

Alma Mater Studiorum – Università di Bologna

DOTTORATO DI RICERCA IN

CHIMICA

Ciclo 33°

Settore Concorsuale: 03/A1

Settore Scientifico Disciplinare: CHIM/12

ADVANCED SPECTROSCOPY FOR THE STUDY OF COLOURANTS IN
CULTURAL HERITAGE

Presentata da: Diego Iván Quintero Balbás

Coordinatore Dottorato

Supervisore

Prof.ssa Domenica Tonelli

Prof. Rocco Mazzeo

Esame finale anno 2021



This research has been carried out at:

Università di Bologna, Ravenna Campus,
Microchemistry & Microscopy Art Diagnostic Laboratory (M2ADL),

<https://site.unibo.it/chemistry-cultural-heritage/en>

Via Guaccimanni 42
48121 Ravenna, Italy

“[...] i raggi del sole formavano su quelle goccioline silicee un immenso arcobaleno che, ogni corpo rinviando i raggi con splendore diverso a seconda della propria natura, aveva molti più colori di quelli che si formano di solito nel cielo dopo un temporale, e a differenza di essi sembrava destinato a brillare in eterno senza mai dissolversi.

Era un rosseggiare di ematiti e cinabri, un baluginare di atramento come se fosse acciaio, un trasvolare di minuzzoli d'auripigmento del giallo all'arancio squillante, un azzurro di armenio, un biancheggiare di conchiglie calcinate, un verdeggiare di malachiti, uno svanire di litargirio in zafferani sempre più pallidi, uno squillare di risigallo, un ruttare di terrume verdaccio che impallidiva in polvere di crisocolla un trionfo di auro musivo, un purpureggiare di biacca bruciata, un fiammeggiare di sandracca, un gatteggiare di creta argentaria, una sola trasparenza di alabastrini.”

Umberto Eco, *Baudolino*

“The nature of all techné is to apply oneself to the genesis of a work of art, to search the technology and the theory of that which is possible to realize, and to find the principle in the person that creates and not in the artwork itself”

*Aristotle, *Éthique à Nicomaque* (translated from French by William Whitney)*

Advanced Spectroscopy for the Study of Colourants in Cultural Heritage

Abstract	i
Resumen	iv
Riassunto	vii
List of Abbreviations	x
List of Figures	xii
List of Equations	xxii
List of Schemes	xxiii
List of Tables	xxv
Introduction	1
Colourant in cultural heritage	2
Spectroscopic methods applied to the study of colourants	6
Outline of this thesis	20
References	21
CHAPTER 1	Enhanced FT-IR methods for studying synthetic organic pigments and dyes and their degradation
1.1 Introduction	35
1.2 Aim of the research	41
1.3 Materials and methods	42
1.3.1 Materials and reagents	42
1.3.2 Paint samples	44
1.3.3 Standard wool samples preparation and artificial aging	46
1.3.4 Wool real samples	46
1.3.5 AgI synthesis and AgI@Au plate preparation	47

1.3.6 Dye extraction protocol	47
1.3.7 μ -XRF analysis	48
1.3.8 MU-ATR analysis	48
1.3.9 AgI@Au MU-ATR analysis	49
1.3.10 AgI@Au TLC analysis	49
1.3.11 ATR-FT-IR measurements and data elaboration	49
2.4 Results and discussion	49
2.4.1 MU-ATR for studying paint samples: pigments, binder and fillers	49
a) Watercolours	51
b) Tempera	57
c) Oil colours	61
d) Conclusions	65
2.4.2 AgI@Au TLC-MU-ATR for studying synthetic dyes and their degradation	66
a) Extraction protocol	67
b) Analyses of the micro extracts with μ -MU-ATR on gold coated glass slides	69
c) Analyses of the micro extracts with TLC μ -MU-ATR on AgI@Au slides	70
d) Real samples	78
e) Conclusions	80
References	81

CHAPTER 2	Effect of silver on the degradation of orpiment in gilding imitation techniques	
	2.1 Introduction	97
	2.2 Aim of the research	102
	2.3 Materials and methods	102
	2.3.1 Real samples	102
	2.3.2 Preparation of paint mock-ups and artificial ageing protocols	104

2.3.3. Stereo and optical microscopy	105
2.3.4 μ -ATR-FT-IR measurements	105
2.3.5 μ -Raman measurements	106
2.3.6 SR-based μ -XRD mapping	107
2.3.7 SR-based μ -XRF and μ -XANES measurements	107
2.4 Results and discussion	109
2.4.1 Real samples: The throne decoration from the Maestà painting	109
2.4.2 Assessing the influence of silver: Unaged mock-ups	113
2.4.3 Assessing the influence of light: Artificial aging with light	116
2.4.4 Assessing the influence of humidity: Orp95%RH and Orp-Ag95%RH	119
2.4.5 Assessing the influence of the binding medium: linseed oil samples	122
2.4.6 Discussion	128
2.5 Conclusion	129
References	130

CHAPTER 3 Spectroscopic study of the crystallization of Pb and Zn carboxylates in different paint binders

3.1 Introduction	141
3.1.1 Metal carboxylates in oil paintings	143
a) Formation of amorphous carboxylates	144
b) Crystallization of carboxylates	145
c) The influence of Zn in oil paintings	148
d) The influence of Pb in oil paintings	148
3.1.2 Metal carboxylates in egg tempera paintings	149
3.1.3 Metal carboxylates in beeswax films	150
3.1.4 Characterization of metal carboxylates	152
3.2 Aim of the study	155
3.3 Materials and methods	156
3.3.1 Mock-up preparation and artificial aging protocol	156

3.3.2 SWIR measurements and Principal Component Analysis (PCA)	158
3.3.3 FT-IR measurement in total reflection mode (rFT-IR)	158
3.3.4 Micro and Macro ATR-FT-IR measurements and data elaboration	160
3.3.5 Cross-section preparation	160
3.3.6 GC-MS measurements	160
3.3.7 XRPD measurements	162
3.4 Results and discussion	163
3.4.1 Study of oil paintings	163
a) Macroscopic effects of the artificial aging	163
b) Non-invasive monitoring	164
c) Monitoring the crystallization of metal carboxylates	171
3.4.2 Study of metal carboxylates in whole egg tempera	177
a) Macroscopic effects of the artificial aging	177
b) Non-invasive monitoring	178
c) Monitoring the crystallization of metal carboxylates	182
3.4.3 Study of metal carboxylates in beeswax films	189
a) Macroscopic effects of the artificial aging	189
b) Non-invasive monitoring	190
c) Monitoring the crystallization of metal carboxylates	192
3.4.4 Discussion	194
3.5 Conclusions	195
References	196
Conclusions	207
Appendices	I-XXIV
Acknowledgements	

Abstract

Colourants in cultural heritage are substances used to change the colour of something, and we classify them into three categories: a) pigments, b) dyes, and c) lakes and hybrid pigments. The first ones are fine powders, both inorganic and organic, that require a binder to maintain cohesion and create a paint layer. Dyes are organic substances with an affinity for the substrate to which they bind and alter their colour, and lakes and hybrid pigments are dyes precipitated or dispersed into inorganic matrices.

Identifying colourants is one of the main goals when studying cultural heritage. It gives information about the artistic technique, can help in dating, and offers insights into the object's condition. Furthermore, the study of the degradation phenomena constitutes a framework for the preventive conservation strategies, provides evidence of the object's original appearance, and contributes to the authentication of works of art. However, the complexity of these systems makes it impossible to achieve a complete understanding using a single technique, making necessary a multi-analytical approach.

This work focuses on the set-up and application of advanced spectroscopic methods for colourant investigation in cultural heritage. The outline consists of three chapters:

The first chapter presents the identification of modern synthetic organic pigments (SOP) using Metal Underlayer-ATR (MU-ATR) and the classification of synthetic dyes extracted from wool fibres using a combination of Thin Layer Chromatography (TLC) coupled to MU-ATR using AgI@Au plates.

The project's objective was to explore the capabilities of MU-ATR to study modern artists' materials commercialized by different companies during the mid-1920 and to develop an alternative methodology for identifying synthetic dyes from wool fibres employing the TLC/MU-ATR technique allowing the identification of dyes even in degraded states.

The results of the modern paint samples evidence the well-known complementarity and mutual exclusion of FT-IR and Raman spectroscopies. In many cases, we identified with MU-ATR one element of the mixture while we characterised the others using Raman spectroscopy.

Moreover, the TLC MU-ATR system efficiently identifies synthetic dyes using just small amounts of sample (less than 0.01 mg). It can be used for identifying rapidly the degradation even at an early stage, thus providing information to the conservators to prevent further degradation.

The second chapter presents the study of the effect of metallic Ag in the photo-oxidation process of orpiment (As_2S_3), and the influence of the different factors, such as light and relative humidity. We used a combination of vibrational and synchrotron radiation (SR)-based X-ray microspectroscopy techniques: micro-Attenuated Total Reflection-Fourier transform Infrared (μ -ATR-FT-IR), μ -Raman, SR-micro-X-ray Fluorescence (μ -XRF), micro X-ray absorption near edge structure (μ -XANES) at S K-, Ag L3- and As K-edges and SR-micro X-ray Diffraction (μ -XRD).

The objective of the research was to evaluate the effect of Ag on the degradation of orpiment and determine which mechanism takes place when these two materials are mixed in a paint layer, as it was identified

in the painting *Maestà* attributed to Cimabue. The results indicate that Ag plays a critical role in the degradation of the orpiment by increasing its oxidation, probably due to an ion interchange mechanism.

The third chapter presents the study of metal carboxylates in paintings, specifically on the formation of Zn and Pb carboxylates in three different binders: stand linseed oil, whole egg, and beeswax. For this research, we used m-ATR-FT-IR, macro-FT-IR in total reflection (rMA-FT-IR), portable Near-Infrared spectroscopy (NIR), macro-X-ray Powder Diffraction (MA-XRPD), X-ray Powder Diffraction (XRPD), and Gas Chromatography Mass-Spectrometry (GC-MS). For the data processing, we explored the data from rMA-FT-IR and NIR with the Principal Component Analysis (PCA).

The objective of this project was to contribute to the knowledge of the pathway of formation and crystallization of lead and zinc carboxylates by monitoring the artificial ageing process of painting mock-ups. The data support the hypothesis of an amorphous state formation at the initial stage of ageing and the simultaneous presence of probably ionomer-like structure and free metal carboxylates. The last one increases with the ageing and degradation of the oil film, migrates, and finally crystallises. After the increase of crystalline carboxylates, the layers started to become fragile. We identified no amorphous carboxylates in egg tempera or beeswax samples.

Resumen

Los materiales colorantes utilizados en el patrimonio cultural son sustancias que cambian el color de un objeto, y pueden clasificarse en tres categorías: a) pigmentos, b) colorantes y c) lacas y pigmentos híbridos. Los primeros son polvos finos, de naturaleza orgánica o inorgánica, que requieren de un aglutinante para mantener su cohesión y formar una capa pictórica. Los colorantes por su parte, son sustancias orgánicas afines al substrato al que se unen y cambian su color. Por último, las lacas y pigmentos híbridos son colorantes precipitados o dispersos en matrices inorgánicas.

La identificación de los materiales colorantes es uno de los principales objetivos cuando se estudia superficies polícromas en objetos del patrimonio cultural. Nos permite obtener información sobre la técnica artística, ayuda en el proceso de datación y ofrece datos sobre el estado de conservación. Además, el estudio de los procesos de deterioro es un referente para el establecimiento de programas de conservación preventiva, permite formular hipótesis sobre la apariencia original del objeto y contribuye a la autenticación de obras de arte. A pesar de estas ventajas, la complejidad de estos sistemas hace imposible entenderlos de manera completa usando solo una técnica de análisis, por lo que es necesario afrontar su estudio de manera multianalítica.

Este trabajo se enfoca en la puesta a punto y aplicación de diferentes métodos espectroscópicos avanzados para el estudio de materiales colorantes en el patrimonio cultural. La tesis se divide en tres capítulos:

En el primero se discute la identificación de pigmentos orgánicos sintéticos utilizando Metal Underlayer-ATR (MU-ATR), y la

identificación de colorantes sintéticos extraídos de fibras de lana usando una combinación de cromatografía de capa fina (TLC) acoplada al MU-ATR utilizando soportes AgI@Au.

El objetivo del proyecto fue explorar la capacidad del MU-ATR para el estudio de materiales artísticos modernos comercializados por diferentes productores a mediados de los años veinte del siglo pasado. Además, se desarrolló una metodología alternativa para la identificación de colorantes sintéticos obtenidos de fibras de lana usando las técnicas TLC/MU-ATR, permitiendo así identificar los colorantes aún cuando están deteriorados.

Los resultados obtenidos de las muestras de pinturas modernas dejan en claro la conocida complementariedad de exclusión mutua de las espectroscopías FT-IR y Raman. En muchos de los casos pudimos identificar uno de los elementos que constituyen la fórmula de la pintura usando MU-ATR, mientras que otros de los compuestos fueron identificados con la espectroscopía Raman.

Además, el sistema TLC/MU-ATR identifica eficientemente colorantes sintéticos usando una pequeña cantidad de muestra (menos de 0.01 mg). Puede ser utilizado para la identificación rápida de sus productos de deterioro aún en las etapas iniciales, ofreciendo así información valiosa para los conservadores-restauradores para prevenir el avance del deterioro.

En el segundo capítulo se aborda el estudio del efecto de la Ag metálica en el proceso de foto-oxidación del pigmento oropimente (As_2S_3), y la influencia de algunos factores como la luz y la humedad relativa. Para este estudio utilizamos una combinación de espectroscopías vibracionales y con radiación de sincrotrón a nivel microscópico: micro-Attenuated Total Reflection-Fourier transform

Infrared (μ -ATR-FT-IR), μ -Raman, SR-micro X-ray Fluorescence (μ -XRF), micro X-ray absorption near edge structure (μ -XANES) de S K-, Ag L3- y As K-edges, así como SR-micro X-ray Diffraction (μ -XRD).

El objetivo de la investigación fue evaluar el efecto de la Ag en el deterioro del oropimente y determinar el mecanismo que se lleva a cabo cuando ambos materiales se encuentran mezclados en una capa pictórica, como es el caso de la pintura *Maestà* atribuida al Cimabue actualmente conservada en la iglesia de Santa Maria dei Servi en Bolonia. Los resultados indican que la Ag juega un papel importante en el proceso de deterioro del oropimente incrementando su oxidación, probablemente a través de un mecanismo de intercambio iónico.

El tercer capítulo aborda el estudio de carboxilatos metálicos en capas pictóricas; en particular se enfoca en la formación de carboxilatos de zinc (Zn) y plomo (Pb) en tres aglutinantes: aceite de linaza cocido, temple de huevo y cera de abeja. Para esta investigación usamos μ -ATR-FT-IR, macro FT-IR en reflexión total (rMA-FT-IR), espectroscopía de Infrarrojo cercano (NIR), macro X-ray Powder Diffraction (MA-XRPD), X-ray Powder Diffraction (XRPD), y cromatografía de gases acoplada a espectrometría de masas (GC-MS). Para el procesamiento de los datos utilizamos el análisis de componentes principales (PCA) para explorar los datos de rMA-FT-IR y NIR.

El objetivo de este proyecto fue contribuir al conocimiento del proceso de formación y cristalización de los carboxilatos de Zn y Pb, monitoreando el proceso de envejecimiento artificial de probetas. Los datos aportan evidencia sobre el estado inicial de formación de una fase amorfa y la presencia simultánea de un ionómero así como

carboxilatos metálicos libres. Estos últimos aumentan con el envejecimiento y deterioro de las capas de óleo, migran y se cristalizan. Después del proceso de cristalización, las capas pictóricas se vuelven frágiles. No identificamos carboxilatos amorfos en el temple de huevo ni en las muestras de cera de abeja.

Riassunto

Nei beni culturali, i materiali coloranti sono sostanze utilizzate per modificare il colore di un oggetto. Li possiamo classificare in tre categorie: a) pigmenti, b) coloranti e c) lacche e pigmenti ibridi. I primi sono una polvere fine, di natura organica oppure inorganica, che richiede un legante per mantenere la coesione e formare un estratto pittorico. I coloranti sono sostanze organiche che hanno un'affinità per il sostrato dove essi si legano e modificano il colore, mentre le lacche e i pigmenti ibridi sono coloranti precipitati o dispersi in matrici inorganiche.

L'identificazione dei materiali coloranti è uno dei principali obiettivi dello studio del patrimonio culturale. Ci permette di ottenere informazioni sulla tecnica artistica, ci aiuta nel processo di datazione e ci offre dati sullo stato di conservazione di un oggetto. Inoltre, lo studio dei processi di degrado è un riferimento per la messa a punto dei piani di conservazione programmata, permette avere un'idea sull'aspetto originale dell'oggetto e contribuisce all'autenticazione delle opere d'arte. Nonostante questi vantaggi, la complessità dei sistemi policromi non consente di completare lo studio utilizzando soltanto una tecnica analitica ed è quindi necessario affrontare lo studio con un'impostazione multianalitica.

La presente tesi si focalizza sulla messa a punto e applicazione di diversi metodi spettroscopici avanzati per lo studio dei materiali coloranti nel patrimonio culturale. La trattazione è divisa in tre capitoli.

Nel primo si discute l'identificazione dei pigmenti organici di sintesi, utilizzando la tecnica Metal Underlayer-ATR (MU-ATR) e l'identificazione di coloranti di sintesi estratti da fibre di lana, tramite la

combinazione della cromatografia di estratto sottile (TLC) e della MU-ATR, usando un supporto AgI@Au.

L'obiettivo di questo progetto è stato definire i limiti e vantaggi dell'utilizzo della MU-ATR per lo studio di materiali artistici moderni, commercializzati da diversi produttori a metà degli anni Venti del secolo scorso e sviluppare una metodologia alternativa per l'identificazione dei coloranti sintetici, anche degradati, estratti da fibre tessili utilizzando le tecniche TLC/MU-ATR

I risultati dei campioni di pittura moderna dimostrano la complementarità di mutua esclusione delle spettroscopie FT-IR e Raman. In molti casi è stato possibile identificare uno dei componenti della formula della pittura con MU-ATR mentre altri composti sono stati accertati con la spettroscopia Raman.

Inoltre, il sistema TLC/MU-ATR permette di identificare in maniera efficace coloranti di sintesi, adoperando una piccola quantità di campione (meno di 0.01 mg). È possibile usare questi sistemi per l'identificazione rapida dei prodotti di degrado anche all'inizio dell'invecchiamento, offrendo così dati importanti per i restauratori, in ottica di prevenzione del deterioramento.

Nel secondo capitolo si tratta l'effetto che l'Ag metallico ha sul processo di foto-ossidazione dell'orpimento (As_2S_3), nonché l'influenza di alcuni fattori, come la luce o l'umidità relativa. Per questo studio abbiamo usato una combinazione di tecniche spettroscopiche vibrazionali e di luce di sincrotrone a livello microscopico: micro-Attenuated Total Reflection-Fourier transform Infrared (μ -ATR-FT-IR), μ -Raman, SR-micro X-ray Fluorescence (μ -XRF), micro X-ray absorption near edge structure (μ -XANES) de S K-, Ag L3- e As K-edges, così come SR-micro X-ray Diffraction (μ -XRD).

L'obiettivo di questa ricerca è stato valutare l'effetto dell'Ag nel degrado dell'orpimento e determinarne il meccanismo quando i due materiali sono miscelati in uno strato pittorico, com'è stato riscontrato nel dipinto *Maestà* attribuito al Cimabue, attualmente conservato nella chiesa di Santa Maria dei Servi a Bologna. I risultati suggeriscono che l'Ag ha un ruolo importante nel processo di degrado, incrementando l'ossidazione dell'orpimento, probabilmente tramite l'intercambio ionico.

Il terzo capitolo si concentra sulla disamina dei carbossilati metallici in strati pittorici, in particolare nella formazione dei carbossilati di Zn e Pb in tre leganti: olio di lino cotto, uovo e cera d'api. Per questa ricerca abbiamo utilizzato μ -ATR-FT-IR, macro FT-IR in riflessione totale (rMA-FT-IR), spettroscopia nel vicino infrarosso (NIR), macro X-ray Powder Diffraction (MA-XRPD), X-ray Powder Diffraction (XRPD), e cromatografia di gas accoppiata a spettrometria di massa (GC-MS). I dati sono stati analizzati con l'Analisi dei Componenti Principali (PCA) per esplorare i dati di rMA-FT-IR e NIR.

L'obiettivo di questo progetto è stato contribuire alla conoscenza del processo di formazione e cristallizzazione dei carbossilati di Zn e Pb, monitorando il processo di invecchiamento artificiale dei campioni. I dati apportano delle evidenze sullo stato iniziale di formazione di una fase amorfa e la presenza simultanea dell'ionomero così come di carbossilati metallici liberi. Questi ultimi incrementano con l'invecchiamento e il degrado dei film di olio, migrano e cristallizzano. Dopo il processo di cristallizzazione, gli estratti pittorici diventano fragili. Non abbiamo identificato carbossilati amorfi nei campioni di tempera all'uovo né nei campioni di cera d'api.

List of Abbreviations

ATR: Attenuated Total Reflection

DRIFT:

FAs: Fatty acids

FFAs: Free Fatty acids

FIR: Far Infrared

FMC: Free Metal carboxylates

FORS: Fibre Optic Reflectance Spectroscopy

FT-IR: Fourier Transform Infrared Spectroscopy

FT-Raman: Fourier Transformed Raman Spectroscopy

GAART: Grazing Angle Attenuated Total Reflection

HIS: Hyperspectral Imaging

HPLC: High Performance Liquid Chromatography

IRR: Infrared Reflectography

MA-rFT-IR: Macro FT-IR in total reflection mode

MA-XRPD: Macro X-ray Powder Diffraction

MS: Mass Spectroscopy

MU-ATR: Metal Underlayer Attenuated Total Reflection
FT-IR

NIR: Near Infrared

Py-GC: Pyrolysis-Gas Chromatography

SEIRA: Surface-Enhanced Infrared Reflection Absorption

SERS: Surface Enhanced Raman Spectroscopy

SOP: Synthetic Organic Pigment

SuGARS: Super Grazing Angle Reflection Spectroscopy

THz: Terahertz

TLC: Thin Layer Chromatography

UV-Vis: Ultraviolet–Visible spectroscopy

XANES: X-ray Absorption Near Edge Structure

XRD: X-ray Diffraction

XRF: X-ray Fluorescence

XRPD: X-ray Powder Diffraction

μ -SORS: Micro Spatially Offset Raman Spectroscopy

List of Figures

Introduction

Figure 1. Malachite and Azurite, two copper (Cu) pigments commonly used in polychrome surfaces. They can be obtained from natural sources or produced artificially. **3**

Figure 2. Cochineal lake (red powder) is produced precipitating of cochineal dye obtained from dry female insects. **3**

Figure 3. In situ XRF analysis of Renaissance wall painting, Museo Casa Romei, Ferrara, 2019. **13**

Figure 4. Portable MA-rFT-IR instrumentation. University of Antwerp. 2019. **16**

Chapter 1

Figure 1. Girl before a mirror by Pablo Picasso, 1932. Museum of Modern Art (MoMA), New York. **35**

Figure 2. Fabric samples of “guarantee unfadable” products by James Morton. 20th century. **36**

Figure 3. Paint sample, 20x, DF. Figure 4. Paint sample, 20x, DF. **44**

Figure 4. Colour chart from Turm-Künstler- Aquarell-Farben (Watercolours) by Redeker & Hennis. Das Deutsche Farbenbuch by Henrich Trillich, 1925. **44**

Figure 5. Gamboge pigment in watercolour. Courtesy of the artist Jane Blundell. **52**

Figure 6. Spectra of Gummigutt, fein by Pelikan (red solid line,) Gummigutte by Turm (black solid line), and Gummi-gutta reference by Kremer (black dashed line). **53**

Figure 7. MU-ATR Spectra in the region 3700-2600 cm^{-1} . Gummigutt, fein by Pelikan (red solid line,) Gummigutte by Turm (black solid line), and Gummi-gutta reference by Kremer (black dashed line). **53**

Figure 8. MU-ATR spectra of Saftgrün dunkel sample. **54**

Figure 9. MU-ATR of Französisch Grün (135). **55**

Figure 10. MU-ATR spectra of Maingrün sample. **56**

<i>Figure 11. MU-ATR spectrum from the sample Krapplack dunkel.</i>	58
<i>Figure 12. Spectra obtained from the sample Echtgelb II.</i>	59
<i>Figure 13. a) The characteristic peaks related to PY1.</i>	60
<i>Figure 14. MU-ATR spectrum of the binder from oily samples.</i>	61
<i>Figure 15. Spectra of the paint sample Dunkel bordeaux 30.</i>	62
<i>Figure 16. Spectra from Parisgelb sample.</i>	63
<i>Figure 17. Spectrum from Ectsaftgrün sample in the range 3800-3100 cm⁻¹.</i>	64
<i>Figure 18. The extraction protocol used on AB74 dyed fibres aged for 20 h.</i>	68
<i>Figure 19. MU-ATR spectra of Standard of BV3 (dashed black line), wool aged for 305 h (dashed red line), BV3 sample aged for 60 h (black solid line), BV3 sample aged for 140 h (red solid line), and aged for 305 h (blue solid line).</i>	69
<i>Figure 20. a) MU-ATR spectra obtained from the double coffee-ring formed over the AgI@Au plate. b) Photograph of the double coffee-ring formed by BV3 over AgI@Au.</i>	70
<i>Figure 21. MU-ATR spectra on AgI@Au plates on the inner coffee-ring formed after spotting the BV1 micro-extracts.</i>	71
<i>Figure 22. MU-ATR spectra on AgI@Au plates of all the BV3 samples.</i>	72
<i>Figure 23. MU-ATR spectra of pre and post TLC analyses on AgI@Au plates of AB74 aged for 60h.</i>	73
<i>Figure 24. MU-ATR spectra of pre and post TLC analyses on AgI@Au plates of Acid Yellow 24 aged for 60h.</i>	74
<i>Figure 25. MU-ATR spectra of pre and post TLC analyses on AgI@Au plates of Acid Red 87.</i>	74
<i>Figure 26. MU-ATR spectra on AgI@Au plates of artificially aged AB74 samples.</i>	76
<i>Figure 27. MU-ATR spectra of the artificially aged AY24 samples obtained over AgI@Au plate.</i>	77
<i>Figure 28. MU-ATR spectra of the artificially aged AR87 samples deposited over AgI@Au plate.</i>	78

Figure 29. MU-ATR spectra of the real sample CH-5. The spectrum shows the characteristic peaks of BV3. **79**

Figure 30. MU-ATR spectra of the real sample CH-6. **80**

Chapter 2

Figure 1. *Maestà* (c. 1280-1285). Attributed to Cimabue. Santa Maria dei Servi, Bologna. Before the 2015 restoration. **98**

Figure 2. Pietro Lorenzetti (active between 1306 – 1345). *Madonna and Child, with the Blessing Christ* [middle panel], probably 1340, tempera on panel transferred to canvas. National Gallery of London. **99**

Figure 3. a) *Maestà* painting attributed to Cimabue, before restoration 2015, the red rectangle indicates the sampling area. b) $CM1_{KBr}$ sample, visible light, 20x. c) $CM1_{KBr}$ sample, UV light, 20x. d) $CM1_{resin}$ sample, visible light, 20x, d) $CM1_{resin}$ sample, UV light, 20x. **103**

Figure 4. μ -ATR-FT-IR mapping elaborated by integrating the area of the corresponding bands. **109**

Figure 5. a) Photomicrograph of the cross-section of sample $CM1_{KBr}$, 20x DF. The number indicate the points of analysis. b) Raman spectra obtained from layer 2. **110**

Figure 6. a) Photomicrograph of cross-section $CM1_{resin}$ taken from a darkened gold decoration of the painting *Maestà* (see Figure 3, page 88, for the sampling location) and b) detail of the area where SR μ -XRD mapping was performed. **111**

Figure 7. RGB composite SR μ -XRF images of a) $S^{II}/S^{VI}/As$ and b) $S^{II}/S^{VI}/Ag$ recorded from the area shown in Figure 6a [map size (vxh): $99.5.8 \times 74.2 \mu m^2$; step size (v x h): $0.5 \times 0.7 \mu m^2$; exp. time: 100 ms/pixel]. Selection of the μ -XANES spectra (black) recorded at the c) S K-edge and d) Ag L3-edge from the spots reported in a,b) and result of the linear combination fitting (LCF) (magenta) of different S- and Ag-based compounds. **112**

Figure 8. Mapping of sample Orp-Ag, arsenolite formed on the surface of the sample and close to the Ag particles. **114**

Figure 9. a) Photomicrograph of the cross-section of sample Orp-Ag (20x, DF), the numbers indicate the points of analysis. b) Raman spectra from sample Orp-Ag from different areas of the cross-section, the spectra are compared with orpiment (dashed black line) and arsenolite (red dashed line) standards. **114**

Figure 10. a) Photomicrograph of Orp-Ag cross-section before aging. b) Composite SR μ -XRD maps of Ag^0 (blue) Ag_2S (green) As_2S_3 (red) [map size (vxh): $150 \times 50 \mu\text{m}^2$; step size (vxh): $1.5 \times 2 \mu\text{m}^2$; exp. time: 1s/pixel; energy: 21 keV]. **115**

Figure 11. a) Photomicrograph sample Orp, 1x. b) Photomicrograph of sample Orp_{UVA-Vis}, 1x, c) Micrograph of sample Orp_{UVA-Vis}, the arsenolite crystals are indicated with white circles, 20x DF. d) μ -FTIR mapping of sample Orp_{UVA-Vis} done integrating the peak area at 803 cm^{-1} , arising from arsenolite. It is located in the surface of the sample. **116**

Figure 12. a) Mapping of the cross-section of sample Orp-Ag_{UVA-Vis} done after integrating the area under the peak at 796 cm^{-1} . b) Spectrum obtained from the surface of the cross-section. **117**

Figure 13. a) Photomicrograph (20x, DF) of the cross-section from mock-up Orp-Ag_{UVA-Vis}, the numbers indicate the different points of analysis. b) The spectra clearly shows the peaks characteristic of orpiment and, only in the surface (04 and 05) of the sample the peaks of arsenolite. The spectrum from one of the black particles (05) also presents the broad band assigned to acanthite. **117**

Figure 14. a) Photomicrograph of Orp cross-section before aging and b) corresponding SR μ -XRD image of As_2S_3 [map size (vxh): $189.5 \times 50 \mu\text{m}^2$; step size (vxh): $1.5 \times 2 \mu\text{m}^2$; exp. time: 1s/pixel; energy: 21 keV]. c) SR μ -XRF image of Stotal [map size (vxh): $84 \times 97 \mu\text{m}^2$; step size (v x h): $1 \times 1 \mu\text{m}^2$; exp. time: 100 ms/pixel; energy: 3.4 keV] and d) selected S K-edge μ -XANES spectrum (black) recorded from the areas shown in c), compared to that of As_2S_3 reference (grey). **118**

Figure 15. a) Photomicrograph of Orp-Ag cross-section after exposure to UVA-Visible light (RH =25%, T = 30°C). b) Composite SR μ -XRD images of Ag^0 (blue) Ag_2S (green) As_2S_3 (red) and As_2O_3 (cyan) [map size (vxh): $150 \times 60 \mu\text{m}^2$; step size (vxh): $1.5 \times 2 \mu\text{m}^2$; exp. time: 1s/pixel; energy: 21 keV]. **114**

Figure 16. FT-IR spectrum from the surface of the sample Orp95%RH (solid red line) and arsenolite standard (dashed black line). **120**

Figure 17. a) μ -FT-IR mapping of sample Orp-Ag_{95%RH} done with the height of the peak b) the spectrum (black solid line) was obtained from the surface of sample Orp-Ag_{95%RH} (01). **120**

Figure 18. Raman spectrum (black solid line) from the surface of sample Orp-Ag_{95%RH}. **121**

Figure 19. a) Photomicrograph (10x) of the cross-section from mock-up Orp-Ag_{95%RH}, the number (01) indicates the point from which the spectrum was obtained. **121**

Figure 20. Photomicrograph of a) Orp_{95%RH} and c) Orp-Ag_{95%RH} cross-section after exposure to RH \geq 95% (T = 40°C, 12 days). b,d) Composite SR μ -XRD images of Ag⁰ (blue) Ag₂S (green) As₂S₃ (red) and As₂O₃ (cyan). **122**

Figure 21. a) Microphotograph of sample Orp_{Oil} and μ -FT-IR map done using the height of the peak at 794 cm⁻¹. **123**

Figure 22. μ -XRD map from sample Orp_{Oil} in addition to orpiment, arsenolite was identified widespread through the sample. **123**

Figure 23. As K-edge and S K-edge μ -XANES maps from sample Orp_{Oil}, it was identified a localized presence of As₂O₃, As^V-species (pts 01As-03As, 07As) and sulphates (pts 01S, 03S, 04S, 06S). **124**

Figure 24. a) Microphotograph of sample Orp_{OilUVA-Vis} and μ -FT-IR map done using the height of the peak at 800 cm⁻¹. **125**

Figure 25. μ -XRD maps from sample Orp_{OilUVA-Vis} some crystals of arsenolite were identified close to the surface of the sample. **125**

Figure 26. μ -XANES mapping and As K-edged and S K-edge spectra. There is a co-localized presence, mainly at the paint surface, of arsenolite, As^V-species (pts 03As-11As, 14As) and sulphates (pts 01S-05S, 08S) that confirm the results obtained from the other analytical techniques. **126**

Figure 27. a) Microphotograph of sample Orp-Ag_{OilUVA-Vis} and μ -FT-IR map done using the height of the peak at 800 cm⁻¹. **126**

Figure 28. The μ -XRD maps of sample Orp-Ag_{OilUVA-Vis} show the formation of arsenolite and acanthite in the surface of the sample. **127**

Figure 29. A layer on the top of the surface contain variable amount of arsenolite and As^V -species (pts 01As-03As, 13As), sulphates, and Ag_2S (pts 01Ag-04Ag). **127**

Chapter 3

Figure 1. Different metal carboxylate coordination. A) Ionic or uncoordinated form, B) Unidentate coordination, C) bidentate chelating coordination, and D) bidentate bridging coordination. **141**

Figure 2. Scheme of the polymerization process of an oil film and the formation of metal carboxylates. A) & B) carboxylate groups are formed in the binder during autoxidative drying; C) metal ions from the pigment surface diffuse and D) form an ionomeric structure. **142**

Figure 3. Scheme crystallization process: a) the crystallization is triggered by the presence of free saturated fatty acids, b) after the formation of initial “units” and recrystallization larger crystals are formed, and c) metal ions (red) and free saturated fatty acids (blue) diffuse toward the growing crystalline metal soap aggregate. **147**

Figure 4. Analysis areas with SWIR. **158**

Figure 5. Points of analysis using rFT-IR. **163**

Figure 6. Photographs of sample $ZWO_{63weeks}$ at different ageing times, it is possible to see the colour change and the damage to the paint layer. The circles under each photograph are a sample of the colour taken from a point of from the surface. **158**

Figure 7. PC12 score plot from sample $ZWO_{63weeks}$. The spectra obtained after 24 h is clearly separate from the data obtained after different times of artificial ageing. Is possible to see a trend that follows the different times of artificial ageing. **165**

Figure 8. PC12 loading plot from the data obtained from the sample $ZWO_{63weeks}$. The band at 1930 nm (5181 cm^{-1}) characterises the spectra obtained after 50 weeks of artificial ageing in the score plot. **165**

Figure 9. a) Comparison of SWIR spectra from $ZWO_{63weeks}$ at different times of artificial ageing, SNV was applied to all the spectra. b) First derivative spectra from $ZWO_{63weeks}$ at different ageing times. **166**

Figure 10. Portable rFT-IR spectra from sample ZWO_{63weeks} after 4 weeks (black line) and 63 weeks (blue line) compare with the spectra obtained in transmission of Zn palmitate (red line). **167**

Figure 11. PC12 score plot from sample LWO_{63weeks}. The spectra obtained after 24 h is clearly separate from the data obtained after different times of artificial ageing. The trend that follows the different times of artificial ageing is less clear in this sample. **168**

Figure 12. PC12 loading plot from the data obtained from the sample LWO_{63weeks}. The band at 1907 nm (5244 cm⁻¹) characterises the spectra obtained after 50 weeks of artificial ageing in the score plot. **168**

Figure 13. Portable rFT-IR spectra from sample LWO_{63weeks} after 24 h (yellow line), 15 weeks (green line) and 63 weeks (blue line) compare with the spectra obtained in transmission of Pb stearate (red line). Is possible to see the derivative-like peak of the crystalline carboxylates identified in the advance ageing stages. It is possible to identify the inverted band ascribable to CO₃²⁻. **169**

Figure 14. PC12 score plot from sample MO_{63weeks}. The spectra obtained after 24 h is not separate from the data obtained after the first weeks of artificial ageing. The trend that follows the different times of artificial ageing is less clear, however is possible to identify clearly the spectra from the advanced stages of ageing. **170**

Figure 15. PC12 loading plot from the data obtained from the sample MO_{63weeks}. The band at 1891 nm (5288 cm⁻¹) characterises the spectra obtained after 50 weeks of artificial ageing in the score plot. **170**

Figure 16. Portable rFT-IR spectra from sample MO_{63weeks} after 24 h (green line), 10 weeks (blue line), after 15 weeks (blue line), and 63 weeks (yellow line) compare with the spectra obtained in transmission of Pb stearate (red line). Is possible to see the derivative-like peak of the crystalline carboxylates identified in the advance ageing stages. **171**

Figure 17. μ -ATR-FT-IR spectra obtained from the surface of the mock-ups ZWO_{63weeks} at different ageing times, the shift towards lower wavenumbers as well as the increase in relative intensity of the band attributed to the $\nu_{as}(\text{COO}^-)$ of carboxylates is very clear. **172**

Figure 18. μ -ATR-FT-IR of sample LWO_{63weeks} and MO_{63weeks} at different ageing times. The higher reactivity of minium (MO_{63weeks}) since the $\nu(\text{COO}^-)$ of carboxylates appeared after 24 h, and after 31 weeks the distribution of crystalline carboxylates is homogenous in the surface, which is not the case for the sample LWO_{63weeks}. **173**

Figure 19. μ -ATR-FT-IR spectra obtained from cross-section samples from the mock-ups after 10 weeks of natural ageing. a) Spectra of the zinc white cross-section sample. The band of the $\nu_{\text{as}}(\text{CO})$ from carboxylates at 1593 cm^{-1} has a higher intensity in the inner part of the paint film. b) Spectra of the minium cross-section sample, the band from carboxylates at 1565 cm^{-1} is more intense in the surface of the sample. c) Spectra from the lead white cross-section sample, a weak band at 1551 cm^{-1} , ascribable to carboxylates, is slightly more intense in the inner part of the paint film. All the spectra were normalized to the C=O band at 1736 cm^{-1} . **175**

Figure 20. μ -ATR-FT-IR of the cross-section sample taken from the lead white mock-up artificially aged. a) Spectra from the sample after 10 weeks of artificial ageing, there are no evident differences in the relative intensity of the broad band from carboxylates. b) Spectra from the sample after 35 weeks of artificial ageing, crystalline carboxylates are detected (peak at 1517 cm^{-1} and shoulder at 1540 cm^{-1}) in the surface of the paint film while two different bands are present in the middle and inner part of it. **176**

Figure 21. Photographs of sample ZWE_{28weeks} at different ageing times, it is possible to see the damage due to the brittleness of the paint layer. The circles under each photograph are a sample of the colour. **178**

Figure 22. PC12 score plot from sample ZWE_{28weeks}. The separation of the different times of artificial ageing is less evident; however, is possible to identify the advance stages of ageing which according to the loading plots, are characterised by the band 1930 nm (5181 cm^{-1}). **179**

Figure 23. PC12 loading plot from the data obtained from the sample ZWE_{28weeks}. The band at 1930 nm (5181 cm^{-1}) characterises the spectra obtained after 20 weeks of artificial ageing in the score plot. **180**

Figure 24. rFT-IR spectra from ZWE_{28weeks} sample, the characteristic peaks of crystalline carboxylates appeared after 2 weeks of artificial ageing and their intensity

increased. Zn palmitate (red line), ZWE_{28weeks} after 24 h (yellow line), after 1 week (green line), after 2 weeks (blue line), and after 24 weeks (purple line). **180**

Figure 25. rFT-IR spectra from LWE_{19weeks} sample, no evidence of carboxylate peaks are observed in the spectra. Lead carbonate (red line), ZWE_{28weeks} after 24 h (blue line), and after 19 weeks (green line). **181**

Figure 26. μ -ATR spectra obtained from the surface of sample ZWE_{28weeks} at different ageing times, the three peaks at 1538 cm^{-1} , 1458 cm^{-1} and 1398 cm^{-1} ascribable to Zn palmitate/stearate are clearly evident after 2 weeks of artificial ageing. Zn palmitate (green line), ZWE_{28weeks} after 24 h (blue line), 1 week (purple line), 2 weeks (yellow line), 6 weeks (red line). **182**

Figure 27. XRPD pattern of a sample from ZWE_{10weeks}, there is no evidence of crystalline carboxylates probably due to the high relative intensity of the characteristic peaks from the pigment ZnO. **183**

Figure 28. XRPD pattern from the samples of Zn palmitate and ZnO at different concentrations. The * indicates peaks produced by a silver plate misalignment, as it can be seen in the range analysed, already at 10 % is complicate to clearly identified the signal characteristic from crystalline Zn palmitate. **184**

Figure 29. Microphotograph and μ -FT-IR spectra obtained from the bottom of the cross-section (red line), the middle part (blue line), and the surface (yellow line). It is clear the different distribution of the carboxylates through the cross-section. The colour circles indicate the point of analysis. **185**

Figure 30. Macro ATR FT-IR spectra of sample LWE_{19weeks}, the peaks of crystalline carboxylates are evident after 7 weeks of artificial ageing. **186**

Figure 31. μ -FT-IR spectra from the surface of sample ME_{63weeks}, the peaks of crystalline carboxylates (i.e. 1537 cm^{-1} and 1512 cm^{-1}) appeared after 2 weeks of artificial ageing (blue line) and increased in intensity. It is evident the strong band at 1398 cm^{-1} assigned to carbonates, which suggest that minium has degrade and transformed into Pb carbonate. ME_{63 weeks} after 24 h (black line), 1 week (purple line), 2 weeks (blue line), 33 weeks (green line), 47 weeks (yellow line), 63 weeks (red line). **187**

Figure 32. μ -ATR spectra obtained from the cross-section of sample ME_{63weeks}, the peaks ascribable to the carboxylates are present mainly in the surface of the sample

(black line). Middle of the sample (purple line), bottom of the sample (red line). The formation of carbonate due to degradation is evident. **188**

Figure 33. Photographs of sample LWB_{62weeks} at different ageing times, it is possible to see the damage due to the ATR analyses. The circles under each photograph are a sample of the colour taken from a point of from the surface. The colour change is related to the deposition of dust over the surface. **189**

Figure 34. PC12 score plot from sample ZWB_{62weeks}. The different times of ageing are mixed together, probably because the small variations on the chemical composition of the mock-ups. **190**

Figure 35. rFT-IR spectra from sample ZWB_{62weeks}, there is no evidence of carboxylates at any ageing time. **191**

Figure 36. μ -FT-IR spectra from the surface of sample ZWB_{62weeks}, the peak of Zn carboxylates (1538 cm^{-1}) present already after 24 h. The intensity increased with the ageing but also variety from point to point, which indicates that the distribution is inhomogeneous. **192**

Figure 37. μ -FT-IR spectra from the surface of the samples. Spectra from LWB_{62weeks} after 24h (purple line), after 6 weeks (dark blue), after 25 weeks (light blue line), after 33 weeks (green line), after 40 weeks (yellow line), and after 60 weeks (red line). Spectra from sample MB_{62weeks} after 24 h (black line), after 6 weeks (grey line), after 25 weeks (yellow line), after 33 weeks (orange line), after 40 weeks (brown line) and after 60 weeks (red line). **193**

List of Equations

Chapter 1

Eq. 1. Synthesis of AgI **47**

Chapter 2

Eq. 1. Oxidation of arsenic trioxide **100**

Eq. 2. Formation of sulphates **101**

List of Schemes

Introduction

- Scheme 1. Classification of colourants in cultural heritage.* **2**
- Scheme 2. Scheme of the stratigraphic composition of a polychrome surface. In general is composed by a preparation layer (0), also called ground layer, that prepares the surface of the support (e.g. wood or textile) making it smooth and reducing the absorption of the paint layers (1-2). In many cases during the time, the original paint layers can be covered by new paint layers applied for modifying the appearance or to repair some damages (3-5).* **4**
- Scheme 3. Scheme of the photophysical phenomena occurring after an electromagnetic beam (B_i) interacts with matter: absorption (A), scattering (S), luminescence (L), and the rest of the beam is transmitted (B_t). Adapted from [1].* **7**
- Scheme 4. Regions or fractions of the electromagnetic spectrum and the type of interaction with the analyte. Adapted from [36].* **8**
- Scheme 5. IR regions and the corresponding interaction with matter* **10**
- Scheme 6. Configuration of a micro Raman instrument and diagram of the Rayleigh and Raman scattering process* **11**
- Scheme 7. Scheme of the X-ray fluorescence phenomenon* **12**
- Scheme 8. a) Scattering of X-rays by a single electron; K_0 and K describe the wave vectors. b) Scheme of diffraction rings, and c) diffraction pattern in the radial profile* **14**

Chapter 1

- Scheme 1. Extraction protocol in three steps. Basic dyes are extracted efficiently in the first while acid dyes required further steps to be extracted. The protocol can be applied in sequence without damaging the sample.* **48**

Chapter 3

Scheme 1. Representation of the “ion hopping” mechanism in an oil film, M^+ is the metal that interacts with the COO^- groups at the end of the side chains in the polymeric network. **146**

Scheme 2. Representation of the Ostwald ripening process, the smaller crystals dissolve and re-crystallise on bigger crystals. **146**

List of Tables

Chapter 1

<i>Table 1. Methods for studying modern materials in artwork.</i>	37
<i>Table 2. Synthetic dyes analysed in this work.</i>	43
<i>Table 3. Paint micro samples analysed in this research.</i>	45
<i>Table 4. Summary of the results from m-Raman/SERS analyses performed at the Doerner Institut. See Appendix I for more information regarding the pigments.</i>	50
<i>Table 5. μ-XRF results.</i>	51
<i>Table 6. Bands arising from the paper support.</i>	52
<i>Table 7. Peaks arising from the binder and their assignation.</i>	61
<i>Table 8. Summary of the materials identified in the set of samples studied.</i>	66
<i>Table 9. Mordents containing sulphate ion and their characteristic FT-IR bands. vw:very weak, m:medium, s: strong, vs:very strong.</i>	75

Chapter 2

<i>Table 1. Summary of artificial aging conditions.</i>	105
<i>Table 2. Summary of the results of the analyses of the real samples from the painting Maestà.</i>	113

Chapter 3

<i>Table 1. Summary of the ageing conditions for each type of mock-up.</i>	157
<i>Table 2. Band assignation of SWIR spectra from oil in the ranges 900-1700 nm and 1200-2200 nm.</i>	164
<i>Table 3. Relative percentages of the quantified free metal carboxylates (FMC) using GC-MS of samples after 10 weeks of natural and artificial ageing.</i>	177
<i>Table 4. Relative percentages of the quantified free metal carboxylates (FMC) using GC-MS of samples after 10 weeks of natural and artificial ageing.</i>	187
<i>Table 5. Some of the characteristic peaks of beeswax identified in the rFT-IR spectra from the three type of samples.</i>	191

Introduction

The chemical and physical effects of light are essential in our daily life: the photosynthesis of green plants is the basis of the food chain, its degradation into heat produces energy, and our vision depends on it [1]. Colour is a physiological phenomenon produced in the human brain [2] as the result of the interaction of three elements: light, the object that interacts with it, and the receptor (our eyes) [3]. There is no real colour of something because when we close the eyes, colour does not exist anymore [4].

Visible light is the part of the electromagnetic spectrum perceptible by the human eye. The electromagnetic spectrum is a range of waves, which are the combination of oscillating electric and magnetic fields in perpendicular planes, divided into different fractions according to their wavelength and frequency, such as X-rays, UV light, and visible light [1].

We see colours thanks to the selective absorption of part of the visible light. For example, we see white the materials that reflect all the wavelengths, while we perceive as black the material that absorbs all of them [1]. If the object absorbs the wavelengths that correspond to the blue (ca. 450 nm) and green (ca. 550 nm) and reflects or transmits the red part (ca. 650-700 nm), we see it red [2].

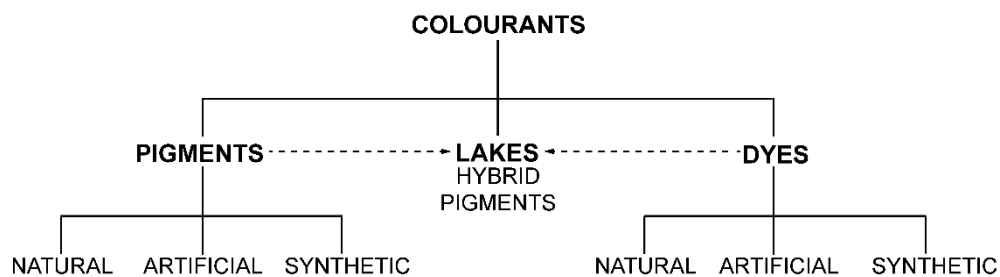
Colours can be the result of different phenomena: a) simple excitation of molecules, b) ligand effects in some metals, c) charge transfer in the molecular orbitals or d) physical effects such as dispersion, scattering, interference or diffraction of the electromagnetic radiations [3].

We cannot imagine cultural heritage without light; we need it for the exhibition and appreciation of the aesthetic values of the objects, and it

allows us to see their colours. Despite its fundamental importance, light and other electromagnetic radiations (e.g., infrared or UV) have also negative effects; they are a factor of long-term cumulative degradation [5]. The undesirable effects of light on cultural heritage have been well-known for a long time; for example, already in historical documents was suggested to reduce light exposure to avoid paintings degradation [6, 7].

Colourants in cultural heritage

Colourants are substances used to add colour or change the colour of something [8]. We can classify colourants in three different categories: pigments, dyes, and lakes/hybrid pigments [3] (Scheme 1). We can subdivide pigments and dyes according to their origin into natural materials (obtained from natural sources), artificial materials (molecules already existing in nature but produced using chemical reactions), and synthetic materials (new molecules not present in nature) [9].



Scheme 1. Classification of colourants in cultural heritage.

Pigments (Figure 1), are fine powders that require a binder, in which they are insoluble, to create a paint layer, maintain cohesion, and attach to the surface. They can be inorganic [10, 11] or organic [12].

Dyes, on the other hand, are organic substances with an affinity for the substrate to which they bind and alter its colour [13]. Some

pigments, for example, Prussian blue ($\text{Fe}_4[\text{Fe}(\text{CN})_6]_3$) or Scheele's green (CuHAsO_3), were used for dyeing textiles [14, 15], but is not possible to use dyes for painting, with some exceptions as indigo and carthamin, reason why artists transformed them into lakes or hybrid pigments.



Figure 1. Malachite and Azurite, two copper (Cu) pigments commonly used in polychrome surfaces. They can be obtained from natural sources or produced artificially.

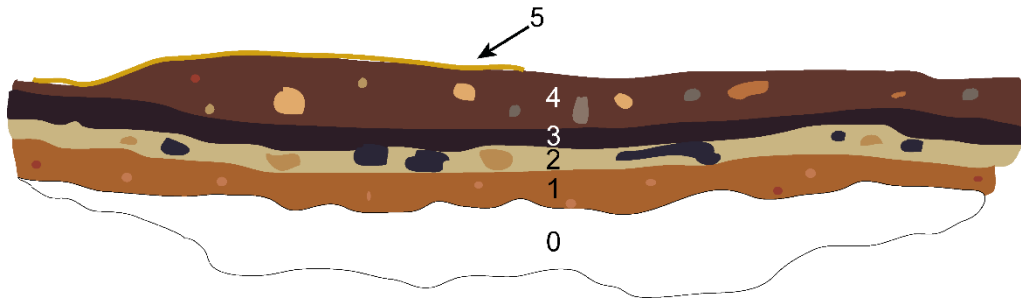


Figure 2. Cochineal lake (red powder) is produced precipitating of cochineal dye obtained from dry female insects.

Lakes and hybrid pigments [16], are dyes precipitated or dispersed into inorganic matrices (also called host); mainly transparent inorganic salts or gels (Figure 2). They keep the translucent properties of dyes that make them good materials for the application of glazes in paintings [10, 11]. Hybrid pigments are obtained when the dyestuff interacts with the host and establishes bonds creating a new material, for example, Maya blue.

Polychrome surfaces constitute complex stratigraphic composites (Scheme 2, next page),

containing pigments and lakes together with binders and sometimes fillers. Easel paintings are the most common example of this kind of objects, but polychrome surfaces are also present in sculptures, manuscripts, watercolours, and mural paintings.



Scheme 2. Scheme of the stratigraphic composition of a polychrome surface. In general is composed by a preparation layer (0), also called ground layer, that prepares the surface of the support (e.g. wood or textile) making it smooth and reducing the absorption of the paint layers (1-2). In many cases, the original paint layers are covered by new paint layers applied to modify the appearance or to repair some damages (3-5).

Dyes merge with fibres and, in many cases, mordents in textiles, for example, tapestries or historical clothes, but also can be part of inks for writing and drawing [17, 18, 19, 20].

The polychrome systems are unstable, undergo internal reactions, and interact with the environment. For example, pigments can react with the binder and produce metal carboxylates [21]; many colourants degrade after interacting with light [22], humidity [23], temperature [24, 25] or atmospheric pollutants (e.g. O₃, NO_x) [26, 27].

During degradation, many colourants produce new molecules that accelerate the damage or interact with other components in the surroundings and lead to further chemical changes. For example, the semiconductor pigments vermilion (HgS), cadmium yellow (CdS and Cd_{1-x}Zn_xS), and minium (Pb₃O₄) undergo self-redox reactions that promote the degradation of other components in their vicinity [28].

For centuries, the colourants available to artists were mainly from natural origin, with some exceptions, such as Egyptian blue, but the advances in chemical synthesis, in particular during the 19th century, provided new materials that revolutionised art. Synthetic pigments, for example, Prussian blue that was developed in Berlin in 1704 by Diesbach [29], modified the artists' palette and today its identification in artwork helps in

dating. The most relevant changes occurred after Perkin discovered mauveine in 1854, and the synthetic dyes Era began [9].

The characterization of colourants is one of the main goals when studying cultural heritage. It gives information about the artistic technique, can help in dating, and offer insights on the condition of the object. And, the study of the degradation phenomena constitutes a framework for the preventive conservation strategies, provides evidence of the object's original appearance, and contributes to the authentication of works of art [28, 30]. However, the complexity of these systems makes it impossible to achieve a complete understanding using a single technique, making necessary a multi-analytical approach [31].

In the scientific literature indexed in Scopus and Web of Science between 1982 and June 2020 (Appendix 1), “pigments/ pigment” are the indexed keywords more often used in the publications related to spectroscopy in cultural heritage, followed by “dyes/dye, “lakes” and “colorant materials”. In particular, many publications associate the term “lakes” with the red colour, such as cochineal and madder lakes. Scientist classify other materials, for example, Maya blue, as “hybrid pigments” or “organic pigments.”

We can divided the studies on colourants in the scientific literature into a) characterization of materials and study of artistic techniques, b) set-up of analytical methodologies, and c) study of degradation mechanisms.

In the last few years, the publication regarding the characterization of materials has decreased since many scientific journals considered less innovative regarding the other type of investigations. The lack of data available about artistic techniques can produce further problems for the authentication of works of art [32, 33] and the misunderstanding of some particular materials used by artists [34].

On the other hand, the set-up of methods is the result of the need to adapt analytical techniques to the particular requirements of the cultural heritage field, for example, the complexity of systems, the materials

degradation, and the sample availability. These investigations focus on the improvement of detection limits, the reduction of sample pre-treatments, the development of methodologies for the characterization of materials in a non-invasive way, and to improve the spatial resolution at a microscopic level to obtain more detailed information from micro-samples.

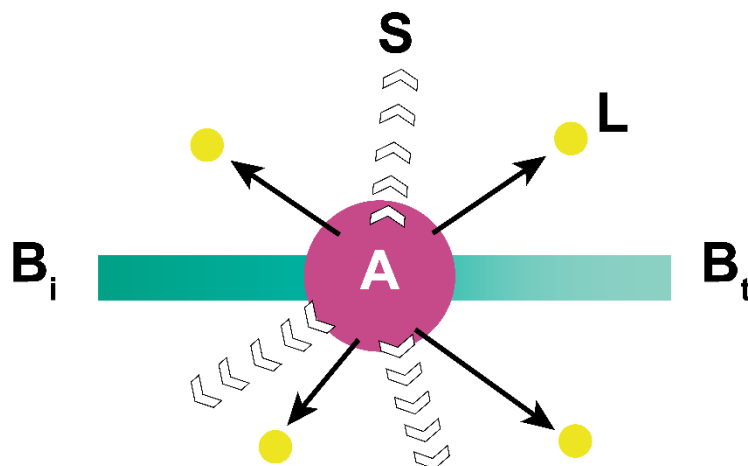
Finally, the study of degradation processes generally is performed under a phenomenological perspective. In general, mock-ups artificially aged are used to imitate the conditions of a real object and evaluate the influence of different factors in the stability and degradation of the materials [7].

The following paragraphs present a general overview of the application of Spectroscopy for the study of colourants in cultural heritage.

Spectroscopic methods applied to the study of colourants

Spectroscopy studies the interaction between the electromagnetic radiations and matter. The spectroscopic methods measure the response (emission or absorption) produced by molecular or atomic species after their irradiation with electromagnetic waves [35].

There are several photophysical and photochemical phenomena that occur after electromagnetic radiation interacts with matter: the incident beam reduces its intensity as the result of the scattering, luminescence and absorption processes (Scheme 3). The absorbed radiation becomes excitation energy and produces an excited state. After releasing the absorbed energy as heat or photons (a phenomenon called luminescence), the matter returns to a lower energy state [1, 35].



Scheme 3. Scheme of the photophysical phenomena occurring after an electromagnetic beam (B_i) interacts with matter: absorption (A), scattering (S), luminescence (L), and the rest of the beam is transmitted (B_t). Adapted from [1].

The spectrophotometers detect the frequency or the wavelength, and the intensity of the energy released by matter and produce a graphic, called spectrum (Scheme 4, next page) [36]. The methods can be classified, based on the phenomena measured, into emission, absorption, or photoluminescence spectroscopy. According to the level of interaction between the radiation and matter, which depends on the energy of the radiation, some spectroscopic methods offer atomic information while others produce molecular data; this depends on the energy of the radiation. For example, X-rays interact with the electron configuration of the atoms and can induce a fluorescence effect that allows us to study the atomic composition with X-ray fluorescence (XRF). On the other hand, infrared radiation modifies the vibrational states of the molecules, offering molecular information from the analyte [35].

Spin change		Orientation change	Configuration change	Electron distribution changes		Nuclear configuration changes	Type of quantum change
10^{-2}	1	100	10^4	10^6	10^8		Wavenumber (cm^{-1})
10 m	1 cm	100 μm	1000 nm	10 nm	100 μm		Wavelength
3×10^6	3×10^{10}	3×10^{12}	3×10^{14}	3×10^{16}	3×10^{18}		Frequency (Hz)
10^{-3}	10	10^3	10^5	10^7	10^9		Energy (J/mol)
NMR	ESR	Microwaves	Infrared	UV-Vis	X-rays	γ rays	Type of spectroscopy

Scheme 4. Regions or fractions of the electromagnetic spectrum and the type of interaction with the analyte. Adapted from [35].

Since the 18th century, scientists got more interested in cultural heritage and influenced the conservation practice. Among different aspects, they started to question about the colour changes of some pigments [37].

During the 19th century, the development of optics and microscopy and the use of different electromagnetic radiations for analytical proposes enriched the studies of cultural heritage [38], and researchers started to investigate the degradation mechanism of some colourants using spectroscopy [30].

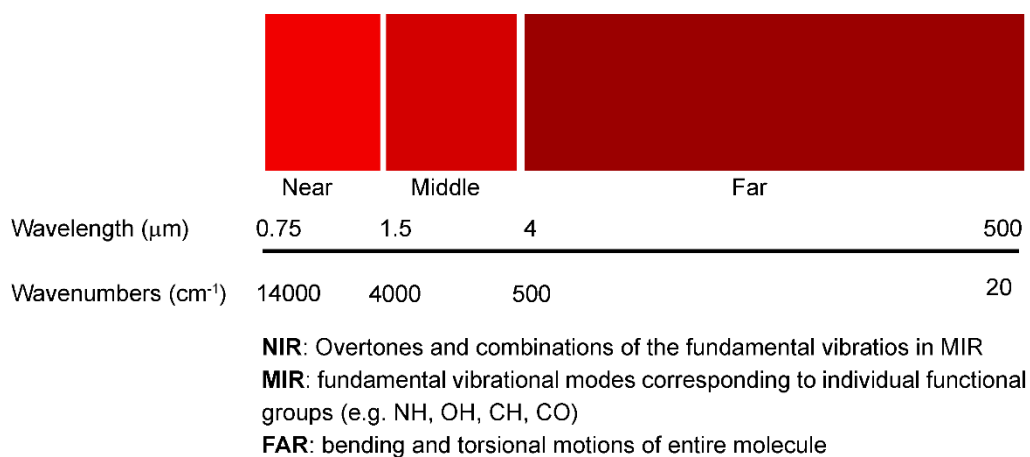
The first pigments investigation published (1800) was the analysis by John Haslam of wall painting samples [39]. In 1806, Désormes and Clément published their results of ultramarine (Pigment blue 29, CI 77007) analysis, focused on the characterization of its chemical composition to manufacture it [39]. Later, in 1809 Sir Humphry Davy (1778–1829) and Jean Chaptal (1756-1832) studied the pigments of the recently discovered wall paintings in Pompeii [40, 39]. In this period, scientists started to use infrared radiation to analyse cultural heritage, but the technique had several limitations [41].

During the early years of the 20th century, the use of analytical methodologies for the study of cultural heritage increased considerably. Scientists used spectroscopic methods to obtain information regarding the morphology and the chemical composition of many materials [40]. The early efforts of Raehlmann in 1910, Laurien in 1914, and later of Joyce Plesters in 1956 are the pioneer works of studying polychrome surfaces by cross-section analysis [42].

After the development of the early FT-IR instrumentation built by Perkin-Elmer Company and the Shell Development Company in the 1940s, scientists increasingly used infrared radiation for analysis and rapidly improved its reproducibility and sample preparation thanks to the invention of Attenuated Total Reflection (ATR) [41, 43].

FT-IR is based on the absorption of infrared radiation, which possess the energy required to produce rotational, translational and vibrational

energy transitions in molecules, the latter being the most important for IR spectroscopy. FT-IR offers molecular information (Figure 3), since functional groups have specific IR absorptions, thus their specific vibrational frequencies allow for their identification. For this reason, FT-IR, in the middle-infrared region, is a powerful tool for the characterization of many colourants, particularly of organic nature due to the presence of functional groups active in that region, such as NH, OH, CH and CO. However, some inorganic colourants (i.e., pigments) exhibit particular vibrational frequencies in FT-IR spectra, for example, the band at 2100-2200 cm^{-1} arising from $\nu(\text{C}=\text{N})$ group from the Prussian blue ($\text{Fe}_4[\text{Fe}(\text{CN})_6]_3$, C.I. Pigment blue 27) [44].



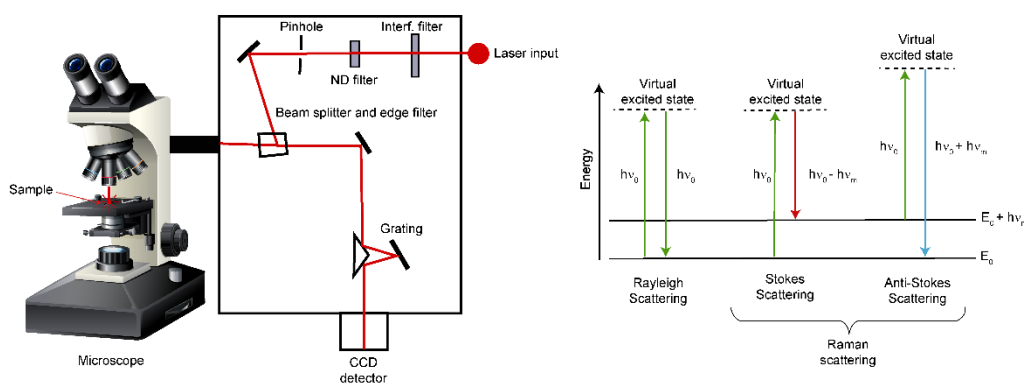
Scheme 5. IR regions and the corresponding interaction with matter. Adapted from [44].

It was in 1966 that Olin published a paper regarding the study of paintings using FT-IR, and later the analysis of pigments and binders using FT-IR became more common among scientists [42]. FT-IR offers information on some inorganic pigments and lakes, but its main drawback lies in the overlapping of bands when studying complex mixtures; however, this is remediable by coupling it with separation methods [45].

After the introduction of lasers as monochromatic radiation sources and the development of semiconductors for detection during the 1960s, the

measurement of the Raman Effect increased, and scientists started to apply it to cultural heritage studies [46].

Raman spectroscopy uses a monochromatic excitation source (i.e., a laser). The lasers used in Raman spectroscopy can be in the UV (244 nm, 355 nm), Vis (532 nm, 633 nm) or NIR (785 nm, 1064 nm) regions. The incident beam used in Raman spectroscopy has a different energy from the energy gap between the ground state and the excited state of the molecule, and thus it exploits the scattering of the light and not the absorption. The incident radiation can produce a nuclei motion in the atoms, giving rise to elastic scattering (the so-called Raman scattering) and thus producing a difference in the energy scattered, both by transferring energy from the laser to the molecule or from the molecule to the scatter energy, the first one produces Stokes scattering while the second anti-Stokes, which are the most used in Raman spectroscopy [47, 48].



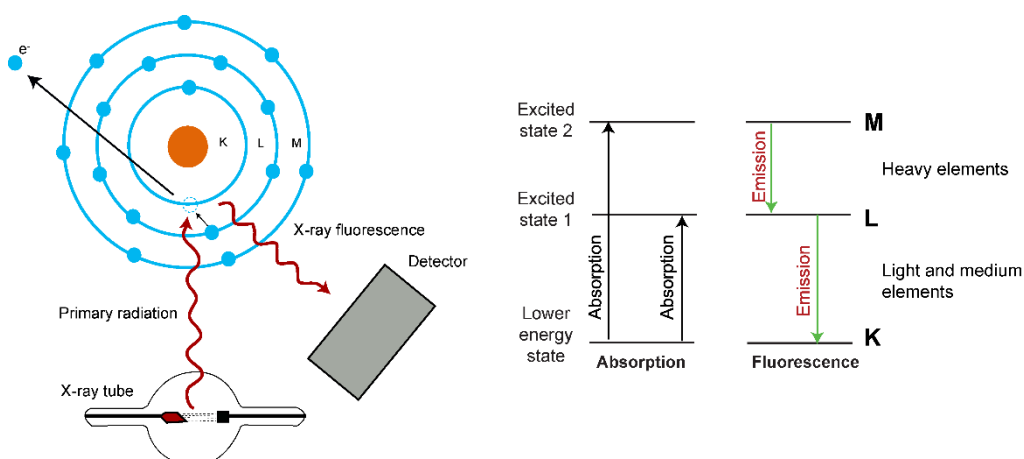
Scheme 6. Configuration of a micro Raman instrument and diagram of the Rayleigh and Raman scattering process. Adapted from [47].

In 1969 early studies of cinnabar (HgS) and orpiment (As_2S_3) using Far Infrared or Terahertz (THz) radiation (wavelength 3000–30 μm) were published, this kind of radiation involves motions of the entire molecule [44]. THz offers fingerprint-like information useful for the characterization of materials; however, the lack of commercial instrumentation limited its application in the cultural heritage field [49].

Even though, since the 1930s researchers used UV-Vis-NIR absorption and emission spectroscopy in the field of cultural heritage, it was until the 1970s that it became commonly used to monitor colour changes and studying polychrome surfaces [50, 51].

It was also during the 1970s that the analysis of pigments using FIR (600-50 cm^{-1}) was published [52], and studies of pigments on their own and mixed with oil were done using the newly available diamond cell for FT-IR analysis in the middle range [42]. In the same decade, researchers analysed with X-ray fluorescence spectroscopy (XRF) a wide range of objects, such as ceramics, mural paintings, and easel paintings, and showed the great utility of XRF for the study of pigments [53].

The X-rays interact at the electronic level of the atoms, and several phenomena occurs, such as the photoelectric effect (i.e., absorption and emission), Compton effect, and Rayleigh effect. The first one takes place when a photon extracts an electron from the atom producing an excited state and a further emission of a photon (fluorescence) as a result of the transition an electron from an outer shell to cover the vacancy produced by the X-rays. This technique offers atomic information, it is very useful for the study of pigments, but it offers no clues about organic materials since it only allows identifying elements with $Z > 15$ [53].



Scheme 7. Scheme of the X-ray fluorescence phenomenon.

Since the 1960s, portable XRF instrumentation was available for military purposes, but scientists seldom applied it to cultural heritage studies because it required particular conditions. With the improvements to the XRF instrumentation, such as the air-cooled X-ray tubes and the thermoelectrically cooled X-ray detectors, portable equipment [54] made possible the analysis of objects *in situ* (Figure 3), and today is possible to map a complete painting thanks to the new data processing methods [55, 56].



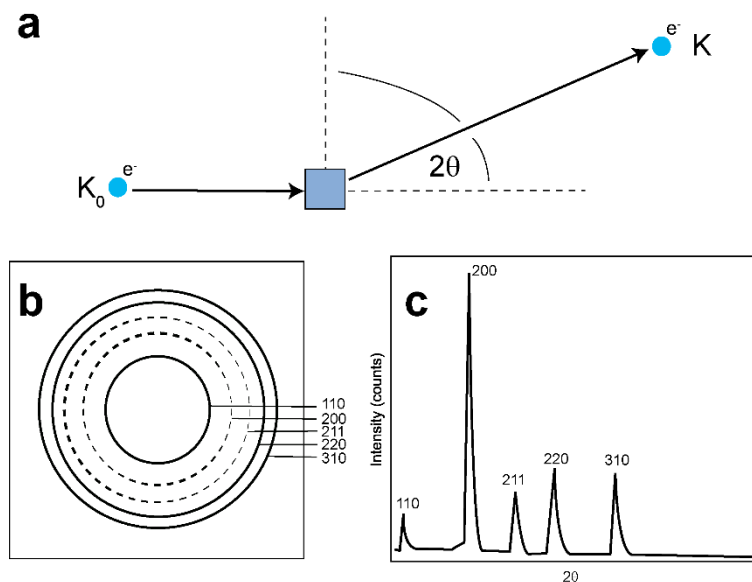
Figure 3. In situ XRF analysis of Renaissance wall painting, Museo Casa Romei, Ferrara, 2019.

The main limitation of non-invasive XRF is the complexity of signal attribution when studying a complex stratigraphy [57]; only on a few analyses, it was possible to estimate the thickness of painting layers using non-invasive XRF [50].

A few years later after the first applications of XRF, researchers started to use X-rays Diffraction (XRD) spectroscopy for pigments analysis [58]. XRD rapidly became a useful technique for studying paintings [59] and for understanding some pigments degradation processes, such as goethite-hematite transformation, and As-based pigments photo-degradation [60, 61].

XRD analysis is based on the X-rays Thompson scattering effect, one of the different phenomena occurring when an X-ray beam impinges matter. Thompson scattering is elastic process and thus the X-ray beam maintain the energy but modifies its direction. The angle difference between the vector of the incident beam and the vector of the scattered beam is called 2θ [62].

The powder diffraction rings, also called diffraction patterns, give information about the crystalline materials present in a sample. The pattern is recorded using a detector and azimuthally integrated in order to obtain a radial profile with the scattering intensity vs scattering angle (2θ) or momentum transfer (Q) [63]. Each phase inside the sample gives rise to a series of diffraction rings that appear as sharp peaks in the radial profile and allow the identification of the material using databases. The patterns are produced by the diffraction of materials with atoms arranged in a crystalline structure, the amorphous materials have no periodic arrays and thus produce no diffraction patterns.



Scheme 8. a) Scattering of X-rays by a single electron; K_0 and K describe the wave vectors. b) Scheme of diffraction rings, and c) diffraction pattern in the radial profile. Adapted from [62].

When the beam size is much larger than the crystals size and they are randomly oriented, the diffraction pattern observed consists of Debye-Scherrer rings, in this case the technique is called X-ray powder diffraction (XRPD) [64].

During the 1980s, cross-section molecular studies were possible thanks to the coupling of microscopy to FT-IR instrumentation and the reduction of the signal-to-noise ratio. This type of analysis became more accessible thanks to the development of commercial instruments and the sampling

methods available for the FT-IR analysis, such as ATR, DRIFT, and diamond cell [44, 41, 65, 42].

In 1984, scientists published the pioneer studies of cultural heritage with Raman spectroscopy [66] focused on the analysis of pigments. These investigations influence the studies of regional palettes, artists' economy, and other historical aspects [67], and then in 1987 was presented the first application of Surface Enhanced Raman Spectroscopy (SERS) for the analysis of alizarin; however, it took around 20 years for SERS to be commonly used in the cultural heritage field [68].

Nowadays, SERS is used in particular for the characterization of lakes. Different substrates have been tested and currently, non-invasive methods, such as the detachable Agar gel or cellulose films doped with nanoparticles, and on-fibre SERS using colloids of metallic nanoparticles have been applied [69, 70, 71].

In the 1990s, Bell and co-workers published a database of Raman spectra from 1850 pigments, and since then, the use of Raman spectroscopy for studying colourants in cultural heritage increased considerably [54].

It was until the 1990s when the application of fibre optics reflectance spectroscopy (FORS) technique in the Vis-UV and NIR ranges (190 nm to 1700 nm) for spot analysis gave good results for the characterization of colourants [72]. Despite the advantages of this technique, its selectivity is reduced since the spectra feature broad bands arising from the electronic transitions, not always allowing the unambiguous characterization of colourants [50].

In the late 1990s, Scott published the study of plastic in a non-invasive way using portable FT-IR instrumentation with a fiber optic [73]. Initially, researchers used non-invasive analytical methods for studying artefacts that could be easily transported to the laboratory, for example, manuscripts or paintings. However, *in situ* studies are preferable due to the risk of moving the objects as well as the high cost of the insurance

makes. For this reason, portable instrumentation was developed and its application has modified the conservation science practice [50].

In 1995 was published the first imaging results using THz in transmission mode. Three years later, in 1998, was published the first application of THz in the field of cultural heritage, initially for dendrochronological analysis [74]. Since then, several techniques have been developed, and their application to cultural heritage studies has increased [75]. Different from NIR or Visible radiation, THz can fully penetrate the painting and allows the observation of reflections from the interfaces of the different layers of the stratigraphic structure at all depths [76].

Finally, in the 2000s, the first application of Hyperspectral Imaging (HSI) for cultural heritage studies appeared. Before the HSI, multiband and multispectral imaging systems were adapted taken advance of the well-known Infrared Reflectography (IRR). HSI led to the use of the terms “imaging spectroscopy” that today is employed for many spectroscopic techniques used in the cultural heritage field to obtain 2D chemical information [72].

Further development in FT-IR instrumentation led to non-invasive and *in situ* analyses by single points and mapping of complete areas in total reflection mode using portable instrumentation (Figure 4) [45, 73, 77, 78].

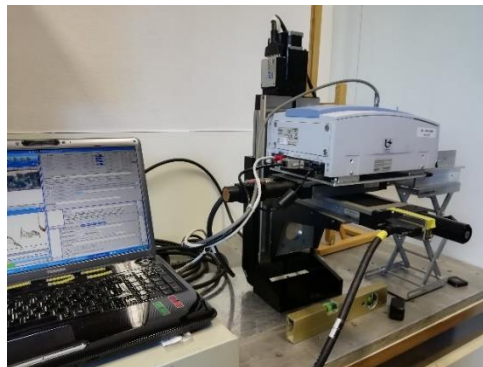


Figure 4. Portable MA-rFT-IR instrumentation. University of Antwerp. 2019.

The FT-IR in reflexion mode (rFT-IR) in the middle infrared region suffers from a strong spectral distortion (bands shape and position) caused by the matrix effect; the data is highly dependent on the surface topography of the object, and it is not possible to predict the distortions that the spectra will have [50].

In 2001 was published the analysis of paintings using a fibre optic probe for the FT-Raman analysis, which led to the development of specific portable instrumentation for the studies of cultural heritage [54].

Since 2002, non-invasive micro and macro XRD mapping have been available for cultural heritage analysis. XRD maps can be obtained both in reflection and transmission mode by acquiring XRD patterns at each pixel of a two-dimensional area. The information can be extracted as single patterns or plot to obtain distribution maps [64, 79, 80].

Two years later, in 2004, the first publication of portable Raman analysis in a museum was published by Vandenabeele and co-workers [40], in 2008 was published online a database of spectra in the THz region [49], and in 2014 were published the first results of the application of Micro Spatially Offset Raman Spectroscopy (μ -SORS) for the study of cultural heritage [81].

Although the clear advantages that portable instrumentation offers and the great advances that in the last few years have been done, some limitations derive from the miniaturization of the optics and some issues can arise from the data interpretation produced by optical and matrix effects, as well as the stratigraphic complexity of polychrome surfaces [50].

Despite the interest in the non-invasive methodologies and the development of macroscopic imaging techniques, also the microscopic analyses have been improved. It was until 2007 when the first FT-IR micro mapping of paint cross-section was published [82]

Further improvements on the signal sensibility of the FT-IR led to the development of enhanced techniques. The surface-enhanced infrared reflection absorption (SEIRA) exploits the IR absorption enhancement effect produced when a sample is absorbed into a metal, mainly with a roughened topology at a nanometre scale [83]. The phenomena occurs when the dielectric properties of the metal are altered by dipoles, induced by IR radiation, produce by the molecule absorbed in the metal,

producing a change in the transmittance or reflectance of it. In addition to the phenomenon explained above, an enhancement of the electromagnetic (EM) field of the analyte is produced when surface Plasmon Polaritons (electromagnetic waves in the Vis and IR frequency traveling along a metal-dielectric interface) are excited, this restricts the enhancement to the vicinity of the molecule (i.e., dielectric) to the surface. Both effects contribute to the SEIRA enhancement [84].

Few publications report on the application of SEIRA to characterized dyes. The method foresees the use of a metal colloid and measurements can be carried out in reflection or attenuated total reflection (ATR) modes [41].

Other methods, such as Super Grazing Angle Reflection Spectroscopy (SuGARS) and Grazing Angle Attenuated Total Reflection (GAATR) enhance FT-IR signal using ATR mode at a high angle of incidence to study thin layers of a sample deposited over a metal or silicon [83]; however, the specific instrumentation required limits their use.

Metal Underlayer attenuated total reflection (MU-ATR) has been recently proposed for the investigation of a thin layer of around 100 nm to 1 μm of thickness of dyes deposited over a high reflective index metal. The advantage of MU-ATR compared with other enhance FT-IR techniques is the capacity of examining thicker layers with commercial instruments, without sample preparation [45].

Researchers used MU-ATR for the analysis of synthetic dyes extracted from fibres [45] and, after coupling it to thin-layer chromatography (TLC), they studied their degradation [85]. Besides, it has been demonstrated that is possible to obtain the SERS effect using the same system [86].

Synchrotron facilities improved the microanalyses because the high brilliance radiation that ranges from infrared to X-rays, the high collimation and polarization, high spatial resolution, and better resolution with a lower amount of sample [31, 87]. In comparison with traditional techniques, many imaging methods, for example, μ -XRD, μ -FT-IR, μ -

XRF, and μ -XANES, offer detailed information, due to the small pixel size and sensibility to the signal-to-noise ratio [30]. Thanks to these features, it is possible to perform spot analysis or obtain 2D and 3D maps with a micrometre-level resolution, and is possible to do multiple analyses in the same sample areas and obtained atomic, molecular and morphological information [88].

The synchrotron analyses are generally performed in cross-section samples that require complex preparation since thin sections are preferred [89].

Publications regarding the study of cultural heritage using synchrotron-based techniques started in 1986 and increased in the last few years [87]. Synchrotron-based X-ray techniques (SR-XR) have revealed very useful for the characterization of pigments [30, 90] and fillers, to understand the degradation process [28, 91], and identified external pollutants [89]. The main drawbacks of the synchrotron techniques are the difficulty to access to the facilities and the reduction of representativeness of the data due to the spot-size [88].

Among all the different spectroscopic methods applied for studying colourants in cultural heritage, today Raman is a leading technique due to its versatility and the different types of objects that can be analysed with it [40]. The keyword occurrence in the scientific literature between 1982 and June 2020 suggests that Raman spectroscopy is the technique most used for the study of colourants in cultural heritage, followed by FT-IR and XRF.

Today the spectroscopic methods are of great importance for the study of cultural heritage, are fundamental for understanding degradation mechanisms, and to determine the hypothetical appearance that some artefacts had in the past.

Outline of this thesis

This work focuses on the set-up and application of advanced spectroscopic methods for the study of colourants in cultural heritage. It addresses both the characterization as well as the understanding of the degradation of some colourants.

The outline consists of three chapters: the first chapter presents the identification of modern synthetic organic pigments (SOP) using Metal Underlayer-ATR (MU-ATR), and the study of synthetic dyes extracted from wool fibres using a combination of Thin Layer Chromatography (TLC) coupled to MU-ATR using AgI@Au plates. This project was done in collaboration with the Doerner Institut (Germany).

The second chapter presents the study of the effect of metallic Ag in the photo-oxidation of orpiment (As_2S_3) and the influence of the different factors, such as light and relative humidity. This research is based on the findings from the study, done by our research group in 2015, of the painting *The Madonna Enthroned with the Child and Two Angels*, also known as *Maestà*, attributed to Cimabue.

We used a combination of vibrational and synchrotron-based X-ray microspectroscopy techniques: micro-Attenuated Total Reflection-Fourier transform Infrared (μ -ATR-FT-IR), μ -Raman, SR-micro X-ray Fluorescence (μ -XRF), micro X-ray absorption near edge structure (μ -XANES) at S K-, Ag L3- and As K-edges and SR-micro X-ray Diffraction (μ -XRD). This project was done in collaboration with the University of Perugia (Italy) and the University of Antwerp (Belgium).

The third chapter presents the study of metal carboxylates in paintings. We studied the formation of Zn and Pb carboxylates in three different binders: stand linseed oil, whole egg, and beeswax. For this research, we used μ -ATR-FT-IR, macro FT-IR in total reflection (rMA-FT-IR), portable Near-Infrared spectroscopy (NIR), macro X-ray Powder Diffraction (MA-XRPD), X-ray Powder Diffraction (XRPD), and Gas

Chromatography Mass-Spectrometry (GC-MS). For the data processing, the data from rMA-FT-IR and NIR were processed with the Principal Component Analysis (PCA). The University of Pisa (Italy) and the University of Antwerp (Belgium) collaborated in this project.

References

- [1] P. Suppan, *Chemistry and Light*, Cambridge: The Royal Society of Chemistry, 1994.
- [2] R. Cozzi, P. Protti and T. Ruaro, *Elementi di analisi chimica strumentale*, Italy: Zanichelli, 2013.
- [3] R. M. Christie, *Colour Chemistry*, Cambridge: Royal Society of Chemistry, 2015.
- [4] R. Falcinelli, *Cromorama. Come il colore ha cambiato il nostro sguardo*, Turin: Einaudi, 2017.
- [5] C. Cuttle, "Damage to museum objects due to light exposure," *Lighting Res. Technology*, vol. 28, no. 1, pp. 1-9, 1996.
- [6] G. Piva, *L'Arte del Restauro*, Milan: Ulrico Hoepli, 2007.
- [7] M. Spring, "Fading, darkening, browning, blanching: a review of our current understanding of colour change and its consequences in Old Master paintings," in *Colour Change in Paintings*, R. Clarricoates, H. Dowding and A. Gent, Eds., London, Archetype Publications Ltd, 2016, pp. 1-14.
- [8] Cambridge University Press, "Cambridge Dictionary," 2019. [Online]. Available:

<https://dictionary.cambridge.org/dictionary/english/colourant>.

[Accessed 17 03 2019].

- [9] P. Le Couteur and J. Burreson, *I bottoni di Napoleone. Come 17 molecole hanno cambiato la Storia*, Milan: TEA, 2018.
- [10] M. Matteini and A. Moles, *La Chimica nel restauro. I materiali dell'arte pittorica*, Florence: Nardini editore, 2010.
- [11] N. Bevilacqua, L. Borgioli and I. Androver Garcia, *I pigmenti nell'arte dalla preistoria alla rivoluzione industriale*, Padua: Il Prato, 2010.
- [12] N. Sonoda, J.-P. Rioux and A. R. Duval, "Identification des matériaux synthétiques dans les peintures modernes. II. Pigments organiques et matière picturale," *Studies in Conservation*, vol. 38, pp. 99-127, 1993.
- [13] S. W. Lewis, "Analysis of dyes using chromatography," in *Identification of textile fibers*, M. M. Houck, Ed., United Kingdom, The Textile Institute, Woodhead Publishing, 2009, pp. 203-223.
- [14] C. Gervais, M.-A. Languille, S. Reguer, C. Garnier and M. Gillet, "Light and anoxia fading of Prussian blue dyed textiles," *Heritage Science*, vol. 2, no. 26, 2014.
- [15] J. C. Whorton, *The Arsenic century. How Victorian Britain was Poisoned at Home, Work and Play*, United States: Oxford University Press, 2011.
- [16] A. A. Polette-Nie, F. S. Manciu, B. Torres, M. Alvarado Jr. and R. R. Chianelli, "Organic/inorganic complex pigments: Ancient colors Maya Blue," *Journal of Inorganic Biochemistry*, vol. 101, pp. 958-1973, 2007.
- [17] O. Díaz-Santana, D. Vega-Moreno and F. Conde-Hardisson, "Gas chromatography-mass spectrometry and high-performance liquid

chromatography-diode array detection for dating of paper ink," *Journal of Chromatography A.*, vol. 1515, pp. 187-195, 2017.

- [18] S. Garrappa, Multi-technical approach for the chemical characterization of modern inks, Ravenna: Alma Mater Studiorum - Università di Bologna, 2017.
- [19] F. C. Izzo, V. Vitale, C. Fabbro and H. Van Keulen , "Multi-analytical investigation on felt-tip pen inks: Formulation and preliminary photo-degradation study," *Microchemical Journal*, 2015.
- [20] A. Vila and J. F. García, "Analysis of the Chemical Composition of Red Pigments and Inks for the Characterization and Differentiation of Contemporary Prints," *Analytical Letters*, vol. 40, no. 10, pp. 1274-1285, 2012.
- [21] M. Cotte, E. Checroun, W. De Nolf, Y. Taniguchi, L. De Viguerie, M. Burghammer, P. Walter, C. Rivard, M. Salomé, K. Janssens and J. Susini, "Lead soaps in paintings: Friends or foes?," *Studies in Conservation*, 2016.
- [22] D. Saunders and J. Kirby, "Wavelength-dependent fading of artists' pigments," *Studies in Conservation*, vol. 39, no. sup 2, pp. 190-194, 1994.
- [23] D. Saunders and J. Kirby, "The effect of relative humidity on artists' pigments," *The National Gallery Technical Bulletin*, vol. 25, pp. 62-72, 2004.
- [24] Y. Taru and K. Takaoka, "Thermal Stability of Organic Pigment (II). Mechanism of Thermal Degradation and Thermal Stability of Azo Lake Pigments," *Journal of the Japan Society of Colour Material*, vol. 48, no. 4, pp. 223-228, 1975.
- [25] A. Coccato, L. Moens and P. Vandenabeele, "On the stability of mediaeval inorganic pigments: a literature review of the effect of

climate, material selection, biological activity, analysis and conservation treatments," *Heritage Science*, vol. 5, no. 12, 2017.

- [26] P. M. Whitmore and G. R. Cass, "The Ozone Fading of Traditional Japanese Colorants," *Studies in Conservation*, vol. 33, no. 1, pp. 29-40, 1988.
- [27] P. M. Whitmore and G. R. Cass, "The Fading of Artists' Colorants by Exposure to Atmospheric Nitrogen Dioxide," *Studies in Conservation*, vol. 34, no. 2, pp. 85-97, 1989.
- [28] C. Miliani, L. Monico, M. J. Melo, S. Fantacci, E. M. Engelin, A. Romani and K. Janssens, "Photochemistry of Artists' Dyes and Pigments: Towards Better Understanding and Prevention of Colour Change in Works of Art," *Angewandte Chemie International Edition*, vol. 57, pp. 7324-7334, 2018.
- [29] Museum of Fine Arts, Boston, "CAMEO: Conservation & Art Materials Encyclopedia Online," 08 05 2018. [Online]. Available: http://cameo.mfa.org/wiki/Prussian_blue. [Accessed 25 04 2019].
- [30] M. Cotte, J. Susini, V. A. Sole, Y. Taniguchi, J. Chillida, E. Checroun and P. Walter, "Applications of synchrotron-based micro-imaging techniques to the chemical analysis of ancient paintings," *J. Anal. At. Spectrom.*, vol. 23, p. 820–828, 2008.
- [31] M. Cotte, E. Welcomme, V. A. Sole, M. Salome, M. Menu, P. Walter and J. Susini, "Synchrotron-Based X-ray Spectromicroscopy Used for the Study of an Atypical Micrometric Pigment in 16th Century Paintings," *Analytical Chemistry*, vol. 79, no. 18, pp. 6988-6994, 2007.
- [32] F. Fiorillo, Assessment of a best practise approach for the attribution and authentication of paintings, Ravenna: University of Bologna, 2020.

- [33] F. Fiorillo, C. Matteucci, M. Cataldo, S. A. Apicella and M. Vandini, "A multi-analytical approach for the characterisation of 20th century paintings," *The European Physical Journal Plus*, vol. 134, p. 373, 2019.
- [34] A. van Loon, P. Noble, A. Krekeler, G. Van der Snickt, K. Janssens, Y. Abe, I. Nakai and J. Dik, "Artificial orpiment, a new pigment in Rembrandt's palette," *Heritage Science*, vol. 5, no. 26, pp. 1-13, 2017.
- [35] D. A. Skoog, D. M. West, F. J. Holler and S. R. Crouch, *Fundamentos de Química Analítica*, Eight ed., Mexico: CENGAGE, 2005.
- [36] M. L. Gómez, *La Restauración. Exámen aplicado a la conservación de obras de arte*, Spain: Cátedra, Intituto del Patrimonio Histórico Español, 2008.
- [37] A. M. Macarrón Miguel, *Historia de la conservación y la restauración. Desde la Antigüedad hasta el siglo XX*, Madrid: Tecnos, 2013.
- [38] I. Pallot-Frossard, "Sciences et conservation du patrimoine culturel. Ou les leçons de Pasteur," *L'actualité chimique*, no. 312-313, pp. 6-9, 2007.
- [39] S. G. Rees-Jones, "Early Experiments in Pigments Analysis," *Studies in Conservation*, vol. 35, no. 2, pp. 93-101, 1990.
- [40] T. Łojewski and B. Łydźba-Kopczyńska, "Spectroscopy in the Analysis of Artworks," in *Molecular Spectroscopy—Experiment and Theory*, A. Koleżyński and M. Król, Eds., Switzerland, Springer Nature, 2019, pp. 483-517.
- [41] F. Rosi, L. Cartechini, D. Sali and C. Miliani, "Recent trends in the application of Fourier Transform Infrared (FT-IR) spectroscopy in

Heritage Science: from micro- to non-invasive FT-IR," *Physical Sciences Reviews*, 2019.

- [42] F. Casadio and L. Toniolo, "The analysis of polychrome works of art: 40 years of infrared spectroscopic investigations," *Journal of Cultural Heritage*, vol. 2, pp. 71-78, 2001.
- [43] M.-M. Blum and H. John, "Historical perspective and modern applications of Attenuated Total Reflectance – Fourier Transform Infrared Spectroscopy (ATR-FTIR)," *Drug Test. Analysis*, no. 4, p. 298–302, 2012.
- [44] M. R. Derrick, S. Stulik and J. M. Landry, *Infrared Spectroscopy in Conservation Science*, Los Angeles: The Getty Conservation Institute, 1999.
- [45] S. Prati, M. Milosevic, G. Sciutto, S. G. Kazarian and R. Mazzeo, "Analyses of trace amounts of dyes with a new enhanced sensitivity FTIR spectroscopic technique: MU-ATR (metal underlayer ATR spectroscopy)," *Analytica Chimica Acta*, no. 941, pp. 67-79, 2016.
- [46] R. J. H. Clark, "Pigment identification by spectroscopic means: an arts/science interface," *C. R. Chimie*, vol. 5, p. 7–20, 2002.
- [47] E. Smith and G. Dent, *Modern Raman Spectroscopy. A Practical Approach*, UK: Wiley, 2005.
- [48] P. Vandenabeele, *Practical Raman Spectroscopy. An Introduction*, Malaysia: Wiley & Sons, 2013.
- [49] K. Fukunaga and I. Hosako, "Innovative non-invasive analysis techniques for cultural heritage using terahertz technology," *Comptes Rendus Physique*, vol. 11, pp. 519-526, 2010.
- [50] B. Brunetti, C. Miliani, F. Rosi, B. Doherty, L. Monico, A. Romani and A. Sgamellotti, "Non-invasive investigations of paintings by

portable instrumentation: The MOLAB experience," *Topics in Current Chemistry*, vol. 374, no. 1, pp. 1-35, 2016.

- [51] Analytical Methods Committee AMCTB No 75, "UV-visible-NIR reflectance spectrophotometry in cultural heritage: Background paper," *Analytical Methods*, vol. 8, p. 5894, 2016.
- [52] S. Prati, J. Edith, G. Sciutto and R. Mazzeo, "New Advances in the Application of FTIR Microscopy and Spectroscopy for the Characterization of Artistic Materials," *Accounts of Chemical Research*, vol. 43, no. 6, pp. 792-801, 2010.
- [53] C. Seccaroni and P. Moiola, *Fluorescenza X. Prontuario per l'analisi XRF portatile applicata a superficie policrome*, Florence: Nardini, 2004.
- [54] P. Vandenberghe and M. K. Donais, "Mobile Spectroscopic Instrumentation in Archaeometry Research," *Applied Spectroscopy*, vol. 70, no. 1, p. 27-41, 2016.
- [55] M. Ferretti, "X-ray Fluorescence Applications for the Study and Conservation of Cultural Heritage," in *Radiation in Art and Archeometry*, D. C. Creagh and D. A. Bradley, Eds., Elsevier Science, 2000, pp. 285-296.
- [56] G. Sciutto, T. Frizzi, E. Catelli, N. Aresi, S. Prati, R. Alberti and R. Mazzeo, "From macro to micro: an advanced macro X-ray fluorescence (MA-XRF) imaging approach for the study of painted surfaces," *Microchemical Journal*, no. 137, pp. 277-284, 2018.
- [57] F. Mederos-Henry and A. L. Camacho-Puebla, *Alcances de la técnica de Fluorescencia de Rayos X (FRX) aplicada al estudio de la distribución estratigráfica de pigmentos en la pintura de caballete novohispana*, Guadalajara: Escuela de Conservación y Restauración de Occidente, 2011.

- [58] Z. Stos-Fertner, R. E. M. Hedges and R. D. G. Evely, "The Application of the XRF-XRD Method to the Analysis of the Pigments of Minoan Painted Pottery," *Archaeometry*, vol. 21, no. 2, pp. 187-194, 1979.
- [59] M. Uda, S. Sassa, S. Yoshimura, J. Kondo, M. Nakamura, Y. Ban and H. Adachi, "Yellow, red and blue pigments from ancient Egyptian palace painted walls," *Nuclear Instruments and Methods in Physics Research, Section B: Beam Interactions with Materials and Atoms*, vol. 161, p. 2000, 758-761.
- [60] J. Simoen, S. De Meyer, F. Vanmeert, N. de Keyser, E. Avranovich, G. Van der Snickt, A. Van Loon, K. Keune and K. Janssens, "Combined Micro- and Macro-scale X-ray powder diffraction mapping of degraded Orpiment paint in a 17th century still life painting by Martinus Nelliuss," *Heritage Science*, vol. 7, no. 83, 2019.
- [61] M. P. Pomiès, G. Morin and C. Vignaud, "XRD study of the goethite-hematite transformation: Application to the identification of heated prehistoric pigments," *European Journal of Solid State and Inorganic Chemistry*, vol. 35, no. 1, pp. 9-25, 1998.
- [62] M. Birkholz, *Thin Film Analysis by X-Ray Scattering*, Germany: Wiley-VCH, 2006.
- [63] K. Janssens, G. Van der Snickt, F. Vanmeert, S. Legrand, G. Nuyst, M. Alfeld, L. Monico, W. Anaf, W. De Nolf, M. Vermeulen, J. Verbeeck and K. De Wael, "Non-Invasive and Non-Destructive Examination of Artistic Pigments, Paints, Paintings by Means of X-Ray Methods," in *Analytical Chemistry for Cultural Heritage*, Switzerland, Springer, 2016, pp. 77-128.
- [64] V. Gonzalez, M. Cotte, F. Vanmeert, W. de Nolf and K. Janssens, "X-ray Diffraction Mapping for Cultural Heritage Science: a Review

of Experimental Configurations and Applications," *Chemistry European Journal*, vol. 25, p. 1–19, 2019.

- [65] A. Hartstein, J. R. Kirtley and J. C. Tsang, "Enhancement of the Infrared Absorption from Molecular Monolayers with Thin Metal Overlayers," *Physical Review Letters*, vol. 45, no. 3, pp. 201-204, 1980.
- [66] F. Casadio, C. Daher and L. Bellot-Gurlet, "Raman spectroscopy of Cultural Heritage materials: overview of applications and new frontiers in Instrumentation, sampling modalities, and data processing," *Topics in Current Chemistry*, no. 374, p. 62, 2016.
- [67] G. D. Smith and R. J. H. Clark, "Raman microscopy in art history and conservation science," *Studies in Conservation*, vol. 46, no. sup 1, pp. 92-106, 2001.
- [68] Analytical Methods Committee AMCTB No. 80, "Surface-enhanced Raman spectroscopy (SERS) in cultural heritage," *Anal. Methods*, no. 9, p. 4338–4340, 2017.
- [69] B. Doherty, B. G. Brunetti, A. Sgamelotti and C. Miliani, "A detachable SERS active cellulose film: a minimally invasive approach to the study of painting lakes," *Journal of Raman Spectroscopy*, vol. 42, pp. 1932-1938, 2011.
- [70] C. Lofrumento, M. Ricci, E. Platania, M. Becucci and E. Castelluci, "SERS detection of red organic dyes in Ag-agar gel," *Journal Raman Spectroscopy*, vol. 44, pp. 47-54, 2013.
- [71] A. Daveri, B. Doherty, P. Moretti, C. Grazia, A. Romani, E. Fiorin, B. G. Brunetti and M. Vagnini, "An uncovered XIII century icon: Particular use of organic pigments and gilding techniques highlighted by analytical methods," *Spectrochimica Acta Part A*:

Molecular and Biomolecular Spectroscopy, vol. 135, p. 398–404, 2015.

- [72] C. Cucci and A. Casini, "Hyperspectral imaging for artworks investigation," in *Hyperspectral Imaging*, J. M. Amigo, Ed., Elsevier, 2020, pp. 583-604.
- [73] S. Legrand, M. Alfeld, F. Vanmeert, W. De Nolf and K. Janssens, "Macroscopic Fourier transform infrared scanning in reflection mode (MA-rFTIR), a new tool for chemical imaging of cultural heritage artefacts in the mid-infrared range," *Analyst*, no. 139, p. 2489–2498, 2014.
- [74] J. B. Jackson, J. Bowen, G. Walker, J. Labaune, G. Mourou, M. Menu and K. Fukunaga, "A Survey of Terahertz Applications in Cultural Heritage Conservation Science," *IEEE Transactions on Terahertz Science and Technology*, vol. 1, no. 1, pp. 220-231, 2011.
- [75] E. Abraham, A. Younus, A. El Fatimy, J. Delagnes, E. Nguéma and P. Mounaix, "Broadband terahertz imaging of documents written with lead pencils," *Optics Communications*, vol. 282, pp. 3104-3107, 2009.
- [76] K. Janssens, J. Dik, M. Cotte and J. Susini, "Photon-Based Techniques for Nondestructive Subsurface Analysis of Painted Cultural Heritage Artifacts," *Accounts of Chemical Research*, vol. 43, no. 6, pp. 814-825, 2010.
- [77] G. Sciutto, S. Legrand, E. Catelli, S. Prati, C. Malegori, P. Oliveri, K. Janssens and R. Mazzeo, "Macroscopic mid-FTIR mapping and clustering-based automated data-reduction: An advanced diagnostic tool for in situ investigations of artworks," *Talanta*, 2019.
- [78] S. Legrand, P. Ricciardi, L. Nodari and K. Janssens, "Non-invasive analysis of a 15th century illuminated manuscript fragment: point-

based vs imaging spectroscopy," *Microchemical Journal*, no. 138, p. 162–172, 2018.

- [79] S. De Meyer, F. Vanmeert, R. Vertongen, A. Van Loon, V. Gonzalez, J. Delaney, K. Dooley, J. Dik, G. Van der Snickt, A. Vandivere and K. Janssens, "Macroscopic x-ray powder diffraction imaging reveals Vermeer's discriminating use of lead white pigments in *Girl with a Pearl Earring*," *Science Advances*, vol. 5, p. eaax1975, 2019.
- [80] F. Vanmeert, N. de Keyser, A. van Loon, L. Klaassen, P. Noble and K. Janssens, "Transmission and reflection mode macroscopic X ray powder diffraction (MA XRPD) imaging for the noninvasive visualization of paint degradation in still life paintings by Jan Davidsz. de Heem," *Analytical Chemistry*, vol. 91, no. 11, pp. 7153-7161, 2019.
- [81] C. Conti, A. Botteon, C. Colombo, D. Pinna, M. Realini and P. Matousek, "Advances in Raman spectroscopy for the non-destructive subsurface analysis of artworks: Micro-SORS," *Journal of Cultural Heritage*, vol. 43, pp. 319-328, 2020.
- [82] S. G. Kazarian and K. L. A. Chan, "Micro- and Macro-Attenuated Total Reflection Fourier Transform Infrared Spectroscopic Imaging," *Applied Spectroscopy*, vol. 64, no. 5, pp. 135A-152A, 2010.
- [83] S. Prati, G. Sciutto, I. Bonacini and R. Mazzeo, "New Frontiers in Application of FTIR Microscopy for Characterization of Cultural Heritage Materials," in *Analytical Chemistry for Cultural Heritage*, Springer, 2016.
- [84] K. Ataka, S. T. Stripp and J. Heberle, "Surface-enhanced infrared absorption spectroscopy (SEIRAS) to probe monolayers of membrane proteins," *Biochimica et Biophysica Acta*, vol. 1828, pp. 2283-2293, 2013.

- [85] D. Quintero Balbas, S. Prati, G. Sciutto, E. Catelli and R. Mazzeo, "Thin-layer chromatography/metal underlayer-ATR FTIR methodology for the study of synthetic dyes extracted from degraded wool fibres," *New Journal of Chemistry*, vol. 43, no. 24, pp. 9411-9419, 2019.
- [86] G. Sciutto, S. Prati, I. Bonacini, L. Litti, M. Meneghetti and R. Mazzeo, "A new integrated TLC/MU-ATR/SERS advanced approach for the identification of trace amounts of dyes in mixtures," *Analytica Chimica Acta*, vol. 991, pp. 104-112, 2017.
- [87] D. Creagh, "Synchrotron Radiation and its Use in Art, Archaeometry, and Cultural Heritage Studies," in *Physical Techniques in the Study of Art, Archaeology and Cultural Heritage*, D. Dudley Creagh and D. Bradley, Eds., Elsevier, 2007, pp. 1-95.
- [88] L. Bertrand, "Synchrotron Imaging for Archaeology, Art History, Conservation, and Palaeontology," in *Physical Techniques in the Study of Art, Archaeology and Cultural Heritage*, D. Creagh and D. Bradley, Eds., Elsevier, 2007, pp. 97-114.
- [89] M. Cotte, E. Pouyet, M. Salomé, C. Rivard, W. De Nolf, H. Castillo-Michel, T. Fabris, L. Monico, K. Janssens, T. Wang, P. Sciau, L. Verger, L. Cormier, O. Dargaud, E. Brun, D. Bugnazet, B. Fayard, B. Hesse, A. E. Pradas del Real, G. Veronesi, J. Langlois, N. Balcar, Y. Vandenberghe, V. Armando Solé, J. Kieffer, R. Barrett, C. Cohen, C. Cornu, R. Baker, E. Gagliardini, E. Papillon and J. Susini, "The ID21 X-ray and infrared microscopy beamline at the ESRF: status and recent applications to artistic materials," *Journal of Analytical Atomic Spectrometry*, vol. 32, pp. 477-493, 2017.
- [90] K. Krug, J. Dik, M. Den Leeuw, A. Whitson, J. Tortora, P. Coan, C. Nemoz and A. Bravin, "Visualization of pigment distributions in

paintings using synchrotron K-edge imaging," *Applied Physics A – Materials Science & Processing*, vol. 83, p. 247–251, 2006.

- [91] G. Van der Snickt, J. Dik, M. Cotte, K. Janssens, J. Jaroszewicz, W. De Nolf, J. Groenewegen and L. Van der Loeff, "Characterization of a Degraded Cadmium Yellow (CdS) Pigment in an Oil Painting by Means of Synchrotron Radiation Based X-ray Techniques," *Analytical Chemistry*, vol. 81, no. 7, p. 2600–2610, 2009.

Chapter 1

Enhanced FT-IR methods for studying synthetic organic pigments and synthetic dyes

1.1 Introduction

Since prehistoric times pigments and dyes were obtained from natural sources (e.g., minerals, plants, and animals); with some exceptions, such as the Egyptian blue [1] and the Mayan blue [2]. But, after the synthesis of mauveine (CI 50245) by Perkin in 1856 [1] the new colourants modified the artist palette and improved the public health (e.g., the toxic lead white pigment $((\text{PbCO}_3)_2 \cdot \text{Pb}(\text{OH})_2)$, CI 77597) was substitute by the zinc white (ZnO , CI 77947) [3, 4]).



Figure 1. Girl before a mirror by Pablo Picasso, 1932. Museum of Modern Art (MoMA), New York.

By 1890, almost the 90% of all the dyes used were synthetic [5], and artists, such as Pablo Picasso (Figure 1), Paul Gauguin and Vincent van Gogh, used synthetic dyes, some of their lakes and synthetic pigments for painting and drawing [6, 7, 8, 9, 10].

According to de Keijzer, to date 50% of artists' materials of quality A and 70% of the quality B in commerce contain compounds discovered during the 20th century [6].

Rapidly, the instability of all these new materials became evident, and manufacturers started testing them to identify the most stable. For example, James Morton (Figure 2) did artificial ageing tests to identify the best synthetic dyes for his textile production, and Prof. Ernst Täuber evaluated the stability of synthetic pigments [11, 12].

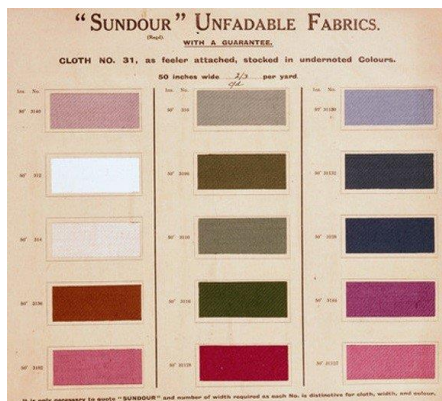


Figure 2. Fabric samples of “guarantee unfadable” products by James Morton. 20th century.

Because the instability of synthetic colourants, by the 1950s the international standards approved only three synthetic organic pigments for artists’ use: Alizarin crimson (Pigment Red 112, CI 12370), phthalocyanine blue (Pigment Blue 15:2, CI 26380) and phthalocyanine green (Pigment green 7, CI 74260) [13].

Nowadays, conservators face several problems regarding the preservation of modern materials in artwork. Their degradation, which includes fading and darkening [14, 15, 16, 17], water sensibility, failure of the pigment dispersants [18, 19], and migration of the additives [20, 21], is influenced by different environmental factors (e.g., relative humidity, O₃, NO_x).

Lightfastness is one of the main concerns [18, 22]. The current standards consider as highly sensitive materials the early synthetic dyes (ISO Blue Wool 1, 2 or 3) that even in low light exposure and UV filtering conditions can present, in a range of 1.5 to 20 years, colour changes evident to the human eye [23]. Today the most common strategy is to reduce light exposure (e.g., 50 luxes for textiles) in combination with the use of UV filters.

For the above mentioned reasons, the identification of colourants and the understanding of their behaviour under different conditions is essential for the conservation of cultural heritage; it contributes to authenticating

[24], dating [25], and establishing informed preventive conservation strategies [26].

Table 1 summarizes the different methodologies used today for studying modern artists' materials [27]. The analysis of the objects can be complemented by the study of artists' materials and palettes found in their studios, and sampling books published by manufacturers. The investigations done so far offer information about paints available to artists in the 19th and 20th centuries [24, 28, 29, 30, 31, 32, 33].

Table 1. Methods for studying modern materials in artwork, from [27].

Method	Description
Documentation	Information regarding the materials used by an artist: letters, photographs, films. Patents, product catalogues, colour charts, and scientific literature.
Interaction with artists	Interviews and visits to artists' studios.
Examination of artwork	Many materials have particular characteristics identifiable by macroscopic examination.
Scientific Analyses	Analytical characterization of samples from artwork, modern materials, samples coming from artists' studios, and mock-ups to imitate the ageing of materials.

The analytical characterization of dyes and pigments is challenging. Dyes are in low concentration; the matrices and their components interfere and scale down the analyte signal [34, 35], for example, the mordents and fibres in textiles, or the complex composition of paint layers that generally contain binders, pigments, and additives (e.g., surfactants, thickeners, and pigment dispersants) [27]. This condition makes necessary the separation of the different components.

The chromatographic methods are powerful tools [36] that help in the identification of the components in a mixture [14, 37], but suffer from the amount of sample required. For example, HPLC analysis requires ≥ 0.2 mg of sample [38], and the complex pre-treatment (e.g., the strong methods with HF vapours or HCl) can produce hydrolysis of the dye extracted from a textile fibre [39, 40, 41, 42].

Other chromatographic methods like Thin-Layer Chromatography (TLC), depend on the solubility of the analytes and required complex sample manipulation to analyse each component after separation, which is the principal drawback [43]. The advances in mass spectrometry complemented the chromatography techniques, for example, Pyrolysis Gas Chromatography-Mass Spectrometry (Py-GC-MS) [44], but suffer from a long time of sample preparation and analysis, as well as poor sensitivity due to the reduced amount of sample [45].

Techniques such as Direct Analysis in Real-Time Mass Spectrometry (DART-MS) and Direct Infusion Electrospray Ionization Mass Spectrometry (DI-ESI-MS) are promising tools for the investigation of degradation mechanisms of synthetic dyes, lakes, and pigments, but among the disadvantages of these methods, DART is not able to separate isomers (that can be intermediate phases of degradation products), and only a few laboratories have the instrumentation required [45].

μ -Raman spectroscopy is also an effective tool, but it requires adequate databases. Currently, several online databases [7, 46, 47] are available and references for the characterization of synthetic organic pigments are available in the scientific literature, but the complexity of the materials makes necessary a multi-analytical approach. Is worth mentioning the [Synthetic Organic Pigments Research Aggregation Network](#) (SOPRANO) that puts together the efforts of different institutions studying synthetic organic pigments since 2014, and offers an online Raman database of different artists' pigments [47].

Non-destructive analytical techniques, for example, on-fibre SERS and Agar gel doped with nanoparticle for SERS are promising methods, but the nanoparticle colloid can stain the surface of the objects and required the partial extraction of the dye [48, 49]. On the other hand, UV-Vis-NIR FORS [14, 50], and the multi and hyper-spectral imaging systems [51, 52] allow the identification and monitoring the degradation of dyes and

pigments, but the object's ageing, the dirt, and environmental contaminants deposited over the surface may interfere in the results and their interpretation. The use of databases is of paramount importance [38], but many of these techniques suffer from poor reproducibility or poor selectivity [50, 53].

Scientists seldom used FT-IR spectroscopy for the analysis of dyes and synthetic organic pigments because of its scarce selectivity and sensitivity in complex samples [27, 53, 54]. Recent developments in FT-IR have increased its sensibility. For example, surface-enhanced infrared reflection absorption (SEIRA) exploits the IR absorption enhancement effect produced when a sample is absorbed into a metal due to physical and chemical phenomena [55]. Researchers used it successfully to study of dyes [56].

Other methods, such as Super Grazing Angle Reflection Spectroscopy (SuGARS) and Grazing Angle Attenuated Total Reflection (GAATR) allow the enhancement of FT-IR signal, arising from thin layer deposited over a metal or silicon respectively, by increasing the electric field of the evanescent waves, and thus producing an increase of the electromagnetic waves and their absorption. To do this, a large angle of incidence is required, reason why special instrumentation is needed [55].

Further improvements led to simpler methods such as Metal underlayer Attenuated Total Reflection (MU-ATR). The absorbance enhancement is produced by a similar phenomenon given rise to SuGARS enhancement: after the deposition of a thin layer of the analyte over a high reflective index material (i.e., a metal) producing an enhancement of the evanescent waves. The main difference between these two techniques is that MU-ATR is capable to analyse layers ranging from 100 nm to 1 μm of thickness, and does not require particular instrumentation to obtain a larger angle of incidence [57].

The use of commercial instrumentation for MU-ATR, with a typical angle of incidence fixed at 45° , does not satisfy the conditions required for total

internal reflection, but the reflectivity of the gold-coated glass used as support prevents the transmission of the electromagnetic waves into a third medium. So far, MU-ATR has been successfully used for the analysis of synthetic dyes extracted from fibres [57].

To overcome the problem of overlapping of signal when studying complex mixtures, researchers used AgI [58] and BaF₂ [59] as stationary phases transparent in the Mid-Infrared region (4000–800 cm⁻¹) for TLC separation and improved the separation quality using a narrow TLC support [60, 61].

Our research group used the AgI system as an improvement to the MU-ATR technique which enhances FT-IR signals, leading to a considerable increase in sensitivity (is possible to study less than 0.5 ng of dye). They used a gold-coated glass slide covered with a thin layer of AgI (Au@AgI plate) to separate by TLC dyes mixtures and identify the components [57]. Also, using the same system is possible to perform SERS analysis [62].

In this work, we study with MU-ATR the composition of modern watercolour, tempera, and oil paints from different commercial brands. The samples come from the book [*Das Deutsche Farbenbuch – II. Die Künstler-farb und Malmittel*](#) published by Heinrich Trillich in 1925. To our best knowledge, this is the first application of MU-ATR to study painting samples. Our objective was testing the possibility of complex samples using a small amount, reducing the sample preparation, and compare the results to other enhanced methods, such as SERS.

This investigation is part of a multi-analytical project in the frame of the Integrated Platform for the European Research Infrastructure ON Cultural Heritage ([Iperion-CH](#)) European project. 81 hues from 10 different colour charts are under study with μ -XRF, μ -Raman and SERS, μ -MU-ATR and Ultra-High-Performance Liquid Chromatography–Diode Array Detector–Tandem Mass Spectrometry (UPLC-DAD/MS) in

collaboration with the Doerner Institut (Germany) and the Rijksdienst voor Cultureel Erfgoed (RCE, The Netherlands).

The second part of this work consists of the application of the Agl@Au TLC/MU-ATR system to analyse synthetic dyes in wool fibres. It required the set-up of a multi-step extraction protocol using solvents suitable for different types of dyes (of different polarity and pH) in sequence. The extraction sequence pre-classifies the dyes and provides clues regarding the mordents employed during dyeing, which may be related to specific time periods of the dyeing industry.

The method was set-up on artificially-aged mock-ups, prepared at the OCW/Rijksdienst voor het Cultureel Erfgoed (The Netherlands) and artificially aged by Centre de Recherche et des Restauration des Musées de France (CR2MF), and validated on two real samples from a pattern book entitled *Tabellarische Uebersicht über die künstlichen organischen Farbstoffe* by Adolf Lehne published in 1893 by Springer in Berlin. This research was part of the W.P.10e *Characterisation of Early Synthetic Colorants* of the European project Cultural Heritage Advanced Research Infrastructure: Synergy for a Multicultural Approach to Conservation/Restoration ([CHARISMA](#)).

1.2 Aim of the research

The aim of this work is to set-up and apply two FT-IR enhanced methodologies for the study and characterization of different modern colourants: modern pigments and synthetic dyes and their degradation. In particular, we aimed to:

- Apply MU-ATR to study modern artists' materials commercialized by different companies during the mid-1920 in a fast a simple way using a small amount of sample. We aim to contribute to the knowledge of the composition of artists' materials available at the beginning of 20th century.

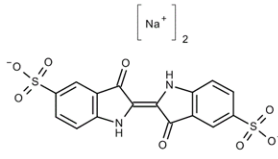
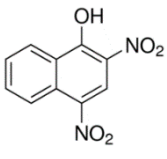
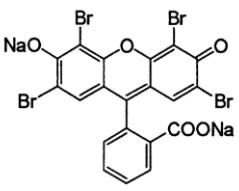
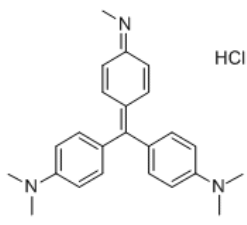
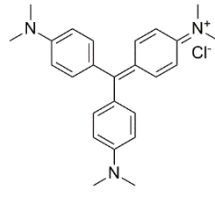
- Develop an alternative methodology for the characterization of synthetic dyes from wool fibres, by means of TLC/MU-ATR technique, using a small amount of sample and allowing the identification of dyes even in degraded states.

1.3 Materials and methods

1.3.1 Materials and reagents

All glassware was cleaned with deionized water and acetone. AgNO₃ and KI were purchased from Sigma-Aldrich® (puriss. p.a.). In all the solutions pure water was employed (>5 MΩcm at 25° C and TOC <30 ppb) obtained from Elix Essential® purification system. Methanol, isopropanol, ammonium hydroxide (28-30% in water), and ammonium hydroxide (puriss. 30-33% in water) were purchased from Sigma-Aldrich® and Ethanol (puriss. analytical) from Honeywell®. Standard dyes were obtained from Sigma-Aldrich® (dye content 85-95%) (Table 2). All solvents were used without any further purification.

Table 2. Synthetic dyes analysed in this work.

Name	Code	Class	Chemical structure
Acid Blue 74 CI 73015	AB74	Indigoid	
Acid Yellow 24 CI 10315	AY24	Nitro	
Acid Red 87 CI 45380	AR87	Xanthene	
Basic Violet 1 CI 42535	BV1	Triarylmethane	
Basic Violet 3 CI 42555	BV3	Triarylmethane	

1.3.2 Paint samples

Paint samples were obtained from colour charts from the book *Das Deutsche Farbenbuch* by Heinrich Trillich published in 1925. Table 3 (next page) summarizes the paint samples (~300 μm, Figure 3) studied in this work. Figure 4 shows one of the colour charts of watercolours from Redeker & Hennis A.-G. Information regarding the paint manufacturers is summarised in Appendix 1.

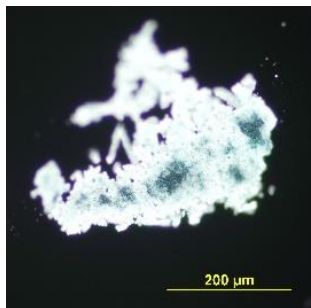


Figure 3. Paint sample, 20x, DF.



Figure 4. Colour chart from *Turm-Künstler- Aquarell-Farben (Watercolours)* by Redeker & Hennis. *Das Deutsche Farbenbuch* by Heinrich Trillich, 1925.

Table 3. Paint micro samples analysed in this research

Type	Brand	Description
Watercolour	Turm“-Künstler-Aquarellfarben von Redeker & Hennis A.-G., Nürnberg	Gummigutte
		Indischgelb
		Gummigutt, fein (268)
	Pelikan Künstler-Wasserfarben	Französisch Grün (135)
		Eilido-Grün, hell (571)
		Maigrün
	Flamuco Künstler-Aquarell-Farben	Paynes-grau
		Saftgrün dunkel
		Englischrot hell
Tempera	Temperafarben (Eitempera) Sorte 700 Herrmann Neisch & Co.	Permanentgrün hell
		Chromoxydgrün feurig
		Krapplack dunkel
	Flamuco Künstler-Tempera-Farben	3 Echtgelb II
		31 Indischgelb imit. II
		Permanentgrün hell
Oil colours	Rubensölfarben Herrmann Neisch & Co.	Wurzelkrapplack O dunkel
		Chromgelb 40
		Dunkelbordeaux 30
		Modellrot 51
		Parisergelb 20 dunkel
	Oelfarben G.Siegle & Co GmbH	Echtsaftgrün A 95
		Seidengrün 29 c
		Zinckgelb
		Emaile blau
		Grün 22
Oelfarben G.Siegle & Co GmbH	Permanentgrün 62	
	Schilderviolet 7621L	
	Schilderviolet S1740	
		Violet 132

1.3.3 Standard wool samples preparation and artificial aging

Dyed wool fibre samples (Bluefaced Leicester, brand: Rowan®, Purelife) were prepared, following the recipe by Adolf Lehne published in 1893. The wool fibres were washed with 10% (wool weight) Marseille soap at 40° C before the dyeing process.

For dyeing two methods were followed according to the dye type. In the case of basic dyes, 750 ml of demineralized water was heated to 70° C and kept at this temperature. 100 mg of a basic dye was weighed and dissolved in the warm water. 10 g of the wool bundle was soaked in the dye bath and put in the oven at 70° C for 30 min. The dye bath was stirred every 5 min to get a homogeneous colour. The bundle was left to cool down in the dye bath and afterwards it was rinsed with demineralized water.

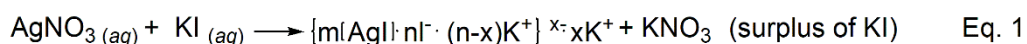
For the acid dyes, 750 ml of demineralized water was heated to 70° C and kept at this temperature during the complete dyeing process. 5 g of sodium sulphate (Na_2SO_4) was added and dissolved. 150 mg of the acid dye was weighed and was dissolved in the solution. 10 g of the wool bundle was soaked in the dyeing solution. 200 μl of concentrate sulphuric acid was added to the beaker. The dye bath was put in the oven at 70° C for 30 min. The dyeing solution was stirred every 5 min to get a homogeneous colour. The bundle was left to cool down in the dye bath and afterwards it was rinsed with demineralized water. The fibres were subsequently artificially aged under UV light (~365 nm) using a Xenon test machine for 20 h, 60 h, 140 h, and 305 h.

1.3.4 Wool real samples

Real samples were taken from the pattern book entitle *Tabellarische Uebersicht über die künstlichen organischen Farbstoffe und ihre Anwendung in Färberei und Zeugdruck* by Adolf Lehne published in 1893 by Springer in Berlin.

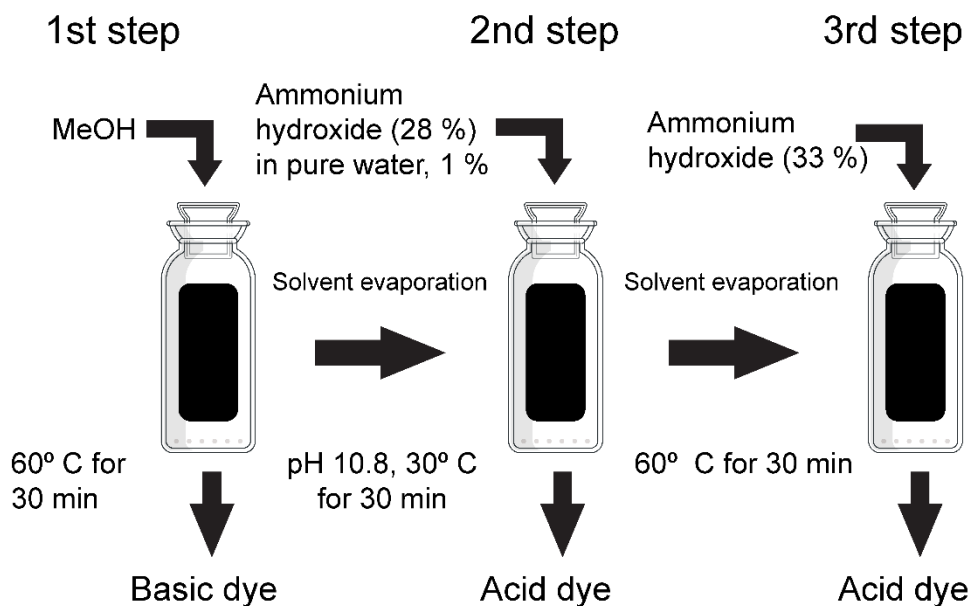
1.3.5 AgI synthesis and AgI@Au plate preparation

The synthesis of AgI (Eq. 1) was performed according to the procedure reported in Sciutto, et al. [62] 0.1 M solutions of AgNO₃ and KI were cooled at 4° C for 30 min. Later the AgNO₃ solution was poured into the KI solution and kept at 4° C for 1 h. Subsequently, the solution was cooled at room temperature (25° C) for 50 min. The AgI solution was filtered under vacuum using a filter paper (pore size <2 μm), and the powder was dried at 40° C for 15 min to 20 min. The procedure was carried out with low light illumination since AgI is photosensitive. 0.1 g of AgI was suspended in 7 ml of isopropanol and sonicated for 30 min a temperature not higher than 30° C. 1 ml of the supernatant was deposited over a gold-coated glass slide and let dry in a chamber saturated with isopropanol for 24h.



1.3.6 Dye extraction protocol

Few wool fibres (< 0.01 mg) were placed in a cone bottom vial with 60 μl of solvent. The extraction was done in a bain-marie at 60° C or 30° C for 30 min following extraction protocol (Scheme 1, next page). The vials were capped with aluminium foil to prevent water entrance and reduce solvent evaporation. Visual examination of the solution colour helped to understand the efficacy of the extraction. A sequence of extractions was set up considering the different properties of the dyes. After the first step, if the extraction solvent remained uncoloured it was evaporated at 40° C and a second solvent was added, up to three different steps until a net colour change was observed. At this point, the fibres were taken out from the solvent, the solution was let to rest at room temperature for 24 h and then it was dried at 40° C. The dye was recovered with 10 μl of pure water.



Scheme 1. Extraction protocol in three steps. Basic dyes are extracted efficiently in the first while acid dyes required further steps to be extracted. The protocol can be applied in sequence without damaging the sample.

1.3.7 μ -XRF analysis

The μ -XRF of the paint samples was carried out at the Doerner Institut with a Bruker M6 Jetstream using a spot size 100 μm with helium flow. The X-ray source is a Rh tube, and 50 kV and 200 μA were used. The analysis time was 100 sec.

1.3.8 MU-ATR analysis

MU-ATR analyses were performed over a gold-coated glass slide (76x26 mm; 200 nm Au thickness) purchased from Ssens bvTM. The paint micro-samples (~300 μm) were pressed using a metal roller wheel to obtain a thin layer.

1.3.9 AgI@Au MU-ATR analysis

1 μl of the extracted dye was spotted over gold-coated glass slide (76x26 mm; 200 nm Au thickness) purchased from Ssens bvTM covered with AgI nanoparticles (AgI@Au plates).

1.3.10 AgI@Au TLC analysis

Chromatographic separation by means of TLC was performed using as eluent a mixture of isopropanol, ethanol, and ammonium hydroxide (33 %) 5:2:3 v/v/v. Only in the case of Acid Blue 74, the ammonium hydroxide was eliminated from the mixture to avoid dye degradation.

1.3.11 ATR-FT-IR measurements and data elaboration

All ATR-FT-IR analyses were performed using a Ge ATR crystal and a Thermo Scientific Nicolet iN 10MX spectrometer. Spectra were recorded in the range 4000-675 cm^{-1} with an optical aperture of 200x200 μm , a spectral resolution of 4 cm^{-1} , and 64 scans. All data were acquired in three or more replicates according to the sample homogeneity. Spectra were processed with Omnic PictaTM and Omnic32TM softwares.

2.4 Results and discussion

2.4.1 MU-ATR for studying paint samples: pigments, binder, and fillers

The μ -Raman/SERS and μ -XRF analyses allowed the characterization of many of the samples contained in the different colour charts analysed. Using those techniques, the researchers from the Doerner Institut were capable to identify a total of 17 different synthetic organic pigments and lakes from 7 different classes: indigoid, anthraquinone, azo, nitroso, triarylmethane, xanthane and azine, and some inorganic pigments and fillers. Table 4 (next page) summarises the different materials identified for every type of paint. The μ -MU-ATR analysis focused on the paint

samples were not conclusively identified by means of Raman/SER or μ -XRF analyses. Table 5 (next page) shows the μ -XRF results from those samples.

Table 4. Summary of the results from *m*-Raman/SERS analyses performed at the Doerner Institut. See Appendix I for more information regarding the pigments.

Type of paint	μ -Raman/SERS
Watercolours	Natural Alizarin lakes, Synthetic Alizarin lakes, Carminic acid lakes, Pigment Red 57:1, Acid Red 51/Pigment Red 172, Pigment Violet 5, Basic Violet 10/ Pigment Violet 1, Basic Violet 2, Acid Green 1/ Pigment green 12, Minium (Pigment Red 105), Chrome yellow (Pigment Yellow 34), Iron oxide red (Pigment red 101), Ultramarine blue (Pigment Blue 29)
Tempera	Pigment Red 3, Pigment Violet 3/Basic Violet 1, Acid Red 87/ Pigment Red 90.
Oil colours	Pigment Red 1, Pigment Red 3, Pigment Red 4, Pigment Red 54, Pigment Red 40, Pigment Red 49, Basic Red 5, Pigment Violet 3, Prussian blue (Pigment blue 27), Vermilion (Pigment Red 106), Baryte (as filler, Pigment White 21/22)

Table 5. μ -XRF results

Type	Sample name	μ -XRF results	
Watercolour	Gummigutte	S, Ca, Si, Cl, Al, K, Sr, As, Fe, Ti	
	Indischgelb	Al, Si, Fe, Ba, Sn (Pb)	
	Gummigutt, fein (268)	Values are below the background signal	
	Französisch Grün (135)	Not measured	
	Eilido-Grün, hell (571)	Not measured	
	Maigrün	Ba, Cr, Ca, Cr, Zn	
	Paynes-grau	P, Al, S, Si, Ca, Cr	
	Saftgrün dunkel	S, Fe, Ca, Sn, Zn (Ba, Al)	
	Tempera	Englischrot hell	P, S, Fe, Si (Zn, Ca)
		Permanentgrün hell	K, Zn, Cr, Ba, Fe, Sr
Krapplack dunkel		P, S, Ba, Ca	
3 Echtgelb II		Na, Ba, Zn, Pb (Cd)	
31 Indischgelb imit. II		Sr, Pb, Cr, Ca, Zn Cd	
Oil colours	Permanentgrün hell	K, Cr, Fe, Zn (Ba)	
	Wurzelkrapplack O dunkel	Al, Si, P, Fe (Hg, Sr)	
	Chromgelb 40	Cr, Sr, Ba, Pb	
	Dunkelbordeaux 30	S, Ba, Sr (Zn)	
	Modellrot 51	Zn, Ba, Pb	
	Pariser gelb 20 dunkel	Ba, S, (Pb, Zn, Sr, Cr)	
	Echtsaftgrün A 95	Ba, Sr, Zn, Pb	
	Seidengrün 29 c	Ba, Pb, Cr, Zn, Sr	
	Zinkgelb	Zn, Ba, Pb	
	Emaill blau	Ba, Pb, Cr, Zn, Sr	
	Grün 22	Ba, Cr, Pb, Sr, (Al, S)	
	Permanentgrün 62	S, Cr, Ba, Zn, Sr	
	Schilderviolet 7621L	Zn, Ba, Pb, (Sr)	
	Schilderviolet S1740	Zn, Ba, Pb, (Sr)	
	Violet 132	S, Zn, Ba, (Pb, Al)	

a) Watercolours

The μ -MU-ATR spectra of all the watercolour samples we analysed have interference from the paper support, in particular in the range 1400-900 cm^{-1} (Table 6). The results offer no information regarding the binder. Despite this interference, we were able to identify different pigments and fillers.

Table 6. Bands arising from the paper support [63, 64, 65].

Wavenumber (cm ⁻¹)	Assignment
1428	(CH ₂) in-plane deformation
1368	(CH) bending
1335	(CH) vibration, (OH) in-plane bending
1314	(CH ₂) wagging
1201	(OH) bending
1158	(C-C) stretching
1054	(OH) 2 nd alcohol stretching
1033	(OH) 1 st alcohol stretching
896	Amorphous region of cellulose

The results confirm the presence of Gummi-gutta or “Gamboge” (Natural Yellow 24) in two of the samples, *Gummigutte* by Redeker & Hennis and *Gummigutt, fein (268)* by Pelikan. Gamboge is a yellow gum-resin, produced by trees of *Garcinia* genus in Asia, constituted of a yellow resinous component (70-80%; morelloflavone) and β -Guttalacton and Gambogic acid [7]. Artists used it in varnishes,



Figure 5. Gamboge pigment in watercolour. Courtesy of the artist Jane Blundell.

as a mordant for gilding on paper and as a watercolour pigment (Figure 5) [8]. Surprisingly, neither Raman nor SERS analyses show characteristic peaks of this resin [66], even though at least one peak in the 1800-1500 cm⁻¹ region assigned to the C=C double bonds could be expected [67].

Since the MU-ATR spectra (Figure 6, next page) suggest that the sample from Pelikan contains mainly gummi-gutta and probably a small amount of material rich in aluminosilicate, and the XRF spectra show no peaks [66], it is probable that the manufacturer used pure Gamboge resin. On the contrary, the sample from Redeker & Hennis is mixed with gypsum (Pigment White 25, CaSO₄·2H₂O) as a filler, as suggested by the bands at 3537 cm⁻¹ and 3400 cm⁻¹ arising from the OH stretching [68] and the SO₄²⁻ band at 1057 cm⁻¹ identified by means of MU-ATR. The small peaks at 3694 cm⁻¹ and 3619 cm⁻¹ from hydroxyl ion suggest the

presence of a material rich in aluminosilicates [69] (Figures 6 and 7). The μ -XRF analysis that identified S, Ca, Si, Al, Fe confirmed these results.

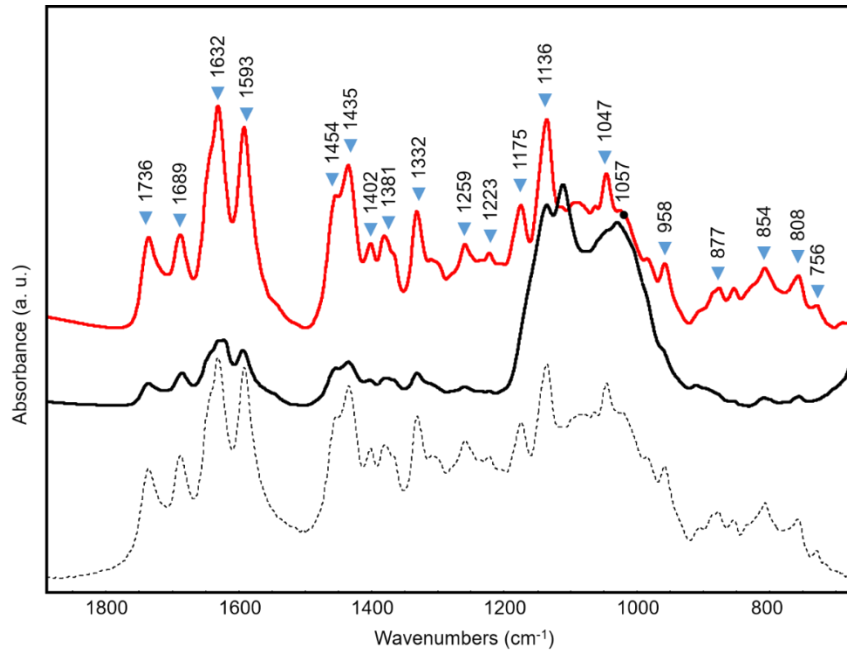


Figure 6. Spectra of Gummigutt, fein by Pelikan (red solid line,) Gummigutte by Turm (black solid line), and Gummi-gutta reference by Kremer (black dashed line). ▼ indicates the characteristic band of gummi-gutta and ● indicates the band assigned to SO_4^{2-} .

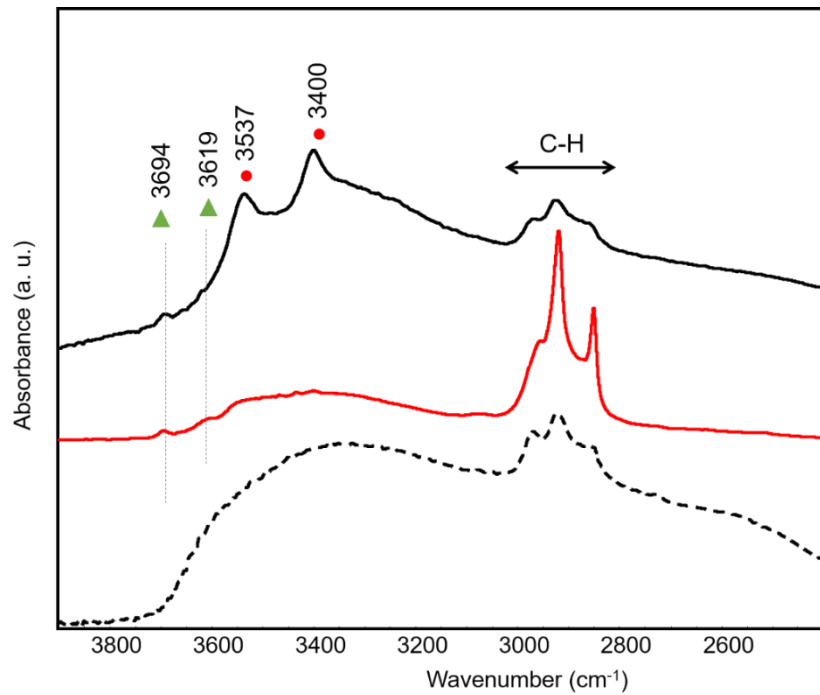


Figure 7. MU-ATR Spectra in the region $3700\text{--}2600\text{ cm}^{-1}$, the bands marked with ● arise from gypsum, and the small peaks marked with ▲ arise from OH stretching. Gummigutt, fein by Pelikan (red solid line,) Gummigutte by Turm (black solid line), and Gummi-gutta reference by Kremer (black dashed line).

Indischgelb (Engl. Indian yellow) colour by Redeker & Hennis contains a material rich in aluminosilicates. The spectra peaks at 3689 cm^{-1} and 3618 cm^{-1} from the OH stretching (*data not shown*) [70]. The μ -XRF results indicate the presence of Al, Si, Fe, Ba, Sn, Pb, and Raman analysis detected minium (Pigment Red 105, Pb_3O_4) that is not active in the middle infrared region.

The green colour *Saftgrün dunkel* (Engl. Sap green, dark), from Flamuco, contains Prussian blue (Pigment Blue 27, $\text{Fe}_4[\text{Fe}(\text{CN})_6]_3 \cdot x\text{H}_2\text{O}$) [71], and baryte (Pigment White 21 or 22, BaSO_4) as filler, which manufacturers added as extender since the 19th century [72]. The detection of S, Fe, Ca, Sn, Zn, Ba, Al using μ -XRF confirmed the MU-ATR results. In this case, the characteristic $\nu(\text{CN})$ at $2150\text{-}2160\text{ cm}^{-1}$ band of Prussian blue in Raman [73] is out of the range reported by the Doerner Institut ($300\text{-}1800\text{ cm}^{-1}$) [66]. However, the μ -MU-ATR spectra contain no clues about the yellow component, while the Raman spectrum features many well-defined peaks that may suggest the presence of a synthetic yellow pigment, but so far, no match has been found (Figure 8).

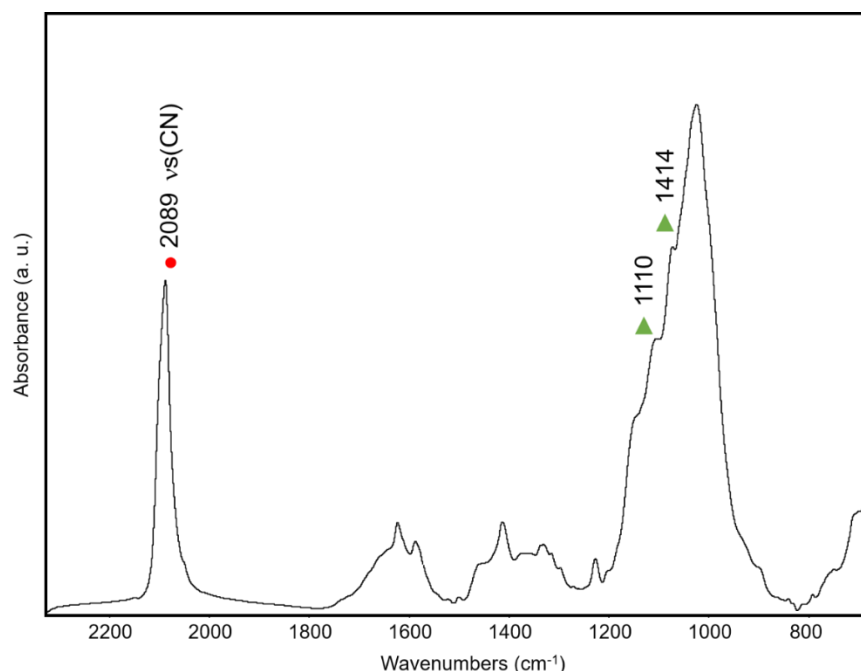


Figure 8. MU-ATR spectra of Saftgrün dunkel sample. The peak marked with ● correspond to Prussian blue, while the bands marked with ▲ relate to baryte. The other bands that are not marked in the spectra arise from the paper support.

The *Französisch Grün* (135) (Engl. French green) by Pelikan contains Emerald green (Pigment Green 21, $\text{Cu}(\text{C}_2\text{H}_3\text{O}_2)_2 \cdot 3\text{Cu}(\text{AsO}_2)_2$). The chemists Russ and Sattler synthesized this green pigment for the first time in 1814 and artists used it for painting despite its instability and toxicity until the 1960s when it was banned [74, 75]. The μ -MU-ATR spectra show the characteristic peaks of Emerald green (Figure 9) [76, 77], surprisingly no spectra were obtained with Raman [66] despite the numerous and well-defined peaks that can be expected in the range $1000\text{-}100\text{ cm}^{-1}$ [78].

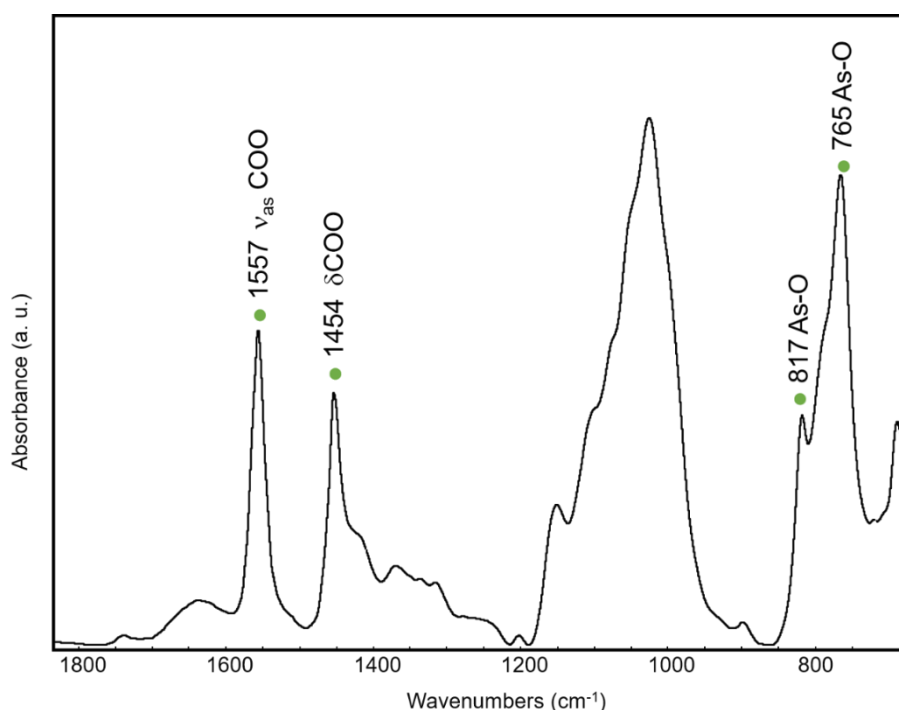


Figure 9. MU-ATR of Französisch Grün (135), the characteristic peaks of Emerald green (●) evident even in presence of paper interference. The other peaks not marked arise from the paper support.

The *Eilido-Grün, hell* (Engl. Eilido green, light) from Pelikan is of particular interest since the name “eilido” indicates a particular product line based on coal-tar pigments that were synthesized in 1909 by Karl König [12]. No Raman spectra were obtained [66], while the μ -MU-ATR spectra obtained from the sample exhibits several bands in the spectrum that suggests the presence of a synthetic pigment or mixture of pigments, however, no match has been found so far.

Based on the μ -MU-ATR analysis, we hypothesize that the green paint *Maigrün* (Engl. Green of May) by Pelikan contains a mixture of a yellow and a blue pigment. The MU-ATR spectra (Figure 10) suggest the presence of zinc yellow (Pigment Yellow 36, $4\text{ZnO}\cdot 4\text{CrO}_3\cdot \text{K}_2\text{O}\cdot 3\text{H}_2\text{O}$) [79, 80]; but no information about the possible blue element is evident in the spectra. The μ -XRF confirmed the presence of Cr and Zn and neither Raman nor SERS spectra were obtained. The manufacturer probably added gypsum and/or baryte as fillers to this paint, as suggested by the shoulders in the range $1200\text{-}1000\text{ cm}^{-1}$ of the MU-ATR spectra, and it was confirmed thanks to the identification of Ba by means of μ -XRF.

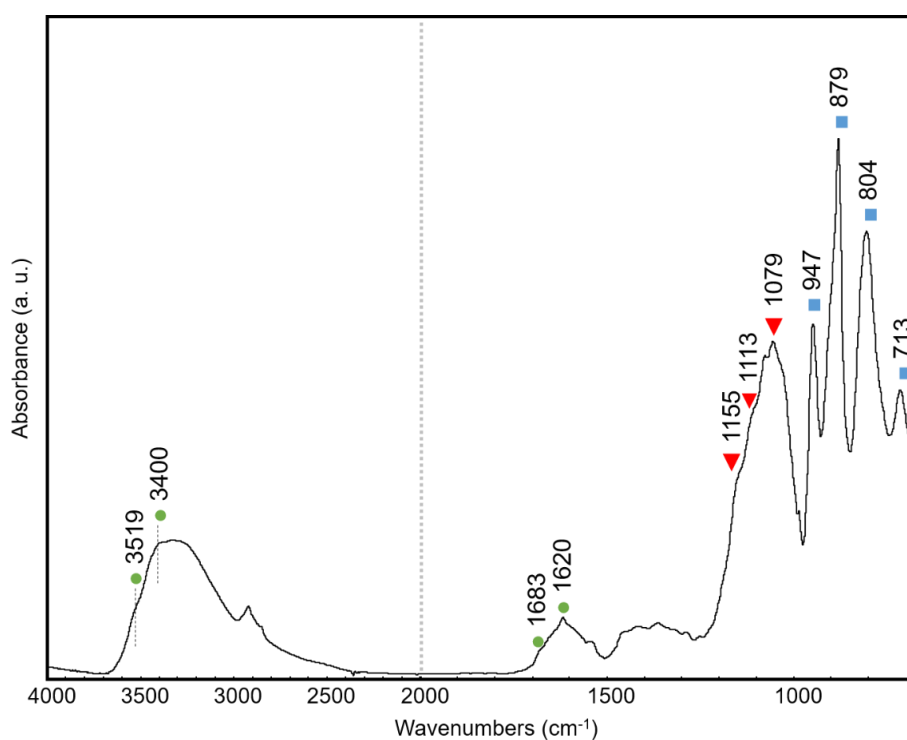


Figure 10. MU-ATR spectra of Maigrün sample. The characteristic peaks of zinc yellow are marked with ■. The peaks that can be attributed to gypsum are marked with ● and the peaks from baryte are marked with ▼.

Finally, the MU-ATR spectra suggest the presence of synthetic ultramarine ($3\text{Na}_2\text{O}\cdot 3\text{Al}_2\text{O}_3\cdot 6\text{SiO}_2\cdot 2\text{Na}_2\text{S}$) in the sample *Paynes-grau* from Flamuco due to the presence of the strong band at 987 cm^{-1} [81].

This result is consistent with the μ -XRF analysis that showed Al (*data not shown*).

b) Tempera

The results from the sample of *Permanentgrün, hell* (Engl. Permanent green) by Herrmann Neisch & Co show no information about the colourant, yet the small sharp peak at 3676 cm^{-1} and the intense peak at 1011 cm^{-1} may suggest the manufacturer added talc (Pigment White 26, $\text{Mg}_3\text{Si}_4\text{O}_{10}(\text{OH})_2$) as filler. Talc helps to reduce settling and separation of paint components, reduce cracking, smooths ridges left by the brush, and is an inexpensive extender [82]. Neither Raman nor SERS produced spectra [66].

The *Englischrot, hell* (Engl. English red) paint produced by the same manufacturer probably contains an earth-based pigment rich in aluminosilicates suggested by the band at 1021 cm^{-1} and gypsum as filler identified thanks to the bands at 3492 cm^{-1} , 3392 cm^{-1} , 1684 cm^{-1} , 1616 cm^{-1} , and 1095 cm^{-1} . The XRF detected Fe, Ca, Si, and S, which supports the MU-ATR results.

Krapplack dunkel (Engl. Madder Lake dark) from Flamuco contains Pigment Red 83 (PR83, CI 58000), also called Alizarin, that was identified by the characteristic band in the μ -MU-ATR spectra, this result was confirmed by the Raman analysis (Figure 11, next page). PR83 is an anthraquinonoid synthetic dye synthesized in 1868 by Carl Graebe and Carl Lieberman [83], the absence of other common constituents of madder dye (e.g., purpurin) indicates that this paint is of synthetic nature. Some silicates are part of this pigment, probably related to the support for the lake [84].

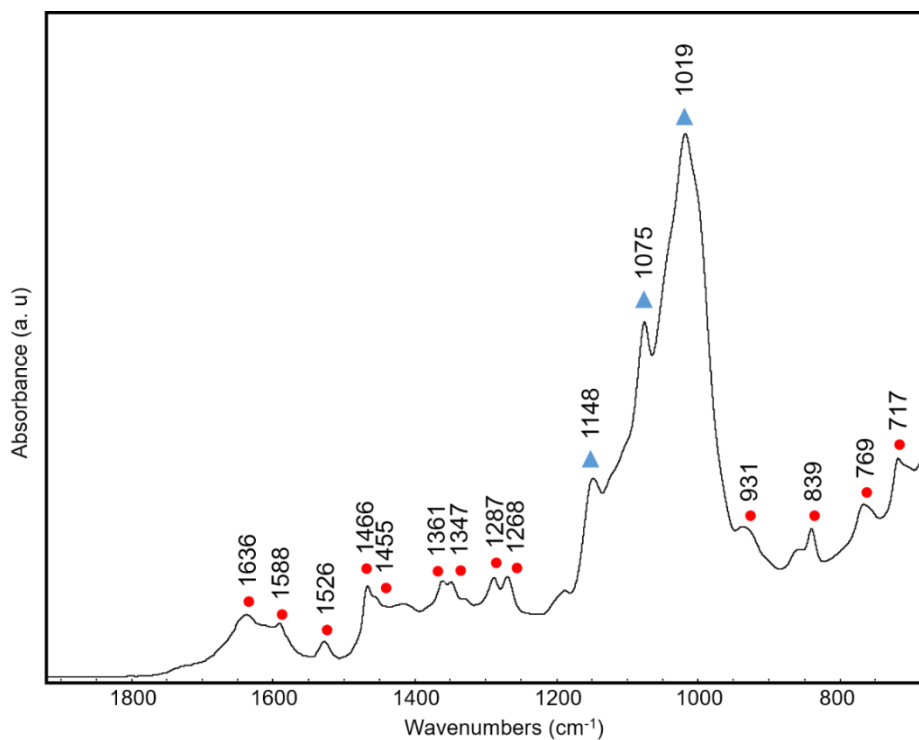


Figure 11. MU-ATR spectrum from the sample Krapplack dunkel. The characteristic peaks of the Pigment Red 83 are marked with ● and the peaks arising from silicates with ▲.

The sample of *Echtgelb II* (Engl. Real yellow) from Bössenroth present peaks attributed to Pigment Yellow 1 (PY1, CI 11680) also called Hansa Yellow or Fast Yellow G, which is a yellow azo dye available as an artists' material around 1915 [85]. In addition, we identified baryte as filler, and an earth-based pigment rich in aluminosilicates (Figure 12, next page).

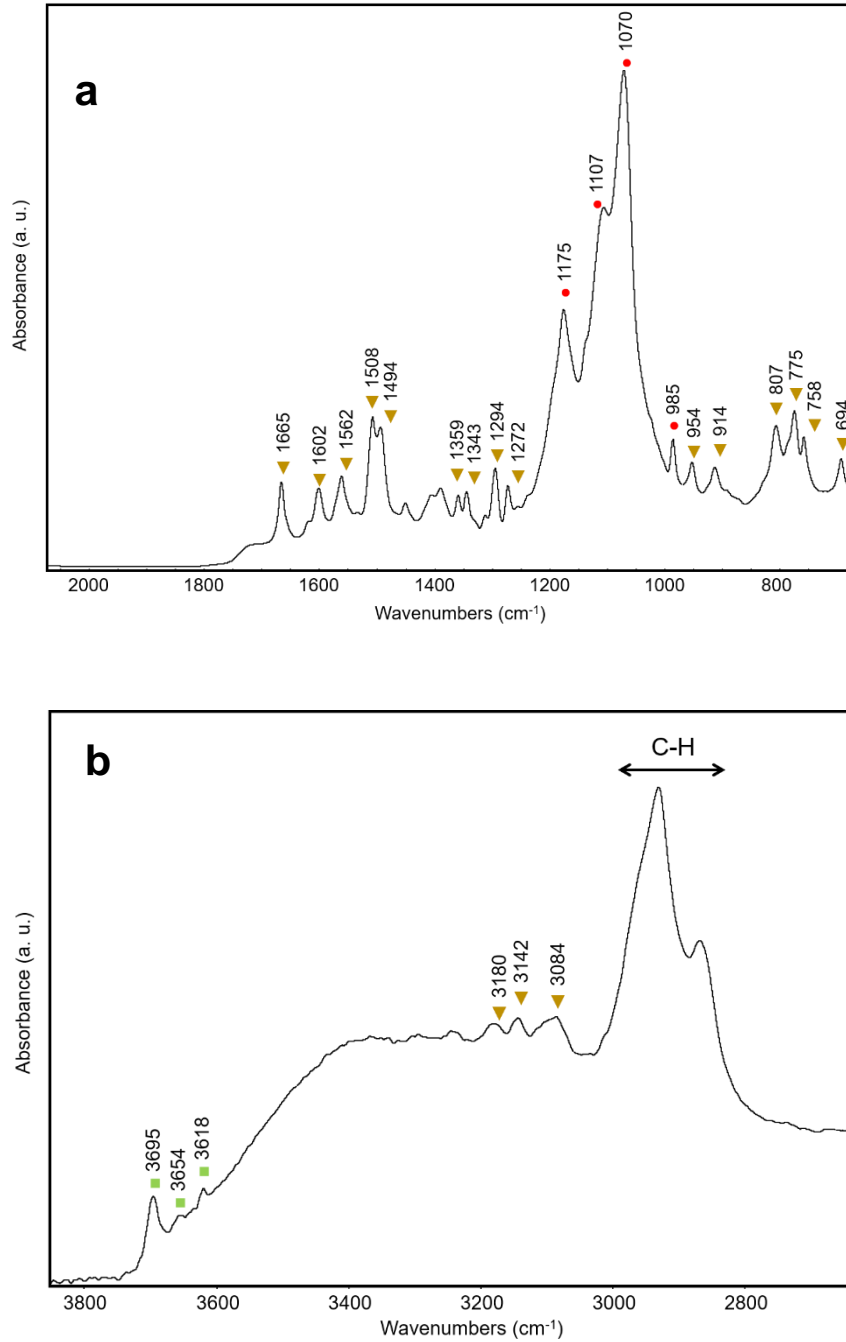


Figure 12. Spectra obtained from the sample Echtgelb II. a) the characteristic peaks of PY1 are marked with ▼ and the peaks from baryte (filler) with ●. b) Spectrum in the range 3800-2600 cm⁻¹. The peaks arising from PY1 are marked with ▼ and the peaks from OH stretching attributed to aluminosilicates with ■.

Indischgelb imit. II (Engl. Indian yellow, imitation) from Bössenroth probably also contains PY1 mixed with strontium chromate (Pigment Yellow 32), which μ -XRF results confirm [80]. As a filler, the manufacturer added gypsum (Figure 13).

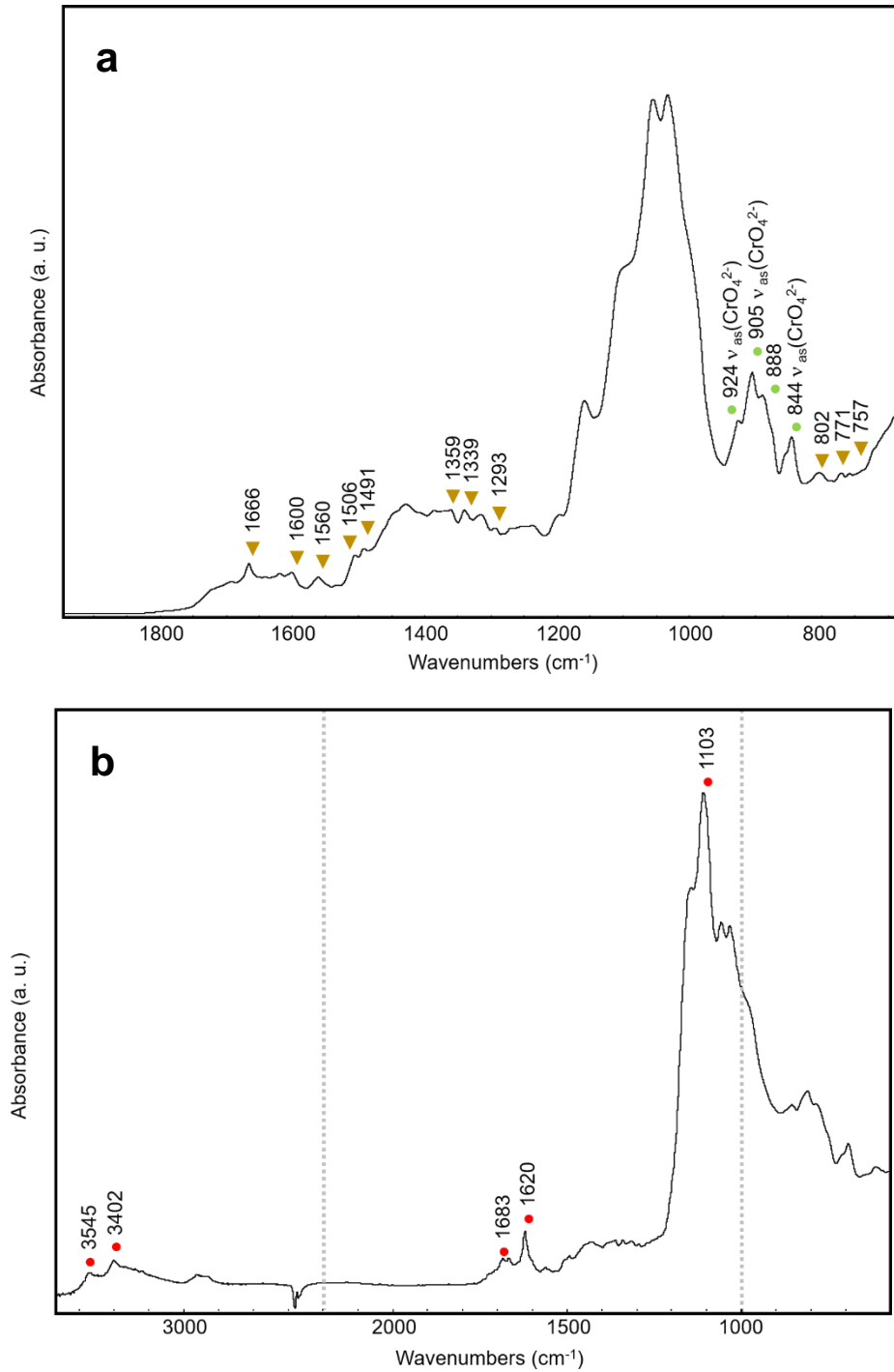


Figure 13. a) The characteristic peaks related to PY1 are marked with ▼ while the peaks from Strontium yellow are indicated with ●. b) In the spectrum ● indicates the characteristic peaks of gypsum.

c) Oil colours

The main feature identified in these samples was the binder that contains a mixture of nitrocellulose and an oily component. Table 7 summarizes the main characteristic bands present in the spectra (Figure 14). During the 1920s artists used nitrocellulose or pyroxylin paints. The properties of the nitrocellulose make necessary the addition of a second resin, for example, an alkyd resin, and some additives [27] to achieve the brushability of nitrocellulose lacquers. Glidden and Sherwin-Williams were the first to add alkyd resins to nitrocellulose in the mid-1920s [86].

Table 7. Peaks arising from the binder and their assignment.

Wavenumber (cm ⁻¹)	Assignment [87] [88]
1727	(CO) symmetric stretching (<i>alkyd resin</i>)
1648	(NO ₂) asymmetric stretching (<i>nitrocellulose</i>)
1456	(CH) (<i>alkyd resin</i>)
1379	(CH) bending (<i>nitrocellulose</i>)
1277	(NO ₂) symmetric stretching (<i>nitrocellulose</i>)
1161	(COC) stretching (<i>nitrocellulose</i>)
1067	(COC) stretching (<i>nitrocellulose</i>)
1005	(COC) stretching (<i>nitrocellulose</i>)
834	(NO) stretching (<i>nitrocellulose</i>)
750	(NO ₂) out-of-plane wagging (<i>nitrocellulose</i>)

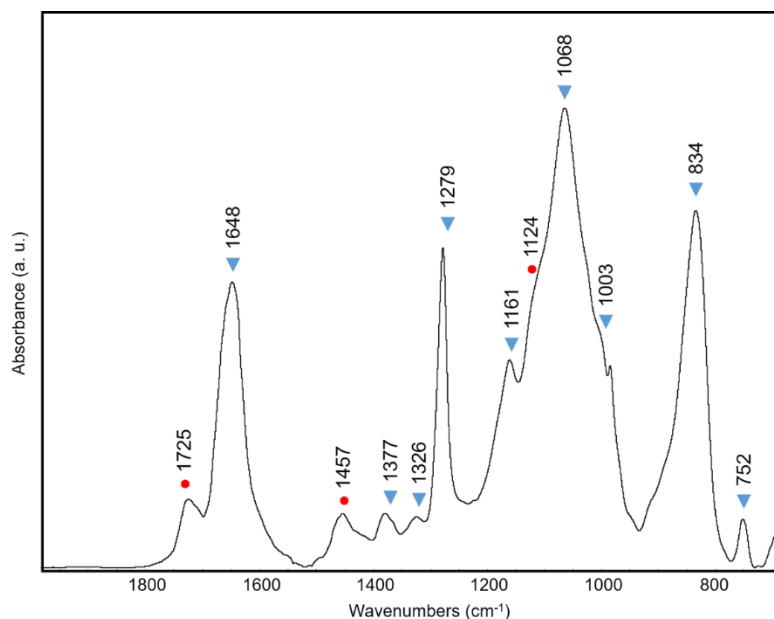


Figure 14. MU-ATR spectrum of the binder from oily samples. The bands arising from nitrocellulose are marked with ▼, and ● indicates the bands from alkyd resin.

The interference of the binder hinders the characteristic bands of other components in the samples *Chromgelb 40* (Engl. Chrome yellow), *Permanentgrun 62* (Engl. Permanent green), *Schilderviolet 7621L*, and *Schilderviolet S1740* from G.Siegle & Co GmbH.

In the *Dunkelbordeaux 30* (Engl. Dark *Bordeaux*) by G.Siegle & Co GmbH paint the spectra (Figure 15) suggest the presence of an earth-based pigment rich in aluminosilicates, and calcium carboxylates as additives [89, 90, 91]. Paint manufacturers commonly add calcium driers as an auxiliary additive to alkyd resin, to improve the hardness and gloss of the paint [92]. These materials are also part of the *Parigelb 20 dunkel* (Engl. Paris yellow, dark) (Figure 16, next page).

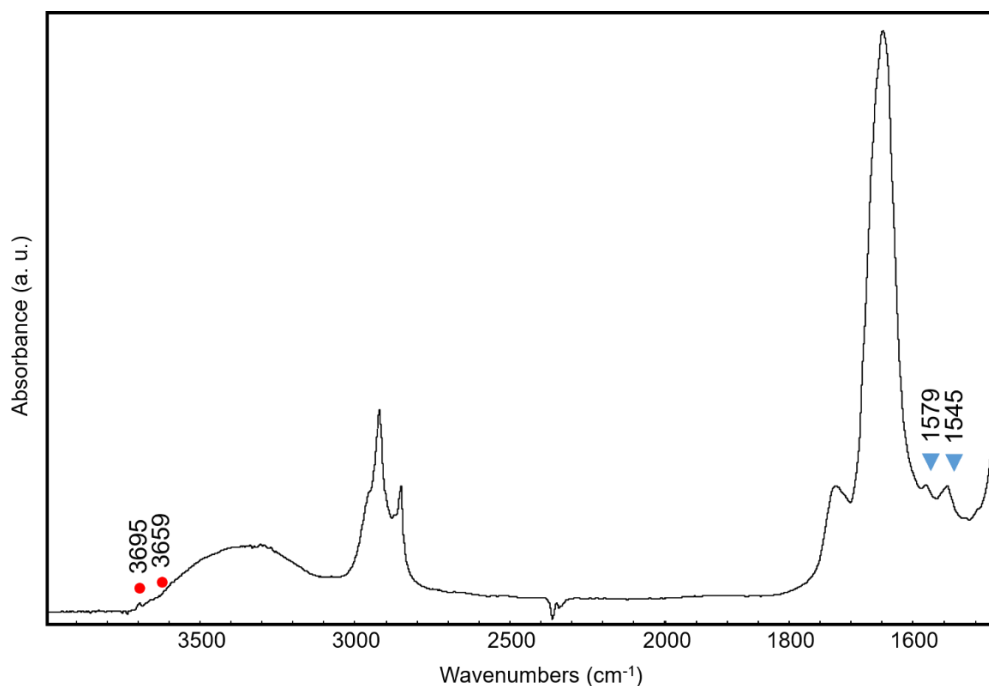


Figure 15. Spectra of the paint sample Dunkel bordeaux 30. The peaks arising from the OH stretching attributed to aluminosilicates are marked with ● and the peaks from Ca carboxylates with ▼.

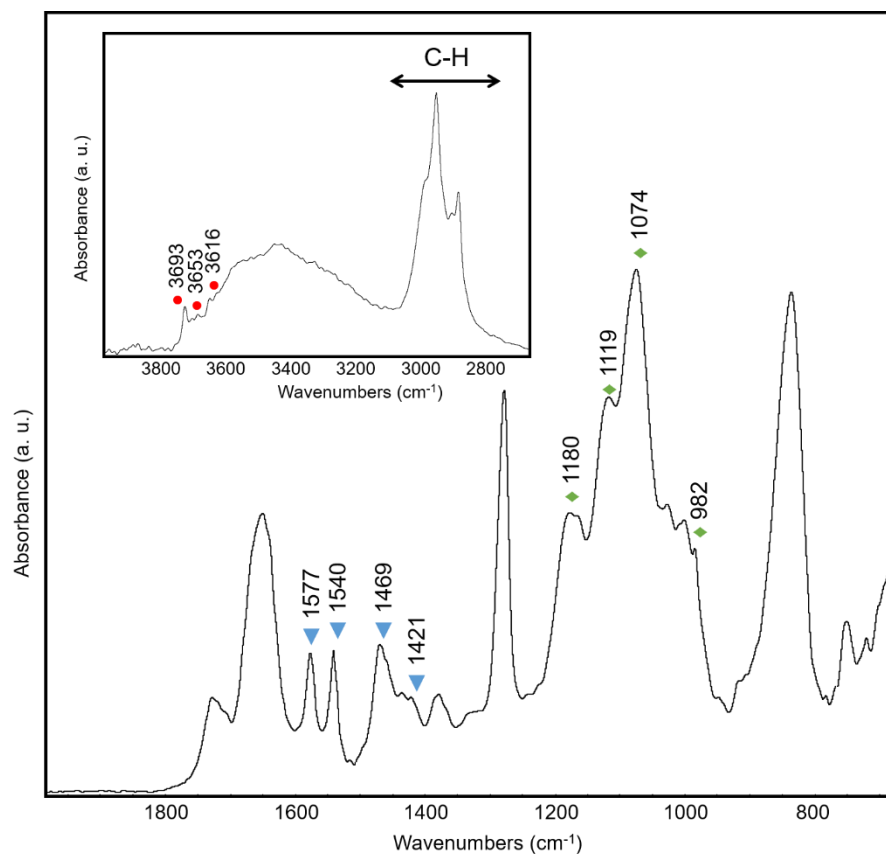


Figure 16. Spectra from Parisgelb sample, ▼ indicates the characteristic peaks of Ca carboxylates, ◆ marks the peaks from baryte, and ● the peaks related to OH stretching attributed to aluminosilicate.

The spectra from the sample *Modellrot 51* suggest, due to the bands at 3535 cm^{-1} and 3403 cm^{-1} that the paint contains gypsum as filler. The identification of Ca and S by $\mu\text{-XRF}$ confirmed it. The spectra show no other pigment signals.

After studying the green sample *Echtsaftgrün A 95* from G. Siegle & Co GmbH, the spectrum (Figure 17) exhibits peaks that suggest the paint contains strontium yellow chromate; the manufacturer added also calcium carboxylates and an aluminosilicates-rich pigment. The blue element used to obtain the green hue was not identified.

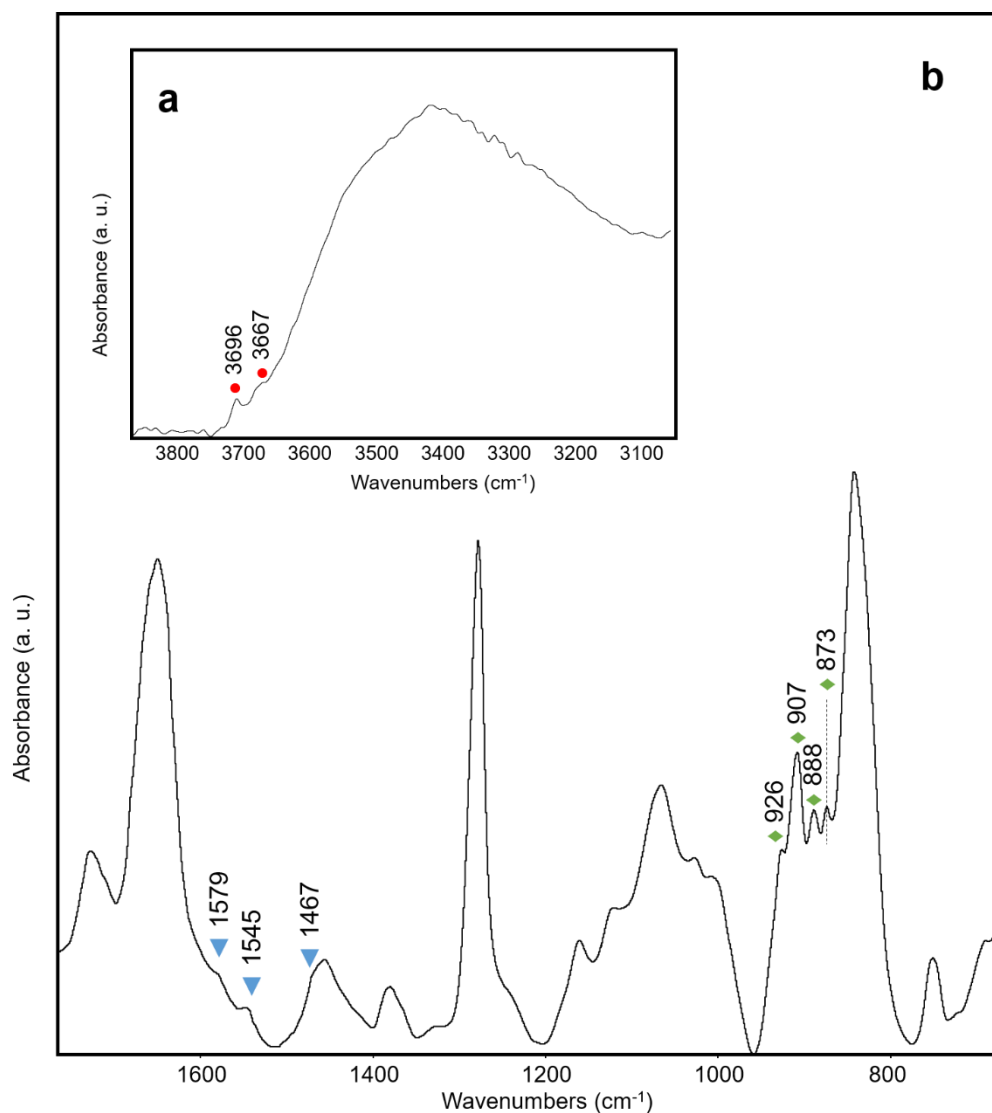


Figure 17. a) Spectrum from *Echtsaftgrün* sample in the range 3800-3100 cm^{-1} , ● indicates the characteristic peaks arising from the pigment rich in aluminosilicates, b) ▼ indicates Ca carboxylates and ◆ marks the characteristic peaks of strontium yellow

The green sample *Seidengrün 29 c* contains a blue pigment, Prussian blue identified with MU-ATR by the band at 2096 cm^{-1} , and probably an unidentified yellow pigment to obtain the green hue.

The manufacturer used baryte as filler in the paints *Zinckgelb*, *Emaille blau*, and *Wagengrün 42*. Nevertheless, was impossible to identify other components in these two samples. In particular, the *Zinckgelb* spectra present a broad band with two maximum one at 1545 cm^{-1} and the other at 1534 cm^{-1} that suggests the presence of zinc carboxylates.

d) Conclusions

The results of this investigation show that MU-ATR technique is a promising method of enhanced spectroscopy that allows the characterization of artists' materials even in complex mixtures in a fast and simple way, and without sample preparation, and using a small amount of sample (around $\sim 300\text{ }\mu\text{m}$). In many cases, it identifies not only the pigment but also the binding media and some additives.

The results also evidence the well-known complementarity and mutual exclusion of FT-IR (i.e., MU-ATR) and Raman spectroscopies that offer information about the vibrations of the molecules [93]. In many of the cases, we identified with MU-ATR one element of the mixture while with Raman we characterised the others. Because of the complexity of the samples, a multi-analytical approach is required for a complete characterization of the materials, mainly in the case of inorganic compounds not active in the mid-infrared region.

The most common filler add by manufacturers is baryte. The μ -XRF results of Siegle pyroxylin paints show a correlation between the presence of Ba and Sr in many of the samples, this may suggest the presence of impurities of Celestine (SrSO_4) and thus the use of natural baryte (Pigment White 22) [94] (introduced as paint material in 1782) [95]. In the other brands, no Sr is related to Ba, which suggests the use of synthetic baryte or *Blanc fixe* (Pigment White 21) use mainly for watercolours until the 1820s, and after that, it was introduced in another kind of paintings as filler, adulterant, and base for lakes [95].

Regarding the green colours, the samples studied indicate that green hues were still obtained mainly by mixing a yellow and a blue pigment (i. e., Prussian Blue, Pigment Blue 27) and in few cases with inorganic synthetic pigments such as the Emerald green (Pigment Green 21), this was common because of the reduced number of stable green pigments before the synthesis of phthalocyanines patented in 1929 [96]. One exception is the lake of Naphthol green (Acid Green 1) or Pigment Green 12 that was available since the last part of the 19th century [97], the researchers of the Doerner Institut identified it using Raman in the watercolours *Saftgrün, gelblich* and *Saftgrün, bläulich* from Redeker & Hennis (*data not showed*). Table 8 summarizes the different compounds identified in this set of samples.

Table 8. Summary of the materials identified in the set of samples studied.

Type of materials	Description
Pigments	Gamboge (Gummigutti), Zinc yellow, Prussian blue, Ultramarine blue, minium, Emerald green, PY1, PR83
Fillers	Gypsum, talc, natural and synthetic baryte, calcium carboxylates, aluminosilicates
Binders	Nitrocellulose, alkyd resin

2.4.2 AgI@Au TLC-MU-ATR for studying synthetic dyes and their degradation

As mentioned before, the second part of this work is focused on the study of synthetic dyes used for wool dyeing and their degradation. The objective was to set-up the AgI@Au system to analyse by means of TLC and MU-ATR the dyes extracted from different wool fibres aged artificially, the results are presented below.

a) Extraction protocol

Depending on the nature of the dye, different extraction methods have been proposed [40, 41]. Basic dyes, such as BV1, BV3 can, for instance, be extracted with methanol. On the other hand, acid dyes, are mainly solubilised with basic solvents [40].

Since it is difficult to know the nature of a dye before the analysis, we propose a multi-step protocol for the extraction of unknown dyed samples. The first step is based on the use of methanol, which is particularly effective for the extraction of basic dyes. Subsequently, extraction with ammonium hydroxide is introduced for acid dyes.

The pH stability is an important issue to consider during the extraction of dyes. Many studies have noted the utility of dyes as pH indicators since they change colour over a range of pH values. Several dyes are unstable at acid pH values, which makes our methodology useful since no acid pH values are used during the extraction.

Ammonium hydroxide, at pH 13.09, was the most effective solvent for the extraction of acid dyes. However, given that some dyes such as AB74, Alizarin, Malachite Green [98] may degrade at a pH higher than 11, we carried out an intermediate step with a solution of ammonium hydroxide (28%) at 1% (pH 10.85). Since the use of diluted ammonium hydroxide showed a lower extraction yield, we only used this method for extracting acid dyes, which are unstable in strong acidic conditions.

Our extraction protocol also enables dyes to be pre-classified. The protocol was performed on a wool sample treated with AB74 (Figure 18, next page), demonstrating that after the first step, the sample can be submitted to the second step without alterations. The effectiveness of the extraction was then proved by means of MU-ATR analyses.

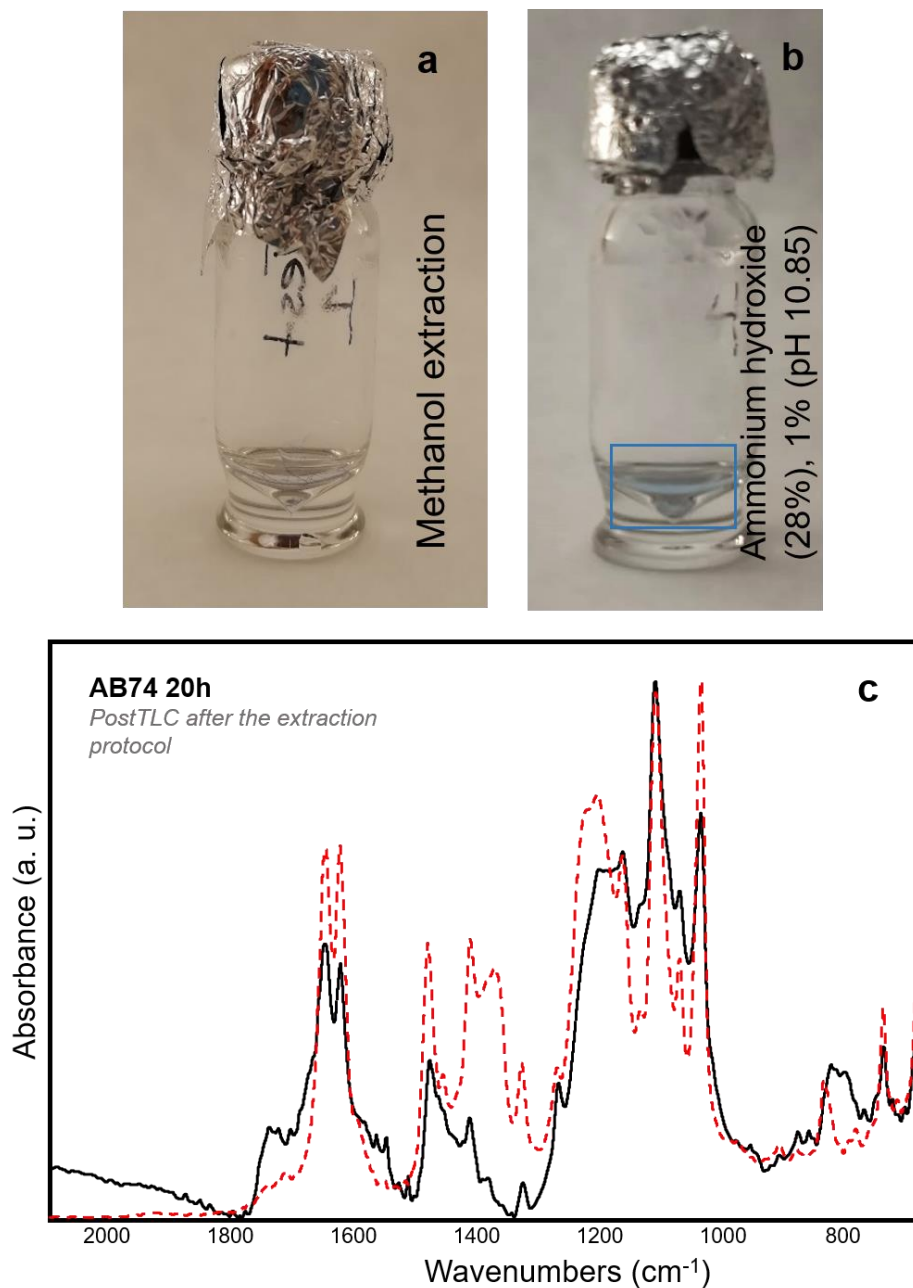


Figure 18. The extraction protocol used on AB74 dyed fibres aged for 20 h. a) Poor extraction using methanol, and b) improvement in the extraction when using a basic solution. c) MU-ATR over AgI@Au spectra show the post TLC analysis after the protocol: the comparison of the standard solution (red dashed line) and the sample analysed (solid black line) suggests that the dye was not modified or degraded after the application of the full extraction protocol.

b) Analyses of the micro extracts with μ -MU-ATR on gold-coated glass slides

Figure 19 reports the MU-ATR spectrum acquired by spotting BV3 micro extracts on gold-coated glass slides. Micro extracts of BV3 fibres aged for 60 h, 140 h, and 305 h were compared with the micro extracts of wool fibres aged and extracted in the same conditions.

In the spectra of the micro extract of the undyed wool fibres after 305 h of ageing, the Amide I band at around 1654 cm^{-1} is clearly visible. This suggests that with ageing, hydrolysis occurred thus forming peptides, which can be solubilised. In the BV3 micro extracts, the identification of the dye was hampered by the superimposition of the protein signals, which increase with ageing. The same behaviour was observed for the other dyed fibres.

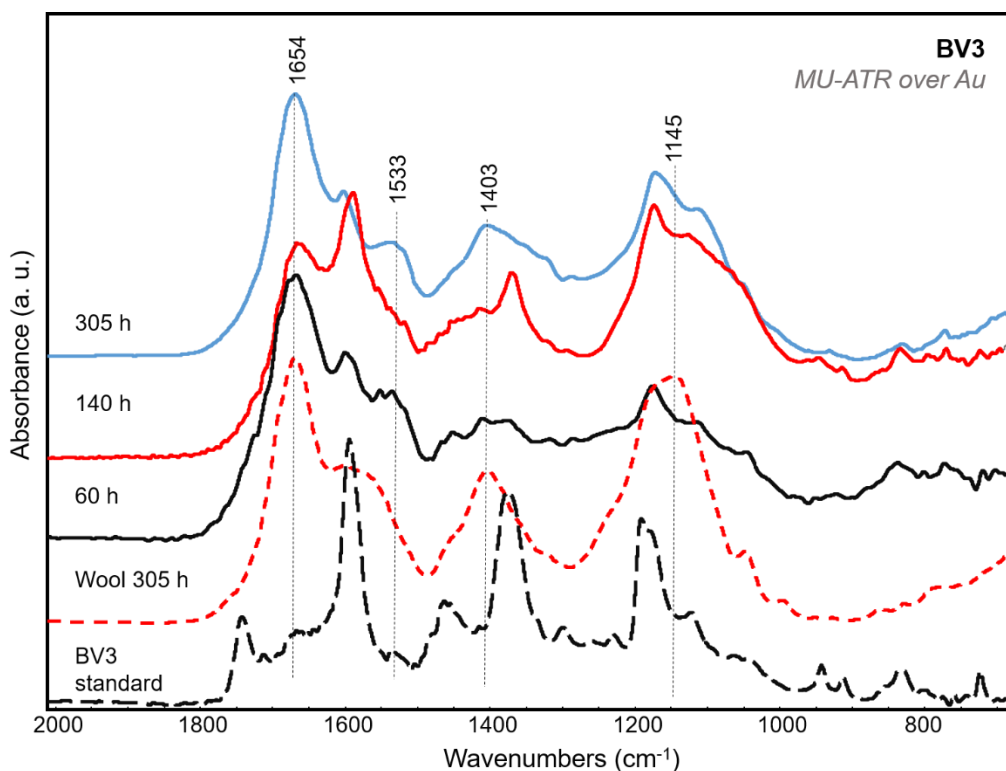


Figure 19. MU-ATR spectra of Standard of BV3 (dashed black line), wool aged for 305 h (dashed red line), BV3 sample aged for 60 h (black solid line), BV3 sample aged for 140 h (red solid line), and aged for 305 h (blue solid line). All the spectra were obtained over Au (MU-ATR).

c) Analyses of the micro extracts with TLC μ -MU-ATR on AgI@Au slides

BV1 and BV3

A double coffee-ring (Figure 20) is formed after BV1 and BV3 micro-extracts are spotted over the AgI@Au plate. The “coffee-ring effect” is a tool for the concentration of analytes in the edge of a droplet when a three-phase contact line between the atmosphere, the droplet and the substrate, creating a capillary flow after the evaporation of the solvent [99].

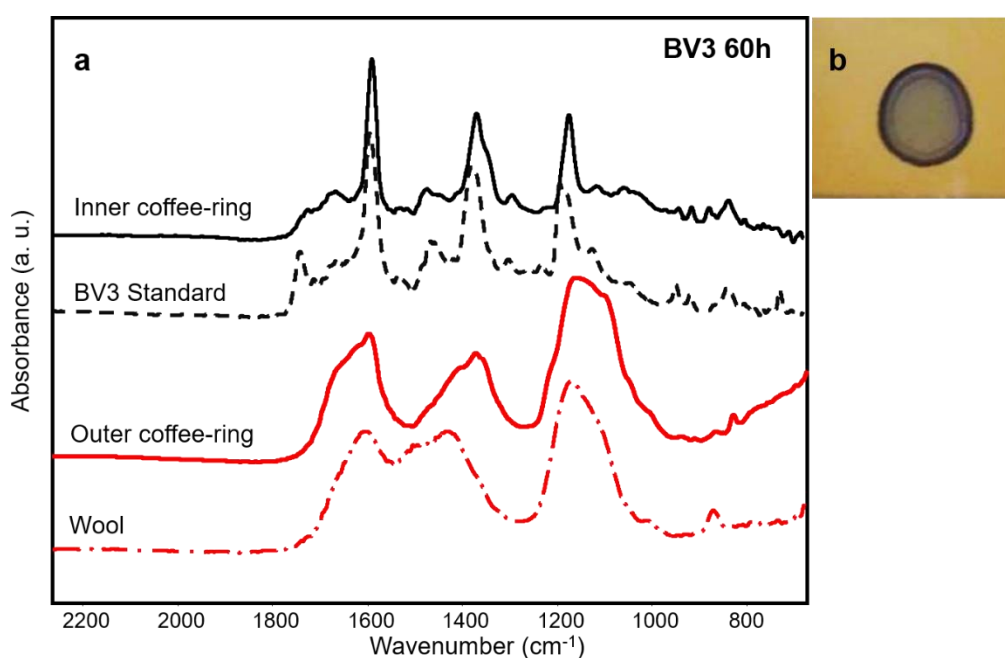


Figure 20. a) MU-ATR spectra obtained from the double coffee-ring formed over the AgI@Au plate. b) Photograph of the double coffee-ring formed by BV3 over AgI@Au.

The MU-ATR analysis on the outer coffee-ring showed the presence of bands at 1660-1630 cm⁻¹ and in some cases, also a second band at 1540cm⁻¹ corresponding to Amide I and II of wool fibres in both the aged and unaged samples. The spectra obtained from the inner coffee-ring clearly indicated the presence of the dyes.

The double ring separation is probably related to the different interactions that the dyes and the wool derivatives have with the AgI particles. This separation prevents interference from the fibres without the TLC

development even for degraded fibres [99]. The different interactions between the dyes/matrix with AgI and their efficient separation reduces the analysis time and the amount of solvent, and also means that no further dilution of the dye micro-extract is required.

The two basic dyes, BV1 and BV3, possess a similar chemical structure. The analyses of both dyes showed an increase in relative intensity of a peak around 1720 cm^{-1} , which suggests the formation of a carbonyl group due to photodegradation (Figure 21 and 22, next page). These results agree with other studies, which report the formation of Michler's ketone, due to the oxidation of the central carbon of the triarylmethane dyes [14]. The presence of Michler's ketone is a sign of progressive degradation since it accelerates the chemical degradation leading to the photo fading of this type of dye. The presence of this product can be considered as a signal of the beginning of degradation, even though the change in colour of aged fibres cannot be seen by the naked eye. Thus, this marker is a sign that conservators should begin preservation strategies in order to limit possible damage.

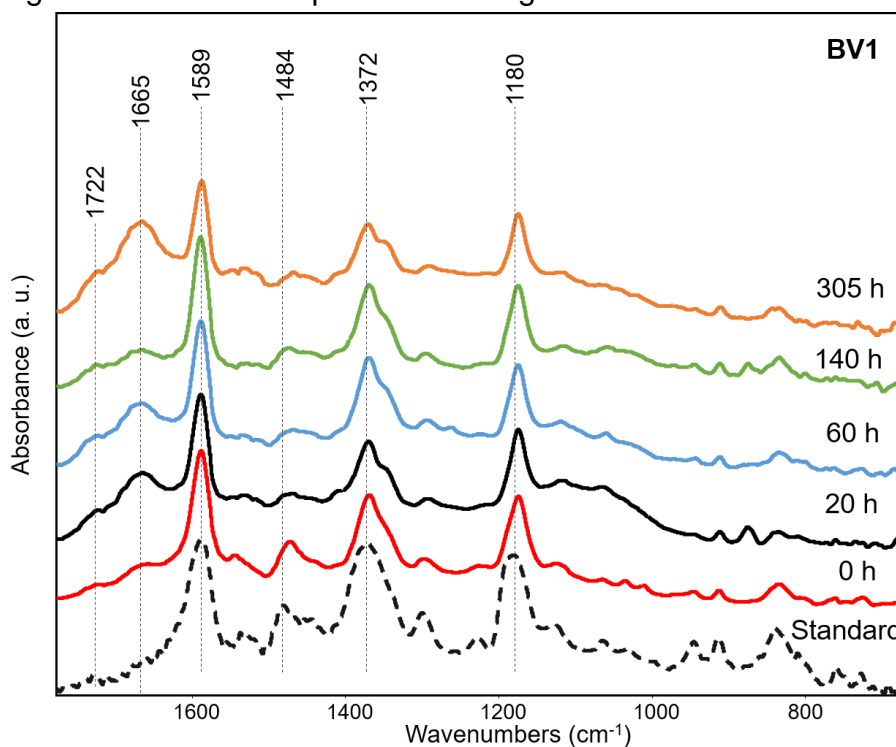


Figure 21. MU-ATR spectra on AgI@Au plates on the inner coffee-ring formed after spotting the BV1 micro-extracts. The band at 1665 cm^{-1} and the shoulder at 1722 cm^{-1} clearly increasing with degradation.

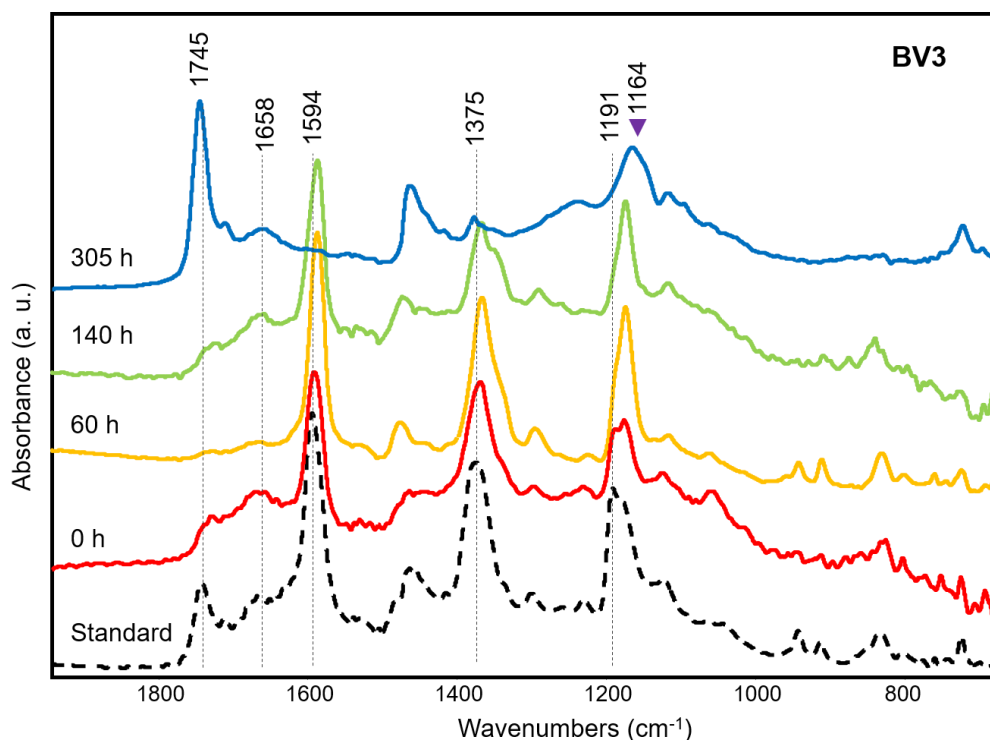


Figure 22. MU-ATR spectra on AgI@Au plates of all the BV3 samples. The increase of the peak at 1745cm^{-1} is very evident, given that the peak shifts from 1190 to 1160 cm^{-1} , suggesting the presence of Michler's ketone.

A band at around 1660 cm^{-1} suggests the contribution of wool fibres in both BV1 and BV3 samples, and its relative intensity increases with ageing since the soluble peptides amount in the extraction solvent probably increases and the AgI separation becomes less effective. However, the peaks of the dye are clearly identified in the inner coffee-ring meanwhile the highest concentration of the wool components remains in the outer coffee-ring.

AY24, AB74, and AR87

These three acid dyes required a mordent for better fixation in the wool fibre. In contrast to what we observed when studying the basic dyes, after the deposition of the micro-extracts, a single coffee-ring was formed. This suggests that the interaction of the dyes, the mordent, and the wool peptides with AgI is not sufficiently different even for a partial separation. The pre-TLC analysis showed a high interference of the mordent. A broad band around 1102 cm^{-1} attributed to SO_4^{2-} covered other peaks characteristic of the dye [68]. Although in many cases some characteristic peaks were identified, the mordent signal was high (Figures 23, 24 and 25, next page).

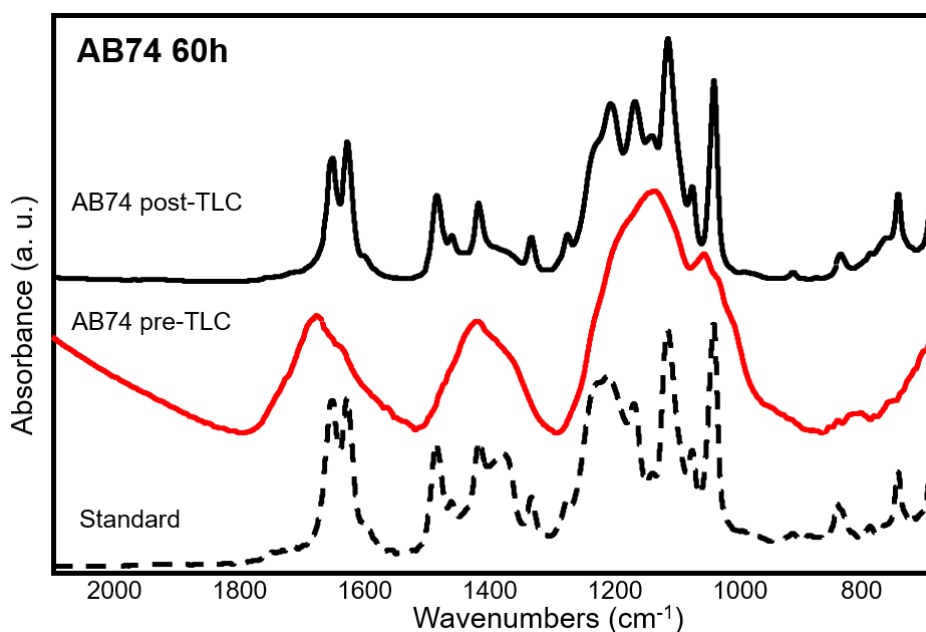


Figure 23. MU-ATR spectra of pre and post TLC analyses on AgI@Au plates of AB74 aged for 60h. The TLC separation reduces considerably the interference of the fibre and the mordent.

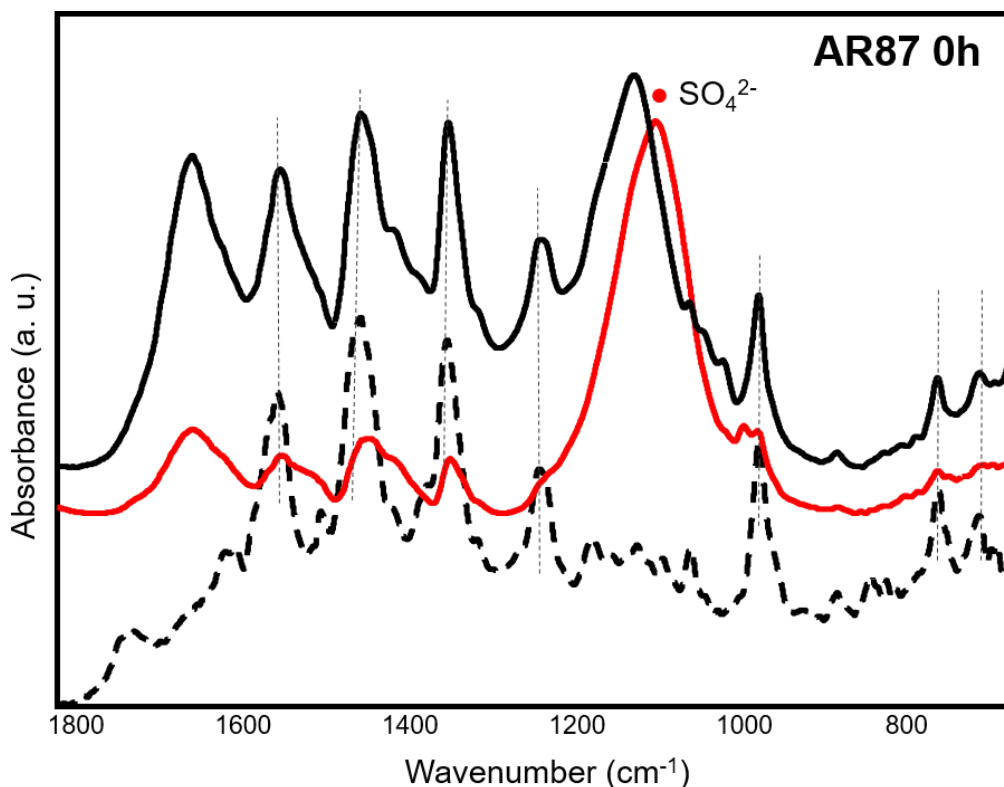


Figure 24. MU-ATR spectra of pre and post TLC analyses on AgI@Au plates of Acid Yellow 24 aged for 60h. The TLC separation considerably reduces the interference of the mordant marked with ●.

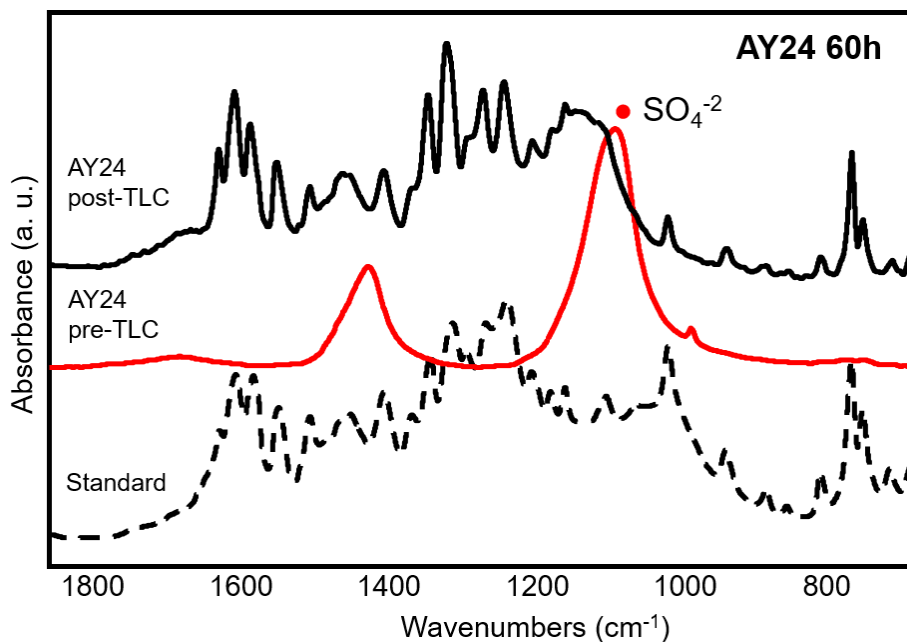


Figure 25. MU-ATR spectra of pre and post TLC analyses on AgI@Au plates of Acid Red 87. Pre-TLC spectrum (red solid line) and post TLC spectrum (black solid line). The TLC separation considerably reduces the interference of the mordant marked with ●. The results are compared with an AR87 standard (dashed black line).

Obtaining additional information regarding the use of a specific mordent is interesting because it can be correlated to the use of particular dyeing recipes. Table 9 summarizes the mordents containing sulphate ion and their characteristic signals in the middle FT-IR region.

Table 9. Mordents containing sulphate ion and their characteristic FT-IR bands. *vw:very weak, m:medium, s: strong, vs:very strong [68, 100].*

Mordent	Characteristic bands in FT-IR (cm^{-1})
Potash alum	1630, 1100, 695, 614
Iron sulphate	1625(m), 1150(m), 1090(vs), 990(vw)
Copper sulphate	1600(vw), 1200(s), 1090(vs), 1020(w), 860(m), 805, 680(m)
Glauber's salt (Na_2SO_4)	1110(vs), 645(w)

We observed that the acid dyes studied present a band at 1110 cm^{-1} , which may be related to two specific mordents, potash alum and Glauber's salt. Given that the characteristic peaks of Glauber's salt are out of the detection range of our instrumentation (645 cm^{-1}), the presence of potash alum can be ruled out due to the absence of 1630 cm^{-1} peak. This confirms the presence of Glauber's salt. Na_2SO_4 was introduced as a dyeing assistant during the 1880s thereby considerably improving the dyeing, especially in the case of Acid Blue 74, which in combination with Na_2SO_4 was considered the best version of the indigotin-disulphonic acid dye available at that time [101, 102].

After TLC developments, MU-ATR spectra clearly showed the characteristic bands of the dyes. Spectra obtained from Acid Blue 74 after TLC separation (Figure 26, next page) showed slight modifications at different aging times. The principal changes were related to the reduction of the 1200 cm^{-1} shoulder that can be assigned to the sulfonate groups. There was also a slight change in the intensity of bands $1630\text{-}1617 \text{ cm}^{-1}$ and 1460 cm^{-1} , which are related to the alkene bonds. All these modifications are in agreement with the findings already reported in the literature [103].

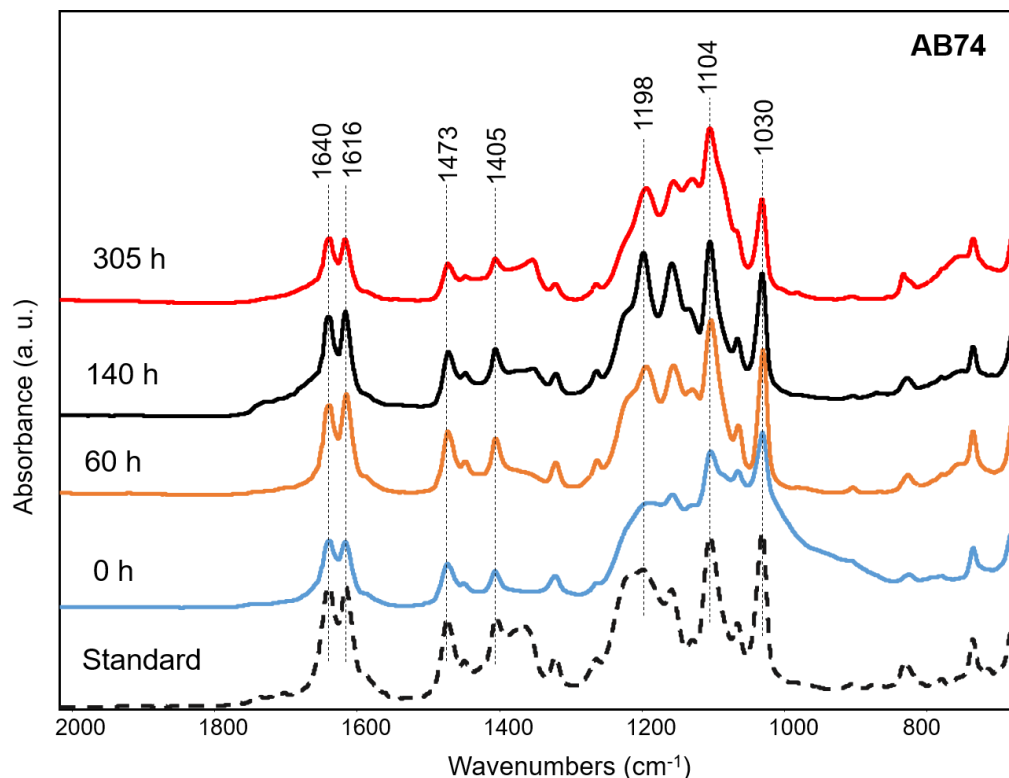


Figure 26. MU-ATR spectra on AgI@Au plates of artificially aged AB74 samples. Few modifications to the spectra can be observed suggesting no evident degradation of the dye.

According to Cao et al. [103], AB74 loses colour turning first yellow and later colourless when it is highly degraded and thus shows the presence of bands related to succinic acid (1685 cm^{-1}) and acetic acid (1416 cm^{-1}). The colour of the samples analysed in our study (still dark blue even at 305 h), in combination with the absence of succinic and acetic acid bands [103] suggested that the dye degradation is at an early stage.

Acid Yellow 24 samples analysed after TLC separation showed a progressive modification of FT-IR spectra at increasing levels of degradation (Figure 27, next page).

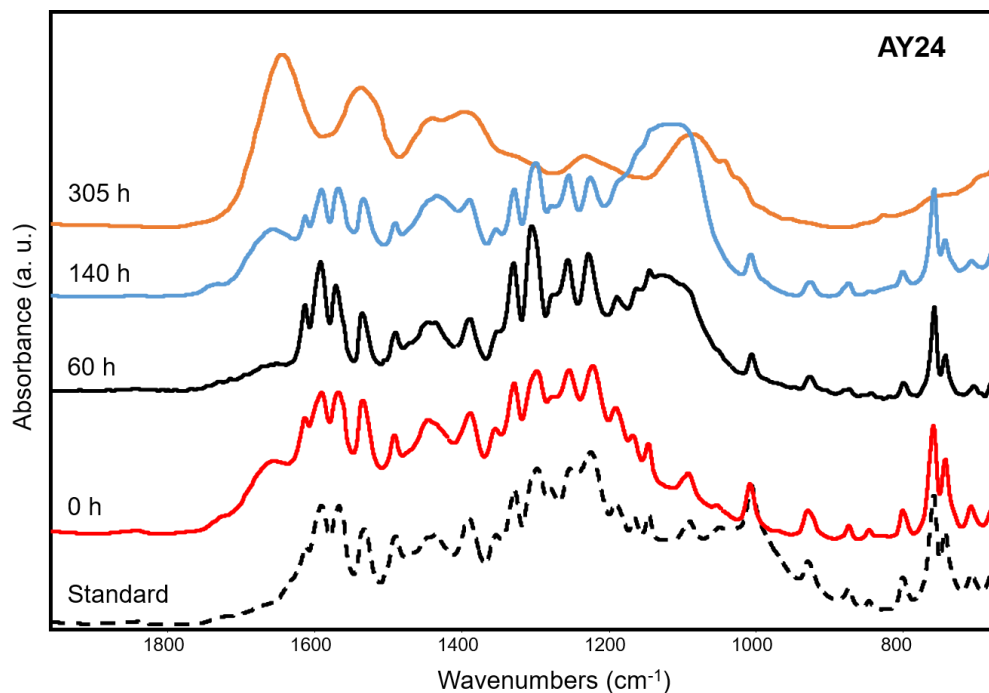


Figure 27. MU-ATR spectra of the artificially aged AY24 samples obtained over AgI@Au plate. It is very evident the complete modification of 305h suggesting an advanced degradation stage of the dye.

The ageing of the sample led to a reduction in dye extraction efficacy; however, it was possible to identify the dye after 140 h, while after 305 h the concentration of the extracted dye is low and the signal is dominated by wool fibre degradation products even after the TLC separation. No information regarding the degradation mechanism of AY24 is reported in the literature, but, the degradation of other nitro dyes such as Acid Orange 3 (AO3, CI 10385), already studied can give some idea of the possible mechanism. The degradation pathway determined by Li et al. [37] suggests the loss of nitro bonds, and in an initial step the formation of hydroxyl groups and finally carbonyl groups. Ahmed et al. [38] propose a similar mechanism for the degradation of Dispersive Yellow 42, forming hydroxyl groups and later carboxylic acids. However, the strong contribution of wool in the sample aged for 305 h hinders any the signals arising from the degradation.

AR87 samples present a high degradation rate, indicating rapid photofading. Even after the TLC separation, the bands related to the wool residues and the mordents can be observed in all the samples at different ageing conditions. Despite those signals, the characteristic peaks of AR87 at 1553 cm^{-1} , 1454 cm^{-1} , 1349 cm^{-1} , and 1237 cm^{-1} can be identified in the micro extracts of the unaged fibres (0 h) and aged for 20 h and 60 h (Figure 28). These features disappear at longer times of light exposure, probably due to the reduction in the concentration of the dye.

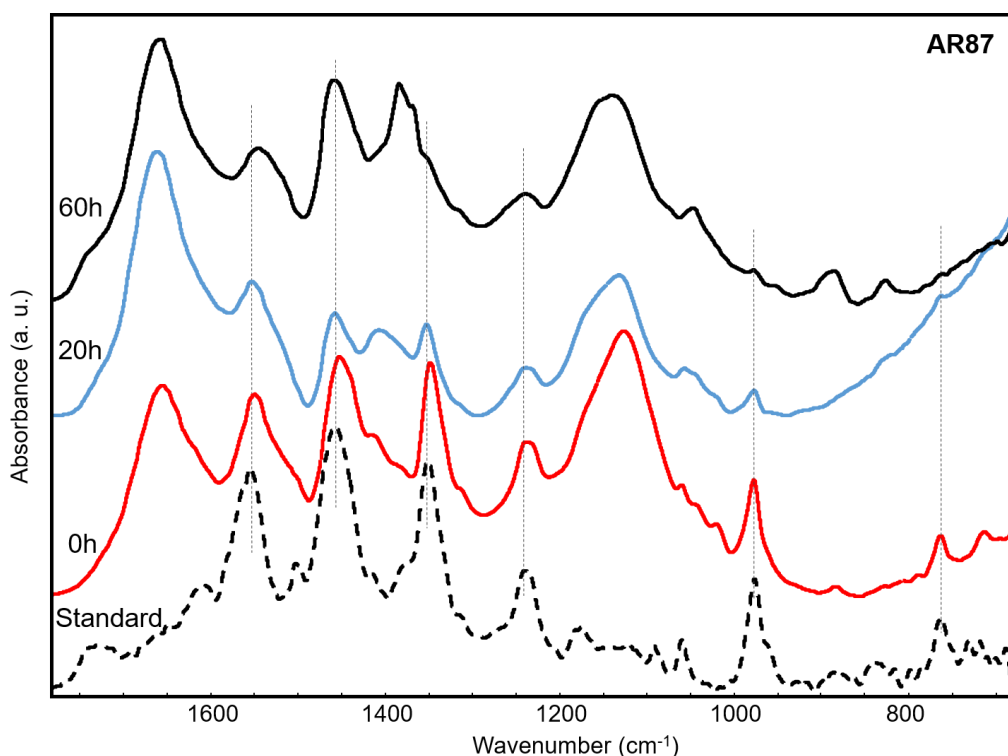


Figure 28. MU-ATR spectra of the artificially aged AR87 samples deposited over AgI@Au plate. The characteristic peaks of dye are evident in unaged sample (0h) and 20h and 60h, however it is evident the interference of wool fibre and mordent in all the spectra.

d) Real samples

To validate the results obtained from artificially aged samples, two historical samples from a pattern book dated 1893 were studied. The information provided in the book gave an idea of the dyes possibly present in each sample.

Using our protocol we analysed the micro-extracts, with the normal MU-ATR set-up on gold-coated glass slides, but, the spectra were dominated by wool residues for CH-5 and wool residues and a sulphate band for CH-6.

When the CH-5 micro-extract was spotted on the AgI@Au plate, a double coffee-ring with purple spots at the centre of the drop was observed. Spectra acquired in the inner ring and in the purple spots, present the characteristic peaks of BV3 (Figure 29) and a peak at 1742 cm^{-1} . This suggests the presence of degradation products, probably Michler's ketone, as observed in the aged standard fibres.

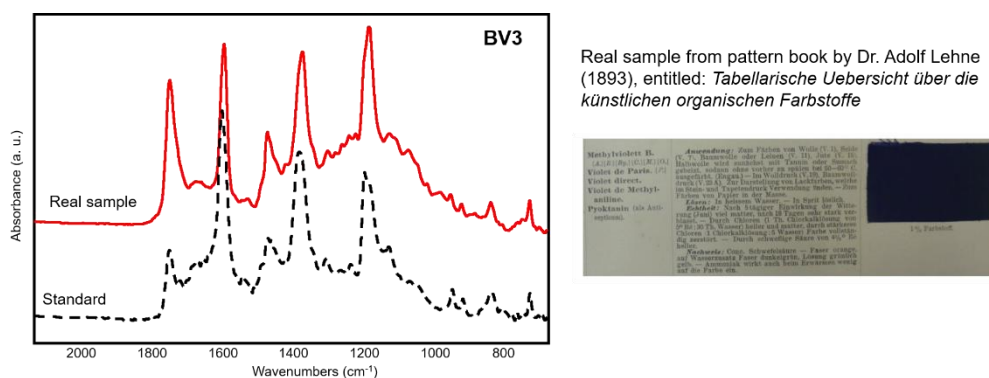


Figure 29. MU-ATR spectra of the real sample CH-5. The spectrum shows the characteristic peaks of BV3.

After the extraction with ammonium hydroxide solution at pH 10.85, the CH-6 micro-extract was spotted on the AgI@Au plate and formed a single coffee ring, in accordance with the results of the artificially aged samples. Spectra related to sample CH-6 before the TLC analysis shows a band at 1100 cm^{-1} attributed to the sulphate group, which could be related to the presence of Glauber's salt since no other peaks are present [35]. This information was confirmed by the dye recipe described in the book. After TLC analysis, the characteristic peaks of AB74 were identified (Figure 30, next page). These results suggest that our methodology can be used for identifying dyes in historical samples and to obtain information on their state of degradation.

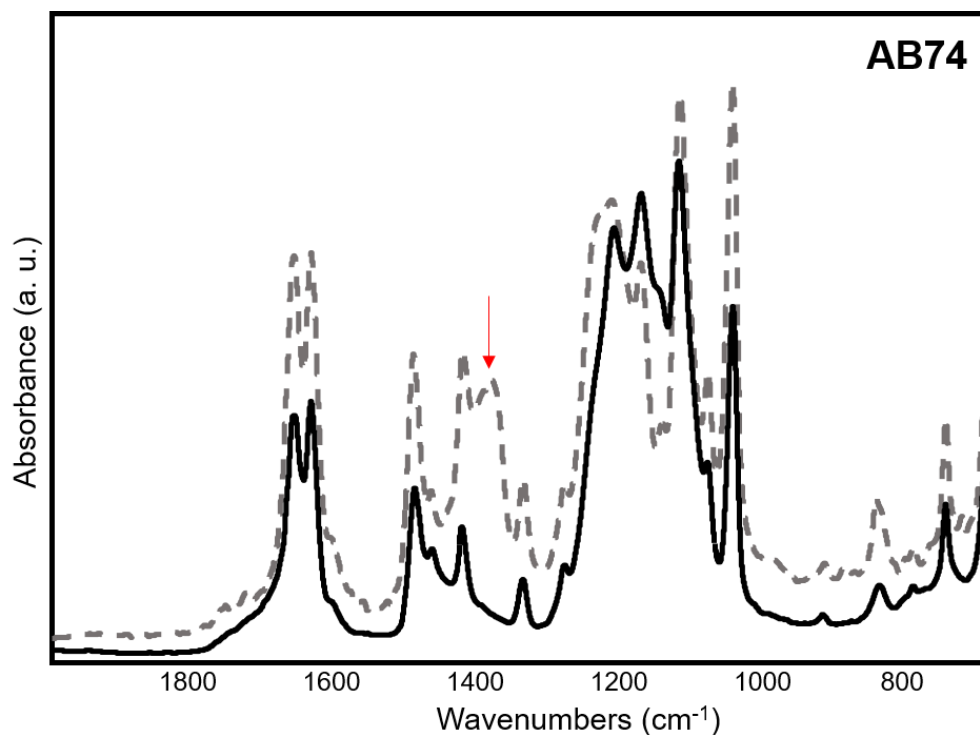


Figure 30. MU-ATR spectra of the real sample CH-6. The spectrum shows the characteristic peaks of AB74. The red arrow indicates the only difference between the standard and the real sample that can be attributed to degradation of the dye.

e) Conclusions

This work presents for the first time, the use of AgI@Au TLC /MU-ATR for analysing aged fibres. Our methodology shows promising results for identifying degraded dyes in a fast and simple way, and this a suitable technique for use in the cultural heritage. We also outlined a multi-step micro-extraction protocol whose first step is a mild solvent for basic dyes and then different weak basic conditions for acid dyes. Being able to modulate the extraction condition is crucial when unknown samples are studied. Our data suggest that with ageing, the dye concentration decreases, and the interference of wool fibre increases. AgI@Au's ability to perform separations is of the utmost importance.

For the basic dyes BV1 and BV3, we observed the formation of a double coffee ring after spotting the micro-extract in the AgI@Au plates. A partial separation occurred, enabling the dye peaks both in the unaged and in the aged samples to be identified without the TLC development. The

double coffee-ring allows reducing analysis times and avoiding dilution effects. On the other hand, the acid dyes, containing a mordant, showed no double coffee-ring separation. In this case, after the TLC development, we isolated the dye signals and observed their degradation pattern. For the most unstable dye, identification was only possible at the earliest stage of ageing. The analyses of historical samples from 1893 enabled us to validate our methodology.

In conclusion, our system efficiently identifies synthetic dyes using just small amounts of sample. It can be used for rapid identification of their degradation even at an early stage, thus providing useful information for conservators in order to prevent further degradation.

The issue of nitro dye degradation should be explored in further research since little is known about the mechanisms that lead to the lightfastness of this class of dyes. We are currently studying whether this methodology could also be applied for the identification of natural dyes and their mixtures commonly present in historical artefacts.

References

- [1] R. M. Christie, *Colour Chemistry*, Cambridge: Royal Society of Chemistry, 2015.
- [2] A. A. Polette-Nie, F. S. Manciu, B. Torres, M. Alvarado Jr. and R. R. Chianelli, "Organic/inorganic complex pigments: Ancient colors Maya Blue," *Journal of Inorganic Biochemistry*, vol. 101, pp. 958-1973, 2007.
- [3] J. P. Murmann, "Chemical Industries after 1850," in *Oxford Encyclopedia of Economic History*, Oxford, Oxford University Press, 2003, pp. 398-406.
- [4] P. Ball, *Colore. Una Biografia*, Milan: Bur Rizzoli, 2015.

- [5] I. Holme, "Sir William Henry Perkin: a review of his life, work and legacy," *Coloration Technology*, vol. 122, pp. 235-251, 2006.
- [6] M. de Keijzer, "The history of modern synthetic inorganic and organic artists' pigments," in *Contributions to conservation: research in conservation at the Netherlands Institute for Cultural Heritage*, J. A. Mosk and N. H. Tennent, Eds., James & James Ltd., 2002, pp. 42-54.
- [7] P. Vandenabeele, L. Moens, H. G. M. Edwards and R. Dams, "Raman spectroscopic database of azo pigments and application to modern art studies," *Journal of Raman Spectroscopy*, vol. 31, p. 509–517, 2000.
- [8] M. de Keijzer, . M. R. van Bommel and M. Geldof, "Synthetic organic pigments used by Vincent van Gogh at the end of his lifetime," in *EU-Artech Symposium on Vincent van Gogh and Contemporaries*, Amsterdam, 2009.
- [9] The Art Institute of Chicago, The Metropolitan Museum of Art, Gauguin, USA: The Lakeside Press, 1959.
- [10] L. A. Kalba, *Color in the Age of Impressionism. Commerce, Technology, and Art*, Pennsylvania State University Press, 2017.
- [11] J. Park and J. Shore, "Dye and fiber discoveries of the twentieth century. Part 1: From the magic of electric light to the nightmare of world war," *Journal of the Society of Dyers and Colourists*, vol. 115, pp. 157-167, 1999.
- [12] H. Skowranek, H. Stege, C. Krekel and C. Steuer, "Eilido colours: sources relating to the introduction of coal-tar colours and their controversial reception in the early 20th century," in *Sources on Art Technology. Back to Basics*, London, Archetype Publications Ltd, 2016, pp. 34-42.

- [13] R. Mayer, *The Artist's Handbook of Materials and Techniques*, USA: Viking, 1981.
- [14] D. Confortin, H. Neevel, M. Brustolon, L. Franco, A. J. Kettelarij, R. M. Williams and M. R. van Bommel, "Crystal violet: study of the photo-fading of an early synthetic dye in aqueous solution and on paper with HPLC-PDA, LCMS and FORS," *Journal of Physics: Conference Series* 231, 2010.
- [15] P. M. Whitmore and G. R. Cass, "The Fading of Artists' Colorants by Exposure to Atmospheric Nitrogen Dioxide," *Studies in Conservation*, vol. 34, no. 2, pp. 85-97, 1989.
- [16] E. Ghelardi, I. Degano, M. P. Colombini, J. Mazurek, M. Schilling, H. Khanjian and T. Learner, "A multi-analytical study on the photochemical degradation of synthetic organic pigments," *Dyes and Pigments*, vol. 123, pp. 396-403, 2015.
- [17] V. Jovanovic, S. Eric, P. Colomban and A. Kremenovic, "Identification of Lithol Red Synthetic Organic Pigment Reveals the Cause of Paint Layer Degradation on the Lazar Vozarevic Painting "Untitled" with Copper Plates," *Heritage*, vol. 2, p. 2612–2624, 2019.
- [18] C. L. Shaver and G. R. Cass, "Ozone and the Deterioration of Works of Art," *Environ. Sci. Technol.*, vol. 17, pp. 748-752, 1983.
- [19] L. Mills, A. Burnstock, F. Duarte, S. de Groot, L. Megens, M. Bisschoff, H. van Keulen and K. J. van den Berg, "Water sensitivity of modern artists' oil paints," *ICOM Committee for conservation*, vol. II, pp. 651-659, 2008.
- [20] J. Lee, I. Bonaduce, F. Modugno, J. La Nasa, B. Ormsby and K. J. van den Berg, "Scientific investigation into the water sensitivity of

- twentieth century oil paints,” *Microchemical Journal*, vol. 138, p. 282–295, 2018.
- [21] S. Genevieve , A. Burnstock, L. Megens, T. Learner, G. Chiari and K. J. van den Berg, “A cause of water-sensitivity in modern oil paint films: The formation of magnesium sulphate,” *Studies in Conservation*, vol. 59, no. 1, pp. 38-51, 2014.
- [22] D. Saunders and J. Kirby, “The effect of relative humidity on artists’ pigments,” *The National Gallery Technical Bulletin*, vol. 25, pp. 62-72, 2004.
- [23] R. Dancause, J. Wagner and J. Vuori, “Caring for textiles and costumes,” Canadian Conservation Institute, 2018. [Online]. Available: <https://www.canada.ca/en/conservation-institute/services/preventive-conservation/guidelines-collections/textiles-costumes.html#a24>. [Accessed 05 12 2019].
- [24] B. Hochleitner, V. Desnica, M. Mantler and M. Schreiner, “Historical pigments: a collection analyzed with X-ray diffraction analysis and X-ray fluorescence analysis in order to create a database,” *Spectrochimica Acta Part B*, vol. 58, p. 641–649, 2003.
- [25] C. Defeyt and D. Strivay, “PB15 as 20th and 21st artists' pigment: Conservation concerns,” *e-Preservation Science*, vol. 11, pp. 6-14, 2014.
- [26] . M. van Bommel and E. Fantini, “Unravelling the colour palette: the reconstruction and analysis of synthetic colour stains,” *e-Preservation Science*, no. 10, pp. 50-58, 2013.
- [27] T. Learner, “A review of synthetic binding media in twentieth-century paints,” *The Conservator*, vol. 24, no. 1, pp. 96-103, 2000.
- [28] M. Van De Laar and A. Burnstock, “With Paint from Claus & Fritz”: A Study of an Amsterdam Painting Materials Firm (1841-1931),”

Journal of the American Institute for Conservation, vol. 36, no. 1, pp. 1-16, 1997.

- [29] M. Wachowiak, 19th century paints of Richard Ainè used by Jan Matejko (1838-1983). Analysis of preserved paints from tubes , palettes and of paintings' surfaces and paint-layers, London: Laser in the Conservation of Artworks VIII, 2011.
- [30] E. West FitzHugh, M. Leona and N. Shibayama, "Pigments in a Paint Box Belonging to Whistler in the Library of Congress," *Studies in Conservation*, vol. 56, no. 2, pp. 115-124, 2011.
- [31] M. Kokkori, F. Casadio, K. Sutherland and M. Vermeulen, "Charting the Development of Oil-Based Enamel Paints Through the Correlation of Historical Paint Technology Manuals with Scientific Analysis," in *Issues in Contemporary Oil Paint*, A. Burnstock, M. de Keijzer, J. Krueger, T. Learner, A. de Tagle, G. Heydenreich and K. J. van den Berg, Eds., Springer, 2014, pp. 117-125.
- [32] F. C. Izzo, C. Zanin, H. van Keulen and C. da Roit, "From Pigments to Paints: Studying original materials from the atelier of the artist Mariano Fortuny y Madrazo," *International Journal of Conservation Science* , vol. 8, no. 4, pp. 547-564, 2017.
- [33] M. . B. Christiansen, E. Baadsgaard, J. Sanyova and K. P. Simonsen, "The artists' materials of P. S. Krøyer: An analytical study of the artist's paintings and tube colours by Raman, SEM-EDS and HPLC," *Heritage Science*, vol. 5, no. 39, 2017.
- [34] A. Burnstock, I. Lanfear, K. J. van den Berg, L. Carlyle, M. Clarke, E. Hendriks and J. Kirby, "Comparison of the fading and surface deterioration of red lake pigments in six paintings by Vincent van Gogh with artificially aged paint reconstructions," in *14th Triennial Meeting the Hague Preprints*, 2005.

- [35] A. M. López-Montes, A. L. Dupont, B. Desmazières and B. Lavédrine, "Identification of synthetic dyes in early colour photographs using capillary electrophoresis and electrospray ionisation-mass spectrometry," *Talanta*, vol. 30, no. 114, pp. 217-226, 2013.
- [36] P. Moretti, G. Germinario, B. Doherty, I. D. van der Werf, L. Sabbatini, A. Mirabile, A. Sgamellotti and C. Miliani, "Disclosing the composition of historical commercial felt-tip pens used in art by integrated vibrational spectroscopy and pyrolysis-gas chromatography/mass spectrometry," *Journal of Cultural Heritage*, no. 35, pp. 242-253, 2019.
- [37] O. Díaz-Santana, D. Vega-Moreno and F. Conde-Hardisson, "Gas chromatography-mass spectrometry and high-performance liquid chromatography-diode array detection for dating of paper ink," *Journal of Chromatography A.*, vol. 1515, pp. 187-195, 2017.
- [38] S. Conti and A. Keller, "Il colore nei materiali tessili antichi: standard di riferimento e caratterizzazione dei colori per mezzodi indagini ottiche," in *Il Restauro dei Materiali Tessili*, M. Ciatti and S. Conti, Eds., Florence, Alpi Lito, 2010, pp. 271-290.
- [39] B. W. Pirok, J. Knip, M. R. van Bommel and P. J. Schoenmakers, "Characterization of synthetic dyes by comprehensive two-dimensional liquid chromatography combining ion-exchange chromatography and fast ion-pair reversed-phase chromatography," *Journal of Chromatography A.*, vol. 1436, pp. 141-146, 2016.
- [40] E. Groves, C. S. Palenik and S. Palenik, "A survey of extraction solvents in the forensic analysis of textile dyes," *Forensic Science International*, vol. 268, pp. 139-144, 2016.

- [41] ASTM, *Standard Guide for Forensic Examination of Non-Reactive Dyes in Textile Fibers by Thin-Layer Chromatography*, ASTM Committee E30 on Forensic Sciences, 2013.
- [42] R. Macrae and K. Smalldon, "The Extraction of Dyestuffs from Single Wool Fibers," *Journal of Forensic Sciences*, vol. 24, no. 1, pp. 109-116, 1979.
- [43] G. A. Milovanovic, M. Ristic-Solajic and T. J. Janjic, "Separation and Identification of Synthetic Organic Pigments in Artists' Paints by Thin-Layer Chromatography," *Journal of Chromatography*, vol. 249, pp. 149-154, 1982.
- [44] J. Russell, B. W. Singer, J. J. Perry and A. Bacon, "The identification of synthetic organic pigments in modern paints and modern paintings using pyrolysis-gas chromatography–mass spectrometry," *Anal. Bioanal. Chem.*, vol. 400, p. 1473–1491, 2011.
- [45] A. Alvarez-Martin, T. P. Cleland, G. M. Kavich, K. Janssens and G. A. Newsome, "Rapid Evaluation of the Debromination Mechanism of Eosin in Oil Paint by Direct Analysis in Real Time and Direct Infusion-Electrospray Ionization Mass Spectrometry," *Analytical Chemistry*, vol. 91, p. 10856–10863, 2019.
- [46] W. Fremout and S. Saverwyns, "Identification of synthetic organic pigments: the role of a comprehensive digital Ramanspectral library," *Journal of Raman Spectroscopy*, vol. 43, p. 1536–1544, 2012.
- [47] W. Fremout, "Synthetic Organic Pigments Research Aggregation Network (SOPRANO)," Royal Institute for Cultural Heritage (KIK-IRPA), [Online]. Available: <https://soprano.kikirpa.be/>. [Accessed 27 02 2020].

- [48] I. Bonacini, . F. Gallazzi, A. Espina, M. Vega Cañamares, S. Prati, R. Mazzeo and S. Sanchez-Cortes, "Sensitive 'on the fiber' detection of synthetic organic dyes by laser photoinduced plasmonic Ag nanoparticles," *Journal of Raman Spectroscopy*, vol. 48, no. 7, pp. 925-934, 2017.
- [49] F. Amato, C. Micciche', M. Cannas, F. . M. Gelardi, B. Pignataro, M. Li Vigni and S. Agnello, "Ag nanoparticles agargel nanocomposites for SERS detection of cultural heritage interest pigments," *The European Physical Journal Plus*, no. 133, p. 74, 2018.
- [50] C. Montagner, M. Bacci, S. Bracci, R. Freeman and M. Picollo, "Library of UV-Vis-NIR reflectance spectra of modern organic dyes from historic pattern-card coloured papers," *Spectrochim Acta A Mol Biomol Spectrosc.*, vol. 79, no. 5, pp. 166-1680, 2011.
- [51] G. M. Atiqur Rahaman, J. Parkkinen, M. Hauta-Kasari and S. H. Amirshahi, "Fiber dye classification by spectral imaging," in *2017 IEEE International Conference on Imaging, Vision & Pattern Recognition (icIVPR)*, Bangladesh, 2017.
- [52] G. Reed, K. Savage, D. Edwards and N. Nic Daeid, "Hyperspectral imaging of gel pen inks: An emerging tool in document analysis," *Science & Justice*, vol. 54, no. 1, pp. 71-80, 2014.
- [53] C. Sessa, R. Weiss, R. Niessner, N. P. Ivleva and H. Stege, "Towards a Surface Enhanced Raman Scattering (SERS) spectra database for synthetic organic colourants in cultural heritage. The effect of using different metal substrates on the spectra," *Microchemical Journal*, vol. 138, pp. 209-225, 2018.
- [54] S. Steger, H. Stege, S. Bretz and O. Hahn, "Capabilities and limitations of handheld Diffuse Reflectance Infrared Fourier Transform Spectroscopy (DRIFTS) for the analysis of colourants

and binders in 20th-century reverse paintings on glass,” *Spectrochim Acta A Mol Biomol Spectrosc.*, vol. 195, pp. 103-112, 2018.

- [55] S. Prati, G. Sciutto, I. Bonacini and R. Mazzeo, “New Frontiers in Application of FTIR Microscopy for Characterization of Cultural Heritage Materials,” in *Analytical Chemistry for Cultural Heritage*, Springer, 2016.
- [56] F. Rosi, L. Cartechini, D. Sali and C. Miliani, “Recent trends in the application of Fourier Transform Infrared (FT-IR) spectroscopy in Heritage Science: from micro- to non-invasive FT-IR,” *Physical Sciences Reviews*, 2019.
- [57] S. Prati, M. Milosevic, G. Sciutto, S. G. Kazarian and R. Mazzeo, “Analyses of trace amounts of dyes with a new enhanced sensitivity FTIR spectroscopic technique: MU-ATR (metal underlayer ATR spectroscopy),” *Analytica Chimica Acta*, no. 941, pp. 67-79, 2016.
- [58] Q. Zhu, X. Su, . H. J. Wu, Y. J. Zhai, J. M. Xia, Buhebate, Y. Z. Xu and J. G. Wu, “The analysis for silver iodide fine particles of TLC/FTIR matrix,” *Spectroscopy and Spectral Analysis*, vol. 32, no. 7, pp. 1790-1794, 2012.
- [59] X. Liu, Q. H. Pan, J. Ding, Q. Zhu, A. Q. He, S. J. Yue, X. P. Li, L. P. Hu, J. M. Xia, C. G. Liu, Y. J. Wei, J. Yu, Z. L. Yang, X. Zhu, Y. Z. Xu and J. G. Wu, “Using barium fluoride fine particles as stationary phase for TLC/FTIR analysis,” *Spectroscopy and Spectral Analysis*, vol. 31, no. 7, pp. 1767-1771, 2011.
- [60] F. Wang, H. Wu, Q. Zhu, K. Huang, Y. Wei, C. Liu, Y. Zhai, Z. Yang, S. Weng, Y. Xu, I. Noda and J. Wu, “Development of narrow-band TLC plates for TLC/FTIR analysis,” *Analytical Methods*, no. 5, pp. 4138-4144, 2013.

- [61] Y. Jiang, X. Kang, D. Gao, A. He, R. Guo, X. Fan, Y. Zhai, J. Xia, Y. Xu, I. Noda and J. Wu, "Finding a suitable separation condition for TLC/FTIR analysis by using multiple-narrow-band TLC technique," *RSC Advances*, no. 5, pp. 21544-21549, 2015.
- [62] G. Sciutto, S. Prati, I. Bonacini, L. Litti and M. Meneghetti, "A new integrated TLC/MU-ATR/SERS advanced approach for the identification of trace amounts of dyes in mixtures," *Analytica Chimica Acta*, vol. 991, pp. 104-112, 2017.
- [63] P. Garside and P. Wyeth, "Identification of Cellulosic Fibres by FTIR Spectroscopy: Thread and Single Fibre Analysis by Attenuated Total Reflectance," *Studies in Conservation*, vol. 48, no. 4, pp. 269-275, 2003.
- [64] F. Xu, J. Yu, T. Tesso, F. Dowell and D. Wang, "Qualitative and quantitative analysis of lignocellulosic biomass using infrared techniques: A mini-review," *Applied Energy*, vol. 104, pp. 801-809, 2013.
- [65] M. Poletto, H. L. Ornaghi Júnior and A. J. Zattera, "Native Cellulose: Structure, Characterization and Thermal Properties," *Materials*, vol. 7, pp. 6105-6119, 2014.
- [66] C. Steuer, "Analysenbericht. 15 handgestrichene Farbmusterkarten verschiedener Hersteller," Doerner Institut, Munich, 2016.
- [67] P. Vandenaabeele, B. Wehling, L. Moens, H. Edwards, M. De Reu and G. Van Hooydonk, "Analysis with micro-Raman spectroscopy of natural organic binding media and varnishes used in art," *Analytica Chimica Acta*, vol. 407, no. 1-2, pp. 261-274, 2000.

- [68] F. A. Miller and C. H. Wilkins, "Infrared Spectra and Characteristic Frequencies of Inorganic Ions," *Analytical Chemistry*, vol. 8, no. 24, pp. 1253-1294, 1952.
- [69] C. Genestar and C. Pons, "Earth pigments in painting: characterisation and differentiation by means of FTIR spectroscopy and SEM-EDS microanalysis," *Anal Bioanal Chem*, vol. 382, p. 269–274, 2005.
- [70] A. Čiuladienė, A. Luckutė, J. Kiuberis and A. Kareiva, "Investigation of the chemical composition of red pigments and binding media," *Chemija*, vol. 29, no. 4, p. 243–256, 2018.
- [71] S.-M. Doncea and R.-M. Ion, "FTIR (DRIFT) analysis of some printing inks from the 19th and 20th centuries," *Revue Roumaine de Chimie*, vol. 59, no. 3-4, pp. 173-183, 2014.
- [72] E. L. Richter and H. Härlin, "A nineteenth-century collection of pigments and painting materials," *Studies in Conservation*, vol. 19, no. 2, pp. 76-82, 1974.
- [73] G. Moretti and C. Gervais, "Raman spectroscopy of the photosensitive pigment Prussian blue," *Journal of Raman Spectroscopy*, vol. 49, pp. 1198-1204, 2018.
- [74] K. Keune, J. J. Boon, R. Boitelle and Y. Shimadzu, "Degradation of Emerald green in oil paint and its contribution to the rapid change in colour of the Descente des vaches (1834–1835) painted by Théodore Rousseau," *Studies in Conservation*, vol. 58, no. 3, pp. 199-210, 2013.
- [75] I. Fiedler and M. A. Bayard, "Emerald Green and Scheele's Green," in *Artists' Pigments. A Handbook of Their History and Characteristics*, vol. 3, E. West Fitzhugh, Ed., London, Archetype Publications, 1997, pp. 219-271.

- [76] D. Buti, F. Rosi, B. G. Brunetti and C. Miliani, "In-situ identification of copper-based green pigments on paintings and manuscripts by reflection FTIR," *Anal. Bioanal. Chem.*, vol. 405, no. 8, p. 2699–2711, 2013.
- [77] J. Suk Oh, J. Eun Choi and Y. Hee Choi, "Study on the Copper-Arsenic Green Pigments used on Shamanic Paintings in the 19~20th century," *Journal of Conservation Science*, vol. 31, no. 3, pp. 193-214, 2015.
- [78] B. Gilbert, S. Denoël, G. Weber and D. Allart, "Analysis of green copper pigments in illuminated manuscripts by micro-Raman spectroscopy," *Analyst*, vol. 128, pp. 1213-1217, 2018.
- [79] T. J. S. Learner, *Analysis of Modern Paints, Canada: The Getty Conservation Institute*, 2004.
- [80] V. Otero, M. F. Campos, J. V. Pinto, M. Vilarigues, L. Carlyle and M. J. Melo, "Barium, zinc and strontium yellows in late 19th–early 20th century oil paintings," *Heritage Science*, vol. 5, no. 46, 2017.
- [81] S. Bruni, F. Cariati, F. Casadio and L. Toniolo, "Spectrochemical characterization by micro-FTIR spectroscopy of blue pigments in different polychrome works of art," *Vibrational Spectroscopy*, vol. 20, p. 15–25, 1999.
- [82] R. L. Virta, "The Talc Industry-An overview," *Bureau of Mines Information Circular*, vol. IC 9220, pp. 2-11, 1989.
- [83] Museum of Fine Arts, Boston, "Conservation and Art Materials Encyclopedia Online (CAMEO). Alizarin, Synthetic," 25 October 2019. [Online]. Available: http://cameo.mfa.org/wiki/Alizarin,_synthetic. [Accessed 10 January 2020].

- [84] A. Vila and J. F. García, "Analysis of the Chemical Composition of Red Pigments and Inks for the Characterization and Differentiation of Contemporary Prints," *Analytical Letters*, vol. 40, no. 10, pp. 1274-1285, 2012.
- [85] Museum of Fine Arts, Boston, "Conservation and Art Materials Encyclopedia Online (CAMEO). Hansa Yellow," 4 November 2019. [Online]. Available: http://cameo.mfa.org/wiki/Hansa_yellow. [Accessed 10 January 2020].
- [86] H. Standeven, "'Cover the Earth": A History of the Manufacture of Household Gloss Paints in Britain and the United States from 1920s to 1950s," in *Modern Paints Uncovered*, London, 2006.
- [87] A. Neves, E. M. Angelin, É. Roldão and M. J. Melo, "New insights into the degradation mechanism of cellulose nitrate in cinematographic films by Raman microscopy," *Journal of Raman Spectroscopy*, p. 1–11, 2018.
- [88] S. M. Cakić and L. B. Bošković, "FTIR Analysis and the Effects of Alkyd/Melamine Resin Ratio on the Properties of the Coatings," *Hemjska industrija*, pp. 637-643, 2009.
- [89] Y. Lu and J. D. Miller, "Carboxyl Stretching Vibrations of Spontaneously Adsorbed and LB-Transferred Calcium Carboxylates as Determined by FTIR Internal Reflection Spectroscopy," *Journal of Colloid and Interface Science*, vol. 256, p. 41–52, 2002.
- [90] M. Cotte, E. Checroun, W. De Nolf, Y. Taniguchi, L. De Viguerie, M. Burghammer, P. Walter, C. Rivard, M. Salomé, K. Janssens and J. Susini, "Lead soaps in paintings: Friends or foes?," *Studies in Conservation*, 2016.
- [91] A. Vichi, G. Eliazyan and S. G. Kazarian, "Study of the Degradation and Conservation of Historical Leather Book Covers with Macro

- Attenuated Total Reflection-Fourier Transform Infrared Spectroscopic Imaging,” *ACS Omega*, vol. 3, pp. 7150-7157, 2018.
- [92] R. v. Gorkum, *Manganese Complexes as Drying Catalysts for Alkyd Paints*, Leiden: Leiden University, 2005.
- [93] K. Hashimoto, V. Ramaiah Badarla, A. Kawai and T. Ideguchi, “Complementary vibrational spectroscopy,” *Nature Communications*, vol. 10, p. 4411, 2019.
- [94] M. Favaro, S. Bianchin, P. A. Vigato and M. Vervat, “The palette of the Macchia Italian artist Giovanni Fattori in the second half of the XIXth century,” *Journal of Cultural Heritage*, vol. 11, pp. 265-278, 2010.
- [95] R. L. Feller, “Barium Sulfate - Natural and Synthetic,” in *Artists' Pigments. A Handbook of their History and Characteristics*, vol. 1, R. L. Feller, Ed., National Gallery of Art, Washington, Archetype, 2012, pp. 47-64.
- [96] N. Bevilacqua, L. Borgioli and I. Androver Garcia, *I pigmenti nell'arte dalla preistoria alla rivoluzione industriale*, Padua: Il Prato, 2010.
- [97] W. Neugebauer, C. Sessa, C. Steuer, T. Allscher and H. Stege, “Naphthol Green – a forgotten artists’ pigment of the early 20th century. History, chemistry and analytical identification,” *Journal of Cultural Heritage*, vol. 36, p. 153–165, 2019.
- [98] E. Bishop, Ed., *Indicators*, Oxford: Pergamon, 1972.
- [99] W. Wang, Y. Yin, Z. Tan and J. Liu, “Coffee-ring effect-based simultaneous SERS substrate fabrication and analyte enrichment for trace analysis,” *Nanoscale*, no. 6, p. 9588, 2014.

- [100] M. V. Barashkov, A. I. Komyak and S. N. Shashkov , “Vibrational Spectra and Structure of Potassium Alum $KAl(SO_4)_2 \cdot 12[(H_2O)_x(D_2O)_{1-x}]$,” *Journal of Applied Spectroscopy*, vol. 71, no. 3, p. 328–333, 2004.
- [101] L. G. García Vedrenne, *Fugitive and Elusive: A Literature Review on Indigo Carmine Dyestuff from a Textile Conservation Point of View*, Glasgow: University of Glasgow, 2017.
- [102] B. Campanella, I. Degano, E. Grifoni, S. Lorenzetti, G. Lorenzetti, S. Pagnotta, F. Poggialini and V. Palleschi, “Identification of inorganic dyeing mordant in textiles by surface-enhanced laser-induced breakdown spectroscopy,” *Microchemical Journal*, vol. 139, pp. 230-235, 2018.
- [103] S. Cao, F. Kang, P. Li, R. Chen, H. Liu and Y. Wei, “Photoassisted hetero-Fenton degradation mechanism of Acid Blue 74 by a γ -Fe₂O₃ catalyst,” *RSC Advances*, vol. 5, no. 81, pp. 66231-66238, 2015.

This chapter is partially based on the paper:

D. Quintero Balbas, S. Prati, G. Sciutto, E. Catelli and R. Mazzeo, “Thin-layer chromatography/metal underlayer-ATR FTIR methodology for the study of synthetic dyes extracted from degraded wool fibres,” *New Journal of Chemistry*, no. 43, pp. 9411-9419, 2019. [DOI: 10.1039/C9NJ01872G](https://doi.org/10.1039/C9NJ01872G)

Acknowledgments

I would like to thank Dr. Heike Stege and Dr. Clarimma Sessa from the Doerner Institut of Munich for sharing the paint samples and the information related to μ -XRF and μ -Raman. I would also like to express my gratitude to the students Gianluca Ghetti and Caterina Bordin for their contribution to this work.

Chapter 2

Silver-assisted degradation of orpiment (As_2S_3) in gilding imitation: a vibrational and synchrotron radiation micro-spectroscopic study

2.1 Introduction

Orpiment (As_2S_3 , Pigment Yellow 39, C.I. 77085, 77086) is a yellow pigment that was used since ancient times in different kinds of artwork, including Egyptian and Chinese wall paintings [1] [2], manuscripts [3, 4] and Mesoamerican codex [5], Greek icons [6], Japanese Ukiyo-e prints [7], Renaissance paintings [8, 9], and decorative panels [10]. It is poor drying in siccativ oil, difficult to grind [7, 8], and toxic [11]; both its natural and artificial forms were often used by artist [8] until it was substituted by less toxic pigments, such as cadmium yellow (CdS), in the 19th century [12]. It has been encountered either alone or in mixture with other colourants, for example indigo, Prussian blue [7, 13, 14], and red oxide [15] to produce green and orange hues. Due to its characteristic yellow colour, the reason why it was called *auripigmentum* (golden pigment) [16], it was used alone or mixed with resins and metal powders to imitate gildings [7, 17, 18, 19].

In previous research, we identified orpiment in the decoration of the throne of the painting *Maestà* (Santa Maria dei Servi church, Bologna, c.1280-1285) attributed to Cimabue (1240-1302) [20] (Figure 2, next page). We

supposed that this decoration had originally a gilding appearance, which was obtained by mixing metallic silver (Ag⁰) powder with orpiment. Probably, as a consequence of the visible darkening of this mixture, the decorations were covered by a brownish layer containing an oily binder and lead-based pigments on top of which traces of a gold leaf were identified [21].

The most similar systems to the throne decoration of the painting are the gold imitation techniques used in manuscripts. These materials have been identified only in few other case, for example in polychrome sculpture [18].

These imitation techniques were produced by mixing powdered Sn and Ag with a golden colourant (i.e., saffron dye) [22]. *Porporina*, another method to imitate gold, was produced with SnS₂, mixed with real gold powder or a mixture of other metals, such as tin and mercury, and some minerals, for example, quartz or calcium carbonate. The *Mappæ Clavicula* manuscript describes complex mixtures of minium (Pb₃O₄), sand, gold powder, alum, vinegar, and orpiment in animal glue; or, brass powder, cadmium, iron sulphide, saffron, orpiment, egg white, and some resins. The *Bologna manuscript* indicates the use of mercury and tin powders to obtain a metallic appearance [23].

Other types of mixtures of orpiment and metallic silver were also observed in two easel paintings by Pietro Lorenzetti (h.1280-1348) [24] (Figure 3, next page). In this case, two separate metallic leaves were used by the painter:



Figure 1. *Maestà* (c. 1280-1285).
Attributed to Cimabue. Santa Maria dei Servi, Bologna. Before the 2015 restoration.

the inner one made of silver and the external one made of gold; both were applied over two coloured mordent layers obtained by mixing orpiment with an oily binder. The silver leaf was extremely degraded; in some points turned dark, while in others it was completely lost.

Until now, researchers have found orpiment used together with metallic leaves in the *Apocalypse* wall painting (14th century) in Westminster Abbey, in a 17th-century German sculpture [24], and in the icon *Proskynetarion* by Isaak Demetrakes (1818) [25].

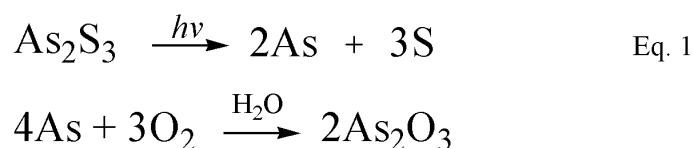
Orpiment is well-known for its sensitivity towards light exposure and humidity, which leads to irreversible changes in the appearance and physical properties of artwork [15, 26, 27, 28]. The paint layers become friable or crumbling and the degradation products migrate into the varnish and produce an unvarnished-like surface [29].

According to the earlier studies [26, 27, 28, 29], such macroscopic modifications are the result of photo-oxidation processes. The photo-degradation of orpiment has been described as a direct oxidation of the pigment to the white arsenic trioxide (arsenolite, As_2O_3) [29, 30] (Eq. 1), in some cases mediated by the primary formation of As-clusters followed by the production of sulphur radicals, which are responsible for the formation of organosulphur derivatives and sulphydric acid (H_2S) [31]. The latter degradation product may explain the well-documented darkening of copper- and/or lead-containing paintings surrounded by arsenic sulphide pigments, being the responsible of the formation of copper and/or lead sulphides [31].



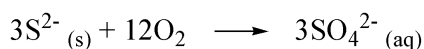
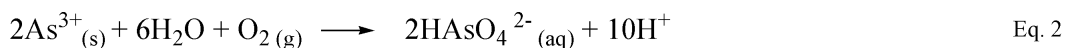
Figure 2. Pietro Lorenzetti (active between 1306 – 1345). Madonna and Child, with the Blessing Christ [middle panel], probably 1340, tempera on panel transferred to canvas. National Gallery of London.

Particular environmental conditions, such as the presence of strong oxidative pollutants (i.e., O₃ and NO₂) [32, 33], may accelerate or promote the oxidation of orpiment even without light exposure, producing the formation of As₂O₃. Besides, in the presence of moisture from the surrounding matrix and depending on the local chemical conditions (e.g., pH, matrix composition), As₂O₃ and/or another arsenite (As^{III}) species might be oxidized to arsenate (As^V) compounds [8, 29, 34, 35, 36, 37].

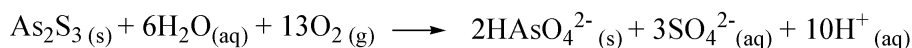


Arsenates are in general present in solution as anions (H₂AsO₄⁻ and HAsO₄²⁻) [36]. Different from other oxyanions, As is particularly movable at a wide range of redox conditions [38]. Ca, Pb, Fe and Al arsenates may be formed from the interaction with the ground layers or with the pigments present in the surroundings [34, 39]. Studies on the removal of arsenic from water showed that anions, such as SO₄²⁻ and CO₃²⁻, influence the formation of arsenate species. The results indicate that high concentrations of CO₃²⁻ ions inhibit the interaction between AsO₄³⁻ and Ca²⁺, meanwhile SO₄²⁻ promotes it [40].

Besides arsenolite and arsenates, researchers identified sulphates as secondary products of orpiment [39]. Keune and co-workers [34] suggested that sulphur transforms into different sulphur species (i.e., sulphides, sulphoxides, and thiol) before becoming sulphates. The sulphates may interact with ions from other pigments in the surroundings (e.g., Pb²⁺, K⁺, Ca²⁺) producing, for example, palmierite (K₂Pb(SO₄)₂) and syngenite (K₂Ca(SO₄)₂·H₂O) [39]. Sulphates (S^{VI}) and other oxidized sulphur-species (S^{II}, S^{IV}, S^V), attributed to organic disulphide, sulphite, monodisulphide or thiol have been detected using S-K edge XANES in paintings either in layers rich in As or in the interference between them and the ground layer [27, 34] (Eq. 2).



.....



The above-mentioned observations suggest a possible synergy between orpiment and Ag^0 in producing degradation pathways in which both chemicals change their nature.

To date, no studies regarding the effect of Ag^0 in the degradation process of orpiment exist in literature. Nevertheless, the deep understanding of such alteration pathways is highly relevant not only to select the most appropriate conservation and restoration conditions for artwork containing both Ag^0 and arsenic sulphide-based pigments but also to hypothesised the original colour and appearance of figurative and decorative details in ancient paintings.

To elucidate which mechanism takes place and to highlight the role played by different environmental agents in the degradation process of mixtures of orpiment and metallic silver, we combined the study of a set of micro-samples taken from darkened areas of the painting *Maestà* and a set of orpiment-based paint mock-ups before and after artificial aging with either UVA-visible light and/or high relative humidity conditions.

Insights into the chemical nature and stratigraphic distribution of sulphur-, silver- and arsenic-based compounds down to the submicrometer scale, were gained by using a combination of vibrational and synchrotron radiation (SR)-based X-ray microspectroscopy techniques, namely: micro-Attenuated Total Reflection-Fourier transform Infrared (μ -ATR-FT-IR), μ -Raman, SR-micro X-ray Fluorescence (μ -XRF), micro X-ray absorption near edge structure (μ -XANES) at S K-, Ag L3- and As K-edges and SR-micro X-ray Diffraction (μ -XRD).

2.2 Aim of the research

This research aims to evaluate the effect of Ag on the degradation of orpiment and determine which mechanism takes place. At this regard, three hypotheses can be formulated on the causes of darkening of the gilding imitation layer:

i) Based on earlier literature [41], the simplest scenario is that due to contact between the metallic silver and H₂S, released by the (photo-)degradation of orpiment, either acanthite (β -Ag₂S) or argentite (α -Ag₂S), both black, are formed.

ii) Alternatively, it is possible to suppose that, under oxidative circumstances, the parallel oxidation of Ag⁰ to Ag⁺ might occur locally, followed by the precipitation of AgAs-based materials, Ag₃AsO₄ and/or Ag₃AsO₃, while As₂S₃ is converted to arsenite- and arsenate-based compounds [42].

iii) As a third pathway, we can hypothesize the photo-dissolution of Ag⁺ cations in the As₂S₃ matrix, with the first step of the reaction involving the direct photo-oxidation of Ag⁰ to Ag⁺ leading to *in situ* formation of Ag₂S, and the subsequent formation of various Ag-As-S ternary compounds as final products.

We also evaluate the influence of the binding medium in the degradation process of the pigment by analysing mock-ups prepared with linseed oil and egg tempera. Based on previous researches [27], we hypothesises that different binder will have a different effect on the degradation rate of the pigment, in particular, we expect a higher degradation in egg tempera samples.

2.3 Materials and methods

2.3.1 Real samples

A sample taken from the painting *Maestà* was divided into different fragments, thus the stratigraphy is similar between them. One of the

samples was embedded in KBr (sample code CM1_{KBr}) as previously described by Prati, et al. [36]. The second sample was cast in Implex® polyester resin (sample code CM1_{resin}), the resin was allowed to cure for 24 h at room temperature and then was hand-polished successively with 120- to 12 000-grit sandpaper to expose the cross-section.

In our previous study [21] was possible to determine that the stratigraphy of the throne's decoration is composed by a white ground made of gypsum and a proteinaceous binder (layer 0), and over it, a yellow layer was applied by mixing a proteinaceous binder with Pb- and Cu-based pigments (layer 1). The original golden decoration was done mixing Ag⁰ with orpiment in a proteinaceous binder. It was covered by a proteinaceous material probably as a varnish (layer 3) [43], and later was covered by a gold leaf (layer 5) using an oily mordant (layer 4), today the Au leaf is almost detached.

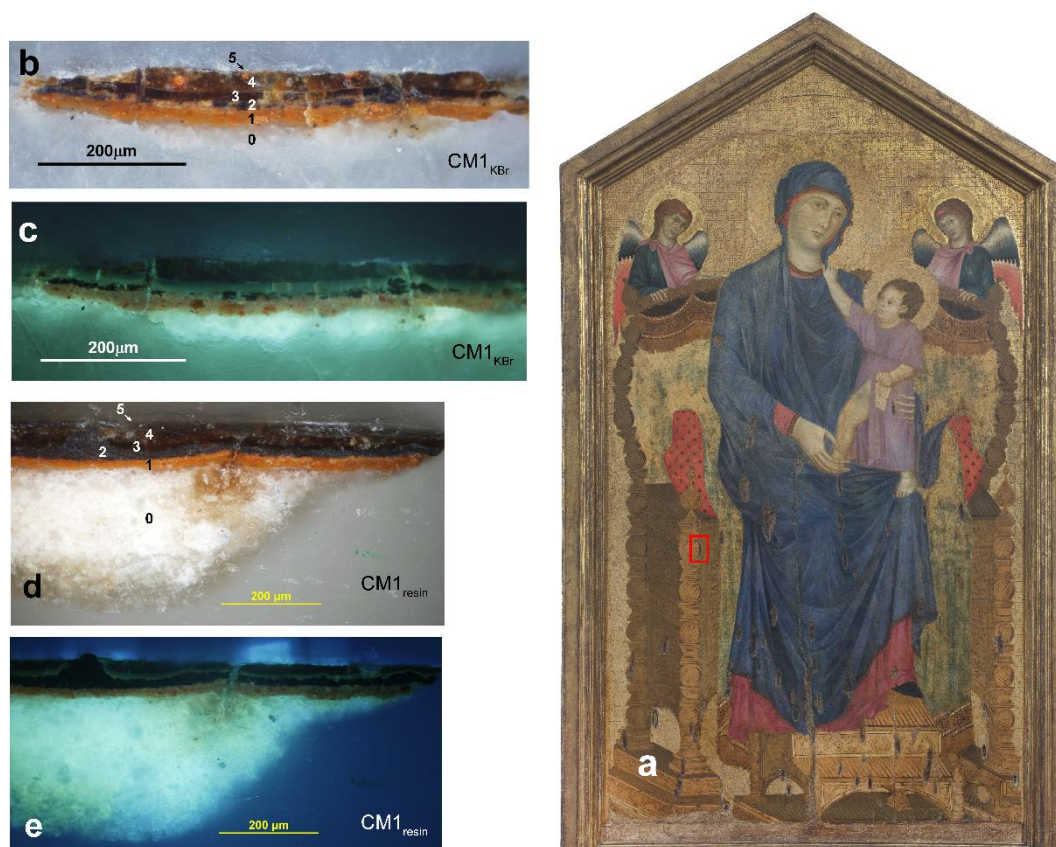


Figure 3. a) Maestà painting attributed to Cimabue, before restoration 2015, the red rectangle indicates the sampling area. b) CM1_{KBr} sample, visible light, 20x. c) CM1_{KBr} sample, UV light, 20x. d) CM1_{resin} sample, visible light, 20x, d) CM1_{resin} sample, UV light, 20x.

2.3.2 Preparation of paint mock-ups and artificial ageing protocols

Four sets of paint mock-ups were prepared over polycarbonate supports. The first set was obtained by mixing natural orpiment (Kremer, 10700) with whole egg as the binder (sample code Orp); the second set contains natural orpiment (Kremer, 10700) and metallic silver powder (Sigma-Aldrich) in the ratio 75:25 (orpiment:Ag) mixed with whole egg as the binder (sample code Orp-Ag).

The mock-ups from the third set were prepared by mixing stand linseed oil with cobalt salts (OLIFA *olio di lino cotto in sali di cobalto* 3340, Zecchi) with natural orpiment (Kremer, 10700); and for the last set the stand linseed oil was mixed with orpiment (Kremer, 10700) and metallic silver powder (Sigma-Aldrich) in the ration 75:25 (orpiment:Ag). Each type of mock-up was prepared in triplicates and subjected to two different types ageing treatments (Table 1).

UVA-visible photochemical aging experiments were performed by allocating the touch-dried paints (i.e., after about one month since their preparation) inside an in-house-made aging chamber, equipped with a UV-filtered 300-W Cermox xenon lamp ($\lambda \geq 300$ nm; see [44] for the corresponding emission spectral profile) at a relative humidity (RH) = 25% (indoor humidity level, measured daily using a thermohygrometer). The measured irradiance and temperature at the sample position were $\sim 1 \times 10^3$ W/m² and 30° C, respectively. Paints were irradiated for ca. 120 hours, thus reaching radiant exposure values of about 1.2×10^5 W/m²-hour (sample codes Orp_{UVA-Vis}, Orp-Ag_{UVA-Vis}, Orp_{OilUVA-Vis}, and Orp-Ag_{OilUVA-Vis}).

High relative humidity aging treatments were performed by placing the touch-dried paints in a vessel maintained in the dark at RH $\geq 95\%$ (achieved using distilled water) and at 40° C for an overall period of 12 days (~ 288 hours) (sample codes Orp_{95%RH} and Orp-Ag_{95%RH}).

Table 1. Summary of artificial aging conditions.

Mock-ups	Light	Relative Humidity	Temperature	Time
Orp, Orp-Ag, Orp _{oil} , and Orp-Ag _{oil}	-	-	-	-
Orp _{UVA-Vis} , Orp-Ag _{UVA-Vis} , Orp _{oilUVA-Vis} , and Orp-Ag _{oilUVA-Vis}	UVA-Vis light with $\sim 1 \times 10^5 \mu\text{m}^2$ irradiance	25%	30° C	123 h
Orp _{95%RH} ; Orp-Ag _{95%RH}	No light	95%	40° C	12 days (~288 h)

For μ -ATR-FT-IR and μ -Raman analyses cross-section samples from each type of mock-up were prepared using KBr as previously describe by Prati et al. [45], and to avoid KBr interference, cross-section samples from Orp, Orp-Ag, Orp_{UVA-Vis}, and Orp-Ag_{UVA-Vis} were cast in polyester resin for the SR-based X-ray analyses.

2.3.3 Stereo and optical microscopy

Microphotographs of the mock-ups were obtained using a Canon Powershot S50 digital camera with 5.0 megapixels coupled to a Leica MZ6 stereomicroscope with an incandescent (tungsten) lighting. The images were processed with a Canon ZoomBrowser Ex 4.5 software.

Microphotographs of cross-sections samples were taken with an Olympus BX51M microscope equipped with a digital camera Olympus DP70 using 10x, 20x, and 100x of magnification.

2.3.4 μ -ATR-FT-IR measurements

Single point analyses on the mock-up surface were performed using a Thermo Scientific Nicolet iN 10MX spectrometer in attenuated total reflection (ATR) mode with a Ge ATR crystal, using a 3% of pressure. Spectra were recorded in the range between 4000-675 cm^{-1} with an optical

aperture of 200x200 μm , a spectral resolution of 4 cm^{-1} , and 64 scans. Six points or more were performed over the surface according to the sample homogeneity.

Using the same spectrometer, maps recorded on the Cimabue cross-section were obtained with an optical aperture of 40x40 μm (corresponding to an effective investigation area of 10x10 μm) and a step size down to 8 μm , while maps on the mock-up cross-sections were performed with an optical aperture of 48x48 μm (effective investigated area of 12x12 μm) and a step size down to 8 μm . Spectra were processed with Omnic Picta and Omnic32 software.

2.3.5 μ -Raman measurements

μ -Raman analyses of sample CM1_{KBr} were performed with a ThermoFisher DXR Raman microscope. Spectra were recorded using a 780 nm frequency-stabilized single-mode diode laser with an excitation power of 5 mW. Spectra were acquired in the 55 cm^{-1} to 3299 cm^{-1} range and with a spectra resolution of 2 cm^{-1} . The acquisition time was 1 sec and 5 scans and a pinhole aperture of 50 μm . The data was processed with Omnic32 software.

μ -Raman single-point analyses were performed on mock-ups surface and cross-section samples using a Bruker Senterra Raman Microscope coupled to an Olympus BX 40 microscope equipped with a CCD camera. Spectra were recorded with a 785 nm He-Ne laser source and with excitation powers of 10 mW and 1 mW. Profiles were acquired in the 1700 cm^{-1} to 400 cm^{-1} range and with a spectral resolution of 3 cm^{-1} to 5 cm^{-1} . Acquisition time was 3 seconds and the number of scans varied from 20 to 15 to maximize the signal-to-noise ratio. All data were acquired in six or more replicates according to the sample homogeneity and in different areas (surface, middle, and inner) to determine the difference in the cross-section profile. Spectra were processed with OPUS and Omnic32 software. The data were compared with orpiment and arsenolite standards obtained from the RRUFF database [46].

2.3.6 SR-based μ -XRD mapping

μ -XRD measurements of both original paint micro-samples and mock-ups were carried out at the microprobe hutch of the Hard X-ray Micro/Nanoprobe beamline P06 of the PETRA III storage ring (DESY, Hamburg, Germany) [47]. The incident energy of the beam (i.e., 21 keV) was selected using a Si(111) crystal monochromator. A Kirkpatrick-Baez mirror system was employed to focus the beam down to $0.46 \times 0.46 \mu\text{m}^2$ (h \times v). XRD signals were acquired in transmission geometry by employing a PILATUS 300K area detector. Calibration of the diffraction setup was performed using a LaB6 reference sample. Crystalline phase distribution maps were produced by full pattern refinement using the XRDUA software package [48].

2.3.7 SR-based μ -XRF and μ -XANES measurements

S, Ag, and As speciation investigations of the paint micro-samples, mock-ups and a set of reference powders were performed at the scanning x-ray microscope (SXM) end station of beamline ID21 and the hard X-ray nanoprobe beamline ID16b of the European Synchrotron Radiation Facility (ESRF, Grenoble, France) [49, 50].

At both beamlines, measurements were carried with a fixed exit double-crystal Si(111) monochromator. A Kirkpatrick-Baez mirror system was used to focus the beam down to ca. $0.6 \times 0.4 \mu\text{m}^2$ (h \times v) and down to around $0.1 \times 0.08 \mu\text{m}^2$ (h \times v) during the investigations at ID21 and ID16b, respectively. XRF signals were collected using a single energy-dispersive silicon drift detector (Xflash 5100, Bruker) a Si drift-diode array detector at ID21 and ID16b, respectively.

At both beamlines, single-point μ -XANES spectra were acquired in XRF mode. Notably, at ID21 data were recorded by scanning the primary energy around the S K-edge (2.46-2.53 keV; energy step: 0.17 eV) and Ag L3-edge (3.34-3.42 keV; energy step: 0.25 eV), while at ID16b spectral profiles were collected by scanning the primary energy around the As K-edge (11.78-12.16 keV; energy step: 1 eV). The energy calibration was performed using

CaSO₄·2H₂O, an Ag foil and As₂S₃ as standards and by setting the position of the peak maximum of their first-order derivative spectrum at 2.4817 keV, 3.3547 keV, and 11.8693 keV, respectively. The normalization and the linear combination fit (LCF) of the spectra against a library of XANES spectra of S, Ag, and As reference compounds were performed using the ATHENA software [51]. The LCF procedure allowed us to quantitatively determine the average relative amount of sulphate (S^{VI}) and sulphide (S^{II}) compounds (expressed as % [S^{VI}]/[S_{total}], and % [S-^{II}]/[S_{total}]) and of different Ag compounds.

At ID21, maps of the same region of interest (ROI) were collected by employing 100 ms/pixel at the three following energies: (i) 2.4718 keV and (ii) 2.4827 keV to favour the excitation of the S^{II}- and S^{VI}-species, respectively and (iii) 3.4 keV to obtain the XRF intensity of all S- and Ag-species. At ID16b, maps of the same ROI were recorded by employing 100 ms/pixel at the three following energies: (i) 11.870 keV and (ii) 11.8754 keV to promote the excitation of the As^{III}-sulphides and As₂O₃/As^V-species, respectively and (iii) 12.0 keV to produce the XRF intensity of all As-species.

The software PyMca [52] was used to fit the XRF spectra and to separate the contribution of different elements. The experimental procedure used for recording and producing the S and As speciation maps is described in previous studies [53, 35].

During the μ -XANES and μ -XRF analysis, attention was paid to ensure that data were not affected by any artefacts due to X-ray beam exposure.

2.4 Results and discussion

2.4.1 Real samples: The throne decoration from the Maestà painting

In layer 2 of sample CM1_{KBr}, orpiment degradation products can be mapped using μ -FT-IR-ATR (Figure 4) thanks to the band at 795 cm^{-1} ; due to the spectral resolution, it is not possible to say unambiguously if this band is related to the As-O stretching mode of arsenolite [54] or arsenate [34, 55]. In the other layers, the band at 795 cm^{-1} is sporadically detected with a lower intensity, simultaneously associated with the band at 1090 cm^{-1} , associated to the Si-H deformation and Si-O-Si stretching of silicates respectively.

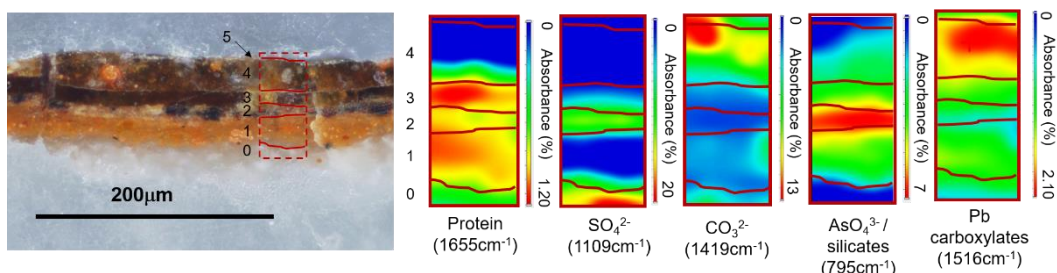


Figure 4. μ -ATR-FT-IR mapping elaborated by integrating the area of the corresponding bands. Proteinaceous material is present in layer 0 to 3 and more concentrate in layers 1 and 3. The presence of arsenates is distribute mainly in the layer 2, while sulphates are present in layers 0 and 2, Pb carboxylates are located in layer 4.

Besides, layer 2 was also characterized by an enrichment of sulphates (band at 1109 cm^{-1}); sulphates have been reported by several authors as part of the degradation products of orpiment [34, 35, 56]; however, the μ -Raman spectra from layer 2 show the main peak of gypsum at 1008 cm^{-1} ; it is not possible to assign the nature of the sulphates using only these two techniques. Also, μ -Raman analysis performed on the black silver particles suggest, thanks to the broad band centred at 218 cm^{-1} from the first longitudinal optical phonon mode, that acanthite (Ag_2S) is present [57].

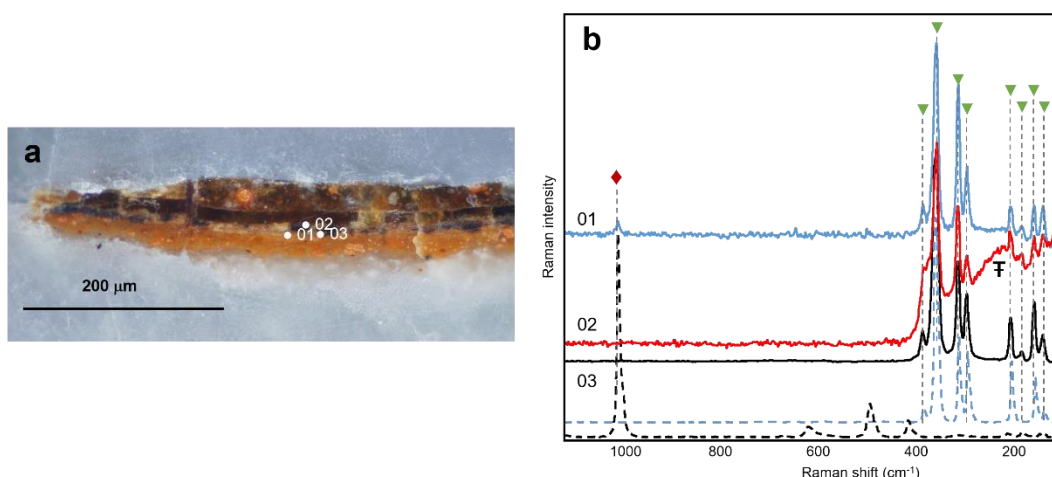


Figure 5. a) Photomicrograph of the cross-section of sample $CM1_{KBr}$, 20x DF. The number indicate the points of analysis. b) Raman spectra obtained from layer 2. The results are compared with orpiment standard (dashed blue line) and gypsum standard (black dashed line). The spectra suggest that apart from orpiment (▼), a small amount of gypsum (01, ◆) is present in the layer 2. In the black particle acanthite (marked with ⊠) was identified.

Sulphates are also mapped with FT-IR in the ground layer (layer 0) associated to gypsum, and Pb carboxylates (characteristic band 1516 cm^{-1} arising from the CO asymmetric stretching [58]) were identified in layer 4, probably due to the degradation associated to the oily binder in the mordant.

The SR- μ -XRD performed on the sample $CM1_{resin}$ confirmed the previous results. Layer 2 contains, in addition to Ag^0 and orpiment, Ag_2S , minium, a small quantity of gypsum, and hydrocerussite (Figure 6, next page). SR- μ -XANES-LCF (Figure 7, page 96) data indicates that S^{VI} and other S species with different oxidation states (IV, V) are present in layer 2, this is in accordance to what Keune [28] reported for the degradation of arsenic pigments suggesting that sulphur transforms into different states of oxidation during the degradation of orpiment.

Besides, the SR- μ -XANES confirmed the presence of As^V species (arsenates) in layer 2, the fact that they were not detected with XRD suggest that they are in a no-crystalline state, probably as ions. Surprisingly arsenolite was detected neither with XRD nor XANES, probably because it completely oxidised and formed As^V compounds.

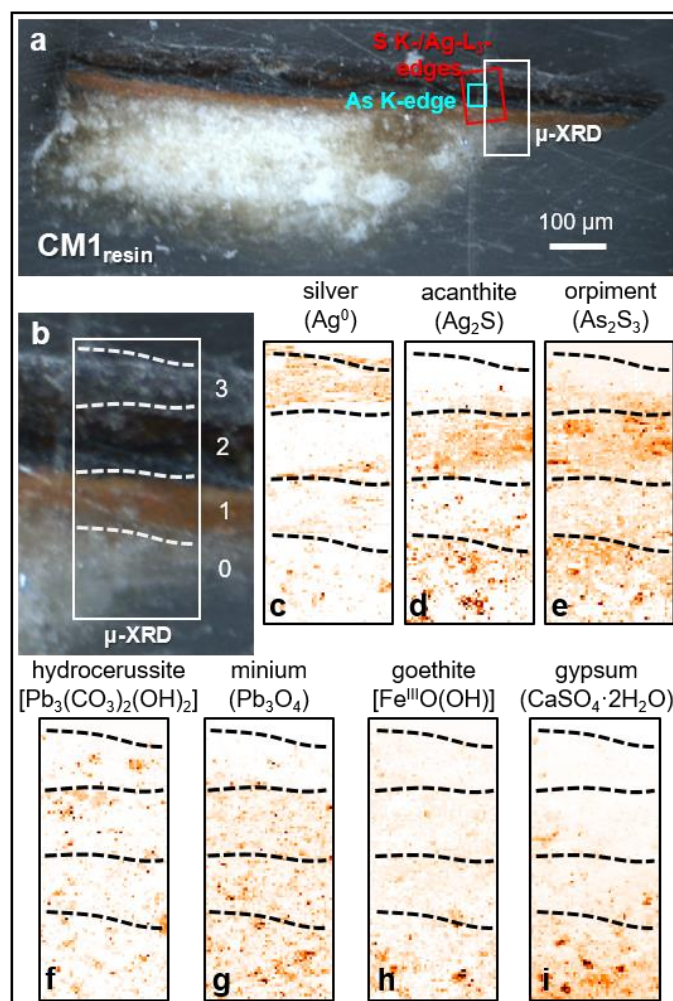


Figure 6. a) Photomicrograph of cross-section CM1_{resin} taken from a darkened gold decoration of the painting *Maestà* (see Figure 3, page 88, for the sampling location) and b) detail of the area where SR μ-XRD mapping was performed. c-i) SR μ-XRD distributions of the identified crystalline phases [map size (v×h): 167 x 75 μm²; step size (v×h): 1.5 x 1.5 μm²; exp. time: 1s/pixel; energy: 21 keV]. In a), the areas analyzed by μ-XANES/μ-XRF are also reported (see Figure 7 for the results). Data kindly provided by Dr. Letizia Monico.

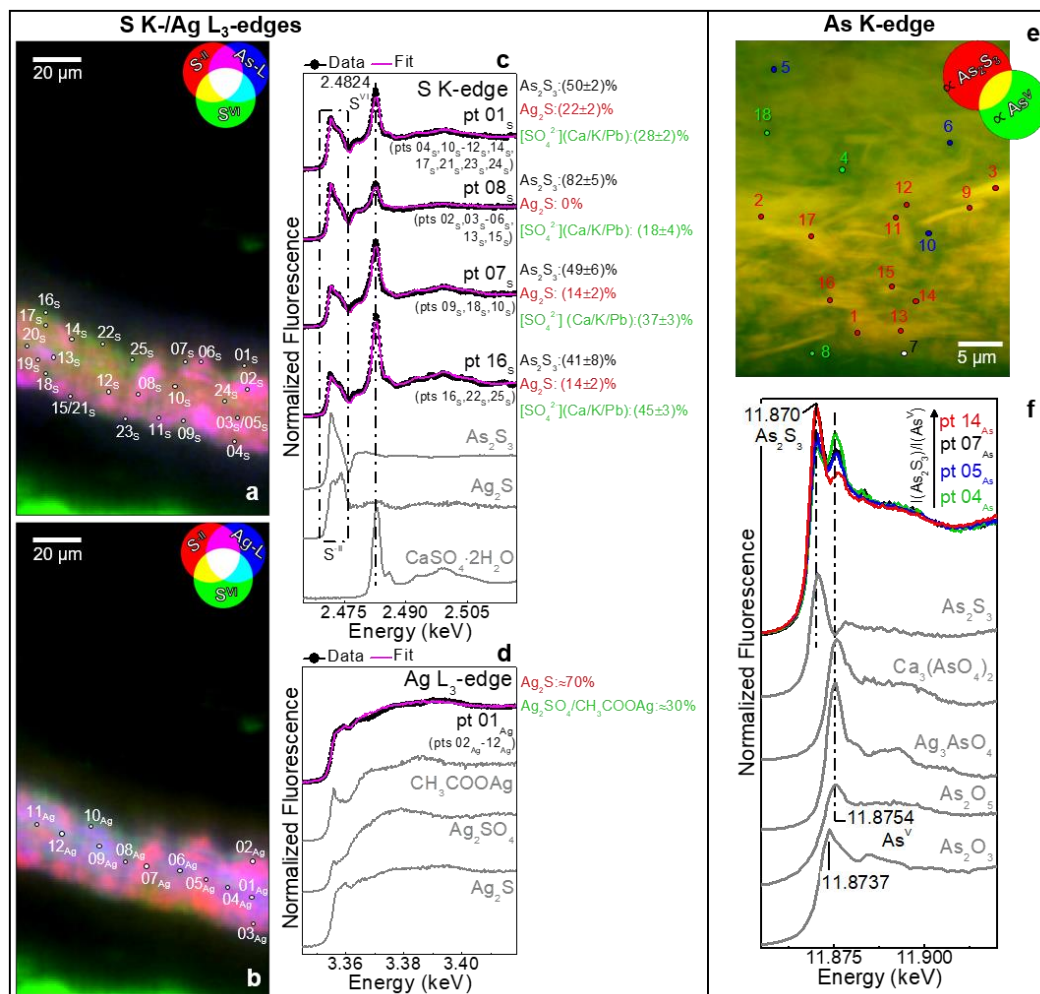


Figure 7. RGB composite SR μ -XRF images of a) $\text{S}^{\text{II}}/\text{S}^{\text{VI}}/\text{As}$ and b) $\text{S}^{\text{II}}/\text{S}^{\text{VI}}/\text{Ag}$ recorded from the area shown in Figure 6a [map size ($v \times h$): $99.5.8 \times 74.2 \mu\text{m}^2$; step size ($v \times h$): $0.5 \times 0.7 \mu\text{m}^2$; exp. time: 100 ms/pixel]. Selection of the μ -XANES spectra (black) recorded at the c) S K-edge and d) Ag L₃-edge from the spots reported in a, b) and result of the linear combination fitting (LCF) (magenta) of different S- and Ag-based compounds. In grey, the spectral profiles of selected reference compounds are reported for comparison. Numbers in brackets refer to the spectra showing similar features to those reported. e) RG composite SR μ -XRF images of $\text{As}_2\text{S}_3/\text{As}^{\text{V}}$ [map size ($v \times h$): $30.7 \times 38.1 \mu\text{m}^2$; step size ($v \times h$): $0.1 \times 0.1 \mu\text{m}^2$; exp. time: 100 ms/pixel] and f) selection of the As K-edge μ -XANES spectra recorded from the spots shown in e) compared to those of various As-references. In e, f), different colours refer to spectra characterized by similar spectral features and that show a variable ratio between the intensity of the white lines of As_2S_3 and As^{V} -compounds. Data kindly provided by Dr. Letizia Monico.

Table 2. Summary of the results of the analyses of the real samples from the painting Maestà.

Layer	μ -ATR-FTIR	μ -Raman	SR- μ -XRD	SR- μ -XRF	SR- μ -XANES-LCF
5	-	-	Ag	Ag, P	Ag, S ^{VI} , Pb compounds, Ag ₂ SO ₄ , Ag ₂ S
4	Pb carboxylates, oily binder, CaCO ₃ (localized)	-	Hydrocerussite, Minium	Pb, Si, Cu, Ca, Cl	-
3	Proteins	-	-	Cl, P	-
2	Arsenate species, protein, sulphates	Ag ₂ S, Orpiment, gypsum	Orpiment, Ag ₂ S, gypsum, minium, hydrocerussite	As, Ag, S, Mg, Na, Cl, Pb, Ca	S ^{II} , S ^{IV} , S ^V , S ^{VI} , As ^V , As ^{III} , phosgenite or laurionite, palmierite, Ag ₂ S, Ag ₂ SO ₄
1	Silicates, protein	-	Minium, goethite	Cl, Si, Pb, Mg	-

2.4.2 Assessing the influence of silver: Unaged mock-ups

Samples Orp and Orp-Ag μ -FT-IR and μ -Raman analyses performed both on the surface and the cross-section samples suggest a peculiar role played by silver in the formation of degradation products.

Indeed, in sample Orp no degradation products were detected (Band assignation of binder and orpiment in Appendix 3). While in sample Orp-Ag μ -FT-IR spectra suggest the presence of sulphates (band at 1160 cm⁻¹) and the band at 796 cm⁻¹ (Figure 8, next page), which can be assigned to the As-O bond stretching either from arsenolite or arsenates. These degradation products are confined to the surface of the cross-section. μ -XANES S-K edge confirmed the presence of sulphates in the sample Orp-Ag, while μ -XRD show that arsenolite is present in a very low concentration (Figure 10, page 99). These results indicate that the presence of Ag seems to promote the degradation of orpiment and, simultaneously, degrades by tarnishing, due to the presence of S compounds.

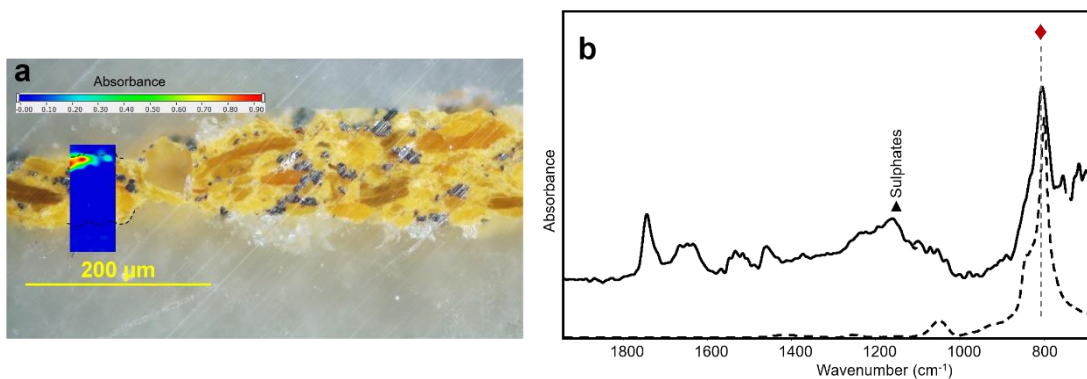


Figure 8. Mapping of sample Orp-Ag, arsenolite formed on the surface of the sample and close to the Ag particles. The spectrum from the surface (black line) shows the characteristic peak of arsenolite/arsenates (♦) (standard dashed line), as well as the presence of sulphates (▲).

The μ -Raman analyses performed on the sample Orp-Ag suggest the presence of As_2O_3 in a very low amount; indeed, just the main band at 369 cm^{-1} (A_{1g}) was detected [27, 29, 30]. μ -Raman spectra acquired on the black silver particles present a broad band centred around 221 cm^{-1} , which may be assigned to the first longitudinal optical phonon mode of acanthite (Ag_2S) [57], this was confirmed by SR- μ -XRD (Figure 10, next page).

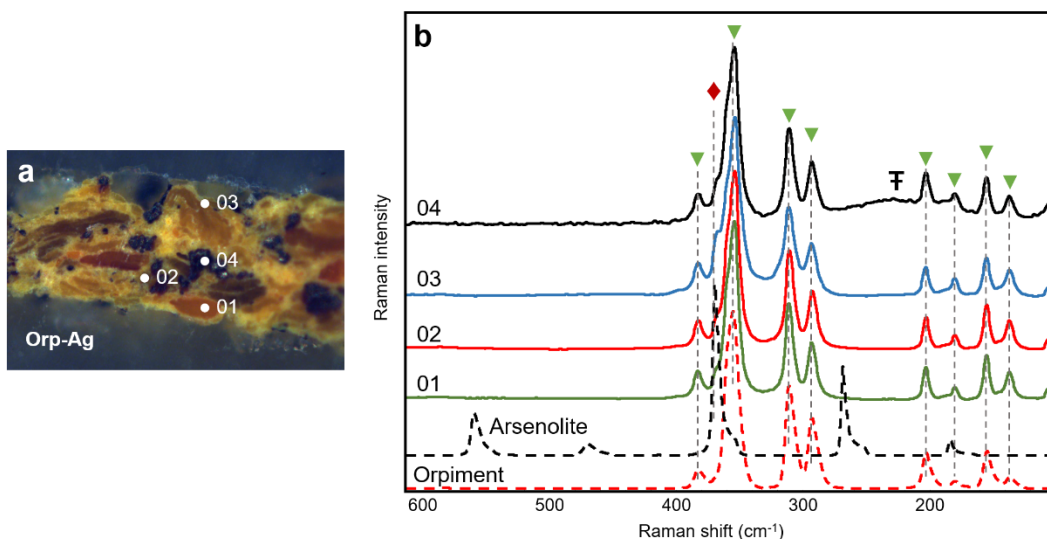


Figure 9. a) Photomicrograph of the cross-section of sample Orp-Ag (20x, DF), the numbers indicate the points of analysis. b) Raman spectra from sample Orp-Ag from different areas of the cross-section, the spectra are compared with orpiment (dashed black line) and arsenolite (red dashed line) standards. The spectra clearly shows the peaks characteristic of orpiment (▼) and arsenolite (03) (♦). The broad band characteristic of acanthite is present in the spectra obtained from the black particle (04) (⊠).

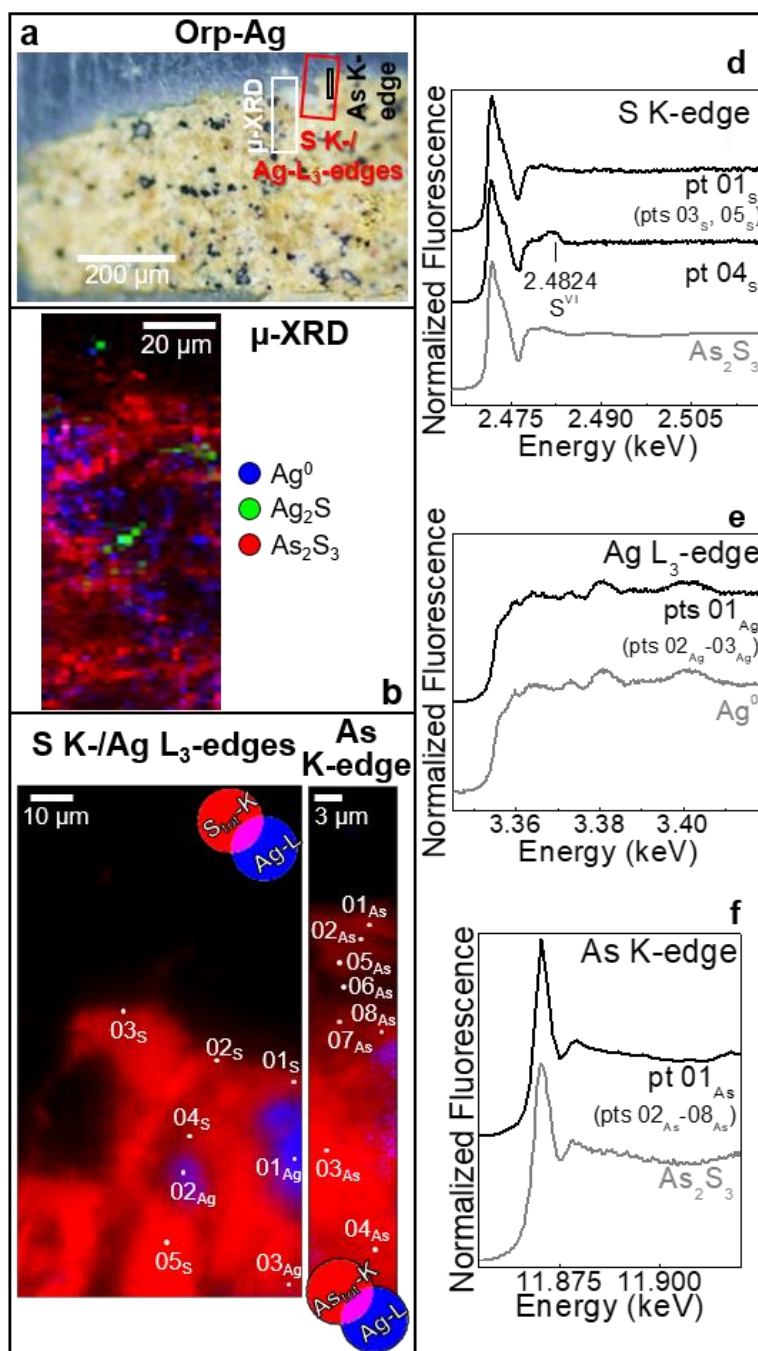


Figure 10. a) Photomicrograph of Orp-Ag cross-section before aging. b) Composite SR μ -XRD maps of Ag^0 (blue) Ag_2S (green) As_2S_3 (red) [map size (vxh): $150 \times 50 \mu\text{m}^2$; step size (vxh): $1.5 \times 2 \mu\text{m}^2$; exp. time: 1s/pixel; energy: 21 keV]. c) RB composite SR μ -XRF images of (left) $S_{\text{total}}/\text{Ag}$ [map size (vxh): $117 \times 65 \mu\text{m}^2$; step size (v x h), $0.86 \times 1 \mu\text{m}^2$; exp. time: 100 ms/pixel; energy: 3.4 keV] and (right) $As_{\text{total}}/\text{Ag}$ [map size (vxh): $56.9 \times 9.9 \mu\text{m}^2$; step size (v x h): $0.1 \times 0.15 \mu\text{m}^2$; exp. time: 100 ms/pixel; energy: 12.00 keV]. Selection of the μ -XANES spectra (black) recorded at the d) S K-edge, e) Ag L3-edge and f) As K-edge from the spots shown in c). In grey the spectral profiles of selected reference compounds are reported for comparison. In a), rectangles show the areas where maps of b,c,f) were recorded. In d-f), numbers in brackets refer to the spectra showing similar features to those reported. Data kindly provided by Dr. Letizia Monico.

2.4.3 Assessing the influence of light: Artificial aging with light

The mock-ups Orp_{UVA-Vis} and Orp-Ag_{UVA-Vis} aged in the presence of light became whitish due to the formation of some transparent As₂O₃ crystals over the surface. μ -FT-IR, μ -Raman, and SR- μ -XRD analyses performed on the cross-section of both the two samples confirm that arsenolite is confined over the first microns of the sample surface, suggesting that the light plays a role in the degradation process. Besides, in both the two types of mock-ups, m-FT-IR and S K-edge m-XANES suggest the presence of sulphates close to the surface.

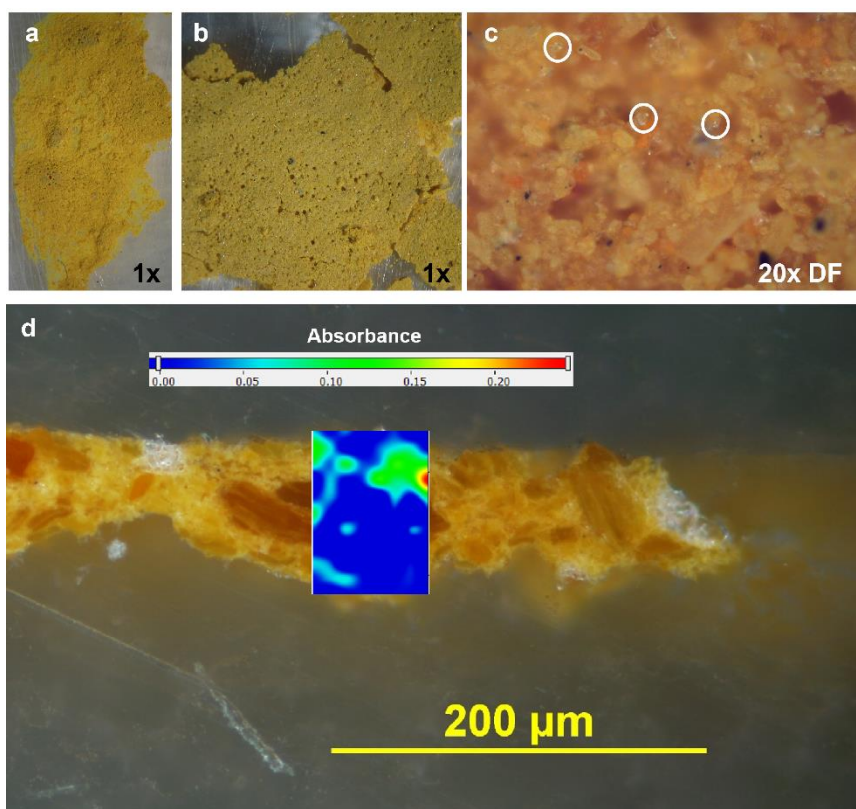


Figure 11. a) Photomicrograph sample Orp, 1x. b) Photomicrograph of sample Orp_{UVA-Vis}, 1x, c) Micrograph of sample Orp_{UVA-Vis}, the arsenolite crystals are indicated with white circles, 20x DF. d) μ -FTR mapping of sample Orp_{UVA-Vis} done integrating the peak area at 803 cm^{-1} , arising from arsenolite. It is located in the surface of the sample.

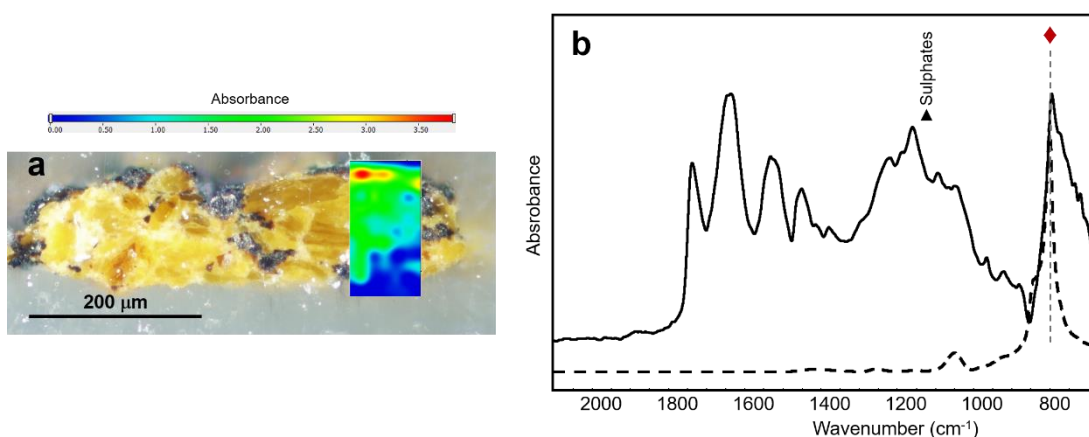


Figure 12. a) Mapping of the cross-section of sample Orp-Ag_{UVA-Vis} done after integrating the area under the peak at 796 cm⁻¹. b) Spectrum obtained from the surface of the cross-section (solid black line) compared with arsenolite (◆) standard (dashed black line). The band attribute to sulphates is also evident (▲).

Moreover, in both the two types of mock-ups, μ -FT-IR and μ -XANES S-K edge suggest the presence of sulphates close to the surface. As in the unaged samples, the broad band ascribable to Ag₂S was detected on the Ag black particles, both by μ -Raman and SR- μ -XRD.

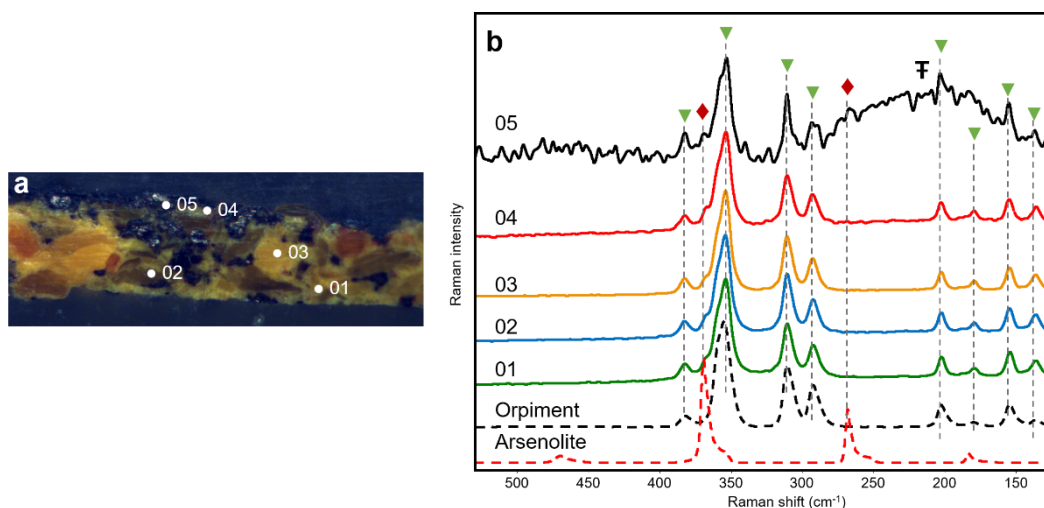


Figure 13. a) Photomicrograph (20x, DF) of the cross-section from mock-up Orp-Ag_{UVA-Vis}, the numbers indicate the different points of analysis. b) The spectra clearly shows the peaks characteristic of orpiment (▼) and, only in the surface (04 and 05) of the sample the peaks of arsenolite (◆). The spectrum from one of the black particles (05) also presents the broad band assignet to acanthite (⌘).

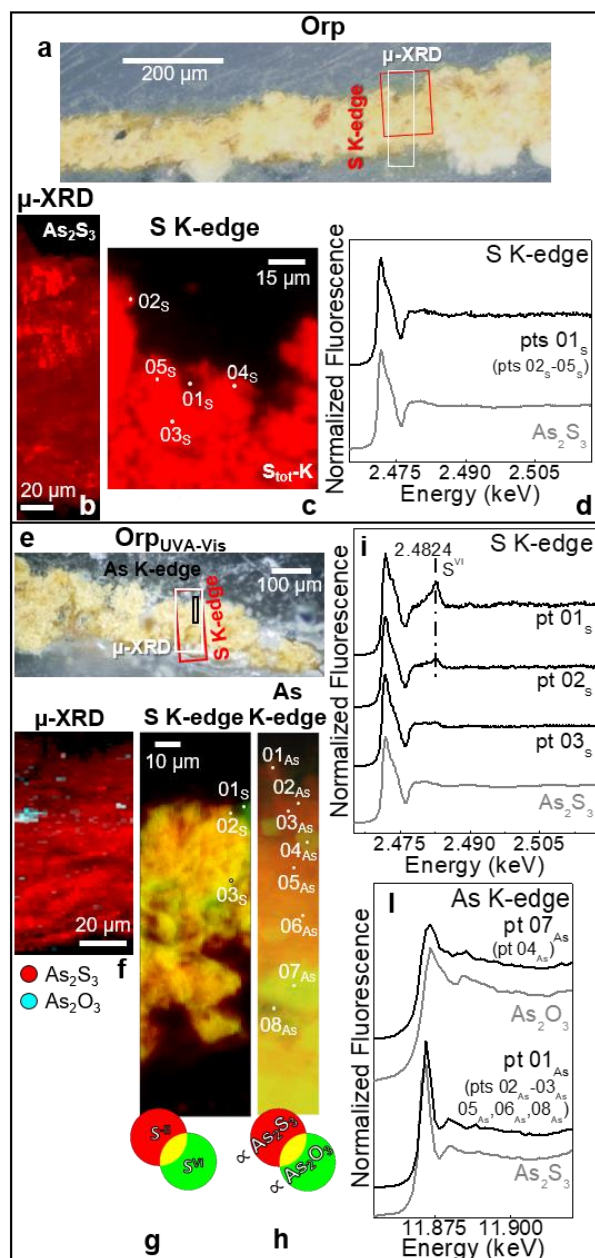


Figure 14. a) Photomicrograph of Orp cross-section before aging and b) corresponding SR μ -XRD image of As_2S_3 [map size (vxh): $189.5 \times 50 \mu\text{m}^2$; step size (vxh): $1.5 \times 2 \mu\text{m}^2$; exp. time: 1s/pixel; energy: 21 keV]. c) SR μ -XRF image of S_{total} [map size (vxh): $84 \times 97 \mu\text{m}^2$; step size (v x h): $1 \times 1 \mu\text{m}^2$; exp. time: 100 ms/pixel; energy: 3.4 keV] and d) selected S K-edge μ -XANES spectrum (black) recorded from the areas shown in c), compared to that of As_2S_3 reference (grey). e) Photomicrograph of Orp-Ag cross-section after exposure to UVA-Visible light (RH =25%, T = 30°C) and f) corresponding composite SR μ -XRD maps of As_2S_3 (red) and As_2O_3 (cyan) [map size (vxh): $145.5 \times 50 \mu\text{m}^2$; step size (vxh): $1.5 \times 2 \mu\text{m}^2$; exp. time: 1s/pixel; energy: 21 keV]. RG SR μ -XRF images of g) $S^{\text{II}}/S^{\text{VI}}$ [map size (vxh): $159 \times 46 \mu\text{m}^2$; step size (v x h): $1 \times 1 \mu\text{m}^2$; exp. time: 100 ms/pixel] and h) $\text{As}_2\text{S}_3/\text{As}_2\text{O}_3$ [map size (vxh): $63 \times 9.9 \mu\text{m}^2$; step size (v x h): $0.1 \times 0.15 \mu\text{m}^2$; exp. time: 100 ms/pixel]. Selection of the μ -XANES spectra recorded at the i) S K-edge and j) As K-edge from the spots reported in g,h), compared to those of a set of reference compounds (gray). In a,e), rectangles show the areas where maps of b,c,f-h) were recorded. In d,i,j), numbers in brackets refer to the spectra showing similar features to those reported. Data kindly provided by Dr. Letizia Monico.

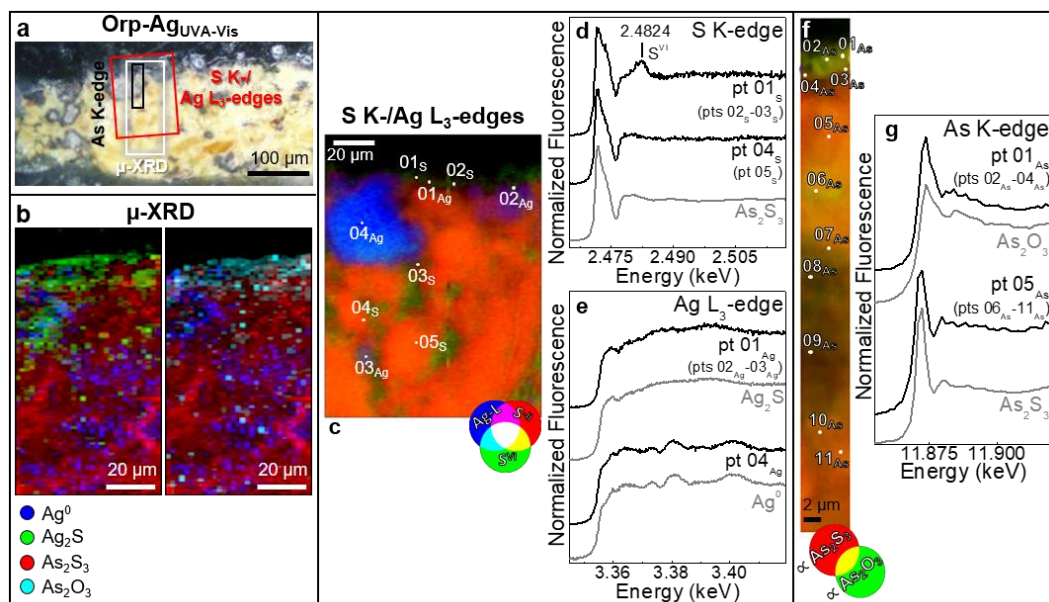


Figure 15. a) Photomicrograph of Orp-Ag cross-section after exposure to UVA-Visible light ($RH=25\%$, $T=30^{\circ}C$). b) Composite SR μ -XRD images of Ag^0 (blue) Ag_2S (green) As_2S_3 (red) and As_2O_3 (cyan) [map size (vxh): $150 \times 60 \mu m^2$; step size (vxh): $1.5 \times 2 \mu m^2$; exp. time: 1s/pixel; energy: 21 keV]. c) RGB composite SR μ -XRF images of S^{II}/S^{VI}/Ag and μ -XANES spectra (black) recorded at the d) S K-edge and e) Ag L₃-edge from the areas shown in c), compared to those of selected reference compounds (gray). f) RG composite SR μ -XRF images of f) As_2S_3/As_2O_3 [map size (vxh): $58.1 \times 5.4 \mu m^2$; step size (vxh): $0.1 \times 0.1 \mu m^2$; exp. time: 100 ms/pixel] and g) selection of the μ -XANES spectra recorded at the As K-edge from the spots reported in f), compared to those of a set of reference compounds (gray). In a), rectangles show the areas where maps of b,c,f) were recorded. In d-e, g), numbers in brackets refer to the spectra showing similar features to those reported. Data kindly provided by Dr. Letizia Monico.

2.4.4 Assessing the influence of humidity: Orp_{95%RH} and Orp-Ag_{95%RH}

A small amount of arsenolite was detected on the surface of sample Orp_{95%RH} using FT-IR. Surprisingly, analyses on the cross-section did not evidence the presence of any degradation product suggesting that the amount formed on the surface is low and not homogeneously distributed. The same findings were confirmed by μ -Raman and μ -XRD analyses.

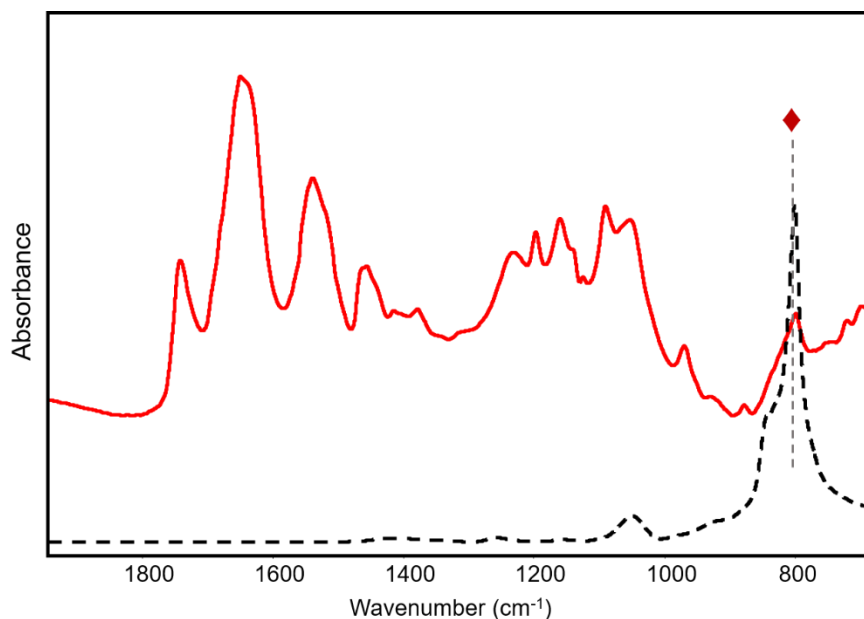


Figure 16. FT-IR spectrum from the surface of the sample Orp95%RH (solid red line) and arsenolite standard (dashed black line), the main characteristic peak of arsenolite is marked with \blacklozenge .

Conversely, FT-IR analyses performed on sample Orp-Ag95%RH showed that arsenolite is distributed through the paint layer at a higher concentration in comparison with sample Orp95%RH. This suggests that even without light exposure arsenolite is formed and confirms the role of Ag in promoting the degradation of orpiment. Sulphates were also detected in sample Orp-Ag95%RH as suggested by the band around 1090cm^{-1} in FT-IR spectra.

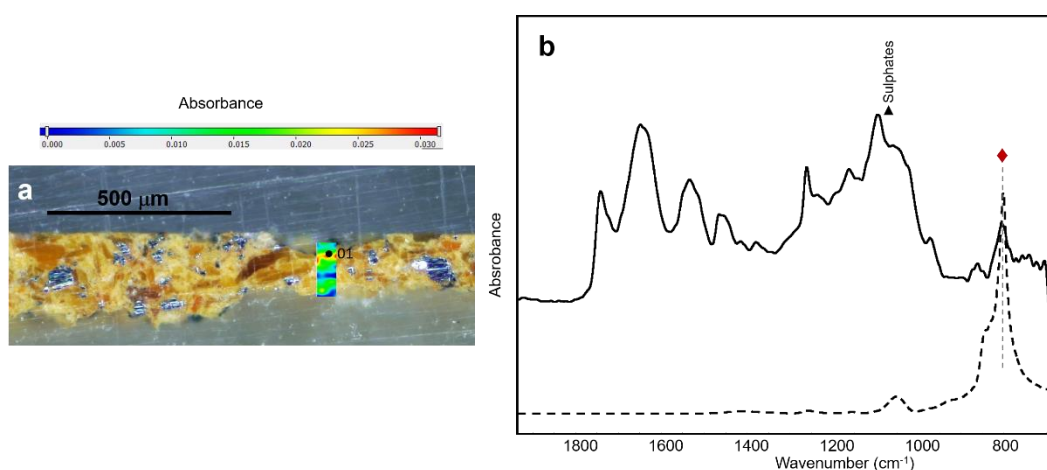


Figure 17. a) μ -FT-IR mapping of sample Orp-Ag95%RH done with the height of the peak b) the spectrum (black solid line) was obtained from the surface of sample Orp-Ag95%RH (01). The spectra shows the peaks characteristic of orpiment (red solid line) (\blacktriangledown), and the peaks of arsenolite (black dashed line) (\blacklozenge).

The presence of arsenolite was confirmed by μ -Raman analysis thanks to the characteristic peaks at 367cm^{-1} and 267cm^{-1} . Similar to the other samples that contain Ag, μ -Raman spectra acquired on the silver particles showed a broad band at 215cm^{-1} that confirms the presence of Ag_2S . These results were also confirmed by μ -XRD analysis. No arsenates were detected in none of the two mock-ups.

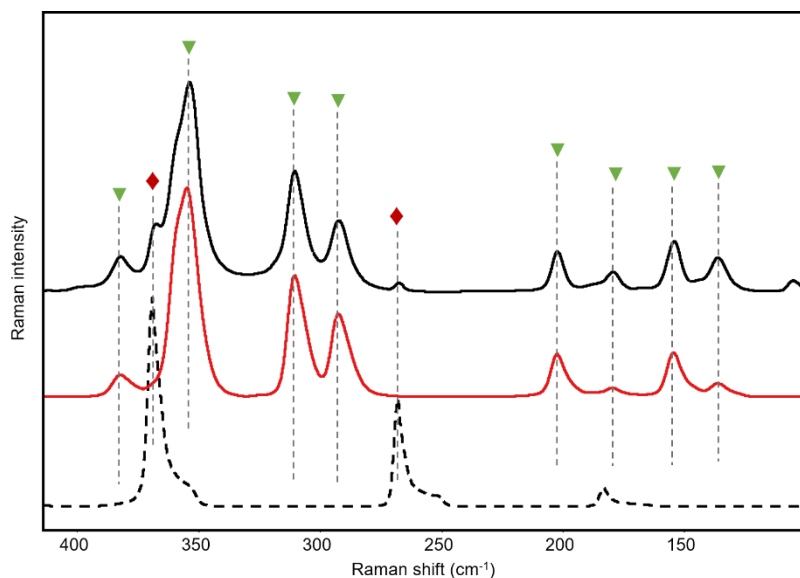


Figure 18. Raman spectrum (black solid line) from the surface of sample Orp-Ag_{95%RH}. The spectra shows the peaks characteristic of orpiment (red solid line) (▼), and the peaks of arsenolite (black dashed line) (◆).

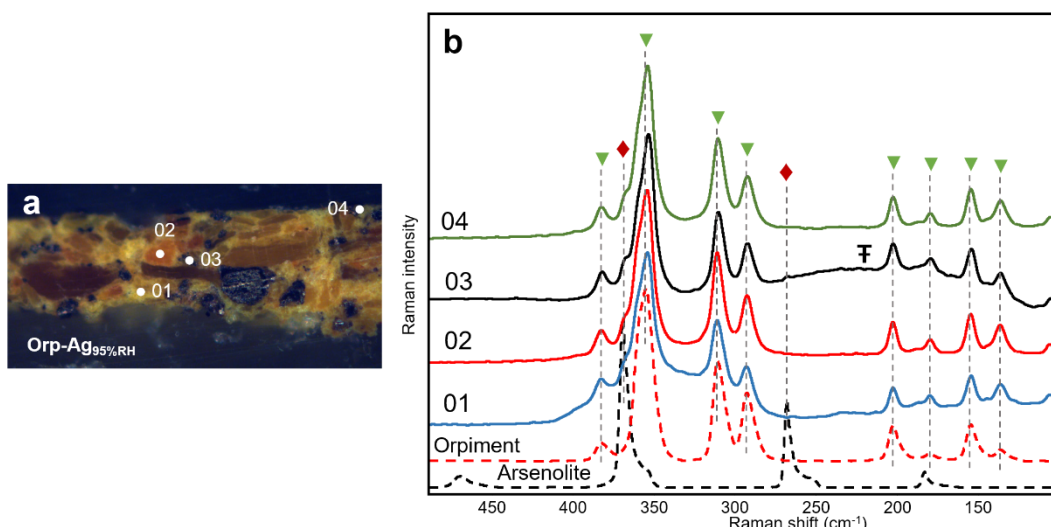


Figure 19. a) Photomicrograph (10x) of the cross-section from mock-up Orp-Ag_{95%RH}, the number (01) indicates the point from which the spectrum was obtained. b) The spectrum shows the peak characteristic of arsenolite (◆) and the band assigned to sulphates (▼).

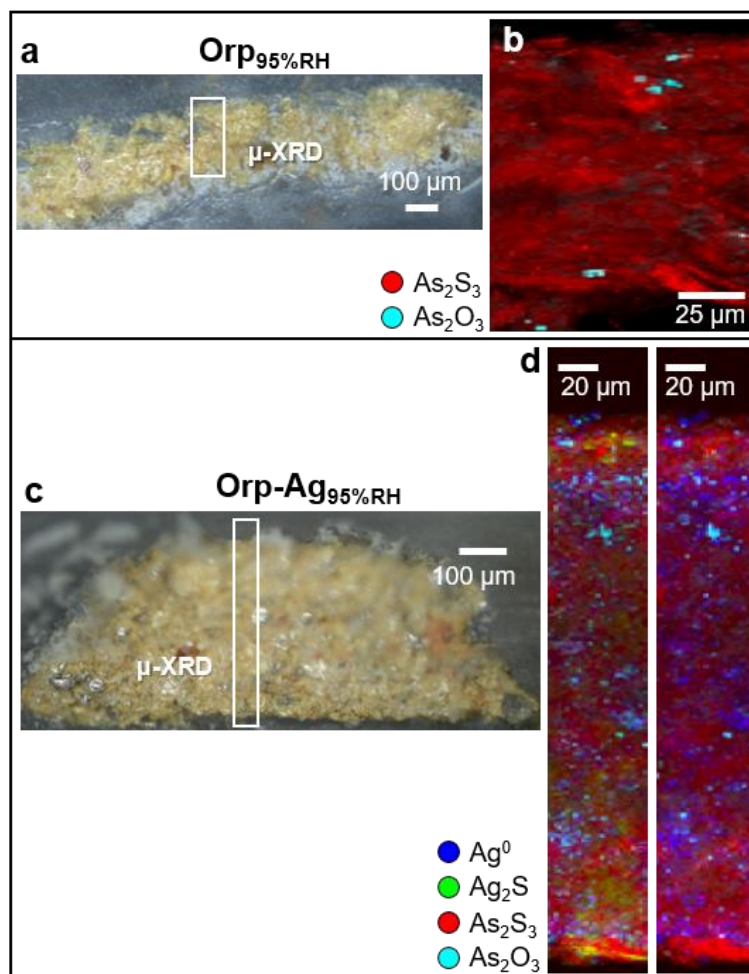


Figure 20. Photomicrograph of a) $\text{Orp}_{95\%RH}$ and c) $\text{Orp-Ag}_{95\%RH}$ cross-section after exposure to $\text{RH} \geq 95\%$ ($T = 40^\circ\text{C}$, 12 days). b,d) Composite SR $\mu\text{-XRD}$ images of Ag^0 (blue) Ag_2S (green) As_2S_3 (red) and As_2O_3 (cyan) recorded from the thermally aged b) $\text{Orp}_{95\%RH}$ [map size (vxh): $239 \times 100 \mu\text{m}^2$; step size (vxh): $1 \times 2 \mu\text{m}^2$; exp. time: 0.5 s/pixel; energy: 21 keV] and d) $\text{Orp-Ag}_{95\%RH}$ paints [map size (vxh): $430.5 \times 50 \mu\text{m}^2$; step size (vxh): $1.5 \times 2 \mu\text{m}^2$; exp. time: 1s/pixel; energy: 21 keV]. In a,c), rectangles show the regions where maps of b,d) were acquired. Data kindly provided by Dr. Letizia Monico.

2.4.5 Assessing the influence of the binding medium: linseed oil samples

The influence of the binder on the degradation of orpiment was already reported by Vermeulen and colleagues [27], the authors suggest an intermediate effect of oil binder, similar to egg white and lower than the effect of the egg yolk. In this research, the egg samples were prepared using equal parts of egg yolk and egg white, the reason why we expected a similar behaviour to the oil, surprisingly our results suggest that linseed oil may accelerate the degradation.

The analyses of mock-ups made with stand linseed oil show differences in the pigment degradation in comparison to the egg tempera samples. We detected arsenolite crystals distributed in the unaged sample Orp_{oil} with μ -FT-IR (intense sharp peak at 794 cm^{-1}) and μ -XRD (Figures 21 and 22). Sulphates were also identified in the vicinity to the area where arsenolite was detected using μ -FT-IR (broad band at 1085 cm^{-1}) and was confirmed with μ -XANES (Figure 23, next page). Similar results were obtained from the sample Orp-Ag_{oil}, in which in addition to arsenolite, acanthite was also identified. This differs from the results obtained from the tempera mock-ups where no degradation products were identified in the sample Orp (unaged).

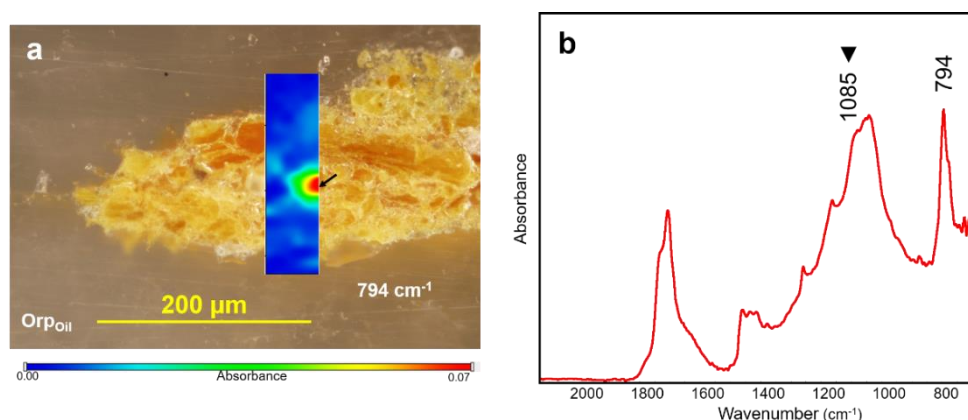


Figure 21. a) Microphotograph of sample Orp_{Oil} and μ -FT-IR map done using the height of the peak at 794 cm^{-1} , it suggests that arsenolite (confirmed by μ -XRD) formed in a localised area of the sample, b) FT-IR spectrum obtained from Orp_{Oil} (indicated with an arrow). In addition to the band at 794 cm^{-1} , the broad band at 1085 cm^{-1} (marked with \blacktriangledown) suggests the presence of sulphates.

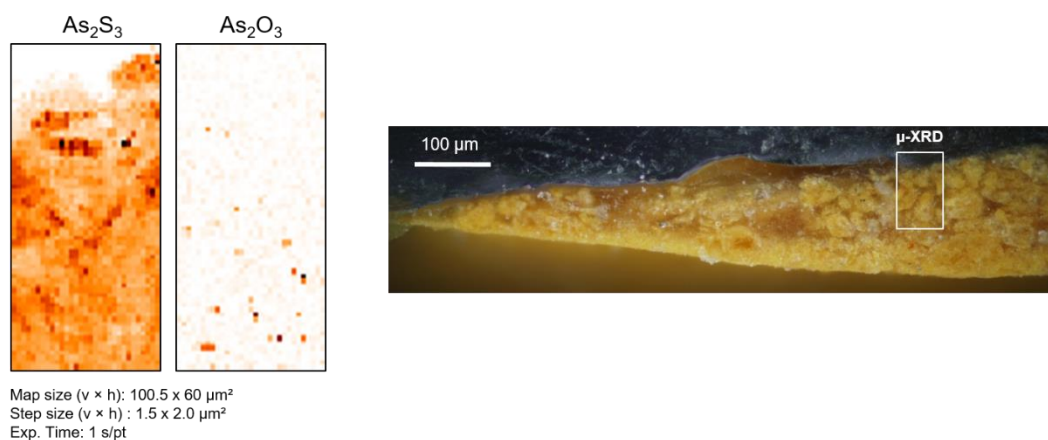


Figure 22. μ -XRD map from sample Orp_{Oil} in addition to orpiment, arsenolite was identified widespread through the sample. These results confirm the attribution of the band 794 cm^{-1} (Figure 21) to arsenolite. Data kindly provided by Dr. Letizia Monico.

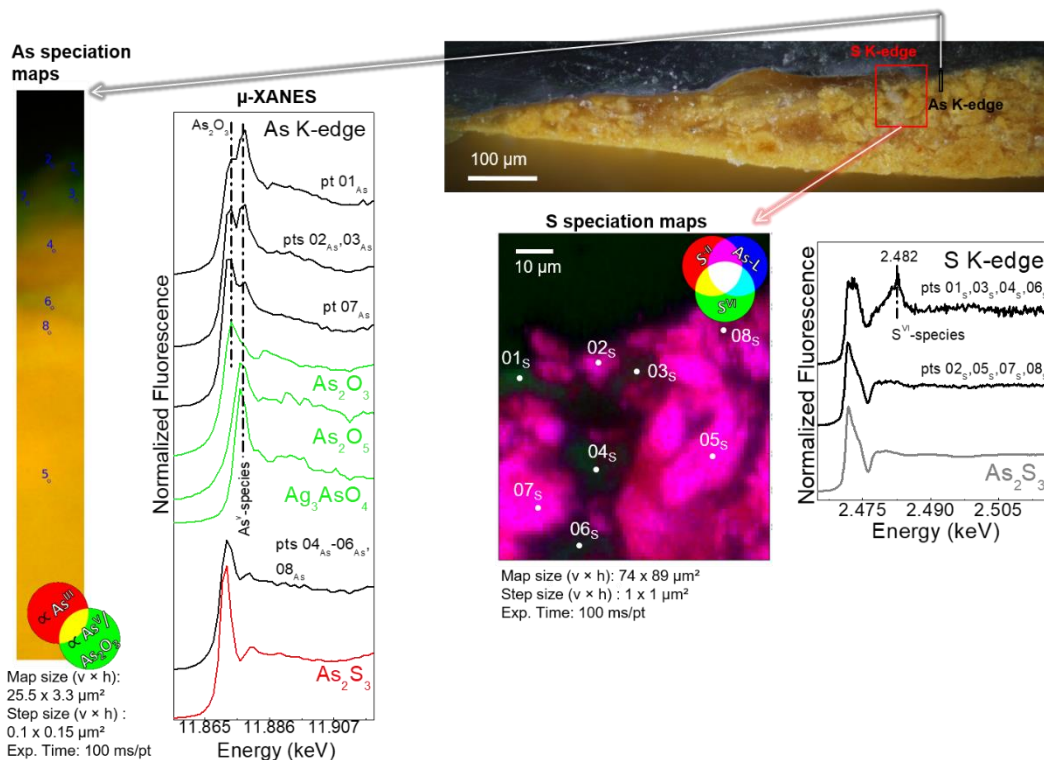


Figure 23. As K-edge and S K-edge μ -XANES maps from sample *Orp_{Oil}*, it was identified a localized presence of As_2O_3 , As^{V} -species (pts 01As-03As, 07As) and sulphates (pts 01S, 03S, 04S, 06S). These results confirmed the results from FT-IR (Figure 21). Data kindly provided by Dr. Letizia Monico.

Arsenolite and sulphates, as well as acanthite for the sample containing silver, were also found in the artificially aged samples *Orp_{OilUVA-Vis}* and *Orp-_{AgOilUVA-Vis}* using μ -FT-IR (Figure 24), μ -XRD, μ -XANES, but in this case As K-edge μ -XANES suggest that in addition to As^{III} species, also As^{V} species are present in both the two samples. The μ -FT-IR maps indicate that arsenolite is mainly localized on the surface of the sample, which suggests the influence of light.

These results confirm the higher reactivity of oil binding media in comparison with the whole egg tempera. In all the cases, the μ -Raman analyses contained a high fluorescence background, produced by the linseed oil, which hindered the signal from degradation products.

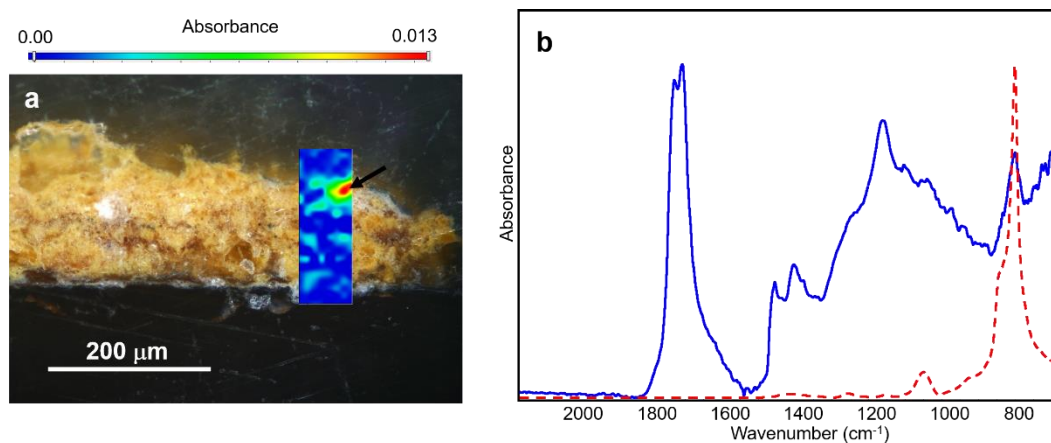


Figure 24. a) Microphotograph of sample *Orp_{OiiUVA-Vis}* and μ -FT-IR map done using the height of the peak at 800 cm^{-1} , it suggest that arsenolite (confirmed by μ -XRD) formed in a localised area in the surface of the sample, b) FT-IR spectrum obtained from *Orp_{OiiUVA-Vis}* (indicated with an arrow). The spectrum is compared with an arsenolite standard (red dashed line).

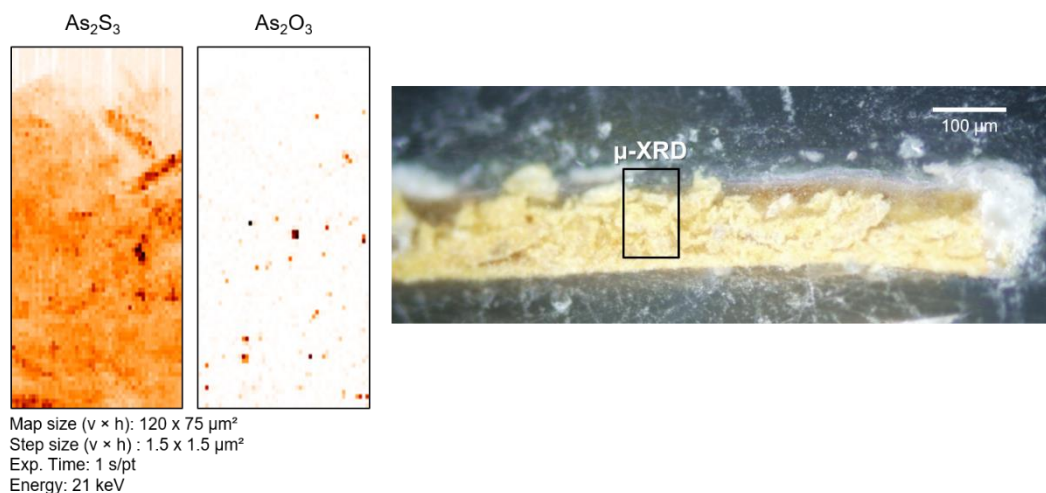


Figure 25. μ -XRD maps from sample *Orp_{OiiUVA-Vis}* some crystals of arsenolite were identified close to the surface of the sample. Data kindly provided by Dr. Letizia Monico.

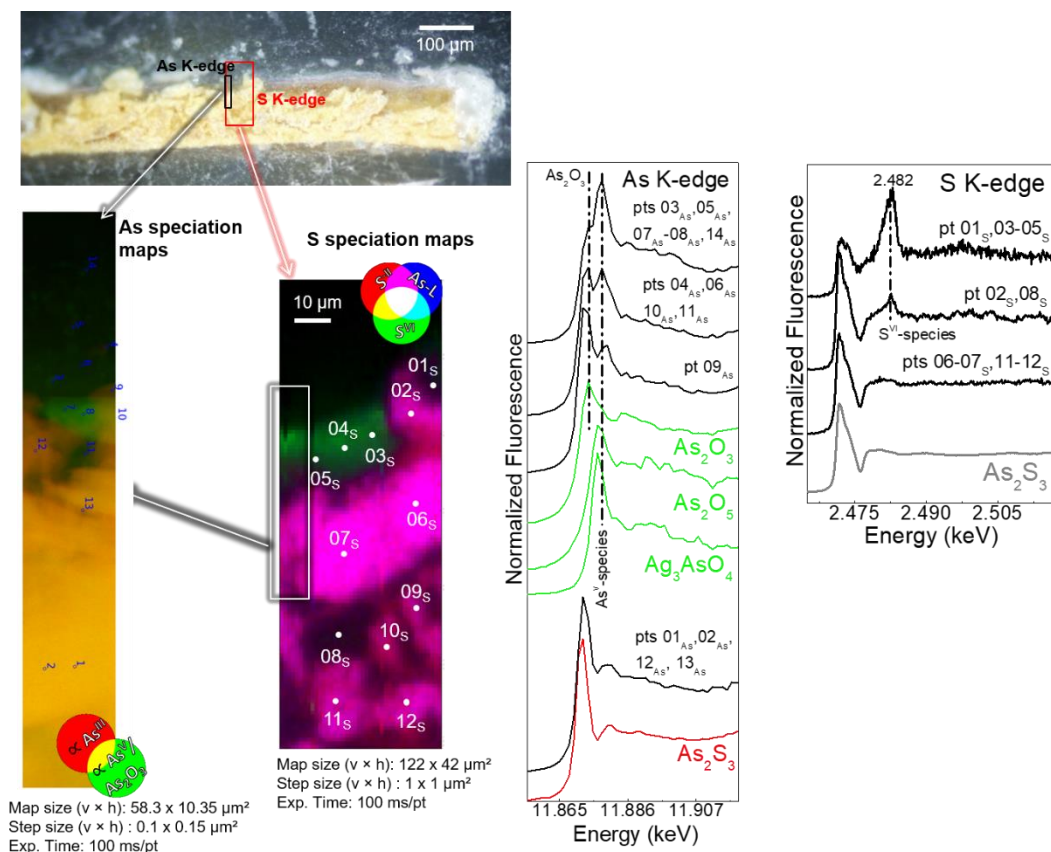


Figure 26. μ -XANES mapping and As K-edge and S K-edge spectra. There is a co-localized presence, mainly at the paint surface, of arsenolite, As^{V} -species (pts 03As-11As, 14As) and sulphates (pts 01S-05S, 08S) that confirm the results obtained from the other analytical techniques. The amount of sulphates identified increased in comparison with the unaged sample. Data kindly provided by Dr. Letizia Monico.

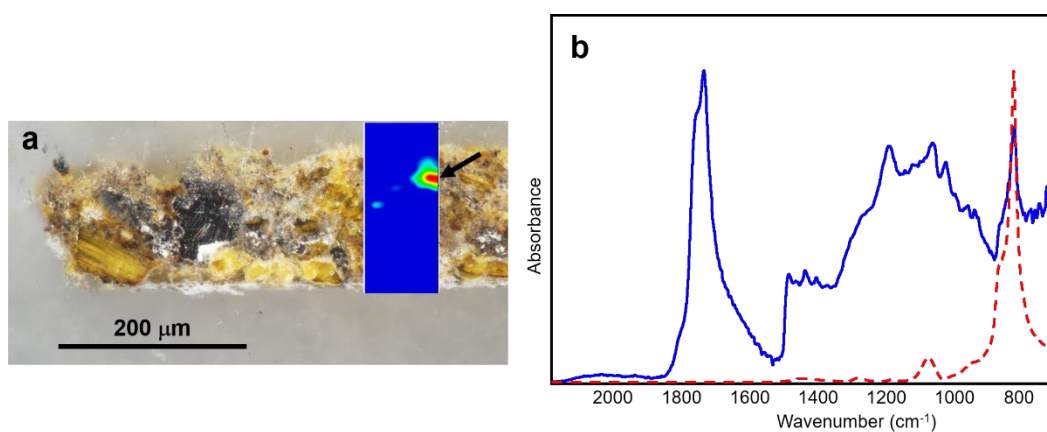


Figure 27. a) Microphotograph of sample Orp-Ag_{OiiIIVA-Vis} and μ -FT-IR map done using the height of the peak at 800 cm^{-1} , it suggests that arsenolite (confirmed by μ -XRD) formed in a localized area close to the surface of the sample, b) FT-IR spectrum obtained from Orp-Ag_{OiiIIVA-Vis} (indicated with an arrow). The spectrum is compared with an arsenolite standard (red dashed line).

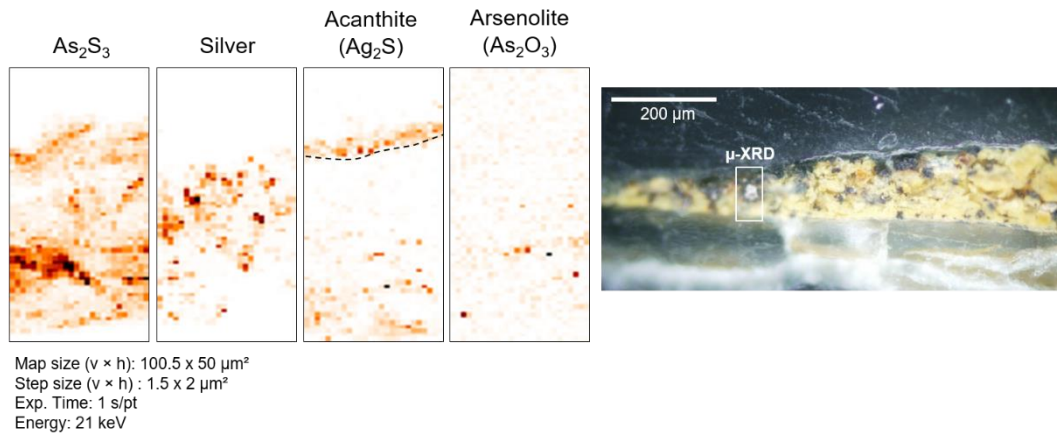


Figure 28. The μ -XRD maps of sample Orp-Ag_{OIUVA-Vis} show the formation of arsenolite and acanthite in the surface of the sample. Data kindly provided by Dr. Letizia Monico.

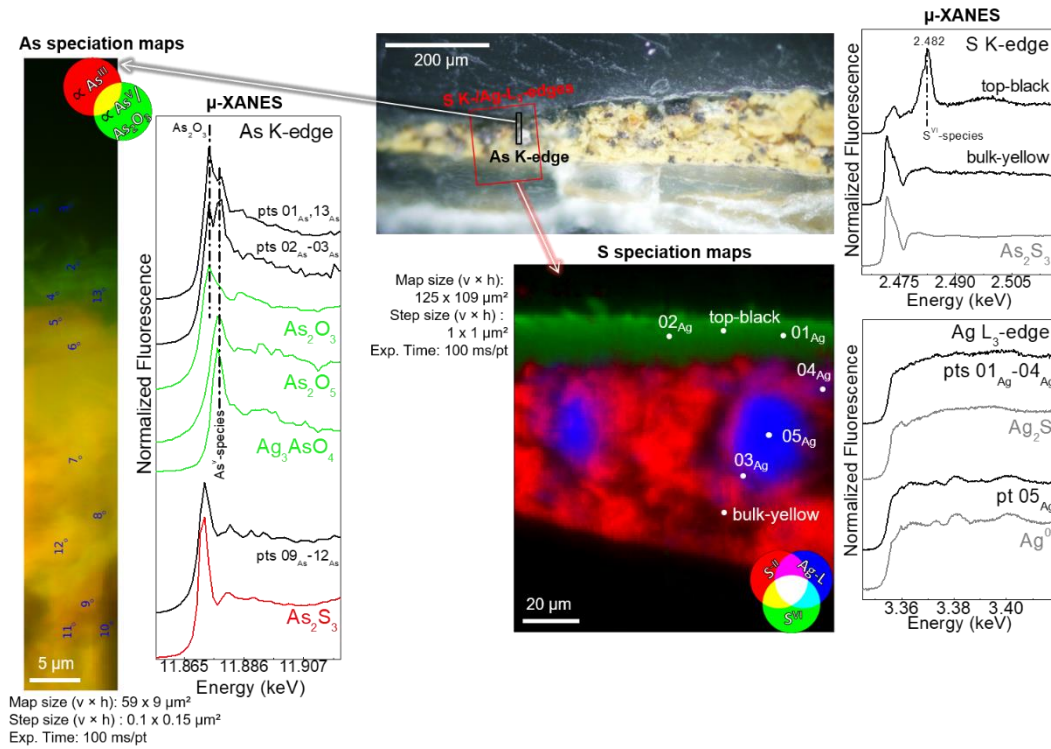


Figure 29. A layer on the top of the surface contain variable amount of arsenolite and As^V-species (pts 01As-03As, 13As), sulphates, and Ag₂S (pts 01Ag-04Ag). Data kindly provided by Dr. Letizia Monico.

2.4.6 Discussion

In summary, the above-discussed results show that Ag plays a role in the degradation process of orpiment (As₂S₃) since, in all the mock-ups that contain it, degradation products such as arsenolite (As₂O₃), sulphates and acanthite were identified. This might be explained by the interaction of the metal with the pigment. According to Zhang and colleagues [59], Ag⁺ can react with MeS minerals through a cationic interchange. Ag⁺ ions from Ag⁰ can be produced by different factors, for example, photo-creation of free holes [60] or Ag dissolution by reaction with S homopolar bonds [60, 61].

The interaction of Ag with homopolar bonds mechanism can explain the simultaneous formation of acanthite (Ag₂S) and orpiment degradation even in the absence of light, as proposed by Jain and co-workers [60, 61]. The S-S and As-As homopolar bonds associated with As₂S₃ have been identified by several authors and are consistent with the observations of Vermeulen and co-workers for painting systems [31].

The influence of light in the process is clear. The higher amount of degradation products was observed in the samples exposed to light; it can be explained by the photo-dissolution mechanism (PD) in which As-S bonds are broken by the absorption of photons producing atoms with a single unpaired electron and the simultaneous formation of Ag⁺ ions which can react with the unpaired electrons [60, 30].

Sulphates as well as other S species formation is in accordance with what has been reported in previous publications. The complexity of S chemistry is well known and the different S oxidation states can be formed during orpiment oxidation, sulphates seem to be the final product of a series of reactions and oxidation of other S species (e.g. sulphite) [36].

The colour change of the paint films containing orpiment and Ag can be associated with two phenomena, the darkening of Ag due to tarnishing and the fading of orpiment as a result of the formation of transparent arsenolite crystals.

Humidity may play also a role in the degradation of the orpiment, as suggested by the sample Op_{r95%RH} where a small amount of arsenolite was identified. The degradation of orpiment by the effect of water was already reported by Pascal in 1958 [62].

Arsenates were not detected in any of the egg tempera mock-ups. This suggests that longer times of exposition or a combination of high humidity and light exposure are required to convert As^{III} into As^V.

On the other hand, the detection of arsenolite in unaged linseed oil muck-ups and the presence of As^V in the samples artificially aged can be related to the curing process of oil binding medium. It is well known that during curing, siccativ oils absorbed a large amount of oxygen and produce peroxidic compounds [63]. The oxygen absorbed in the paint film, and the formation of radicals or peroxide groups may induce the oxidation of As; the oxidation of As^{III} into As^V by the action of oxygen and peroxide has been already reported, and it has been detected that the process is catalysed by UV radiation [64]. This may explain the higher oxidative effect of linseed oil in comparison with the whole egg tempera and the presence of As^V in the samples exposed to light.

Fi the localize presence of As^V (only in layer 2) in the *Maestà* sample may suggest reduced mobility of the arsenate species inside the painting stratigraphy.

2.5 Conclusions

In this chapter, a multi-analytical approach was used to understand the effect that metallic Ag, in combination with visible and UV light and humidity, have on the degradation of orpiment. ATR-FT-IR is suitable for the identification of the main degradation products of orpiment (i.e. arsenolite/arsenates and sulphates), while Raman spectroscopy confirms the presence of some of those degradation products and allow us to identify acanthite (Ag₂S) as the main degradation product of silver.

Regarding the SR-based techniques, μ -XRD confirms the results obtained with FT-IR and Raman, and the speciation As and S methods allow to gain deep knowledge on the nature of the oxidation state, it was complementary since that information is not provided by the other methods used.

All the samples containing Ag present degradation products both from the orpiment and from the silver, this indicates that Ag plays a key role in the degradation of the pigment when it is mixed with it, by increasing the oxidation of the pigment probably due to an ion interchange mechanism.

Within the artificial aging conditions employed, no oxidation of As^{III} into As^V was reached, probably that process requires longer exposition times or more aggressive conditions in which light exposure and high relative humidity conditions are combined.

The results of this study offer information useful for the establishment of preventive conservation conditions for artefacts in which orpiment and silver are mixed or in close contact.

References

- [1] M. Uda, "Characterization of Pigments Used in Ancient Egypt," in *X-rays for Archaeology*, M. Uda, G. Demortier and I. Nakai, Eds., Dordrecht, Springer, 2005, pp. 3-26.
- [2] Q. Cui, Z. Shan, b. Shui, W. Zhang and Z. Yu, "Study on the material and production technology of mural paintings in the 8th cave in Mogao Grottoes, Dunhuang," *Relics and Museology*, pp. 91-95, 2018.
- [3] M. Clarke, "Anglo-Saxon Manuscript Pigments," *Studies in Conservation*, vol. 49, no. 4, pp. 231-244, 2004.
- [4] S. P. Best, R. J. H. Clark, M. A. M. Daniels, C. A. Porter and R. Withnall, "Identification by Raman Microscopy and Visible Reflectance

Spectroscopy of Pigments on an Icelandic Manuscript,” *Studies in Conservation*, vol. 40, no. 1, pp. 31-40, 1995.

- [5] D. Domenici, C. Miliani and A. Sgamellotti, “Cultural and Historical Implications of Non-destructive Analyses on Mesoamerican Codices in the Bodleian Libraries,” in *Mesoamerican Manuscripts. New Scientific Approaches and Interpretations*, Leiden, Brill, 2019, pp. 160-174.
- [6] L. Burgio, R. J. H. Clark and K. Theodoraki, “Raman microscopy of Greek icons: identification of unusual pigments,” *Spectrochimica Acta Part A*, vol. 59, pp. 2371-2389, 2003.
- [7] S. Zaleski, Y. Takahashi and M. Leona, “Natural and synthetic arsenic sulfide pigments in Japanese woodblock prints of the late Edo period,” *Heritage Science*, vol. 6, no. 32, pp. 1-8, 2018.
- [8] A. van Loon, P. Noble, A. Krekeler, G. Van der Snickt, K. Janssens, Y. Abe, I. Nakai and J. Dik, “Artificial orpiment, a new pigment in Rembrandt's palette,” *Heritage Science*, vol. 5, no. 26, pp. 1-13, 2017.
- [9] U. Birkmaier, A. Wallert and A. Rothe, "Technical examinations of Titian's Venus and Adonis : a note on early Italian oil painting technique," in *Historical painting techniques, materials, and studio practice : preprints of a symposium, University of Leiden, the Netherlands*, 1995.
- [10] M. Vermeulen, S. Jana and K. Janssens, “Identification of artificial orpiment in the interior decorations of the Japanese tower in Laeken, Brussels, Belgium,” *Heritage Science*, vol. 3, no. 9, 2015.
- [11] C. Cennini, *Il libro dell'arte*, Vicenza: Neri Pozza Editore, 2017.
- [12] N. Bevilacqua, L. Borgioli and I. Androver Garcia, *I pigmenti nell'arte dalla preistoria alla rivoluzione industriale*, Padua: Il Prato, 2010.

- [13] V. S. Muralha, L. Burgio and R. J. Clark, "Raman spectroscopy analysis of pigments on 16–17th c. Persian manuscripts," *Spectrochimica Acta Part A: Molecular and Biomolecular Spectroscopy*, no. 92, pp. 21-28, 2012.
- [14] C. Nikolla, D. Ornela and R. J. H. Clark, "Identification of pigments used on late 17th century Albanian icons by total reflection X-ray fluorescence and Raman microscopy," *Cultural Heritage*, no. 6, pp. 157 - 164, 2005.
- [15] M. A. Garrote, M. D. Robador and J. L. Perez-Rodriguez, "Analytical investigation of Mudéjar polychrome on the carpentry in the Casa de Pilatos palace in Seville using non-destructive XRF and complementary techniques," *Spectrochimica Acta Part A: Molecular and Biomolecular Spectroscopy*, no. 173, pp. 279-291, 2017.
- [16] N. Eastaugh, V. Walsh, T. Chaplin and R. Siddall, *Pigment Compendium. A Dictionary and Optical Microscopy of Historical Pigments*, United Kingdom: Elsevier, 2008.
- [17] T. Dias, E. Murta, C. Barrocas Dias and V. Serrão, "All that glitters is not gold: silver leaf gilding, another means to an end," *Conservar Património*, no. 22, pp. 29-40, 2015.
- [18] S. Bogović-Zeskoski, "Gold and not so real gold in Medieval treatises," *Conservar Património*, no. 22, pp. 51-58, 2015.
- [19] A. Daveri, B. Doherty, P. Moretti, C. Grazia, A. Romani, E. Fiorin, B. G. Brunetti and M. Vagnini, "An uncovered XIII century icon: Particular use of organic pigments and gilding techniques highlighted by analytical methods," *Spectrochimica Acta Part A: Molecular and Biomolecular Spectroscopy*, vol. 135, p. 398–404, 2015.

- [20] R. D'Amico, *La Terra promessa. Conoscenza e Conservazione. Attività di catalogazione e di restauro nelle Chiese della città e della Diocesi di Bologna*, Bologna: Alfa, 1981.
- [21] G. Sciutto, T. Frizzi, E. Catelli, N. Aresi, S. Prati, R. Alberti and R. Mazzeo, "From macro to micro: an advanced macro X-ray fluorescence (MA-XRF) imaging approach for the study of painted surfaces," *Microchemical Journal*, no. 137, pp. 277-284, 2018.
- [22] D. V. Thompson, *The Materials and Techniques of Medieval Painting*, New York: Dover Art Instruction, 1956.
- [23] E. López Zamora and C. Dalmau Moliner, "Materiales y técnicas de dorado a través de las antiguas fuentes documentales," *PH Boletín del Instituto Andaluz del Patrimonio Histórico*, no. 61, pp. 110-129, 2007.
- [24] H. Howard and J. Najorka, "An unusual gilding technique on two panels by Pietro Lorenzetti," in *ICOM-CC 18th Triennial Conference*, Copenhagen, 2017.
- [25] H. Dick, "The painting technique of the proskynetarion by Isaak Demetrakes, 1818, Palestine," in *Istanbul Congress. Conservation and the Eastern Mediterranean*, Istanbul, 2010.
- [26] L. Bindi and P. Bonazzi, "Light-induced alteration of arsenic sulfides: A new product with an orthorhombic crystal structure," *American Mineralogist*, vol. 92, pp. 617-620, 2007.
- [27] M. Vermeulen, K. Janssens, J. Sanyova, V. Rahemi, C. Mcglinchey and K. De Wael, "Assesing the stability of arsenic sulfide pigments and influence of the binding media on their degradation by means of spectroscopic and electrochemical techniques," *Microchemical Journal*, no. 138, pp. 82-91, 2018.
- [28] K. Trentelman and L. Stodulski, "Characterization of Pararealgar and Other Light-Induced Transformation Products from Realgar by Raman

- Microspectroscopy,” *Analytical Chemistry*, no. 68, pp. 1755-1761, 1996.
- [29] K. Keune, J. Mass, A. Mehta, J. Church and F. Meirer, “Analytical imaging studies of the migration of degraded orpiment, realgar, and emerald green pigments in historic paintings and related conservation issues,” *Heritage Science*, vol. 4, no. 10, pp. 2-14, 2016.
- [30] J. S. Berkes, S. W. Ing Jr. and W. J. Hillegas, “Photodecomposition of Amorphous As₂Se₃ and As₂S₃,” *Journal of Applied Physics*, vol. 42, no. 12, pp. 4908-4916, 1971.
- [31] M. Vermeulen, J. Sanyova, K. Janssens, G. Nuyts, S. De Meyer and K. De Wael, “The darkening of copper- or lead-based pigments explained by a structural modification of natural orpiment: a spectroscopic and electrochemical study,” *J. Anal. At. Spectrom.*, vol. 32, p. 1331–1341, 2017.
- [32] P. M. Whitmore and G. R. Cass, “The Ozone Fading of Traditional Japanese Colorants,” *Studies in Conservation*, vol. 33, no. 1, pp. 29-40, 1988.
- [33] P. M. Whitmore and G. R. Cass, “The Fading of Artists' Colorants by Exposure to Atmospheric Nitrogen Dioxide,” *Studies in Conservation*, vol. 34, no. 2, pp. 85-97, 1989.
- [34] K. Keune, J. Mass, F. Meirer, C. Pottasch, §. van Loon, A. Hull, J. Church, E. Pouyet, M. Cotte and A. Mehta, “Tracking the transformation and transport of arsenic sulfide pigments in paints: synchrotron-based X-ray micro-analyses,” *Journal of Anal. Spectrom.*, vol. 30, pp. 813-827, 2015.
- [35] M. Vermeulen, G. Nuyst, J. Sanyona, A. Vila, D. Buti, J.-P. Suuronen and K. Janssens, “Visualization of As(III) and As(V) distributions in degraded paint micro-samples from Baroque- and Rococo-era

- paintings,” *Journal of Anal. At. Spectrom.*, no. 31, pp. 1913-1921, 2016.
- [36] M. F. Lengke and R. N. Tempel, “Reaction rates of natural orpiment oxidation at 25 to 40°C and pH 6.8 to 8.2 and comparison with amorphous As₂S₃ oxidation,” *Geochimica et Cosmochimica Acta*, vol. 66, no. 18, p. 3281–3291, 2002.
- [37] N. Bhandari, R. J. Reeder and D. R. Strongin, “Photoinduced Oxidation of Arsenite to Arsenate in the Presence of Goethite,” *Environmental Science and Technology*, vol. 46, pp. 8044-8051, 2012.
- [38] P. Smedley and D. Kinniburgh, “A review of the source, behaviour and distribution of arsenic in natural waters,” *Applied Geochemistry*, vol. 17, p. 517–568, 2002.
- [39] J. Simoen, S. De Meyer, F. Vanmeert, N. de Keyser, E. Avranovich, G. Van der Snickt, A. Van Loon, K. Keune and K. Janssens, “Combined Micro- and Macro scale X-ray powder diffraction mapping of degraded Orpiment paint in a 17th century still life painting by Martinus Nelliuss,” *Heritage Science*, vol. 7, no. 83, 2019.
- [40] J. Lei, B. Peng, Y.-J. Liang, X.-B. Min, L.-Y. Chai, Y. Ke and Y. You, “Effects of anions on calcium arsenate crystalline structure and arsenic stability,” *Hydrometallurgy*, vol. 177, p. 123–131, 2018.
- [41] M. B. Mcneil and J. Little, “Corrosion mechanisms for copper and silver objects in near-surface environments,” *Journal of the American Institute of Conservation*, vol. 31, pp. 355-366, 1992.
- [42] X. Zheng-miao and R. Naidu, “Factors influencing bioavailability of arsenic to crops,” in *Managing arsenic in the environment: from soil to human health*, R. Naidu, E. Smith, G. Owens and P. Bhattacharya, Eds., CSIRO publishing, 2006, pp. 223-234.

- [43] J. Imbrogno, A. Nayak and G. Belfort, "Egg White Varnishes on Ancient Paintings: A Molecular Connection to Amyloid Proteins," *Angew. Chem. Int. Ed.*, vol. 53, pp. 7014-7017, 2014.
- [44] L. Monico, K. Janssens, M. Cotte, A. Romani, L. Sorace, C. Grazia, B. G. Brunetti and C. Miliani, "Synchrotron-based X-ray spectromicroscopy and electron paramagnetic resonance spectroscopy to investigate the redox properties of lead chromate pigments under the effect of visible light," *Journal of Analytical Atomic Spectrometry*, vol. 7, no. 30, pp. 1500-1510, 2017.
- [45] S. Prati, G. Sciutto, E. Catelli, A. Ashasina and R. Mazzeo, "Development of innovative embedding procedures for the analyses of paint cross section in ATR FTIR microscopy," *Analytical and Bioanalytical Chemistry*, vol. 405, no. 2-3, pp. 895-905, 2013.
- [46] B. Lafuente, R. T. Downs, H. Yang and N. Stone, "The power of databases: The RRUFF project," in *Highlights in Mineralogical Crystallography*, Switzerland, De Gruyter, 2015, pp. 1-29.
- [47] U. Boesenberg, C. G. Ryan, R. Kirkham, D. P. Siddons, M. Alfeld, J. Garrevoet, T. Núñez, T. Claussen, T. Kracht and G. Falkenberg, "Fast X-ray microfluorescence imaging with submicrometer-resolution integrating a Maia detector at beamline P06 at PETRA III," *Journal of Synchrotron Radiation*, vol. 23, pp. 1550-1560, 2016.
- [48] W. De Nolf, F. Vanmeert and K. Janssens, "XRDU: crystalline phase distribution maps by two-dimensional scanning and tomographic (micro) X-ray powder diffraction," *Journal of Applied Crystallography*, vol. 47, pp. 1107-1117, 2014.
- [49] M. Cotte, E. Pouyet, M. Salomé, C. Rivard, W. De Nolf, H. Castillo-Michel, T. Fabris, L. Monico, K. Janssens, T. Wang, P. Sciau, L. Verger, L. Cormier, O. Dargaud, E. Brun, D. Bugnazet, B. Fayard, B. Hesse, A. E. Pradas del Real, G. Veronesi, J. Langlois, N. Balcar, Y.

- Vandenbergh, V. Armando Solé, J. Kieffer, R. Barrett, C. Cohen, C. Cornu, R. Baker, E. Gagliardini, E. Papillon and J. Susini, "The ID21 X-ray and infrared microscopy beamline at the ESRF: status and recent applications to artistic materials," *Journal of Analytical Atomic Spectrometry*, vol. 32, pp. 477-493, 2017.
- [50] G. Martínez-Criado, J. Villanova, R. Tucoulou, D. Salomon, J.-P. Suuronen, S. Labouré, C. Guilloud, V. Valls, Raymond Barrett, R. Barrett, E. Gagliardini, Y. Dabin, R. Baker, S. Bohic, C. Cohen and J. Morse, "ID16B: A Hard X-ray Nanoprobe Beamline at the ESRF for Nano-Analysis," *Journal of Synchrotron Radiation*, vol. 23, no. 1, pp. 344-52, 2016.
- [51] B. Ravel and M. Newville, "ATHENA, ARTEMIS, HEPHAESTUS: Data Analysis for X-ray Absorption Spectroscopy Using IFEFFIT," *Journal of Synchrotron Radiation*, vol. 12, no. Pt. 4, pp. 537-541, 2005.
- [52] M. Cotte, T. Fabris, G. Agostini, D. Motta Meira, L. De Viguerie and V. Armando Solé, "Watching Kinetic Studies as Chemical Maps Using Open-Source Software," *Analytical Chemistry*, vol. 88, no. 12, pp. 6154-6160, 2016.
- [53] M. Cotte, J. Susini, N. Metrich, A. Moscato, C. Gratziu, A. Bertagnini and M. Pagano, "Blackening of Pompeian Cinnabar Paintings: X-ray Microspectroscopy Analysis," *Analytical Chemistry*, vol. 78, no. 21, pp. 7484-7492, 2006.
- [54] W. B. White and R. Roy, "Infrared spectra-crystal structure correlations: II. Comparison of simple polymorphic minerals," *The American Mineralogist*, vol. 49, pp. 1670-1687, 1964.
- [55] S. C. B. Myneni, S. J. Traina, G. A. Waychunas and T. J. Logan, "Vibrational spectroscopy of functional group chemistry and arsenate coordination in ettringite," *Geochimica et Cosmochimica Acta*, vol. 62, no. 21/22, pp. 3499-3514, 1998.

- [56] S. I. Sadovnikov, E. G. Vovkotrub and R. A. A. Rempela, "Micro-Raman Spectroscopy of Nanostructured Silver Sulfide," *Doklady Akademii Nauk*, vol. 480, no. 6, p. 684–687, 2018.
- [57] S. J. Gilliam, C. N. Merrow, S. J. Kirkby, J. O. Jensen, D. Zeroka and A. Banerjee, "Raman spectroscopy of arsenolite: crystalline cubic As₄O₆," *Journal of Solid State Chemistry*, vol. 173, no. 54–58, 2003.
- [58] M. Cotte, E. Checroun, W. De Nolf, Y. Taniguchi, L. De Viguerie, M. Burghammer, P. Walter, C. Rivard, M. Salomé, K. Janssens and J. Susini, "Lead soaps in paintings: Friends or foes?," *Studies in Conservation*, 2016.
- [59] G. Zhang, X. Chao, P. Guo, J. Cao and C. Yang, "Catalytic effect of Ag⁺ on arsenic bioleaching from orpiment (As₂S₃) in batch tests with *Acidithiobacillus ferrooxidans* and *Sulfobacillus sibiricus*," *Journal of Hazardous Materials*, vol. 283, p. 117–122, 2015.
- [60] D. Tsiulyanu and I. Stratan, "On the photodissolution kinetics of silver in glassy As₂S₃," *Journal of non-crystalline solids*, vol. 356, pp. 147–152, 2010.
- [61] H. Jain, A. Kovalskiy and A. Miller, "An XPS study of the early stages of silver photodiffusion in Ag/a-As₂S₃ films," *Journal of Non-Crystalline Solids*, vol. 352, p. 562–566, 2006.
- [62] E. West Fitzhugh, "Orpiment and Realgar," in *Artists' Pigments: A Handbook of Their History and Characteristics*, vol. vol.3, Washington, National Gallery of Art, Washington, 1997, p. 47.
- [63] M. Lazzari and O. Chiantore, "Drying and oxidative degradation of linseed oil," *Polymer Degradation and Stability*, vol. 65, pp. 303-313, 1999.

- [64] S. Sorlini, F. Gialdini and M. Stefan, "Arsenic oxidation by UV radiation combined with hydrogen peroxide," *Water Science & Technology*, vol. 61, no. 2, pp. 339-344, 2010.

Acknowledgments

I would like to thank Dr. Letizia Monico and Prof. Aldo Romani from the University of Perugia for the artificially aged samples, and for sharing the SR-X-ray analysis results. I would also like to thank Zelan Li, Gianluca Chiaponi and Dr. Emilio Catelli for the invaluable help to this project.

I want to express my gratitude to Dr. Flavia Fiorillo, Dr. Sara Fiorentino and Prof. Mariangela Vandini from the Cultural Heritage department of the University of Bologna for the access to the μ -Raman instrumentation.

Chapter 3

Spectroscopic study of the crystallization of Pb and Zn carboxylates in different paint binders

3.1 Introduction

Metal carboxylates result from the bonding (Figure 1) of a metal with an ester or an acid group from fatty acids. Their general formula is $M(\text{RCOO}^-)_m$, where M stands for a metal and R is a fatty acid [1].

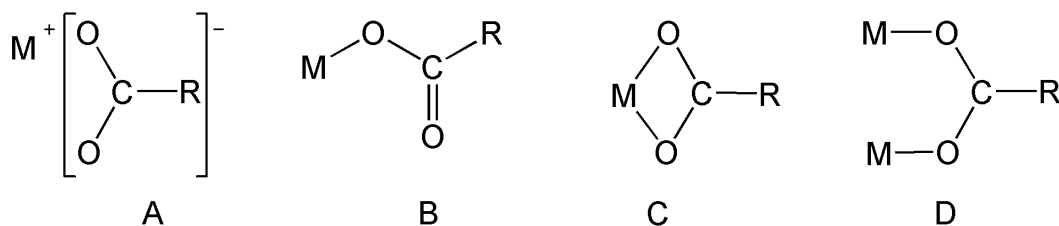


Figure 1. Different metal carboxylate coordination. A) Ionic or uncoordinated form, B) Unidentate coordination, C) bidentate chelating coordination, and D) bidentate bridging coordination. Adapted from [65].

Today, the formation mechanism of carboxylates in paintings is not completely understood. The early investigations suggest two possible mechanisms: a) a simple replacement of the hydrogen from a carboxylic group of a fatty acid with a metal by the action of a base (e.g., hydroxide or oxide), or b) the saponification of glycerides or other esters of the fatty acids with a base or metallic oxide [2].

Not all the metal carboxylates are the result of the interaction of metals from the pigments and the binding medium. In modern paint formulations manufacturers add carboxylates (e.g., Pb, Mn, and Co carboxylates) as additives to improve the rheological properties of the paint or facilitate

pigment grinding [1, 2, 3, 4, 5]. Besides, some metal carboxylates (i.e., Na carboxylates) are used as corrosion inhibitors to protect Fe, Pb, and Zn artefacts from pollutants in museum environments [6, 7].

Today, two different types of carboxylates have been identified; the so-called amorphous carboxylates, which are disordered complexes of metal ions, and the crystalline carboxylates that are organized structures (crystals) [8].

The structure of amorphous carboxylates is still under debate and different hypothesis have been proposed. It is believed that they can be constitute by a) carboxylates groups absorbed into the surface of a pigment, b) non-organized metal complexed of free fatty acids (i.e., metal soaps), and/or c) the ionomer-like structure characterized by an ion-containing polymer [9, 10, 8].

Despite the positive effects that metal carboxylates have (e.g., drying effect and swelling reduction of the paint layer) they can produce damage in paintings by modifying the surface due to the formation of whitish protrusions and crusts, and contribute to the delamination or loss of cohesion and opacity of painting layers [1, 4, 11, 12, 13]

The so-called protrusions are localized aggregations of fatty acids, metals ions, and metal carboxylates gels; they can deform the surface of a painting when their volume increases, and craters are produced when the material contained inside the protrusion is lost [10].

Metal carboxylates have been identified in paintings with binding medium that contains fatty acids, such as, siccative oils (e.g., linseed oil, poppy seed oil or walnut oil), egg tempera, and encaustic (beeswax). Pb and Zn carboxylates, have been extensively found in paintings; the former tend to produce aggregates while the latter generally are distributed homogeneously through the paint layer [3]. Ca, Cu, Cd, Mn, K, and Al also produce carboxylates in paintings and metallic coatings [1, 9, 14, 15].

3.1.1 Metal carboxylates in oil paintings

Siccative oils are a group of oils constituted by a mixture of vegetal unsaturated triglycerides. The double bonds in the fatty acids are the main characteristic that allow these oils to cure, by polymerization, and produce a film [16].

The “drying” of siccative oils is a complex process that is not completely understood. The oils undergo autoxidation of the C=C bonds of fatty acids into peroxides, and a simultaneous transformation of non-conjugated double bonds to conjugated double bonds. The absorption of large amounts of O₂ from the air produces the isomerisation of unconjugated bonds to *cis-trans* and *trans-trans* peroxy radicals, which in further steps led to the formation of radicals, alcohols and aldehydes [17]. These processes are followed by a polymerization, produced by the decomposition of hydroperoxides and formation of alcohol and carboxylic functionalities, the bimolecular combination of radicals, and/or the direct addition of radicals into the double bonds of the polymeric chains [18, 19].

The results obtained by Baij and colleagues [19] indicate that the autoxidation of the oil network during curing is the main pathway that produce metal carboxylates. According to the authors, in absence of hydrolysis, one carboxylic group is formed per triacylglycerol, and the carboxylic functionalities tend to form carboxylates as long as the pigment is available to complex.

In the initial stages of curing, the oil films seem to be more resistant to hydrolysis, but high relative humidity influences the formation of carboxylates [19]. This was confirmed by the reproduction and study of some ancient recipes to prepare linseed oil for painting and pharmaceutical plasters; the results suggest that the high levels of relative humidity or the addition of water during the preparation of stand linseed oil have a catalytic effect on the formation of carboxylates. Water also facilitates the slow ion release from pigments that later interact with the triglycerides, producing metal carboxylates [20].

NMR analysis offered further information regarding the water diffusion in oil film; it depends on the physical characteristic of the film (e.g., porosity, voids, etc.), on the degree of cross-linking of the polymer, and on the level of hydrolysis of the glyceride esters. Water diffuses faster inside an oil film at higher relative humidity conditions, and after the evaporation of water, the researchers identified the formation of Pb carboxylates in paint mock-ups containing lead white [21].

a) Formation of amorphous carboxylates

According to the investigations of Hermans and colleagues [9], an ionomer-like structure is formed by the reaction between the carboxylic acid side-chains produced during the curing of the oil and metal ions from the pigment (Figure 2). Simultaneously, free saturated fatty chains naturally present in the composition of the linseed oil (i.e., stearic [3.4% to 4.6%] and palmitic acids [~7%]), interact with the ions and form metal soaps that can be constrained by the polymeric network in an amorphous state [3, 9].

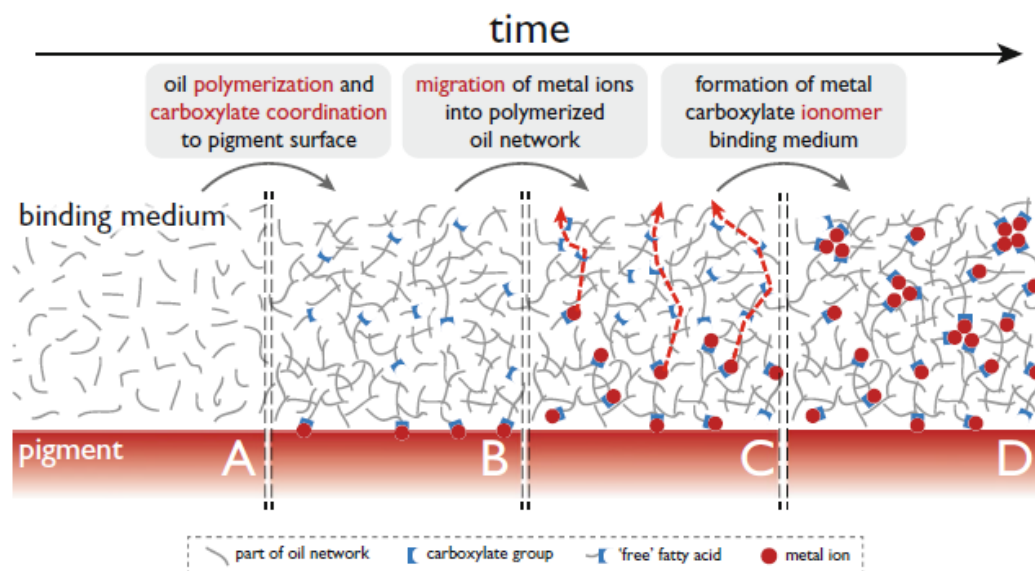


Figure 2. Scheme of the polymerization process of an oil film and the formation of metal carboxylates. A) & B) carboxylate groups are formed in the binder during autoxidative drying; C) metal ions from the pigment surface diffuse and D) form an ionomeric structure. Illustration from [3].

Divalent metal ions (e.g., Cu, Pb and Zn) may coordinate to two carboxylic functionalities, and form additional cross-linking to the polymeric network (i.e., ionomer structures) [3]. Besides, when they react with dicarboxylic acid groups, produce metal dicarboxylates, called halatopolymers, which can produce both crystalline and ionomer-like structures. When the halatopolymers are bonded to the backbone of a polymeric network, such as in oil films, are called halatotelechelic polymers [15].

b) Crystallization of carboxylates

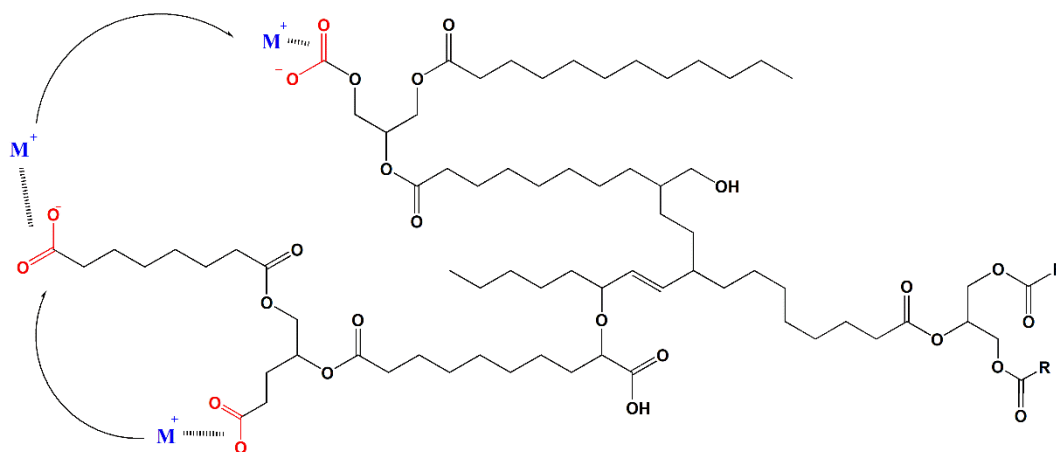
During the degradation of oil films, the hydrolysis of the oil network, which is enhanced by the destabilization of the polymer by the carboxylate groups formed in the initial stages of curing (i.e., ionomer), produce free fatty acids and free metal carboxylates that can diffuse through the paint film. The hydrolysis of the polymeric network is the main cause for the formation of free fatty acids and free metal carboxylates; however external sources, such as restoration treatments (e.g., resin-wax lining) can contribute to the addition of free fatty acids into the system [3].

Because of the film system is not in a thermodynamic equilibrium, the free metal carboxylates tend to move until reach a final state of well-organized structures. The migration process takes longer times than the coordination between the fatty acids in the polymer network and the metal ions, which is why the crystalline carboxylates are identified in the advance stages of degradation while the ionomer-like structure is detected in the initial stages of curing [9].

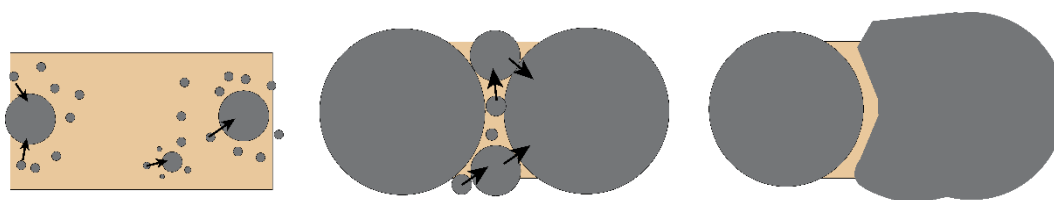
The research of Hermans and co-workers suggest that the main factor that drives the rate of crystallization is the energy barrier for the formation of the first metal soap “unit”, in the case of the long chain free metal carboxylates, the energy barrier corresponds to the alignment of the alkyl chains to maximize the Van der Waals interactions. Different factors such as crystallization and melting temperatures produce influence the behaviour of carboxylates, for example, the zinc soaps tend to be trapped in an

amorphous state because they require higher temperatures for crystallization, while lead carboxylates that require lower temperatures tend to crystallize relative fast [3].

After the initial nucleation, the local concentrations of metal ions and fatty acids close to crystalline metal soaps drop, producing a concentration gradient and the free fatty acids and the metal ions diffuse towards the crystalline phase, favouring further crystallization (Figure 3, next page). According to Hermans, the initial nucleation can be explained by the migration of metal ions through the paint system towards specific areas, this phenomenon occurs by the scission of the bond between the ion and the carboxylic group and the transference of the ion to other side chain in the polymeric network following the “ion hopping” mechanism (Scheme 1), and the formation of bigger crystals can be explained by the Ostwald ripening mechanism (Scheme 2) [3].



Scheme 1. Representation of the “ion hopping” mechanism in an oil film, M^+ is the metal that interacts with the COO^- groups at the end of the side chains in the polymeric network. Adapted from [11].



Scheme 2. Representation of the Ostwald ripening process, the smaller crystals dissolve and re-crystallise on bigger crystals.

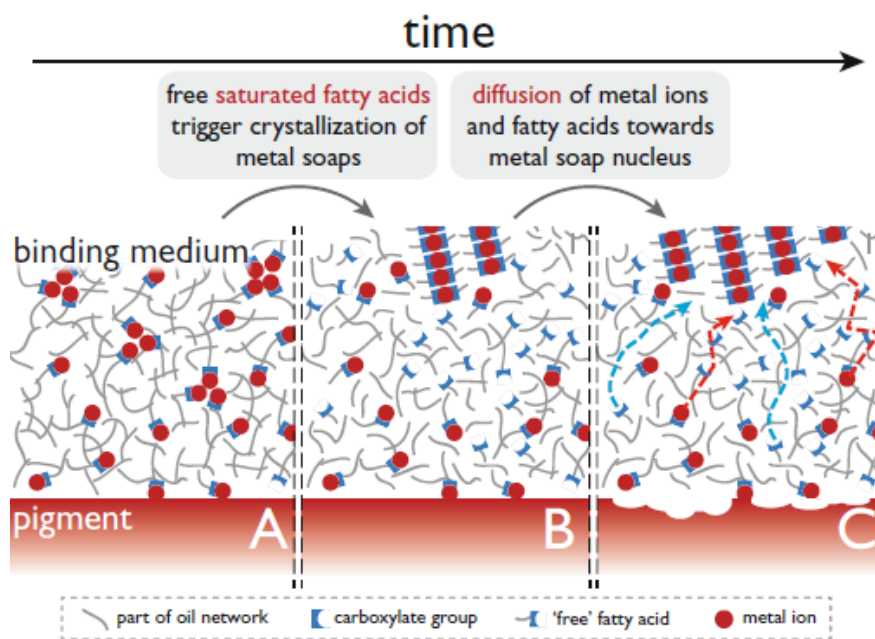


Figure 3. Scheme crystallization process: a) the crystallization is triggered by the presence of free saturated fatty acids, b) after the formation of initial “units” and recrystallization larger crystals are formed, and c) metal ions (red) and free saturated fatty acids (blue) diffuse toward the growing crystalline metal soap aggregate. Taken from [3].

The hypothesis of migration of metal carboxylates inside the paint layer, is supported by investigation using deuterium NMR spectroscopy. At room temperature, a fraction of palmitic acid is mobile in a linseed oil film and can migrate to areas where the pigment is located, this supports the hypothesis of migration of free fatty acids towards the areas of initial nucleation. The study also investigated the mobility of lead palmitate and showed that its mobility is higher with the increasing of the temperature and mainly in films containing higher amount of oil, demonstrating that its mobility is dependent on the composition of the matrix [22].

Moreover, TEM images have shown that metal soaps can crystallise in any area of the polymeric network, even far from the pigment particles, thus ion migration may explain the nucleation [3].

c) The influence of Zn in oil films

The high reactivity of Zn and its proclivity to form metal carboxylates in paintings is well-known. Zn^{2+} introduces successfully ions into a polymer due to its electronegativity [23]. ZnO has a highly catalytic effect for the transesterification of vegetable oils; due to the surface defects of the particles. The differences of the crystal defects between different batches of ZnO pigment have been already identified and studied to determine their reactivity in oil paintings [24, 25]. Different to Pb ions, it has been reported that Zn produce carboxylates even if present in low concentration and the amount of carboxylates increase with the increasing of the amount of pigment in the layer [26].

The investigation of Hermans focused on the role of Zn in the formation of metal carboxylates in oil paintings suggest that ZnO tends to release ions during the curing process of oil films, producing in the initial ionomer-like structure, this step lead to the further formation of free metal carboxylates that have been linked to brittleness, loss of opacity and delamination of the paint layers and in some cases to the formation of protrusions [26]. It has been also detected that zinc carboxylates tend to crystallise in the lower areas of the stratigraphy [3].

d) The influence of Pb in oil paintings

As mentioned by Cotte and co-workers [1], Pb carboxylates are a major problem in the conservation of oil paintings. Pb can be added to an oil film as pigment or as drier, and the formation of Pb soaps can have both positive and negative effects on the conservation of the painting.

The research of Garrappa and colleagues [26] indicate that in mock-ups containing minium and oil, a non-crystalline metal carboxylates and Pb formate is formed. The occurrence of metal carboxylates changed depending on the type of lead pigment. In two months of artificial ageing at 40% RH, no evidence of metal carboxylates were recorded for mock-ups containing lead white and lead tin yellow, while minium showed a broad

band after 60 h as well as the formation of lead formate, which indicates the instability of the pigment in acidic conditions. However, the mock-ups aged at 70% of RH showed evidence of metal carboxylates after two weeks for lead white and lead tin yellow, while for minium the broad band appeared after 2 h, showing clearly that relative humidity accelerates the formation of Pb carboxylates [26].

Different to what has been reported for Zn carboxylates, the free Pb carboxylates tend to crystallize on the surface of the paint film and produce protrusions due to a higher mobility inside the film [4]. Moreover, it has been reported the mineralization of Pb carbonates, chlorides, oxides and sulphates as a secondary product of the lead soaps aggregations [28].

3.1.2 Metal carboxylates in egg tempera paintings

Egg tempera is the most commonly used tempera in art, it can be done using the whole egg, only the egg yolk or only the egg white. Dry egg white is mainly constituted by proteins while dry egg yolk contains both proteins and fatty acids (~60% of dried weight of egg yolk are lipids). Because the high content of fatty acids, egg yolk was widely used by painters since it produces a stable film with good qualities [16, 27].

In comparison to siccativ oils, egg yolk contains a lower amount of unsaturated fatty acids, thus during ageing dicarboxylic fatty acids are formed in a lower quantity [27]. According to Meilunas and co-workers, the lower degree of unsaturation and the presence of proteins prevent for the formation of additional ester groups during ageing of egg tempera films [28]. After the initial drying process due to water evaporation and the further oxidative polymerization, free fatty acids form due to ageing as in the siccativ oils [29].

Colombini and colleagues [27] reported a drying pathway similar to the one produce in oil films (i.e., oxidation and cross-linking) in egg tempera paintings; however, they notice that the increase in the reactivity of fatty

acids during ageing favours other reactions with amine moieties from the protein.

Researchers identified metal soaps in several egg tempera paintings [14, 30, 31, 32]. Differently from siccativ oils, in egg tempera only crystalline carboxylates have been identified [31]. So far carboxylates of Cd, Cu, Mn, Al, Pb and Zn have been identified in tempera [14].

The research conducted by Svarcova and colleagues showed that in comparison with oil films, in egg films, carboxylates are present in the form of crystalline inclusions with a lamellar structure. Moreover, in lead tin yellow-egg yolk samples crystalline carboxylates were formed within a month while in lead tin yellow -linseed oil films no crystalline structures were detected even after 6 months [31].

3.1.3 Metal carboxylates in beeswax films

Beeswax is produced by the insect *Apis Mellifica*, its composition is variable but it can be considered in general that contains around 75% of saturated esters and 11% of fatty acids. It is well-known that due to the high content of esters, beeswax can easily form soaps after hydrolysis by the action of bases [16]. The hydrolysis of esters present in the beeswax can led to the formation of palmitic acid in a low concentration [33]. Other degradation products of beeswax are dicarboxylic fatty acids, saturated and unsaturated fatty acids and esters [34].

Beeswax was commonly used for encaustic and for restoration treatments (e.g., protective coatings and lining of paintings). The technique of encaustic painting was complex, there were two methods: the “hot” method in which the wax is applied in molten state, and the “cold” method that required the treatment of beeswax to purified it and eliminate the yellow colour; this recipe was called “Punic wax”. The Punic wax required the emulsification of beeswax with seawater which produce Na soaps; other recipes include the addition of linseed oil soaps or alkalis. The differentiation between the “hot”

and the “cold” method is complicated since the formation of metal carboxylates due to the ageing of beeswax can bias the results [35].

The analysis of reconstruction of different encaustic techniques suggest that metal carboxylates derive from the interaction of the beeswax with some components during the preparation, from the addition of oil soaps or from the interaction between the pigment and the binder. For example, Na carboxylates were identified in samples prepared following the Punic wax and in samples where oil soaps were added, in both the two cases, XRD analyses indicate that those carboxylates were crystalline. On the other hand, Pb carboxylates were identified as degradation product produced by the interaction between the binder and minium [36, 35].

When the carboxylates are produced by the interaction between the wax and the pigment, two mechanisms of formation were identified: a) carboxylates formed by saponification of the fatty acids of the binder by interaction with the pigment, and b) by an ion exchange between the pigment and oil soaps (i.e., Na carboxylates) [35].

Lead carboxylates have been identified in different mummy portraits using FT-IR [34]. In addition, researchers have also found Cu carboxylates in beeswax samples from Egyptian artefacts; their formation is attributed to the reaction between the saturated fatty acids from the beeswax and the pigments [37].

The formation of carboxylates is also a problem for the conservation of sculptures (e.g., wax models, reliefs, anatomical models). The contact of the wax with metallic armatures in the sculpture can produce carboxylates, which promote colour changes, modification of the physical properties of the wax and promote the hydrolysis due to oxidation [38]. The presence of carboxylates also changes the solubility of wax; which represent a technical problem for the cleaning process.

3.1.4 Characterization of metal carboxylates

As it was mentioned above, so far, the mechanisms of formation and crystallization of metal carboxylates is not completely understood. Today, some hypotheses have been proposed based on the evidence available obtained using different analytical methods.

Several analytical techniques have been used to characterize and study carboxylates in paintings. Both the two types of metal carboxylates (i.e., amorphous and crystalline) can be characterized using FT-IR spectroscopy. Crystalline structures exhibit a sharp COOM band at 1538 cm^{-1} for zinc carboxylates and at 1510 cm^{-1} with a shoulder at 1540 cm^{-1} for lead carboxylates, while amorphous carboxylates (i.e., ionomer) exhibit a broad band at higher wavenumbers, for example at $1570\text{-}1590\text{ cm}^{-1}$ for zinc carboxylates and at 1530 cm^{-1} for Pb carboxylates [9, 8].

There are several hypotheses in literature regarding the nature of carboxylates identified using FT-IR. The broad band has been attributed to the amorphous structure however, until now is not clear if it is related to ionomer-like, free metal carboxylates in amorphous state or absorbed into the pigment surface.

The research of Hermans and co-workers [8] used FT-IR in ATR mode in order to offer information regarding the nature of the broad band arising from carboxylates. They calculated the relative concentration of metal carboxylates groups (COOM) in oil films containing Pb and Zn pigments. For example, the CO band at 1738 cm^{-1} in the FT-IR spectra of zinc carboxylates at 1738 cm^{-1} was used as internal standard, and the concentration was calculated using a linear relationship between the COOM band area and the ratio of COOM and ester groups (COOM/COOR). The results of these calculations show suggest that probably the amount of possible carboxylate groups absorbed in the surface of a common pigment particle in a real painting (average size $0.5\text{-}3\text{ }\mu\text{m}$), is not enough to reach the experimental values of 0.43 for the formation of an intense broad band in FT-IR.

In addition, to address the problem of the possible contribution of amorphous metal soaps not linked to the ionomer to the broad band, the Hermans and co-workers [8], used a similar quantification method to offer information to the hypothesis of the ionomer-like structure. They considered that in a typical linseed oil, saturated fatty acids represent about the 7–13% of the total number of fatty acids present. If all the saturated fatty acids have become available for metal binding through hydrolysis, which is rather unrealistic, of their triglyceride ester bond while all other ester bonds connected to unsaturated fatty acids remain intact, the maximum ratio COOM/COOR is still limited to 0.075–0.15, depending on the exact saturated fatty acid content, thus they considered highly unlikely in the amorphous metal soaps hypothesis that the COOM/COOR ratio approaches the typical experimental value of 0.43 or higher that produce the broad band in FTIR spectra [8].

In addition, further investigation by the same authors suggest that even when some semi-crystalline lamellar structure aggregates, identified using backscattering Scanning Electron Microscope (SEM) images and Transmission Electron Microscopy (TEM), are already formed and are located far from the pigment particle, This hypothesis is supported by the investigations that show that even if in a broad band centred at 1587 cm^{-1} appears in a bulk ATR-FT-IR analysis spectra. Moreover, a broad band centred at 1587 cm^{-1} appears, some semi-crystalline lamellar structure aggregates, identified using backscattering Scanning Electron Microscope (SEM) images and Transmission Electron Microscopy (TEM), are already formed and are located far from the pigment particle. Those aggregates show weak crystalline features in XRD. These results suggest that at this stage the zinc soap aggregations are too disordered to exhibit a sharp peak in IR spectra [39].

As it can be seen, these researches have offered some data that support the hypothesis of the attribution of the broad band to the ionomer structure however, more researches are require to prove it.

FT-IR spectroscopy has been used to also allow quantifying the concentration of reaction products and find potential in model oil films, which is as a useful tool for the evaluation of the different formation rates according to different pigments [3, 8].

XRD has also revealed as a useful tool for the identification of the crystalline carboxylates. Researchers have recorded the diffraction patterns of different pure metal soaps, mainly palmitates and stearates [40, 41]. According to the results, well-resolved peaks can be identified under 20° for Zn, Pb and Cu soaps, however in this region no differences between saturated and unsaturated soaps are evident. The differences produced by double bonds are visible in the weak peaks between 20° to 30° [41]. The investigations using XRPD done by Hermans and co-workers showed that crystalline Zn carboxylates have a layered metal-coordinated structures independent of the chain length from $n=8-18$ [42].

Regarding Gas Chromatography/ Mass Spectrometry is a promising tool for the quantification of free metal soaps in a sample. The methodology developed by La Nasa and co-workers [5] overcome the problem of insolubility of metal soaps in many solvents and allow the clear differentiation between metal soaps and free fatty acids. The methodology is based in a double derivatization using HMDS to derivatise free fatty acids, and BSFTA for derivatise both the free fatty acids and the metal carboxylates, thus the quantification of free metal carboxylates is obtained after subtracting the total of free fatty acids, to the total of free fatty acids and metal carboxylates. The same methodology allow quantifying the amount free fatty acids and dicarboxylic acids and thus offers information of the degradation degree of the oil film analysed [5].

In the last few years, researchers studied metal soaps, combining SR- μ -FT-IR and SR-X-rays techniques, in ancient cosmetic samples [43], painting cross-section samples both from reconstructions and real samples, studying the interaction between oil and egg binders and different pigments (e.g., Pb,

Zn, Cu, Ca, Al) and the carboxylate distribution throughout the paint layers [30, 29, 44, 45, 46].

These investigations suggested that crystallization of lead soaps occur even in a short period of time [44] and that the type of binder can produce differences in the carboxylates typology formed (e.g., more crystalline in egg than in oil) [29]. These methods allow understanding the spatial distribution of metal soaps. For example, the study of Zn carboxylates in oil showed a difference between the surface and the inner part of the layer; more crystalline products (bands around 1540 cm^{-1}) appear in the inner part, while broader bands ($1560\text{-}1620\text{ cm}^{-1}$) related to amorphous, carboxylates distribute towards the surface, probably due to a difference in polarity [46].

The latest investigation made by Hageraats and co-workers suggest that deep-UV photoluminescence is a useful tool for the identification of crystalline metal soaps at a microscale in cross-section samples, it is a complementary tool that in combination with μ -FT-IR in ATR mode data, can produce multispectral images [47].

3.2 Aim of the study

This research aims to contribute to the knowledge of the pathway of formation and crystallization of lead and zinc carboxylates, by monitoring the artificial ageing process of painting mock-ups. We evaluated three different binding media to determine the different pathways according to the differences on the chemical composition of the binder.

3.3 Materials and Methods

3.3.1 Mock-up preparation and artificial ageing protocol

The painting models were prepared following the recipes reported by Cennino Cennini in his painting treatise [48]. Lead White ($2\text{PbCO}_3 \cdot \text{Pb}(\text{OH})_2$) was purchased from Sigma-Aldrich®, Minium (Pb_3O_4) purchased from Kremer® and Zinc White (ZnO) from Carlo Erba.

Stand linseed oil with cobalt salts (*OLIFA olio di lino cotto in sali di cobalto 3340*) was purchased from Zecchi®. Whole egg was used for the tempera mock-ups; some drops of white vinegar were added to avoid the presence of microorganisms. Beeswax has heated until melt and later mixed with pigments. The mixture was then spread over the glass slide using a spatula.

Two of the replicates for each combination were artificial aged inside a chamber with a relative humidity of ~99 %, a temperature of $40^\circ \text{C} \pm 2.3^\circ \text{C}$, and no light exposure. One of those replicates was taken out the chamber after 10 weeks of artificial ageing while the other remain in the chamber and the ageing still in process. The third replicate was naturally aged without light exposure at room temperature (Table 1, next page).

Table 1. Summary of the ageing conditions for each type of mock-up.

Sample code	Pigment	Binder	Ageing conditions
ZWO _{natural}			Natural ageing
ZWO _{10weeks}	Zinc white (ZnO)	Stand linseed oil	Artificial ageing for 10 weeks
ZWO _{63weeks}			Artificial ageing in process
MO _{natural}			Natural ageing
MO _{10weeks}	Minium (Pb ₃ O ₄)	Stand linseed oil	Artificial ageing for 10 weeks
MO _{63weeks}			Artificial ageing in process
LWO _{natural}			Natural ageing
LWO _{10weeks}	Lead white (2PbCO ₃ ·Pb(OH) ₂)	Stand linseed oil	Artificial ageing for 10 weeks
LWO _{63weeks}			Artificial ageing in process
ZWE _{natural}			Natural ageing
ZWE _{10weeks}	Zinc white (ZnO)	Whole egg	Artificial ageing for 10 weeks
ZWE _{28weeks}			Artificial ageing for 28 weeks*
ME _{natural}			Natural ageing
ME _{10weeks}	Minium (Pb ₃ O ₄)	Whole egg	Artificial ageing for 10 weeks
ME _{63weeksl}			Artificial ageing in process
LWE _{natural}			Natural ageing
LWE _{10weeks}	Lead white (2PbCO ₃ ·Pb(OH) ₂)	Whole egg	Artificial ageing for 10 weeks
LWE _{19weeks}			Artificial ageing for 19 weeks*
ZWB _{natural}			Natural ageing
ZWB _{10weeks}	Zinc white (ZnO)	Beeswax	Artificial ageing for 10 weeks
ZWB _{62weeksl}			Artificial ageing in process
MB _{natural}			Natural ageing
MB _{10weeks}	Minium (Pb ₃ O ₄)	Beeswax	Artificial ageing for 10 weeks
MB _{62weeksl}			Artificial ageing in process
LWB _{natural}			Natural ageing
LWB _{10weeks}	Lead white (2PbCO ₃ ·Pb(OH) ₂)	Beeswax	Artificial ageing for 10 weeks
LWB _{62weeksl}			Artificial ageing in process

* the sample was removed from the artificial ageing chamber due to the development of fungi.

3.3.2 SWIR measurements and Principal Component Analysis (PCA)

The short-wave infrared (SWIR) diffuse reflectance measurements were carried out with two portable NIR infrared probes MicroNIR (VIAVI Solutions®), one in the range 900-1700 nm and other in the range 1200-2200 nm. A Spectralon® (Labsphere, Inc.) with a diffuse reflectance >99% was used as a diffuse reflectance standard. The data acquisition was done with the MicroNIR (VIAVI Solutions®) software and the processing was performed with Microsoft Excel.

For each mock-up, five points (area of the sample point approx. 5 x 3 mm) were collected for each range (Figure 4). The heating

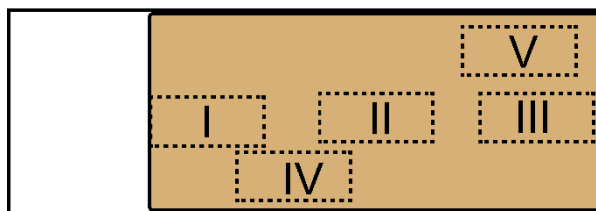


Figure 4. Analysis areas with SWIR.

temperature in which the data was collected was between 30° C and 35° C, the range in which the probes have the lowest noise contribution.

The data analysis was done using MATLAB (MathWorks®) in-house routines. Row pre-treatments (i.e., Standard Normal Variation (SNV), a Savitzky-Golay first derivative [third polynomial order, 11 data point gap], and column centring) were applied to minimise systematic variations that affect the signal. Column centring was applied prior to the calculation of the Principal Component Analysis (PCA) [49].

For the PCA, five components were calculated and only the first, second and third were considered in the score and loading plots; in order to visualize better the differences between the spectra of different ageing periods.

3.3.3 FT-IR measurements in total reflection mode

We used two systems of FT-IR in total reflection (rFT-IR). At the M2ADL we used a spectrometer Cary 630 FT-IR (Agilent Technologies®). We recorded five points for each mock-up (Figure 3, next page) using a spot size of 2.3 mm of diameter, collecting 256 scans with a spectral resolution of 4 cm⁻¹ in

the range of 5500-650 cm^{-1} . The background was acquired with 256 scans every 25 minutes using a gold reflective diffuse standard.

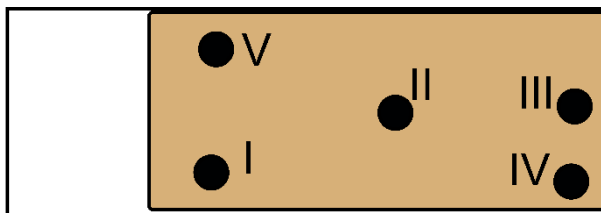


Figure 5. Scheme of points of analysis using rFT-IR.

The area analysed was registered with a Microsoft® Webcam of a VGA 640 x 480 HD sensor (1080p) sensible to infrared radiation and ArcSoft Webcam Companion 3 software in order to be able to see the beam. The distance between the surface of the mock-ups and the instrument was 2.3 cm.

The data was processed using the MicroLab FT-IR Software (Agilent Technologies®) and then OMNIC32™ Spectra software (Thermo Fisher Scientific™).

The second system used was the MA-FT-IR from the AXES group at the University of Antwerp. We performed all the measurements in total reflection mode using a Bruker Alpha FT-IR spectrometer, equipped with a frontal reflection module (20°/20° geometry) and a coaxial visual camera. The spectral range was 7500-375 cm^{-1} . The scan time was 12 sec (10 scans), the step size was 1mm and we collected the background for 15 min. The spectral resolution was of 4 cm^{-1} . For each sample, we performed two lines (vertical and horizontal) and the beam focus was in the centre of the sample [50].

All spectra were processed with Matlab and R software packages. A Principal Component Analysis (PCA) was performed to determine the homogeneity of the mock-up. The pre-processing of the spectra was: spectra range selection (4000-375 cm^{-1}), SNV correction, Savitzky-Golay filtering (order 3, frame 11), and column centering. In the PCA model 10 principal components (PC) were calculated.

A 2D imaging of the integration of the band related to the carboxylates was done using PyMCA software to have an image of the homogeneity of the sample.

3.3.4 Micro and Macro ATR-FTIR measurements and data elaboration

All μ -ATR-FTIR analyses were performed using a Ge ATR crystal and a Thermo Scientific Nicolet iN 10MX spectrometer. Spectra were recorded in the range 4000 to 675 cm^{-1} with an optical aperture of 150x150 μm (effective aperture 37.5 μm), a spectral resolution of 4 cm^{-1} and 64 scans. All data were acquired in six or more replicates according to the sample homogeneity. Spectra were processed with Omnic Picta and Omnic32 software.

The macro ATR-FT-IR measurements were performed with an ATR spectrometer Nicolet 5700 ATR-FTIR (Thermo Electron Company) with a 4 mm diameter ATR diamond crystal. The spectra were recorded using a resolution of 4 cm^{-1} , 64 scans and 64 scan of background. The spectra was processed with EZ Omnic and Omnic32 software packages.

3.3.5 Cross-section preparation

The cross-sections samples were prepared following the methodology proposed in Prati, et. al. [51]. The collected sample was embedded in Potassium bromide (KBr) salt (FT-IR grade, purity 99%) purchased from Sigma-Aldrich, and latter was mounted in Implex® polyester resin from Rohm & Haas©. The samples were polished with abrasive paper Micro-mesh™ grit 1200-12000 (~15 μm to ~2 μm).

All solvents were used without further purification. Ethanol (purity 96-97.2%) and acetone (purity \geq 99%) were purchased from Sigma-Aldrich®.

3.3.6 GC-MS measurements

All solvents were used without further purification. Iso-octane 99% was purchased from Riedel- de Haën and acetone HPLC grade (purity \geq 99.8%) was purchased from Sigma-Aldrich.

For the GC-MS calibration, a standard solution was prepared by dissolving a mixture of fatty acids (Sigma Aldrich products of purity >99%) in acetone. The composition was: lauric acid (4.88 ppm), myristic acid (4.82 ppm), palmitic acid (4.95 ppm), oleic acid (4.78 ppm), stearic acid (4.97 ppm), azelaic acid (4.83 ppm), suberic acid (4.93 ppm) and sebacic acid (4.88 ppm). A solution of tridecanoic acid (Sigma-Aldrich of purity >99%) dissolved in iso-octane in an unknown concentration and a solution of heptadecanoic acid (Sigma-Aldrich of purity > 99%) dissolved in the same solvent (152.27 ppm) were used as derivatization standards for the GC-MS analyses. Hexadecane (purity 99%; Sigma-Aldrich) in a solution of iso-octane (142.00 ppm) was used as internal standard for injection.

The derivatizations were carried out with N,O-bis(trimethylsilyl)trifluoroacetamide (BSTFA) + 1% trimethylchlorosilane (TMCS) and 1,1,1,3,3,3-hexamethylidisilazane (HMDS) (Sigma-Aldrich of purity > 99%).

The sample were submitted to a double derivatization pre-treatment to differentiate between fatty acids from free metal soaps following the methodology reported by La Nasa and co-workers [5].

As reported by Dávalos Navarro [52], after each derivatization, the system was injected with 2µl of the sample using the injector in splitless mode at 280° C. The operational program of the chromatograph oven was: 80° C, isothermal for 2min, 20° C/min up to 280° C, 280° C isothermal for 30 min. The separation took place in a HP-5MS fused silica capillary column (5% diphenyl/95% dimethyl-polysiloxane, 30 m x 0.25 mm i.d., 0.25 µm film thickness, J&W Scientific, Agilent Technologies, Palo Alto, CA). The tubing assembly included a deactive silica precolumn (2 m x 0.32 mm i.d., J&W Scientific Agilent Technologies, Palo Alto, CA). Operative conditions implied a constant (1.2 ml/min) flow of carrier gas (He, purity 99.995%)

The temperature of the MS transfer lines was 280° C, while those of the MS ion source and the MS quadrupole were 230° C and 150° C, respectively. The mass spectrometer was operated in the EI positive mode (70eV) with a

m/z 50-800 scan range. Quantitative analyses were performed in both TIC mode and SIM, using calibration curves and daily injections of standards to evaluate changes in the response of the instrument.

Analyses were performed in triplicate and the amount of carboxylic acids was estimated by comparing the areas of their corresponding peaks of the SIM signal and the areas of the peaks of the calibration curves.

After compute the amounts of carboxylic acids, obtaining the ratios of fatty acids such as palmitic/stearic (P/S), azelaic/palmitic (A/P), oleic/stearic (O/S), and the percentage of total amount of dicarboxylic acids (Σ Dic.), can provide information about the degree and type of oxidation that the fatty acids underwent.

3.3.7 XRPD measurements

Two XRPD systems were used in this research, both of them at the AXES group of the University of Antwerp. The Macro XRPD system (MA-XRPD) was done with a X-ray micro source (30 W, $1\mu\text{S-Cu}$, Incoatec GmbH, DE), a primary excitation energy (Cu $K\alpha$; 8.04 keV), 50 kV, 1 mA, 60 sec, and 10 repetitions. The flux was 7.0×10^8 photons s^{-1} . An incident angle of 13° was chosen between the primary X-ray beam and the surface, resulting in an enlarged beam footprint of around 2 mm in the horizontal direction and around 0.3 mm in the vertical direction. A PILATUS detector was positioned on an angle below 30° between the area detector and the sample [53].

The second system is a XRPD Huber Guinier camera G670 with an ImagePlate detector Cu $K\alpha$, 40 kV, 30 mA. We used 6 repetitions, 15 min, and 3 scan lops. The data of both the two systems was processed using XRDUA software [54].

3.4 Results and discussion

3.4.1 Study of oil paintings

a) Macroscopic effects of the artificial degradation

Samples LWO_{63weeks}, and ZWO_{63weeks} became yellow, but the colour change was more evident in the mock-ups artificially aged. In contrast, the colour modification of the sample MO_{63weeks} was moderated.

In the advanced stages of ageing, the sample ZWO_{63weeks} became crumbling, fragile and it detached from the glass support (Figure 6). The mock-ups LWO_{63weeks} also started detaching from the support but it was more stable in comparison to the ZWO_{63weeks} sample, while MO_{63weeks} was the most stable of the three.

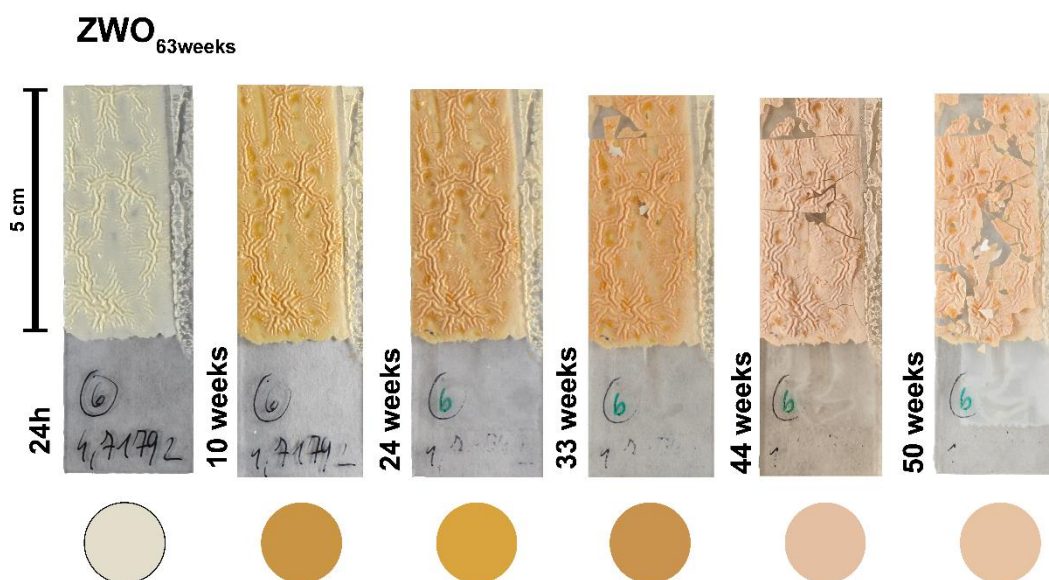


Figure 6. Photographs of sample ZWO_{63weeks} at different ageing times, it is possible to see the colour change and the damage to the paint layer. The circles under each photograph are a sample of the colour taken from a point of from the surface.

b) Non-invasive monitoring

Table 2 summarises the characteristic bands of linseed oil in the SWIR spectra. The lead white is characterised by the band at 6915 cm^{-1} (1st overtone $\nu(\text{OH})$) [55], while the spectra from the ZnO pigment show the bands at 6738 cm^{-1} , 5162 cm^{-1} , 4730 cm^{-1} from the OH overtones that are typical features produced by gases chemisorbed in the surface of the particles [56, 57]. Minium show no characteristic bands in the ranges used.

Table 2. Band assignation of SWIR spectra from oil in the ranges 900-1700 nm and 1200-2200 nm [55, 58].

Band (cm^{-1})	Assignment
8298	2 nd overtone $\nu(\text{CH}_2)$
6882	1 st overtone $\nu(\text{OH})$
5804	1 st overtone $\nu_a(\text{CH}_2)$
5703	1 st overtone $\nu_s(\text{CH}_2)$
5161	2 nd overtone $\nu(\text{C}=\text{O})$

The results arising from the PCA elaboration of all the data from sample ZWO_{63weeks} shows a trend that follows the ageing. The spectra obtained after 24 h are separated from the data obtained after the mock-up was put inside the ageing chamber (Figure 7, next page). The PC12 scree plot shows a difference between the data of the first 10 weeks of artificial ageing and the data after 10 weeks. The loading plot suggests that the data obtained after 50 weeks of artificial ageing is characterised by the band at 1930 nm (5181 cm^{-1}) arising from the 2nd overtone from $\nu(\text{C}=\text{O})$ of COOR [59] (Figure 8, next page and Figure 9, page 162), which is possible to associate to the formation of metal carboxylates.

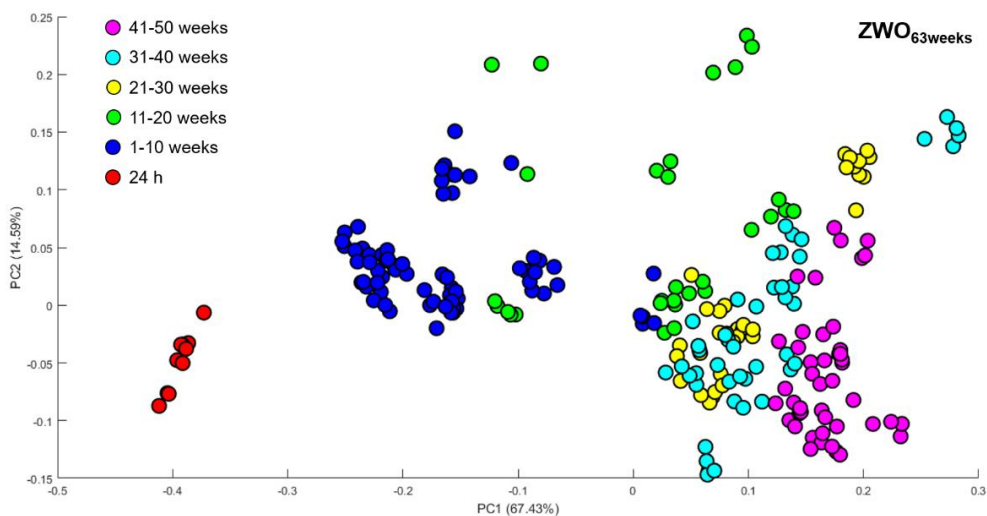


Figure 7. PC12 score plot from sample ZWO_{63weeks}. The spectra obtained after 24 h is clearly separate from the data obtained after different times of artificial ageing. It is possible to see a trend that follows the different times of artificial ageing.

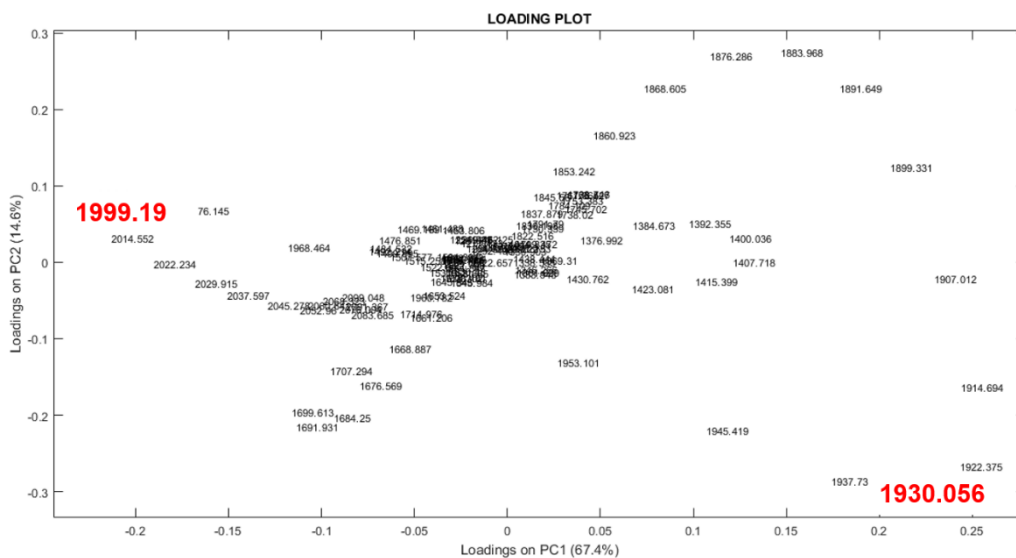


Figure 8. PC12 loading plot from the data obtained from the sample ZWO_{63weeks}. The band at 1930 nm (5181 cm⁻¹) characterises the spectra obtained after 50 weeks of artificial ageing in the score plot (Figure 7).

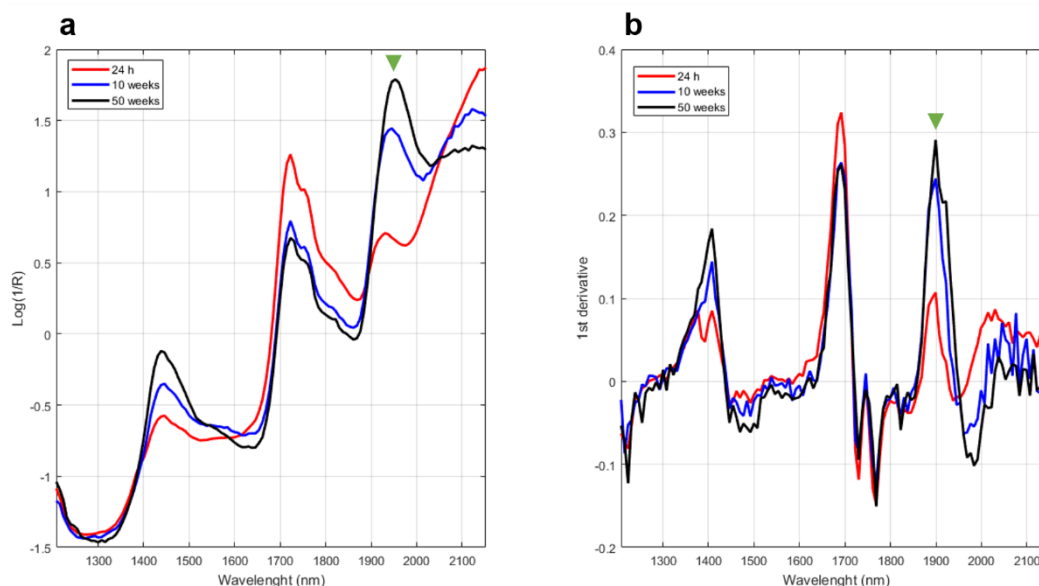


Figure 9. a) Comparison of SWIR spectra from ZWO_{63weeks} at different times of artificial ageing, SNV was applied to all the spectra. b) First derivative spectra from ZWO_{63weeks} at different ageing times. The band at 1930 nm that characterises the measurements during the artificial ageing is marked with ▼.

The data obtained by the portable rFT-IR complemented the SWIR results. The spectra showed already after 24 h a broad band falling in the range of 1450 cm^{-1} to 1650 cm^{-1} . The band intensity increased with the ageing. As previously reported, this band arises from metal carboxylates, however, its attribution to a particular typology of carboxylates (i.e., crystalline or amorphous) is complicated since it seems to contain a contribution of both inverted and derivative-like peaks [60]. The spectra obtained after 28 weeks, and in particular in the more advance states of ageing (i.e., 63 weeks), show three derivative-like peaks at 1538 cm^{-1} , 1458 cm^{-1} and 1395 cm^{-1} , arising from Zn stearate/palmitate. These results suggest that is possible to attribute the broad band in the range of 1450 cm^{-1} to 1650 cm^{-1} to the amorphous carboxylate, while the crystalline metal soaps show clearly inverted peaks in the total reflection spectra (Figure 10, next page).

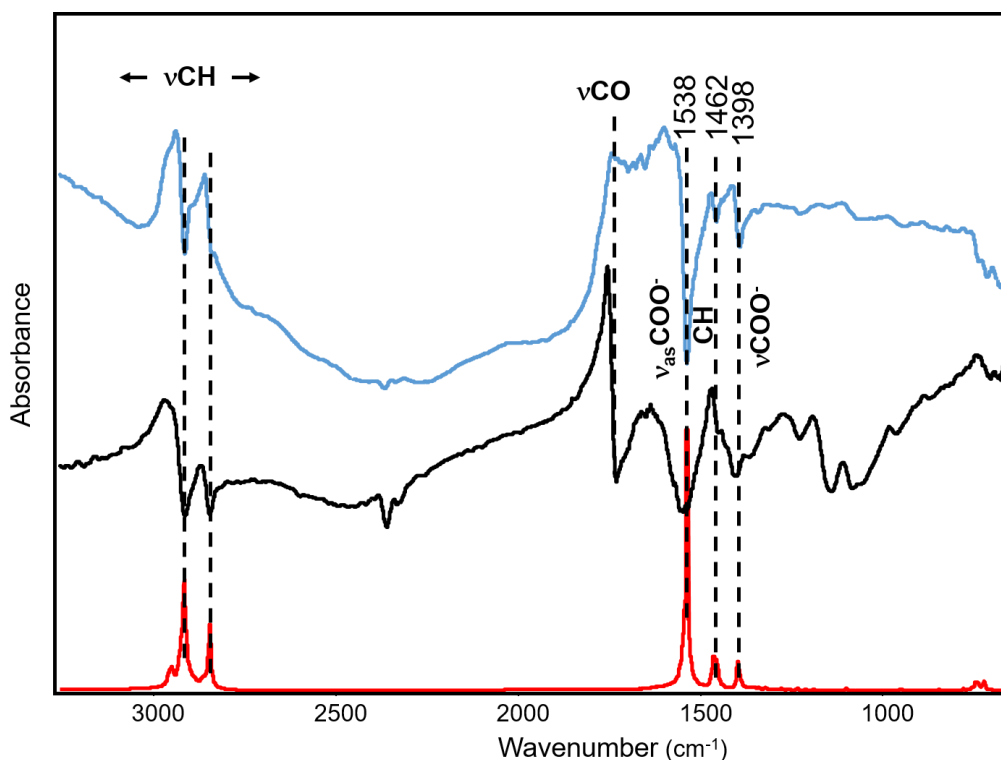


Figure 10. Portable rFT-IR spectra from sample ZWO_{63weeks} after 4 weeks (black line) and 63 weeks (blue line) compare with the spectra obtained in transmission of Zn palmitate (red line). It is possible to see the difference between the carboxylate broad band in the early stages of ageing, assigned to amorphous carboxylates, and the three derivative-like peaks of the crystalline carboxylates identified in the advanced ageing stages.

These results show the complementarity of the two techniques. Both of them allow to monitor changes in the painting film during ageing; SWIR data shows general modifications influenced by the COOR bonds, but it does not allow the identification of the carboxylates type while it is possible to identify the difference among crystalline and amorphous structures using the rFT-IR.

The data obtained from the sample LWO_{63weeks} is less informative (Figures 11 and 12, next page), since the separation of the different ageing times is less evident; however, it is still possible to observe a similar trend in the PC12 scree plot, and the band at 1907 nm (5244 cm⁻¹), characterises the advanced ageing stages.

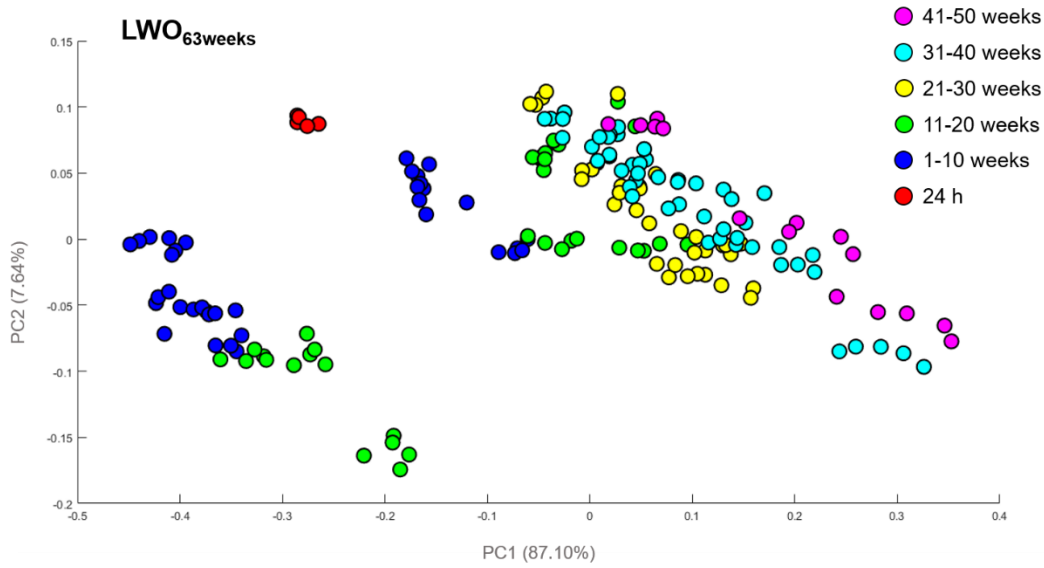


Figure 11. PC12 score plot from sample LWO_{63weeks}. The spectra obtained after 24 h is clearly separate from the data obtained after different times of artificial ageing. The trend that follows the different times of artificial ageing is less clear in this sample.

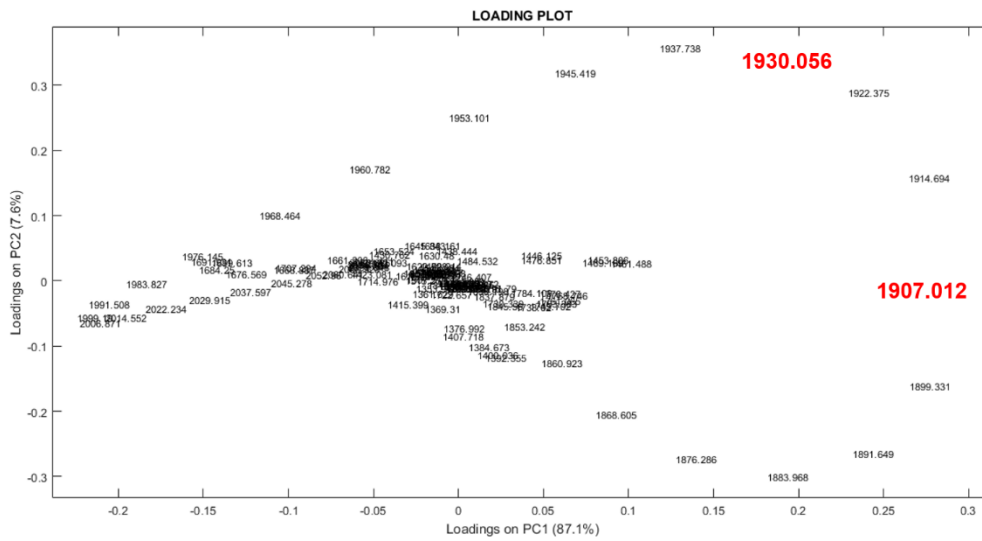


Figure 12. PC12 loading plot from the data obtained from the sample LWO_{63weeks}. The band at 1907 nm (5244 cm^{-1}) characterises the spectra obtained after 50 weeks of artificial ageing in the score plot (Figure 11).

The rFT-IR spectra (Figure 13) allow to identified a weak broad band during the early stages of ageing, while a derivative-like peak at 1512 cm^{-1} , ascribable to crystalline carboxylates, was identified in the advanced stages of ageing, however, the difference was less evident in comparison with the Zn sample, probably due to the influence of the carbonate inverted band at 1399 cm^{-1} .

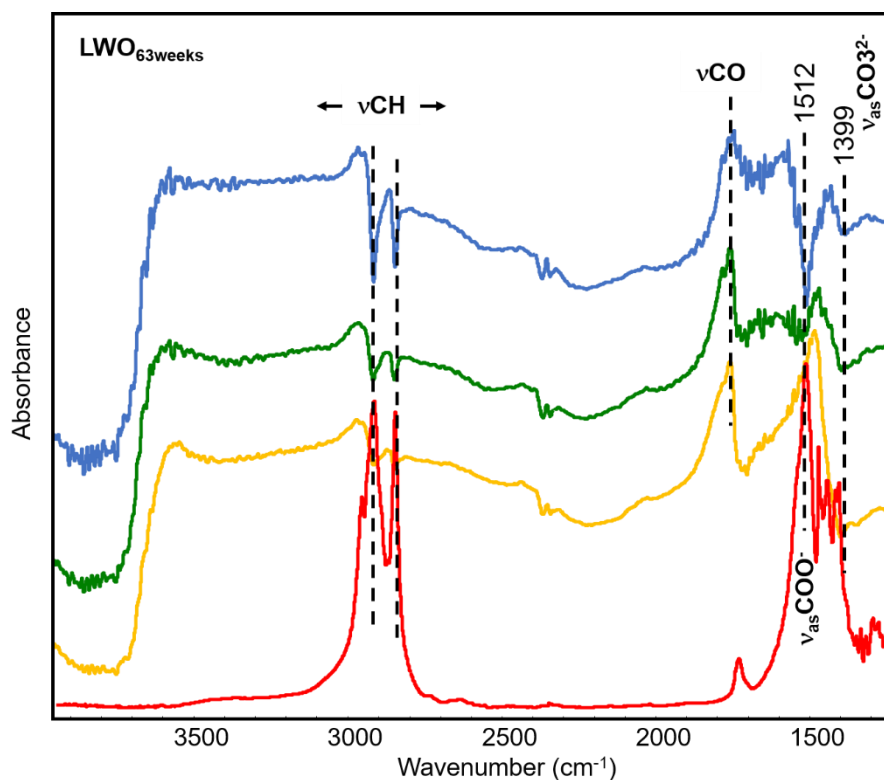


Figure 13. Portable rFT-IR spectra from sample $LWO_{63weeks}$ after 24 h (yellow line), 15 weeks (green line) and 63 weeks (blue line) compare with the spectra obtained in transmission of Pb stearate (red line). It is possible to see the derivative-like peak of the crystalline carboxylates identified in the advance ageing stages. It is possible to identify the inverted band ascribable to CO_3^{2-} .

Finally, the SWIR spectra from the $MO_{63weeks}$ sample (Figures 14 and 15, next page) produce a less informative PC12 Score plot since is not possible to differentiate from the spectra obtain after 24h and the spectra from the first 10 weeks, but is possible to see a trend similar to the one from $LWO_{63weeks}$ sample for the advance ageing stages and the spectra obtained after 51 weeks is clearly differentiated. The band that influences this separation its around 5288.21 cm^{-1} (1891 nm).

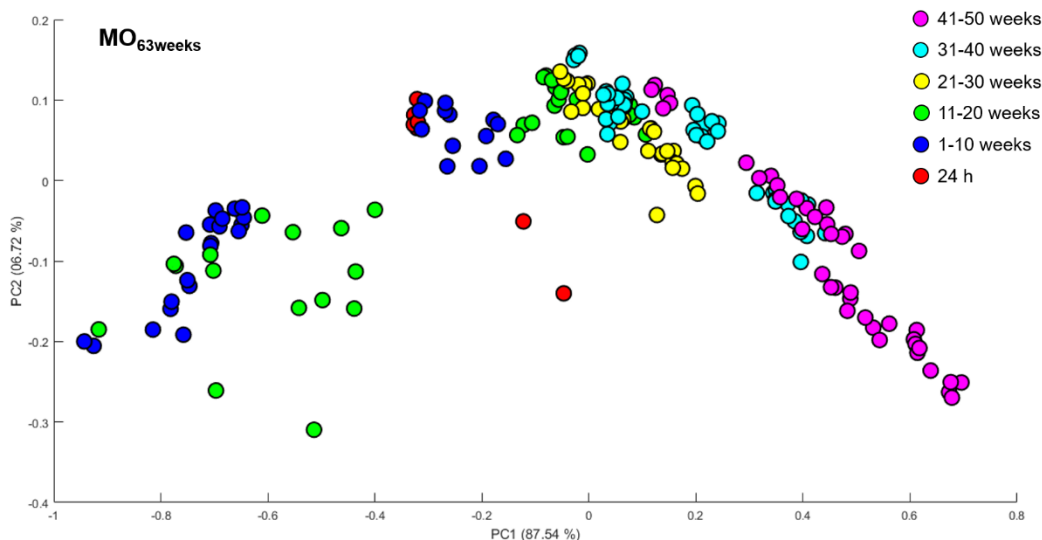


Figure 14. PC12 score plot from sample MO_{63weeks}. The spectra obtained after 24 h is not separate from the data obtained after the first weeks of artificial ageing. The trend that follows the different times of artificial ageing is less clear, however is possible to identify clearly the spectra from the advanced stages of ageing.

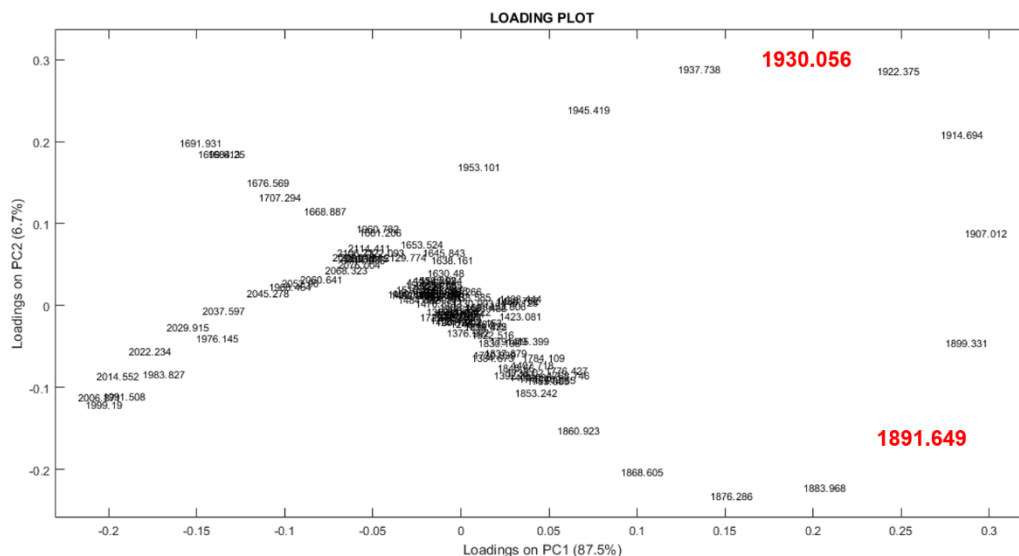


Figure 15. PC12 loading plot from the data obtained from the sample MO_{63weeks}. The band at 1891 nm (5288 cm^{-1}) characterises the spectra obtained after 50 weeks of artificial ageing in the score plot (Figure 14).

The rFT-IR show clearly a derivative-like band at 1512 cm^{-1} ascribable to crystalline carboxylates, the intensity of the band increases with the ageing time. Different from the sample LWO_{63weeks}, the data from MO_{63weeks} show (Figure 16, next page) the band at early times and with a higher intensity, probably due to a higher reactivity of the pigment.

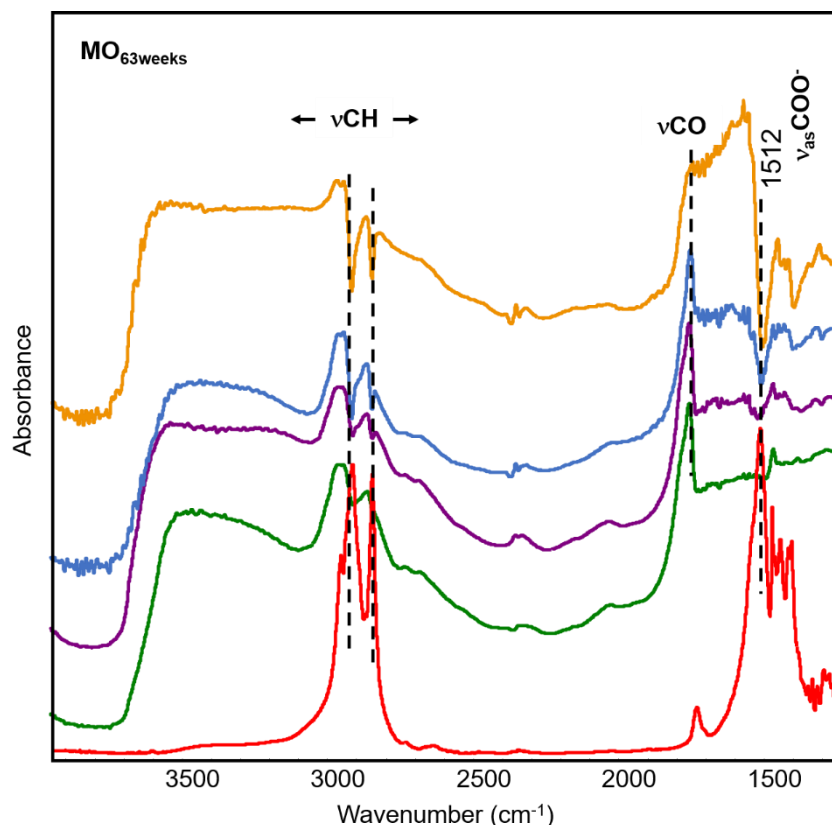


Figure 16. Portable rFT-IR spectra from sample $MO_{63weeks}$ after 24 h (green line), 10 weeks (blue line), after 15 weeks (blue line), and 63 weeks (yellow line) compare with the spectra obtained in transmission of Pb stearate (red line). It is possible to see the derivative-like peak of the crystalline carboxylates identified in the advance ageing stages.

c) Monitoring the crystallization of metal carboxylates

The three pigments showed a different reactivity; as it was expected, the most reactive pigment was ZnO; the spectra from sample $ZWO_{63weeks}$ featured a broad band centred at 1595 cm^{-1} after 24 h, while the $MO_{63weeks}$ sample after the same period of time showed a band at 1627 cm^{-1} arising from conjugated double bonds [61] and a broad band centred at 1545 cm^{-1} ascribable to the carboxylates. The distribution of the carboxylates in the $MO_{63weeks}$ sample was heterogenous as suggested by the differences in the intensity of the broad band among the different points of analysis.

The lead white samples showed a weak shoulder ascribable to the conjugated double bonds at 1630 cm^{-1} [61] after 24 h, and the broad band arising from carboxylates appeared after one week of artificial ageing, in

some points it was centred at 1592 cm^{-1} , while in others shifted towards 1547 cm^{-1} .

The behaviour of the three types of samples during ageing was similar, in general the intensity of broad band increased and it shifted towards lower wavenumbers, as reported in previous researches [3, 61].

The spectra from the sample $ZWO_{63\text{weeks}}$ showed the peaks attributed in literature to crystalline carboxylates [19, 61, 1] after 28 weeks, however the distribution of crystalline carboxylates was inhomogeneous since in some points only the broad band was identified. The three peaks at 1538 cm^{-1} ($\nu_{\text{as}}\text{COO}^-$), 1456 cm^{-1} (CH), and 1398 cm^{-1} (νCOO^-) are associated to Zn stearate/palmitate [62] (Figure 17).

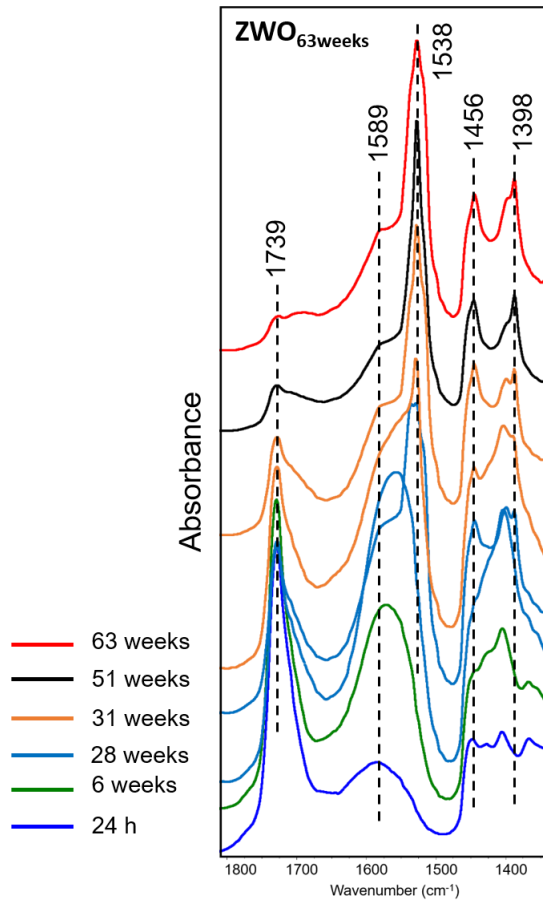


Figure 17. μ -ATR-FT-IR spectra obtained from the surface of the mock-ups $ZWO_{63\text{weeks}}$ at different ageing times, the shift towards lower wavenumbers as well as the increase in relative intensity of the band attributed to the $\nu_{\text{as}}(\text{COO}^-)$ of carboxylates is very clear.

After 63 weeks the sharp peak of crystalline carboxylates (1538 cm^{-1}) was identified in all the point of analysis, but the broad band was still evident as a shoulder centred at 1589 cm^{-1} , which suggest the simultaneous presence of amorphous and crystalline carboxylates.

On the other hand, in the samples $MO_{63weeks}$ the peak arising from crystalline carboxylates at 1509 cm^{-1} appeared after 32 weeks, and for the $LWO_{63weeks}$ the peak at 1511 cm^{-1} was evident after 31 weeks; however, even in advance degradation stages lead white and minium have some differences, the mock-up $LWO_{63weeks}$ presented a higher variability in the distribution of the degradation products in the surface, since after 51 weeks some points exhibit only the broad band at 1523 cm^{-1} while other presented the sharp peak at 1511 cm^{-1} (Figure 18). These results support the previous hypothesis about the crystallization of carboxylates, the initial stages are dominated by amorphous carboxylates and after degradation of the polymeric network and diffusion of metal soaps, the crystallization occurs.

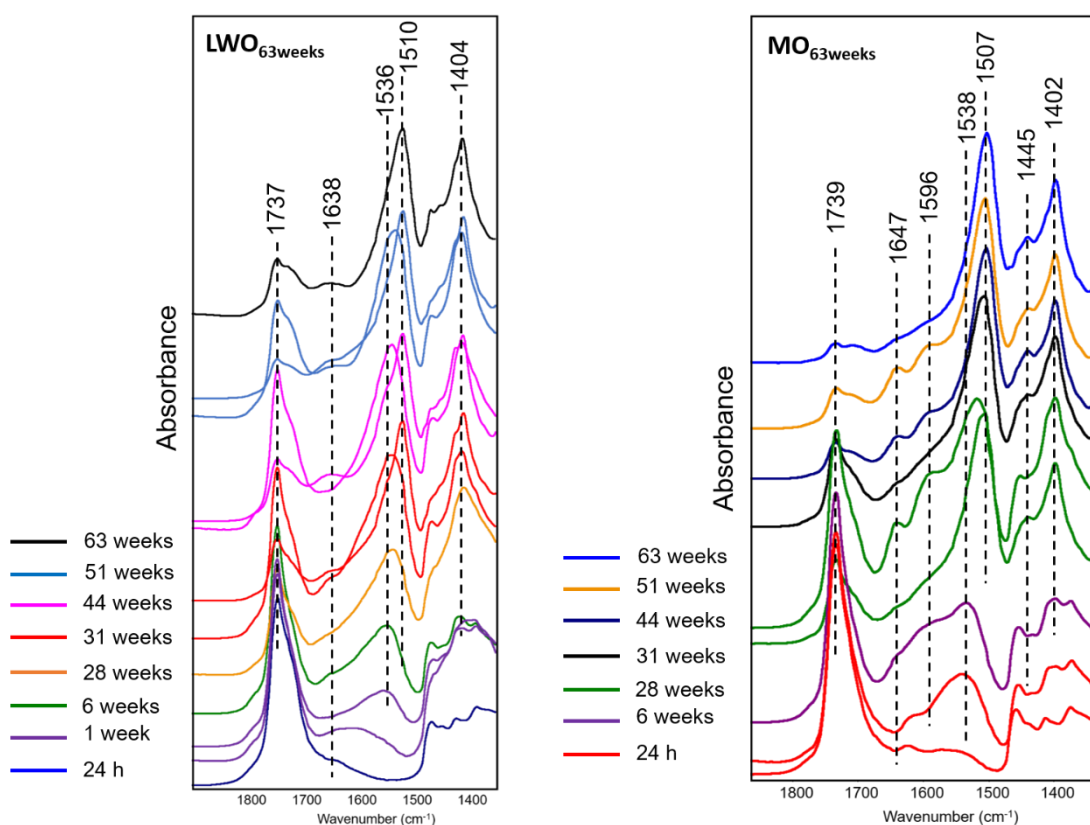


Figure 18. μ -ATR-FT-IR of sample $LWO_{63weeks}$ and $MO_{63weeks}$ at different ageing times. The higher reactivity of minium ($MO_{63weeks}$) since the $\nu(\text{COO}^-)$ of carboxylates appeared after 24 h, and after 31 weeks the distribution of crystalline carboxylates is homogenous in the surface, which is not the case for the sample $LWO_{63weeks}$.

Surprisingly, the bulk analysis in transmission mode of ZWO_{63weeks} after 44 weeks of artificial ageing shows no peaks of crystalline carboxylates, probably hinder by the intensity of the broad band that seems to be formed by the contribution of a band centred at 1584 cm⁻¹ and a peak at 1553 cm⁻¹. This result suggest that the crystalline carboxylates are not distributed through all the paint film and that considering the whole paint layer the dominant contribution is the amorphous carboxylates.

The distribution of the carboxylates in the film was evaluated by studying cross-section samples (Figure 19, next page). In the cross-section sample of all the three types of mock-ups (ZWO_{natural}, LWO_{natural}, MO_{natural}) after 10 weeks of natural ageing, the broad band of the carboxylates was recorded through all the paint film and not particular clusters were identified, however, some differences in intensity were observed. The ZWO_{natural} sample seems to have a higher concentration of carboxylates in the inner part of the paint film, and the MO_{natural} sample showed the higher intensity of the carboxylate band in the surface, while the LWO_{natural} sample surprisingly showed a very weak band at 1547 cm⁻¹, the intensity of the band was variable but slightly higher in the inner part of the sample.

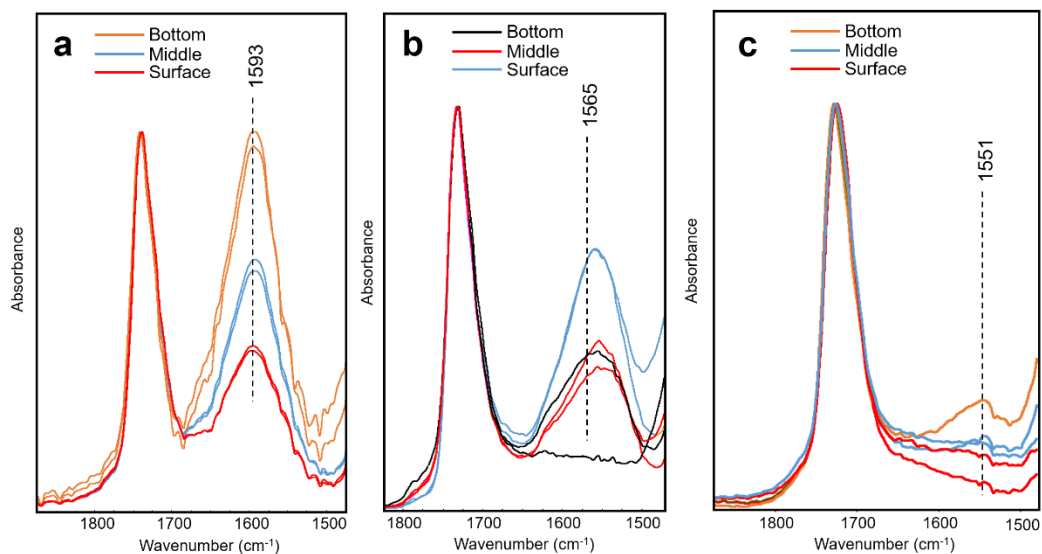


Figure 19. μ -ATR-FT-IR spectra obtained from cross-section samples from the mock-ups after 10 weeks of natural ageing. a) Spectra of the zinc white cross-section sample. The band of the $\nu_{\text{as}}(\text{CO})$ from carboxylates at 1593 cm^{-1} has a higher intensity in the inner part of the paint film. b) Spectra of the minium cross-section sample, the band from carboxylates at 1565 cm^{-1} is more intense in the surface of the sample. c) Spectra from the lead white cross-section sample, a weak band at 1551 cm^{-1} , ascribable to carboxylates, is slightly more intense in the inner part of the paint film. All the spectra were normalized to the C=O band at 1736 cm^{-1} .

This particular behaviour has been already reported in previous investigations [3], Pb carboxylates easily migrate to the surface of the paint film and Zn carboxylates have been reported to distribute in the inner part of mock-up paint films. The fact that there is a differential intensity through the film may suggest a migration of free metal soaps in amorphous state occurring inside the polymeric network or a higher concentration of metal ions that interact with the polymer and form the ionomer.

After the artificial ageing, the differences of intensity through the paint film were less evident. In the sample LWO_{63weeks} (Figure 20a, next page), after 10 weeks of artificial ageing the broad band centred at 1579 cm^{-1} increased in relative intensity in comparison with the LWO_{natural} sample; however, the intensity of the band was similar in different areas of the paint film.

After 35 weeks of artificial ageing (Figure 20b, next page), in the sample LWO_{63weeks} the broad band shifted towards lower wavenumbers and sharpened; in the surface, crystalline carboxylates were identified (peak at

1517 cm^{-1} and shoulder at 1540 cm^{-1}), while in the middle and inner part of the paint film two bands (1536 cm^{-1} and 1611 cm^{-1}) were observed, the same two bands were identified in some points in the superficial analysis. These results confirmed the simultaneous presence of amorphous and crystalline carboxylates in the film and, as it has been reported in literature, that the crystalline carboxylates migrate and concentrated in the surface, reason why the band is very intense in the spectra from superficial analysis.

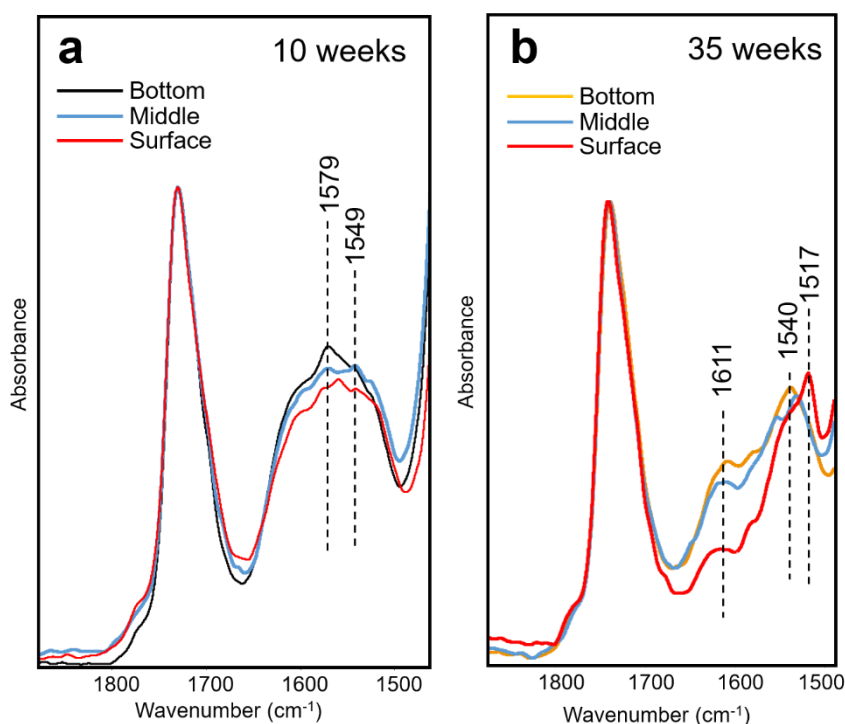


Figure 20. μ -ATR-FT-IR of the cross-section sample taken from the lead white mock-up artificially aged. a) Spectra from the sample after 10 weeks of artificial ageing, there are no evident differences in the relative intensity of the broad band from carboxylates. b) Spectra from the sample after 35 weeks of artificial ageing, crystalline carboxylates are detected (peak at 1517 cm^{-1} and shoulder at 1540 cm^{-1}) in the surface of the paint film while two different bands are present in the middle and inner part of it. All the spectra were normalized to the C=O band at 1736 cm^{-1} .

These results confirm what previous was hypothesised about the crystallization of carboxylates. The cross-section analysis suggests a migration of free metal carboxylate to the surface of the paint film. Only after advanced degradation, the peaks from crystalline carboxylates were identified.

To assess the contribution of free metal carboxylates to the band identified by ATR-FT-IR spectroscopy, bulk samples from the mock-ups were taken from the samples naturally aged and artificially aged after 10 weeks, and studied with GC-MS, the results are summarised in table 3.

Table 3. Relative percentages of the quantified free metal carboxylates (FMC) using GC-MS of samples after 10 weeks of natural and artificial ageing, the complete data is reported in Appendix 4 and in [52]. σ = standard deviation.

Mock-up	Natural aging (w %)			Artificial aging (w %)		
	FFA	FFA+FMC	FMC	FFA	FFA+FMC	FMC
ZWO	0.3 (σ 0.1)	0.6 (σ 0.1)	0.3	0.4 (σ 0.2)	1.2 (σ 0.1)	0.8
MO	0.2 (σ 0.0)	0.4 (σ 0.1)	0.2	0.6 (σ 0.1)	1.2 (σ 0.1)	0.6
LWO	0.8 (σ 0.3)	1.9 (σ 0.0)	1.1	0.9 (σ 0.1)	2.3 (σ 0.3)	1.4

The results indicate a clearly increasing in the amount of free metal carboxylates (FMC) in the samples artificially aged, however, the overall concentration is low to contribute to the broad band clearly identified using FT-IR. In particular, lead white seems to be the pigment that produced the higher amount of FMC. Despite the presence of free metal carboxylates, the FT-IR spectra showed no evidence of crystalline carboxylates characterised by sharp peaks, supporting the hypothesis of the metal soaps constrained in an amorphous phase [3, 39].

3.4.2 Study of metal carboxylate in whole egg tempera

a) Macroscopic effects of the artificial degradation

The samples of egg tempera are more fragile in comparison with the oil mock-ups, *craqueleure* appeared already after 24 h in samples containing zinc white and lead white (Figure 21, next page). As well as in the case of oil samples, the mock-ups containing zinc white lost cohesion and detached from the support. Something similar occurred to the samples with minium, the most stable ones seem to be the samples with lead white.

The colour change in the egg tempera mock-ups was less evident, the yellowing of many of the samples was the result of the formation of fungi in the surface.

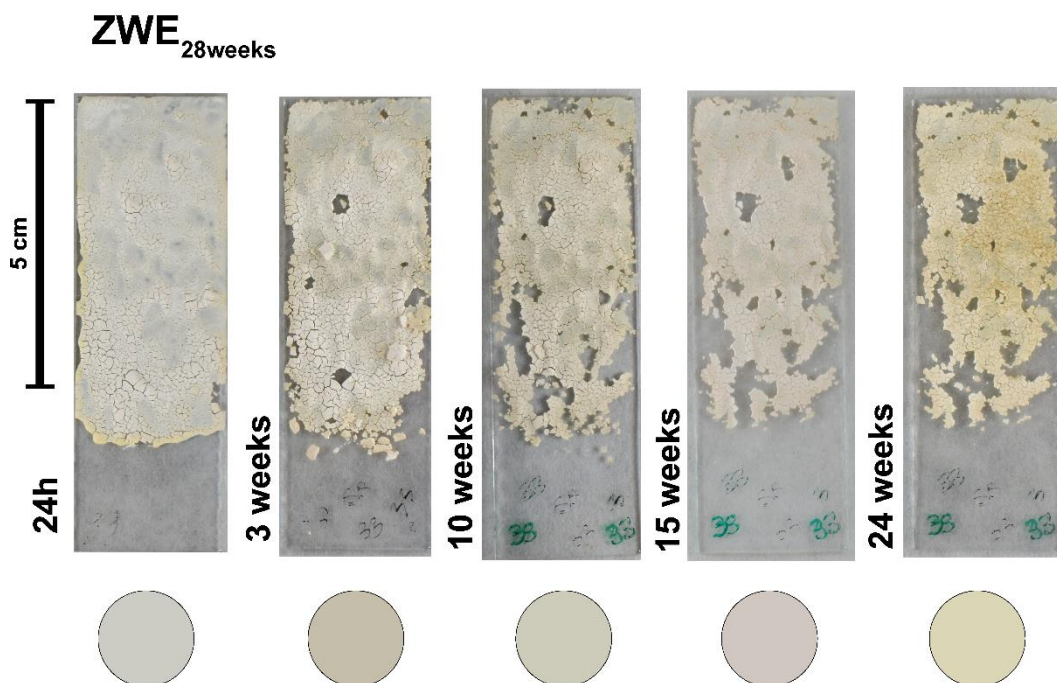


Figure 21. Photographs of sample ZWE_{28weeks} at different ageing times, it is possible to see the damage due to the brittleness of the paint layer. The circles under each photograph are a sample of the colour taken from a point of from the surface. The colour change evident at 24 weeks is produced by fungi hyphae in the surface.

b) Non-invasive monitoring

The SWIR data of the egg tempera mock-ups was less informative than the data obtained from the linseed oil samples. The egg binding medium is characterised by the $\nu(\text{CH}_2)$ 1st overtone at 5799 cm^{-1} , the $\nu(\text{CH}_2)$ 1st overtone at 5653 cm^{-1} and the combinations bands of $\nu(\text{OH})+\delta(\text{OH})$ at 5140 cm^{-1} and $\nu(\text{NH})+\delta(\text{NH})$ at 4852 cm^{-1} [55, 58].

Even if is less evident, the PC12 score and loading plots from sample ZWE_{28weeks} suggest that spectra obtained after 20 weeks of artificial ageing are characterised by the band at 1930 nm (5181 cm⁻¹) attributed to the presence of carboxylates (Figures 22 and 23, next page). The data from sample LWE_{19weeks} and ME_{63weeks} showed no clear trend related to the ageing (data not showed).

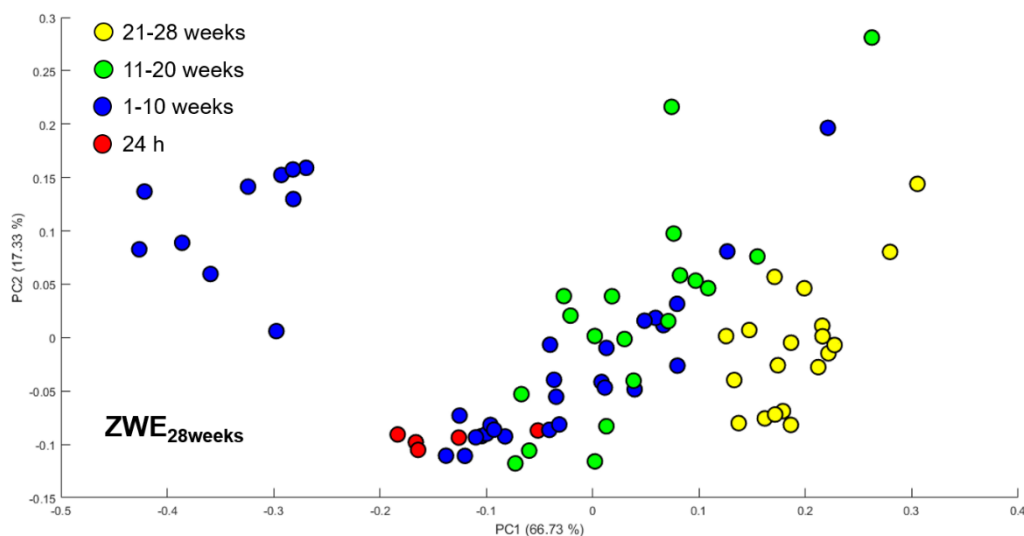


Figure 22. PC12 score plot from sample ZWE_{28weeks}. The separation of the different times of artificial ageing is less evident; however, is possible to identify the advance stages of ageing which according to the loading plots (Figure 21, next page), are characterised by the band 1930 nm (5181 cm⁻¹).

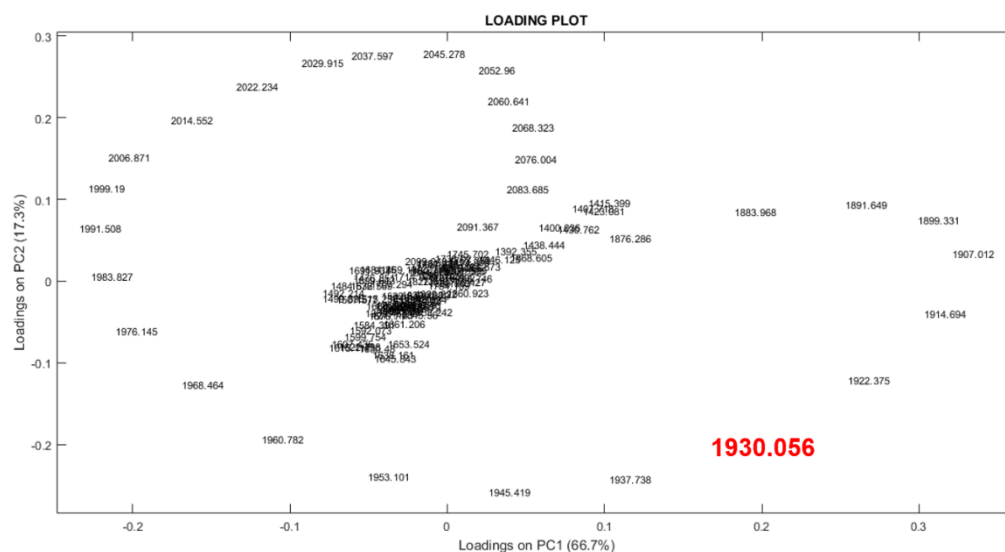


Figure 23. PC12 loading plot from the data obtained from the sample ZWE_{28weeks}. The band at 1930 nm (5181 cm⁻¹) characterises the spectra obtained after 20 weeks of artificial ageing in the score plot (Figure 22, previous page).

After 2 weeks of artificial ageing, the rFT-IR spectra of sample ZWE_{28weeks} exhibited the 3 derivative-like peaks at 1538 cm⁻¹, 1464 cm⁻¹, and 1397 cm⁻¹ ascribable to Pb palmitate/stearate, which suggest that crystalline carboxylates have been formed. The intensity of the 3 peaks increased with the ageing time (Figure 24).

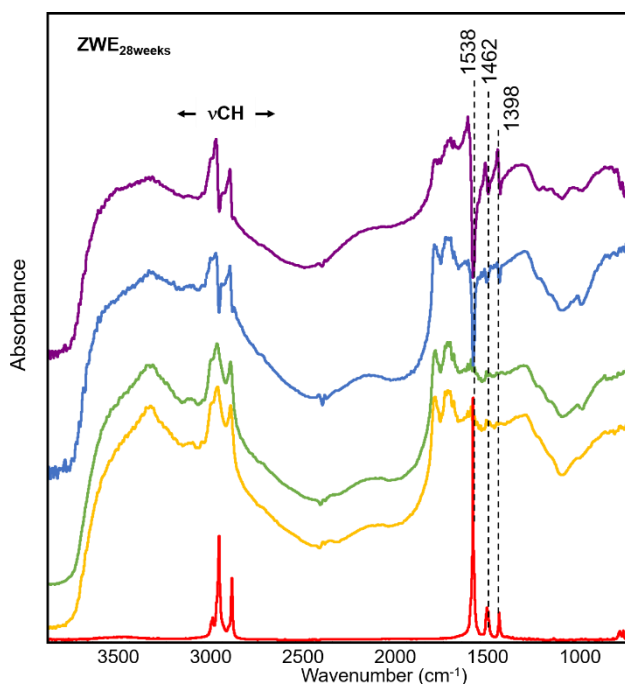


Figure 24. rFT-IR spectra from ZWE_{28weeks} sample, the characteristic peaks of crystalline carboxylates appeared after 2 weeks of artificial ageing and their intensity increased. Zn palmitate (red line), ZWE_{28weeks} after 24 h (yellow line), after 1 week (green line), after 2 weeks (blue line), and after 24 weeks (purple line).

Is probable that because the reduced modifications at the different ageing

times, the PCA of the SWIR data shows no clear differences. No amorphous phase was identified at the early stages of artificial ageing.

The sample $\text{LWE}_{19\text{weeks}}$ no evidence of carboxylates, probably because the intensity of inverted carbonate band at 1403 cm^{-1} hinders the characteristic bands (Figure 25). The same situation presented in the sample $\text{ME}_{63\text{weeks}}$, no evidence of carboxylates were identified using rFT-IR (data not showed). These results are in agreement with the SWIR data that did not show a clear differentiation between the different ageing times. This also confirms the higher reactivity of ZnO in comparison with the Pb pigments.

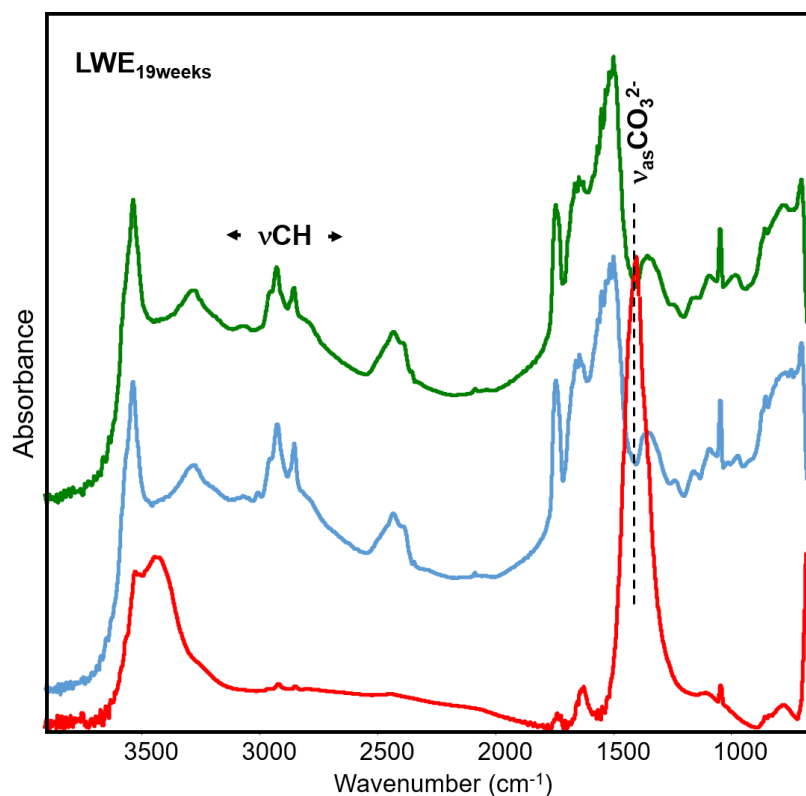


Figure 25. rFT-IR spectra from $\text{LWE}_{19\text{weeks}}$ sample, no evidence of carboxylate peaks are observed in the spectra. Lead carbonate (red line), $\text{ZWE}_{28\text{weeks}}$ after 24 h (blue line), and after 19 weeks (green line).

The results of the analyses of the three types of mock-ups suggest that SWIR and rFT-IR is less effective for monitoring the formation of carboxylates in egg tempera paintings, probably because the reduced formation of soaps caused by the lower content of FAs. The relative intensity of the amide I $\nu(\text{C}=\text{O})$ band at 1644 cm^{-1} and amide II $\delta(\text{N-H})$ band at 1542 cm^{-1} , as well as the $\nu(\text{CO}_3^{2-})$ band in the case of the $\text{LWE}_{19\text{weeks}}$ sample may hind the characteristic peaks of carboxylates.

Is worth noting that due to the development of fungi in two of the mock-ups (i.e., Zn and Pb white) the artificial ageing did not reach the same time as in the case of the oil sample, and was not possible to monitor the sample for long time.

c) Monitoring the crystallization of metal carboxylates

The μ -ATR-FT-IR spectra obtained from the surface of the sample $ZWE_{28weeks}$ (Figure 26) showed the characteristic peaks of crystalline carboxylates (1538 cm^{-1} , 1458 cm^{-1} , and 1396 cm^{-1}) after 2 weeks of artificial ageing, no evidence of amorphous carboxylates were identified at any time and the intensity of the peaks increased with the ageing. These results show the clear differences between the formation of carboxylates in oil films and egg tempera. In the last case, no amorphous stages are formed.

From a qualitative point of view, the comparison between the results obtained from the $ZWO_{63weeks}$ sample and the

$ZWE_{28weeks}$ sample supports the hypothesis already proposed regarding the carboxylates formation pathway. In oil films the process implies an initial state (i.e., amorphous) where the carboxylates are linked to the polymeric network or trapped and after the hydrolysis of the network, the free

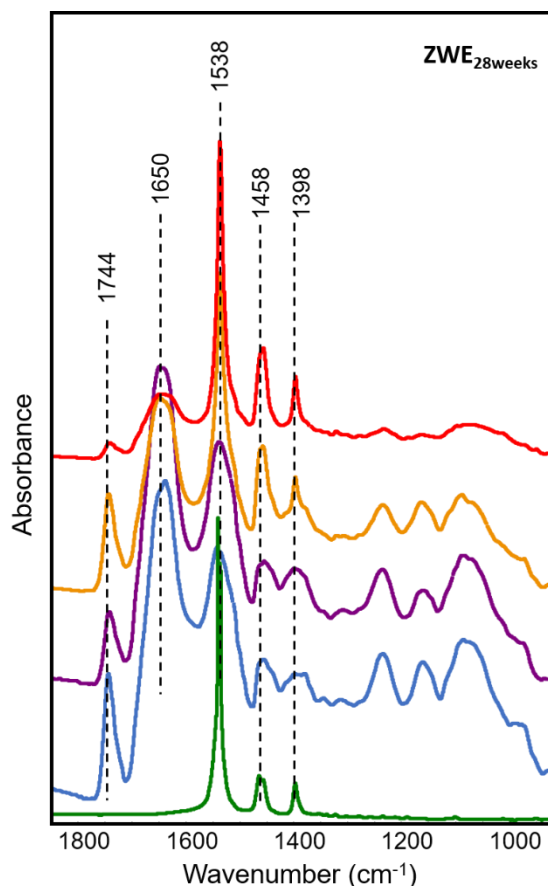


Figure 26. μ -ATR spectra obtained from the surface of sample $ZWE_{28weeks}$ at different ageing times, the three peaks at 1538 cm^{-1} , 1458 cm^{-1} and 1398 cm^{-1} ascribable to Zn palmitate/stearate are clearly evident after 2 weeks of artificial ageing. Zn palmitate (green line), $ZWE_{28weeks}$ after 24 h (blue line), 1 week (purple line), 2 weeks (yellow line), 6 weeks (red line).

carboxylates crystallise. On the other hand, in egg tempera films, even if the FAs in the egg follow a process of cross-linking similar to the oil, the degree of crosslinking is lower and thus more FFAs are easily formed and can form FMCs that crystallise.

To confirm the presence of crystalline structure in the sample, we took a chip from the ZWE_{10weeks} after 10 weeks of artificial ageing and analysed it using a Huber XRPD diffractometer; however, no evidence of crystalline compounds apart from the pigment are present in the pattern. Thus, to determine in a qualitative way the detection limit of Zn palmitate mixed with ZnO we analysed standard mixtures of the two components at different concentrations. The results show that to identify zinc palmitate in presence of zinc white (ZnO) is required a concentration higher than 10% of Zn palmitate (w/w %).

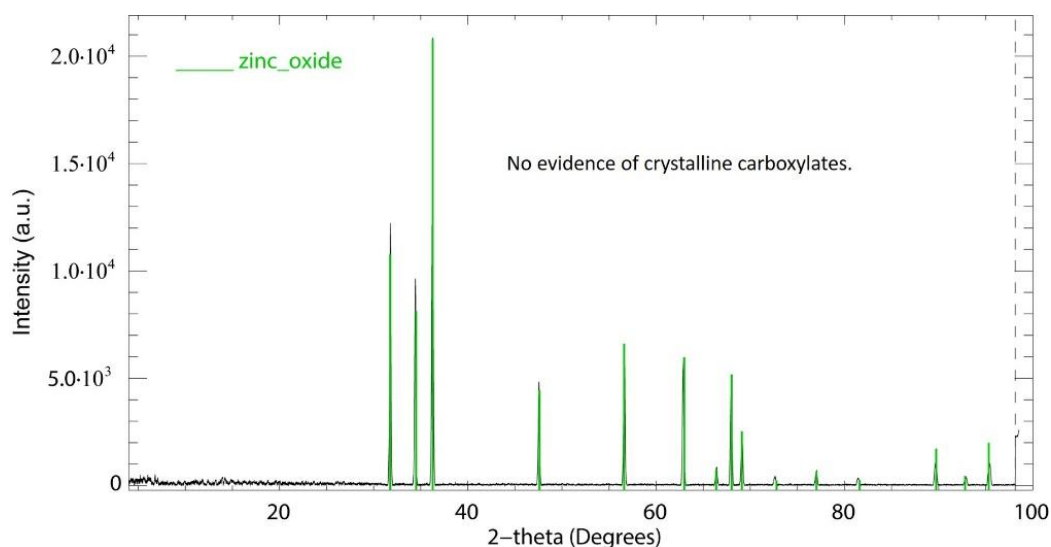


Figure 27. XRPD pattern of a sample from ZWE_{10weeks}, there is no evidence of crystalline carboxylates probably due to the high relative intensity of the characteristic peaks from the pigment ZnO.

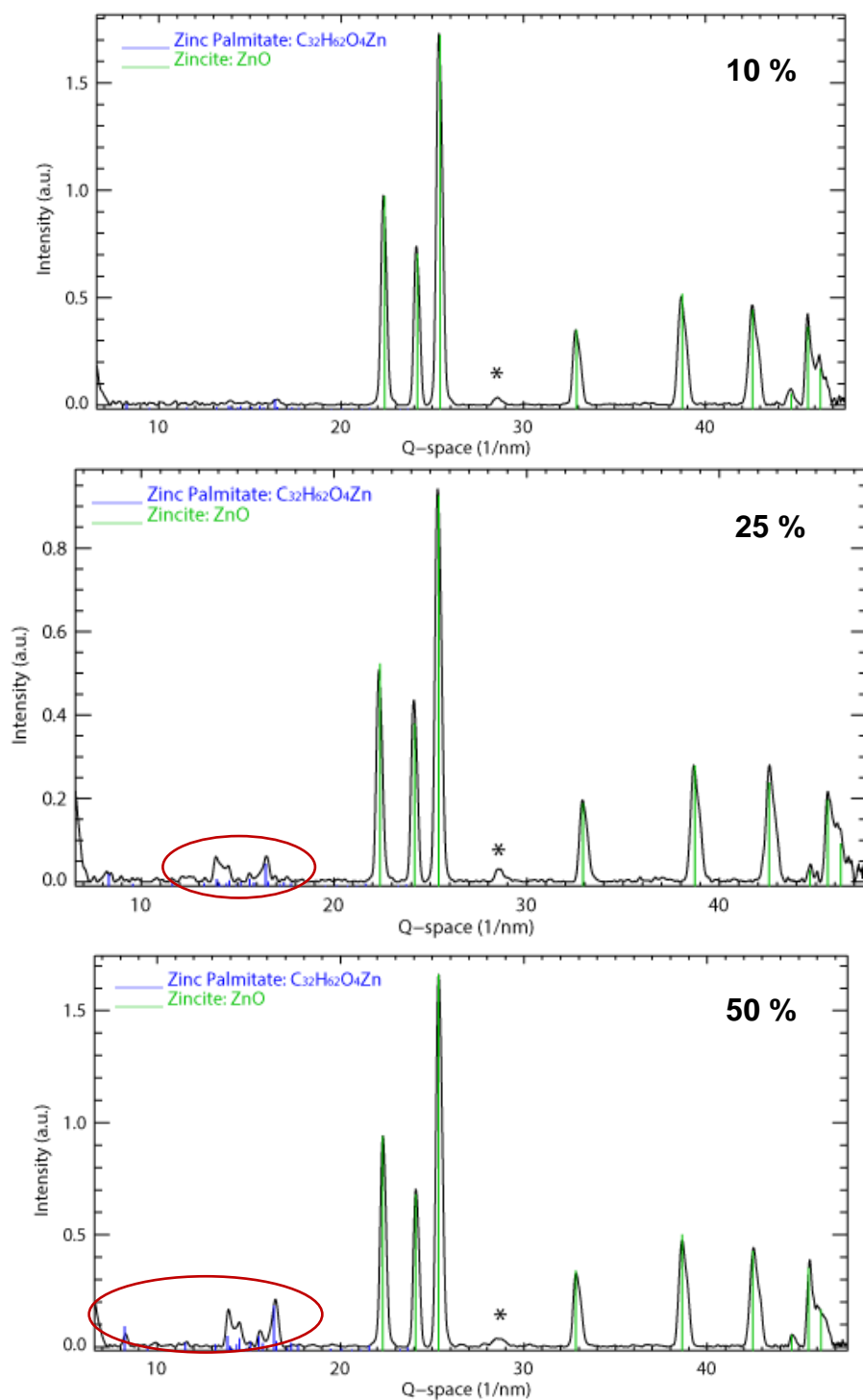


Figure 28. XRPD pattern from the samples of Zn palmitate and ZnO at different concentrations. The * indicates peaks produced by a silver plate misalignment, as it can be seen in the range analysed, already at 10% is complicate to clearly identified the signal characteristic from crystalline Zn palmitate.

These results are in accordance with the data obtained from the GC-MS analysis. Indeed, the values obtained from the measurements of the sample ZWE_{10weeks} suggest that the amount of free metal carboxylates is around 1.4% (w/w %) (Complete data in Appendix 4). The fact that we observed in FT-IR strong peaks suggest that the crystalline carboxylates are located in the surface, probably as the result of the migration. The distribution of the carboxylates was assessed by analysing a cross-section of sample ZWE_{10weeks}. The results confirmed that the carboxylates are confined to the surface of the layer.

The spectra also shows that the peak at 1741 cm^{-1} , 1255 cm^{-1} , 1158 cm^{-1} , and 1088 cm^{-1} , attributed to the triglycerides ester linkages. According to Meilunas and colleagues [28], these features are not visible in dry egg films, in addition, the shift of the band at 1736 cm^{-1} in the spectra obtained from the bottom of the cross-section can be attributed to triglyceride derived aldehydes produced by the degradation of the binder.

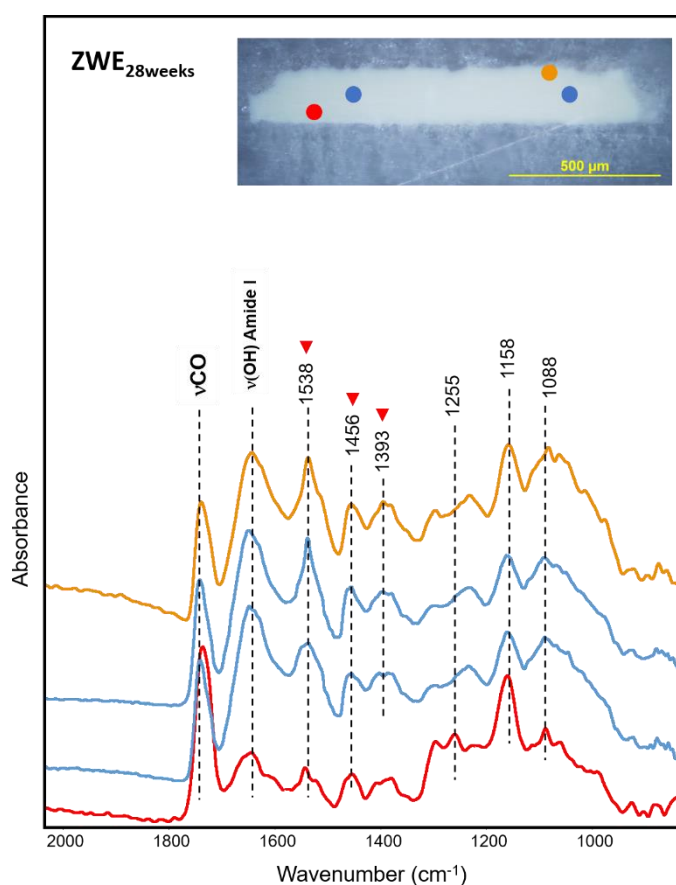


Figure 29. Microphotograph and μ -FT-IR spectra obtained from the bottom of the cross-section (red line), the middle part (blue line), and the surface (yellow line). It is clear the different distribution of the carboxylates through the cross-section. The colour circles indicate the point of analysis.

On the other hand, we observed clear evidence of crystalline carboxylates (i.e., peak at 1536 cm^{-1} and 1512 cm^{-1}) in the sample $\text{LWE}_{19\text{weeks}}$ after 7 weeks of artificial ageing (Figure 27). In this case, the strong carbonate band at 1391 cm^{-1} and the amide II $\delta(\text{NH})$ at 1542 cm^{-1} interfere and probably hinder the carboxylate band in the early stages of ageing.

The formation of carboxylates was clearer in the sample $\text{ME}_{63\text{weeks}}$ (Figure #) because there was no influence of the carbonate band and, as it was notice also in the analysis of oil samples, minium is more reactive than

lead white. We identified the characteristic peaks of crystalline Pb carboxylates (i.e., 1512 cm^{-1} and 1536 cm^{-1}) after 2 weeks of artificial ageing, the distribution was inhomogeneous in the surface. Because the sample remained inside the ageing chamber for a longer time, it was possible to monitor their changes; the intensity of the carboxylate band increased with the ageing time.

We also observed a strong band at 1398 cm^{-1} assigned to CO_3^{2-} group that increased with the ageing, it can be attributed to the degradation of the pigment as it was already reported in previous researches [14, 1]. As in the case of $\text{ZWE}_{28\text{weeks}}$ sample, neither in sample $\text{LWE}_{19\text{weeks}}$ nor $\text{ME}_{63\text{weeks}}$ broad bands ascribable to amorphous carboxylates were identified in the spectra.

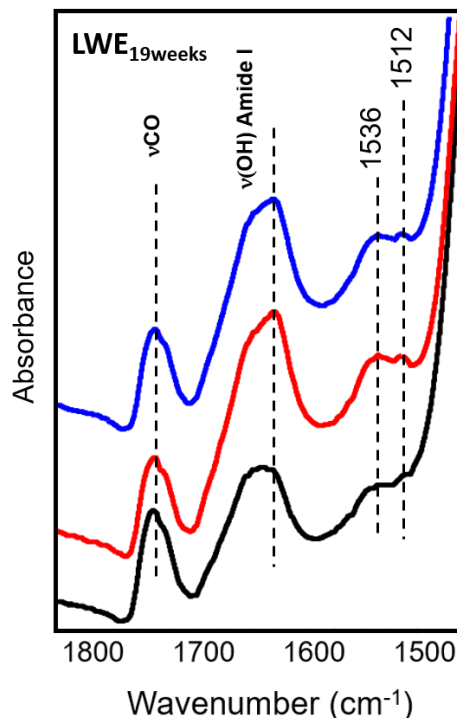


Figure 30. Macro ATR FT-IR spectra of sample $\text{LWE}_{19\text{weeks}}$, the peaks of crystalline carboxylates are evident after 7 weeks of artificial ageing.

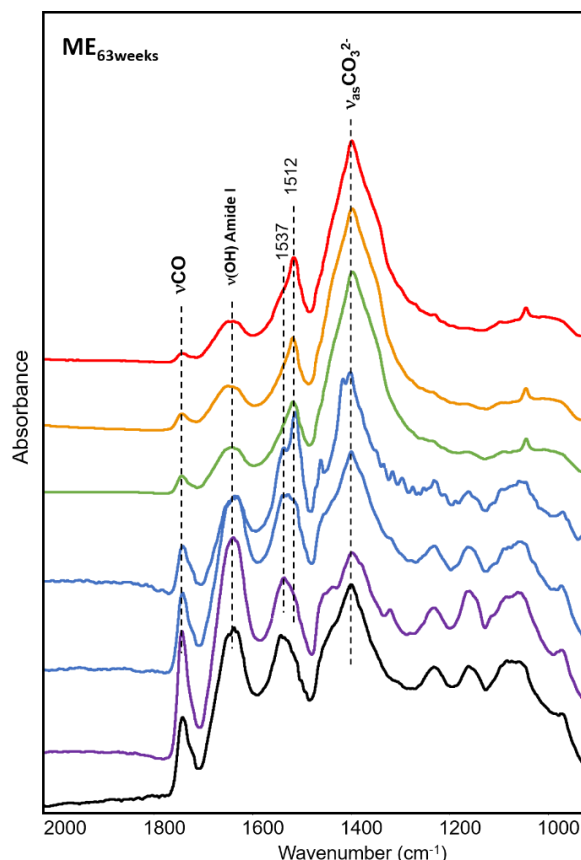


Figure 31. μ -FT-IR spectra from the surface of sample ME63weeks, the peaks of crystalline carboxylates (i.e., 1537 cm^{-1} and 1512 cm^{-1}) appeared after 2 weeks of artificial ageing (blue line) and increased in intensity. It is evident the strong band at 1398 cm^{-1} assigned to carbonates, which suggest that minium has degrade and transformed into Pb carbonate. ME63 weeks after 24 h (black line), 1 week (purple line), 2 weeks (blue line), 33 weeks (green line), 47 weeks (yellow line), 63 weeks (red line).

The CG-MS data, summarised in table 4, obtained from samples $\text{LWE}_{10\text{weeks}}$ and $\text{ME}_{10\text{weeks}}$ after 10 weeks of artificial ageing indicate that the former contains lower quantity of FMCs than the latter, which is in accordance to the FT-IR results.

Table 4. Relative percentages of the quantified free metal carboxylates (FMC) using GC-MS of samples after 10 weeks of natural and artificial ageing, the complete data is reported in Appendix 4 and in [52]. σ = standard deviation.

Mock-up	Natural aging (w %)			Artificial aging (w %)		
	FFA	FFA+FMC	FMC	FFA	FFA+FMC	FMC
ZWE	0.3 (σ 0.1)	0.7 (σ 0.4)	0.4	1.2 (σ 2.0)	2.6 (σ 0.5)	1.4
ME	0.4 (σ 0.2)	1.0 (σ 0.7)	0.6	1.7 (σ 0.4)	3.8 (σ 2.0)	2.2
LWE	0.6 (σ 0.1)	1.1 (σ 0.3)	0.6	0.8 (σ 0.3)	1.1 (σ 0.3)	0.5

The analyses of cross-section samples confirm that carboxylates are present in low concentration and probably are distributed mainly in the surface. In the spectra obtained from a sample from the mock-up ME_{63weeks}, taken after 35 weeks, the characteristic bands of carboxylates are hindered by the amide II band, only in the surface of the sample some features at 1540 cm⁻¹ and 1524 cm⁻¹ suggest the presence of carboxylates.

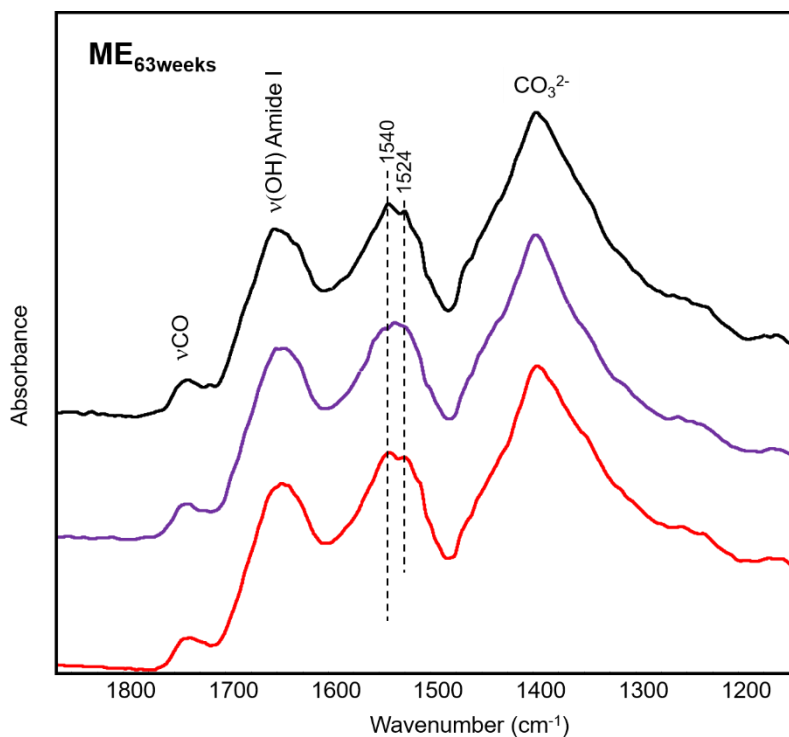


Figure 32. μ -ATR spectra obtained from the cross-section of sample ME_{63weeks}, the peaks ascribable to the carboxylates are present mainly in the surface of the sample (black line). Middle of the sample (purple line), bottom of the sample (red line). The formation of carbonate due to degradation is evident.

3.4.3 Study of metal carboxylates in beeswax films

a) Macroscopic effects of the artificial degradation

The changes of the samples of beeswax are related to the deposition of dust over the surface. The ageing did not produce particular changes. Since the binding medium is very sticky, damage produced by the ATR analysis modified the surface, however also the physical properties of the film remain unaltered after ageing.

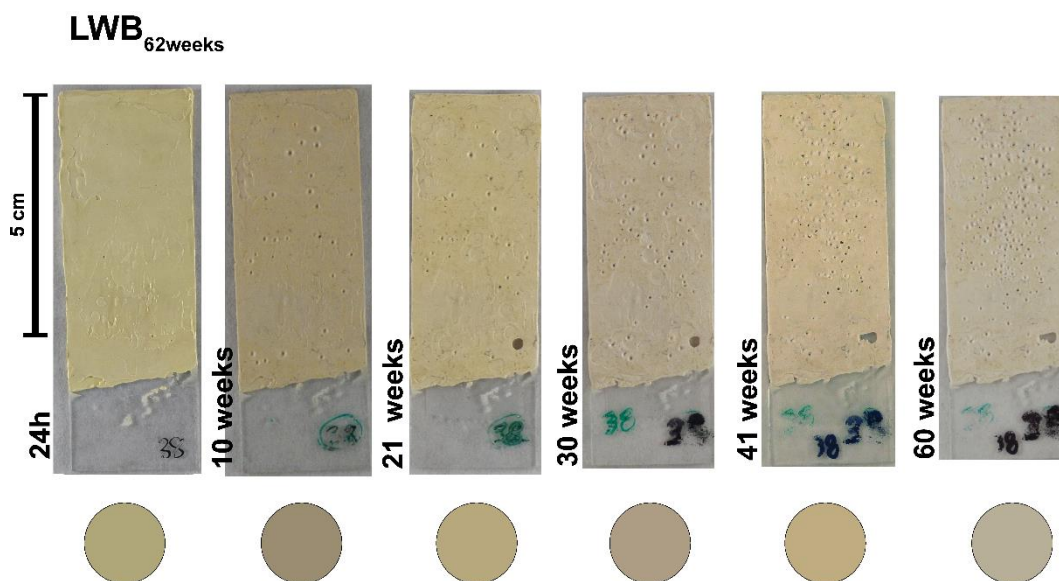


Figure 33. Photographs of sample LWB_{62weeks} at different ageing times, it is possible to see the damage due to the ATR analyses. The circles under each photograph are a sample of the colour taken from a point of from the surface. The colour change is related to the deposition of dust over the surface.

b) Non-invasive monitoring

SWIR spectra show the bands of the $\nu_a(\text{CH})$ 2nd overtone at 8230 cm^{-1} , the $\nu_a(\text{CH}_2)$ 1st overtone at 5780 cm^{-1} , and the $\nu_s(\text{CH}_2)$ 1st overtone at 5678 cm^{-1} from the beeswax. The PCA of SWIR data from sample $\text{ZWB}_{62\text{weeks}}$ does not show particular differences between the different ageing times, this suggest that there are few modifications. Sample $\text{LWB}_{62\text{weeks}}$ and $\text{MB}_{62\text{weeks}}$ showed the same results (data not showed).

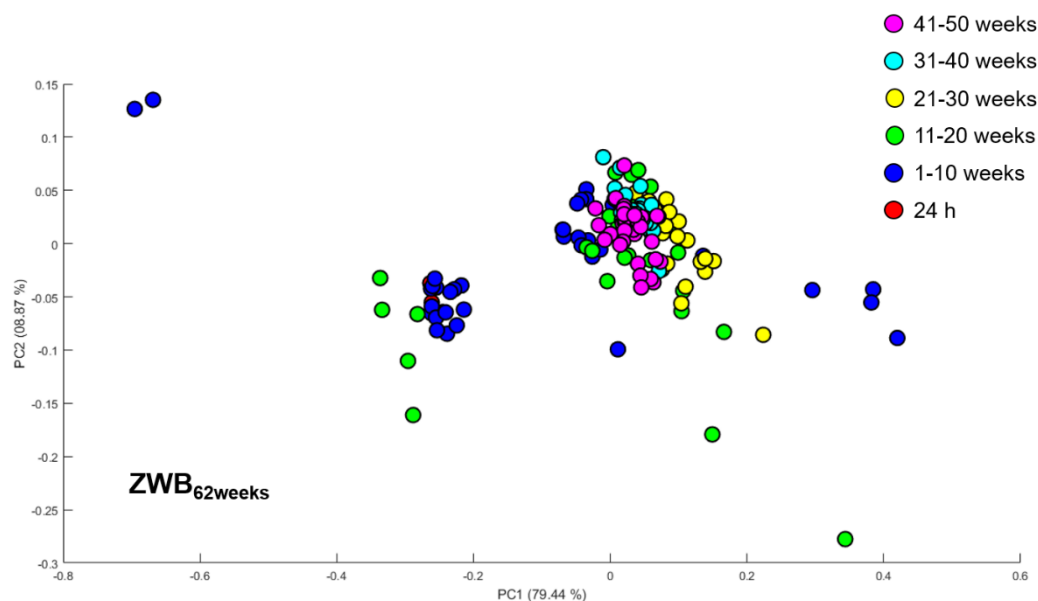
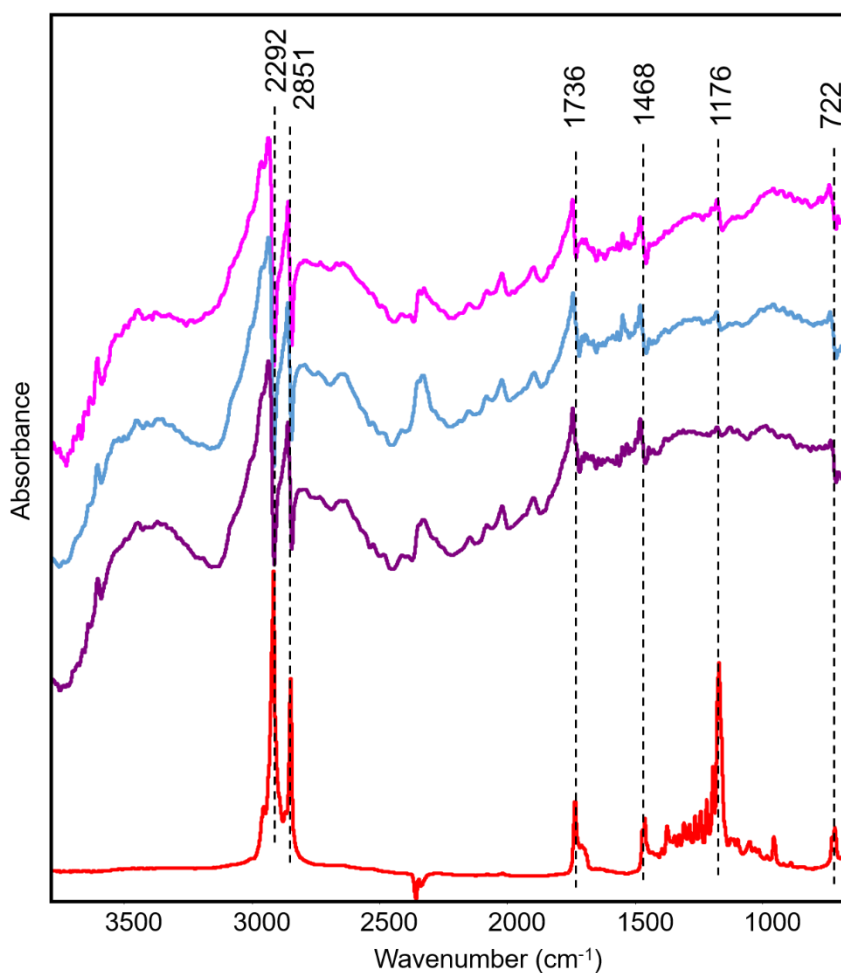


Figure 34. PC12 score plot from sample $\text{ZWB}_{62\text{weeks}}$. The different times of ageing are mixed together, probably because the small variations on the chemical composition of the mock-ups.

In agreement with the SWIR data, the rFT-IR spectra from $\text{ZWB}_{62\text{weeks}}$ show no evidence of carboxylates at any ageing time (from 1 week to 60 weeks) (Figure 34, next page). The spectra show only the characteristic peaks of the binding media (Table 4, next page). The same results were obtained from $\text{LWB}_{62\text{weeks}}$ and $\text{MB}_{62\text{weeks}}$ samples.

Table 5. Some of the characteristic peaks of beeswax identified in the rFT-IR spectra from the three type of samples [63].

Band (cm^{-1})	Assignment	Deformation
2922	$\nu_{\text{as}}(\text{CH}_2)$	Derivative
2851	$\nu_{\text{s}}(\text{CH}_2)$	Derivative
1736	$\nu\text{C}=\text{O}$	Derivative
1468	CH_2 scissoring indicating the semicrystalline structure of beeswax	Derivative
1176	CO	Derivative
722	CH_2 rocking indicating the semicrystalline structure of beeswax	Derivative

**Figure 35.** rFT-IR spectra from sample $\text{ZWB}_{62\text{weeks}}$, there is no evidence of carboxylates at any ageing time. Beeswax standard (red line), sample $\text{ZWB}_{62\text{weeks}}$ after 24 h (purple line), after 6 weeks (blue line), and after 60 weeks (magenta line).

c) Monitoring the crystallization of metal carboxylates

Despite the fact that no evidence of carboxylates was identified using non-invasive methods, in the sample ZWB_{62weeks} shows an intense and well define peak at 1538 cm⁻¹ attributed to crystalline Zn carboxylates (Zn stearate/palmitate) already after 24 h, with the ageing time its intensity increases. After 4 weeks the spectra show peak splitting into doublets at 1735 cm⁻¹ attributed to ν C=O of esters and at 1722 cm⁻¹ attributed to C=O from ketone/acids or free fatty acids [64, 63].

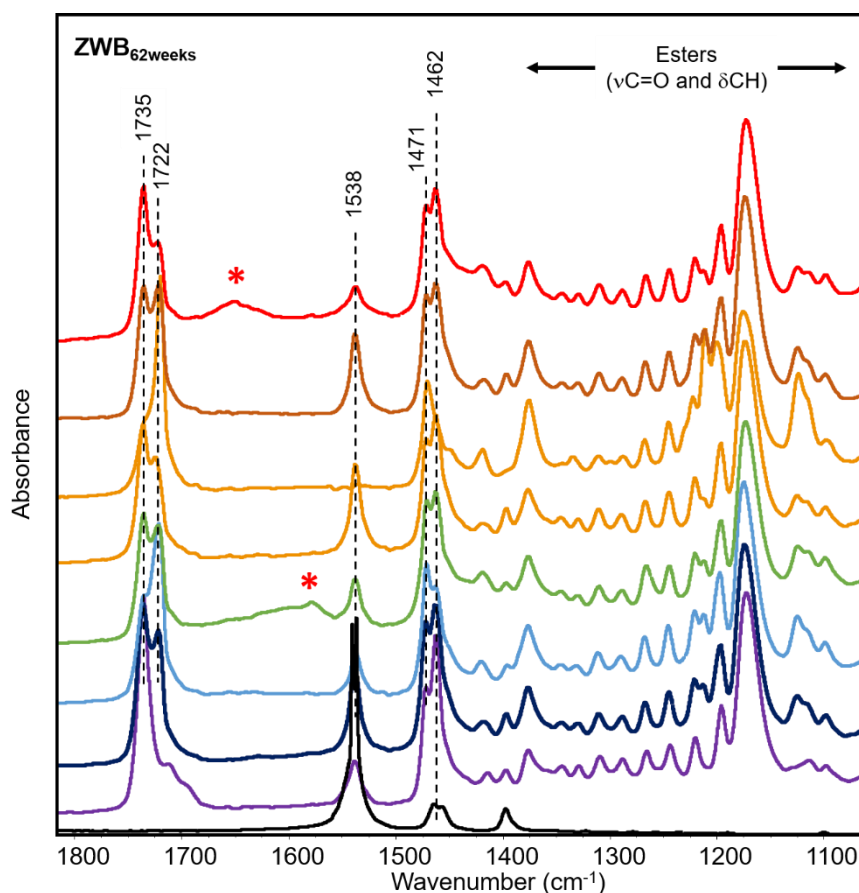


Figure 36. μ -FT-IR spectra from the surface of sample ZWB_{62weeks}, the peak of Zn carboxylates (1538 cm⁻¹) present already after 24 h. The intensity increased with the ageing but also variety from point to point, which indicates that the distribution is inhomogeneous. In some point bands were identified in the region 1700-1600 cm⁻¹ (marked with *) derived from dirt deposition or water condensation over the surface because the sample were cooled before analysis to harden. Zn palmitate standard (black line), ZWB_{62weeks} after 24 h (purple line), after 4 weeks (dark blue line), after 6 weeks (light blue line), after 25 weeks (green line), after 33 weeks (yellow lines), after 40 weeks (orange line), after 60 weeks (red line).

We observed a similar behaviour in the sample LWB_{62weeks}, the peaks of crystalline Pb carboxylates at 1509 cm⁻¹ and a shoulder at 1540 cm⁻¹, appear already after 24 h, but the high relative intensity of the CO₃²⁻ band from the pigment at 1400 cm⁻¹ partially hindered them. The intensity increased with the ageing. The peak at 1722 cm⁻¹ appeared after 2 weeks. The intensity increases of the carboxylate peak at 1515 cm⁻¹ associated to the ageing was more evident in the MB_{62weeks} sample. The degradation of the pigment was also evident after 33 weeks since the band at 1392 cm⁻¹ assigned to CO₃²⁻ suggest minium partially transformed into Pb carbonate. In any of the three types of mock-ups containing beeswax as binding medium features of amorphous carboxylates were identified at any time. Different from egg tempera, all the three pigments formed carboxylates after 24 h.

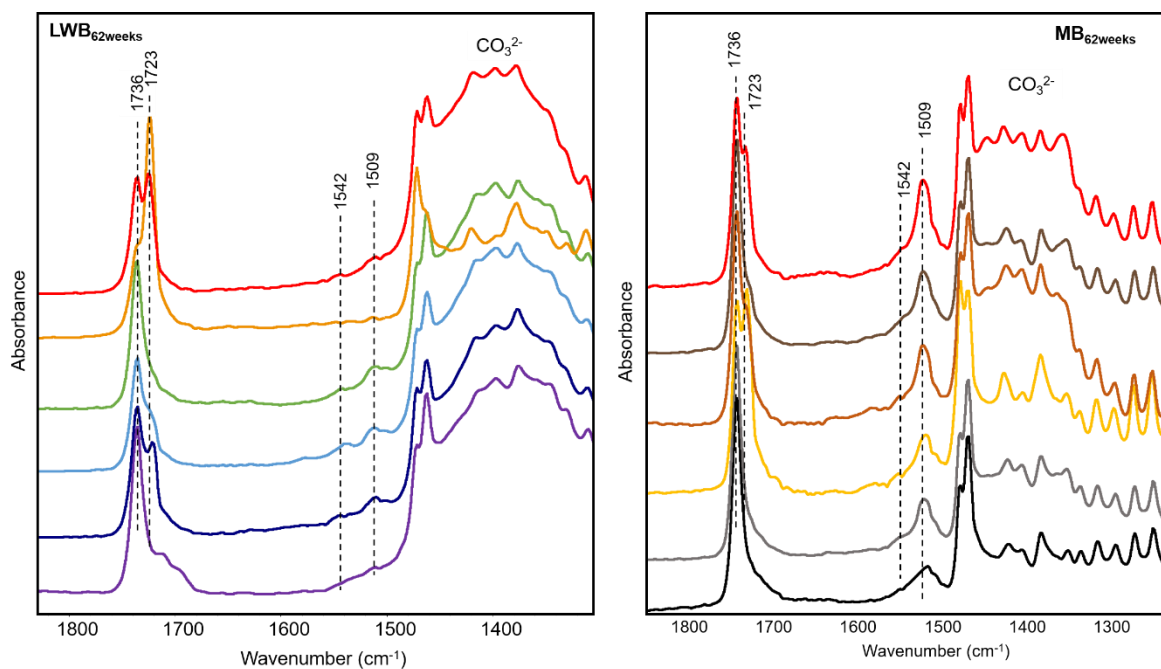


Figure 37. μ -FT-IR spectra from the surface of the samples. Spectra from LWB_{62weeks} after 24h (purple line), after 6 weeks (dark blue), after 25 weeks (light blue line), after 33 weeks (green line), after 40 weeks (yellow line), and after 60 weeks (red line). Spectra from sample MB_{62weeks} after 24 h (black line), after 6 weeks (grey line), after 25 weeks (yellow line), after 33 weeks (orange line), after 40 weeks (brown line) and after 60 weeks (red line).

The cross-section analyses after 32 weeks showed a homogenous distribution of carboxylates trough the film in samples ZWB_{62weeks} and

MB_{62weeks}, which suggest no migration is produced. On the other hand, in the sample LWB_{62weeks}, was contaminated and Ca carboxylates formed as suggested by the two intense band at 1577 cm⁻¹ and 1544 cm⁻¹ assigned to the $\nu_a\text{COO}^-$ [65], which suggest that even deposited materials may produce Ca carboxylates in beeswax films, and thus complicate the characterization of recipe used for the preparation of the film.

3.4.4 Discussion

The results described previously support the hypothesis of the formation of an ionomer-like structure [3, 8, 26] during the curing of oil films. In all the FT-IR spectra of the early stages are dominated by a broad band. The GC-MS data indicates that only a low amount of free metal carboxylates were formed after 10 weeks of artificial ageing indicating that amorphous free metal soaps are not enough to be the dominant specie that produces the broad band.

In the advanced stages, the formation of crystalline carboxylates can be related to the degradation of the oil ionomer since no other source of free fatty acids was present. Physical damage also appeared after the crystalline carboxylates were identified, being possible to linked the damaged with the formation of crystalline carboxylates. The cross-section analyses offers evidence about the migration of free metal carboxylates, since they were mainly localized in the surface of the sample. The results also showed that after 63 weeks is still possible to identify the broad band of the ionomer simultaneously with the features of the crystalline carboxylates, suggesting that there is not a complete hydrolysis of the ionomer.

The results also show the clear difference between binding media and pigments. Regarding the pigments, as it was already reported [9, 24], the most reactive was zinc white, followed by minium [61] and the least reactive of the three pigments studied was lead white.

The whole egg tempera and the beeswax showed no evidence of broad band arising from amorphous carboxylates, this is in accordance to what

has been previously reported [30, 31]. Between these two binders, beeswax seems produce faster the crystalline carboxylates in comparison with the whole egg tempera but it is more stable, since no damage was identified in any of the mock-ups.

Finally, regarding the non-invasive methodologies tested, SWIR allow to monitor the ageing process only in the cases where bigger chemical changes were produced (i.e., oil mock-ups), however, it does not allow to differentiate the type of carboxylate formed. On the other hand, despite the deformation in the reflectance spectra, it was possible in many of the cases to identify the type of carboxylate, but it depends on the concentration and thus the intensity of the bands in order to be identified.

3.5 Conclusions

In summary the results of the analyses of the three typologies of mock-ups suggest clear differences on the mechanism of formation of metal carboxylates in the different binders as well as difference in the reactivity of the pigments.

The most reactive pigment was zinc white which led to a fast formation carboxylates and crystallisation, it was also the pigment that produce higher damage to film, since it became very fragile. As it was already reported [61], among the Pb pigments the most reactive was minium, which also degraded transforming into Pb carbonate [14] and was the only pigment that effectively inhibited the formation of fungi in egg tempera films.

The data supports previous hypothesis, in oil films, the initial stage of formation is characterised by an amorphous state [3, 8], the FT-IR and GC-MS results suggest the simultaneous presence of probably ionomer-like structure and free metal carboxylates. The last one increase with the ageing and degradation of the oil film, migrate and crystallise. After the increasing of crystalline carboxylates, the films started to become fragile, so is possible to associate the presence of crystalline carboxylate with the damage of the paintings.

No amorphous carboxylates were identified in egg tempera or beeswax samples, and the most stable binder was beeswax that even in the presence of metal soaps kept its properties and colour.

References

- [1] M. Cotte, E. Checroun, W. De Nolf, Y. Taniguchi, L. De Viguerie, M. Burghammer, P. Walter, C. Rivard, M. Salomé, K. Janssens and J. Susini, "Lead soaps in paintings: Friends or foes?," *Studies in Conservation*, 2016.
- [2] M. P. Luxán and F. Dorrego, "Reactivity of earth and synthetic pigments with linseed oil," *Surface Coatings International*, vol. 8, pp. 390-402, 1999.
- [3] J. J. Hermans, K. Keune, A. Van Loon and P. D. Iedema, "Toward a Complete Molecular Model for the Formation of Metal Soaps in Oil Paints," in *Metal Soaps in Art*, F. Casadio, K. Keune, P. Noble, A. Van Loon, E. Hendriks, S. A. Centeno and G. Osmond, Eds., Springer, Cham, 2019, pp. 47-67.
- [4] F. Gabrieli, F. Rosi, A. Vichi, L. Cartechini, L. Pensabene Buem, S. G. Kazarian and C. Miliani, "Revealing the Nature and Distribution of Metal Carboxylates in Jackson Pollock's Alchemy (1947) by Micro-Attenuated Total Reflection FT-IR Spectroscopic Imaging," *Analytical Chemistry*, vol. 89, no. 2, pp. 1283-1289, 2017.
- [5] J. La Nasa, F. Modugno, M. Aloisi, A. Lluveras-Tenorio and I. Bonaduce, "Development of a GC/MS method for the qualitative and quantitative analysis of mixtures of free fatty acids and metal soaps in paint samples," *Analytica Chimica Acta*, vol. 1001, pp. 51-58, 2018.
- [6] E. Cano and D. Lafuente, "Corrosion inhibitors for the preservation of metallic heritage artefacts," in *Corrosion and Conservation of cultural*

heritage metallic artefacts, P. Dillmann, D. Watkinson, E. Angelini and A. Adriaens, Eds., WoodHead Publishing. European Federation of Corrosion, 2013, pp. 570-594.

- [7] F. Mirambet, S. Reguer, E. Rocca, S. Hollner and D. Testemale, "A complementary set of electrochemical and X-ray synchrotron techniques to determine the passivation mechanism of iron treated in a new corrosion inhibitor solution specifically developed for the preservation of metallic artefacts," *Applied Physics A*, vol. 99, pp. 341-349, 2010.
- [8] J. J. Hermans, K. Keune, A. van Loon, R. W. Corkery and P. D. Iedema, "Ionomer-like structure in mature oil paint binding media," *RSC Adv.*, vol. 6, p. 93363–93369, 2016.
- [9] J. J. Hermans, K. Keune, A. van Loon and P. D. Iedema, "An infrared spectroscopic study of the nature of zinc carboxylates in oil paintings," *J. Anal. At. Spectrom.*, vol. 30, p. 1600–1608, 2015.
- [10] J. J. Boon, J. van der Weerd, K. Keune, P. Noble and J. Wadum, "Mechanical and chemical changes in Old Master paintings: dissolution, metal soap formation and remineralization processes in lead pigmented ground/intermediate paint layers of 17th century paintings," in *13th Triennial ICOM meeting Rio de Janeiro*, Rio de Janeiro, 2002.
- [11] J. Hermans, *Metal soaps in oil paint: Structure, mechanisms and dynamics*, Amsterdam: University of Amsterdam, 2017.
- [12] Y. Shimadzu and K. van den Berg, "On metal soap related colour and transparency changes in a 19th C painting by Millais," in *Reporting Highlights of the De Mayerne Programme*, J. J. Boon and E. S. Ferreira, Eds., The Hague, Netherlands Organisation for Scientific Research, 2006, pp. 43-52.

- [13] L. Chua, "Whitish haze, soapy globules: micro-analysis of degraded burmese paintings on zinc supports," *Heritage Science*, vol. 7, no. 46, 2019.
- [14] R. Mazzeo, S. Prati, M. Quaranta, E. Joseph, E. Kendix and M. Galeotti, "Attenuated total reflection micro FTIR characterisation of pigment–binder interaction in reconstructed paint films," *Anal. Bioanal. Chem.*, vol. 392, p. 65–76, 2008.
- [15] L.-C. Pavlopoulou and D. Watkinson, "The degradation of oil painted copper surfaces," *Studies in Conservation*, vol. 51, no. Sup1, pp. 55-65, 2006.
- [16] M. Matteini and A. Moles, *La Chimica nel restauro. I materiali dell'arte pittorica*, Florence: Nardini editore, 2010.
- [17] L. de Viguerie, P. A. Payard, E. Portero, P. Walter and M. Cotte, "The drying of linseed oil investigated by Fourier transform infrared spectroscopy: Historical recipes and influence of lead compounds," *Progress in Organic Coatings*, vol. 93, p. 46–60, 2016.
- [18] M. Lazzari and O. Chiantore, "Drying and oxidative degradation of linseed oil," *Polymer Degradation and Stability*, vol. 65, pp. 303-313, 1999.
- [19] L. Baij, L. Chassouant, J. J. Hermans, K. Keune and P. D. Iedema, "The concentration and origins of carboxylic acid groups in oil paint," *RSC Advances*, vol. 9, p. 35559–35564, 2019.
- [20] M. Cotte, E. Checroun, J. Susini, P. Dumas, P. Tchoreloff, M. Besnard and P. Walter, "Kinetics of oil saponification by lead salts in ancient preparations of pharmaceutical lead plasters and painting lead mediums," *Talanta*, vol. 70, p. 1136–1142, 2006.
- [21] V. Di Tullio, N. Zumbulyadis, S. A. Centeno, J. Catalano, M. Wagner and C. Dybowski, "Water Diffusion and Transport in Oil Paints as

- Studied by Unilateral NMR and ^1H High-Resolution MAS-NMR Spectroscopy,” *Chem Phys Chem*, vol. 21, p. e1900858, 2020.
- [22] J. Catalano, A. Murphy, Y. Yao, N. Zumbulyadis, S. A. Centeno and C. Dybowski, “Molecular dynamics of palmitic acid and lead palmitate in cross-linked linseed oil films: Implications from deuterium magnetic resonance for lead soap formation in traditional oil paintings,” *Solid State Nuclear Magnetic Resonance*, vol. 89, p. 21–26, 2018.
- [23] T. A. Ibidapo, “The Characterization of the Halatopolymers: A Review,” *Polymer Engineering and Science*, vol. 36, no. 14, pp. 1920-1927, 1996.
- [24] L. Bertrand, M. Réfrégiers, B. Berrie, J.-P. Échard and M. Thoury, “A multiscale photoluminescence approach to discriminate among semiconducting historical zinc white pigments,” *Analyst*, vol. 138, no. 16, pp. 4463-4469, 2013.
- [25] S. Hageraats, K. Keune, S. Stankic, S. Stanescu, M. Tromp and M. Thoury, “X-ray Nanospectroscopy Reveals Binary Defect Populations in Submicrometric ZnO Crystallites,” *The Journal of Physical Chemistry C*, vol. 124, pp. 12596-12605, 2020.
- [26] J. J. Hermans, L. Baij, M. Koenis, K. Keune, P. D. Iedema and S. Woutersen, “2D-IR spectroscopy for oil paint conservation: Elucidating the water-sensitive structure of zinc carboxylate clusters in ionomers,” *Sci. Adv.*, vol. 5, p. eaaw3592, 2019.
- [27] M. P. Colombini, F. Modugno, R. Fuoco and A. Tognazzi, “A GC-MS study on the deterioration of lipidic paint binders,” *Microchemical Journal*, vol. 73, p. 175–185, 2002.
- [28] R. J. Meilunas, J. G. Bentsen and A. Steinberg, “Analysis of Aged Paint Binders by FTIR Spectroscopy,” *Studies in Conservation*, vol. 35, pp. 33-51, 1990.

- [29] N. Salvadó, S. Butí, J. Nicholson, H. Emerich, A. Labrador and T. Pradell, "Identification of reaction compounds in micrometric layers from gothic paintings using combined SR-XRD and SR-FTIR," *Talanta*, vol. 79, p. 419–428, 2009.
- [30] N. Salvadó, S. Butí, T. Pradell, V. Beltran, G. Cinque and J. Juanhuix, "Identification and Distribution of Metal Soaps and Oxalates in Oil and Tempera Paint Layers in Fifteenth-Century Altarpieces Using Synchrotron Radiation Techniques," in *Metal Soaps in Art*, F. Casadio, K. Keune, P. Noble, A. Van Loon, E. Hendriks, S. A. Centeno and G. Osmond, Eds., Springer, Cham, 2019, pp. 195-210.
- [31] S. Svarcová, E. Kocí, J. Plocek, A. Zhankina, J. Hradilová and P. Bezdick, "Saponification in egg yolk-based tempera paintings with lead-tin yellow type I," *Journal of Cultural Heritage*, vol. 38, pp. 8-19, 2019.
- [32] E. Kočí, J. Rohlíček, L. Kobera, J. Plocek, S. Švarcová and P. Bezdička, "Mixed lead carboxylates relevant to soap formation in oil and tempera paintings: the study of the crystal structure by complementary XRPD and ssNMR," *Dalton Transactions*, vol. 48, pp. 12531-12540, 2019.
- [33] R. J. Stacey, "The composition of some Roman medicines: evidence for Pliny's Punic wax?," *Anal Bioanal Chem*, vol. 401, p. 1749–1759, 2011.
- [34] J. Mazurek, M. Svoboda and M. Schilling, "GC/MS Characterization of Beeswax, Protein, Gum, Resin, and Oil in Romano-Egyptian Paintings," *Heritage*, vol. 2, pp. 1960-1985, 2019.
- [35] R. J. Stacey, J. Dyer, C. Mussell, A. Lluveras-Tenorio, M. P. Colombini, C. Duce, J. La Nasa, E. Catisani, S. Prati, G. Sciutto, R. Mazzeo, S. Sotiropoulou, F. Rosi, C. Miliani, L. Cartechini, J. Mazurek and M. Schilling, "Ancient encaustic: An experimental exploration of

- technology, ageing behaviour and approaches to analytical investigation," *Microchemical journal*, vol. 138, pp. 472-487, 2018.
- [36] J. Shen, Spectroscopic investigations of degradation products in artistic and historical samples, Ravenna: University of Bologna, 2017.
- [37] J. Liang and D. A. Scott, "Green-copper containing waxy paint on two Egyptian polychrome artifacts: A technical study," *Studies in Conservation*, vol. 59, no. 6, pp. 391-403, 2014.
- [38] D. Gramtorp, K. Botfeldt, J. Glastrup and . K. P. Simonsen, "Investigation and conservation of Anne Marie Carl-Nielsen's wax models," *Studies in Conservation*, vol. 2, no. 60, pp. 97-106, 2015.
- [39] J. Hermans, G. Osmond, A. van Loon, P. Iedema, R. Chapman, J. Drennan, K. Jack, R. Rasch, G. Morgan, Z. Zhang, M. Monteiro and K. Keune, "Electron Microscopy Imaging of Zinc Soaps Nucleation in Oil Paint," *Microscopy and Microanalysis*, vol. 24, p. 318–322, 2018.
- [40] R. D. Vold and G. S. Hattikvgdi, "Characterization of Heavy Metal Soaps by X-Ray Diffraction," *Industrial and Engineering Chemistry*, vol. 41, no. 10, pp. 2311-2320, 1949.
- [41] M.-C. Corbeil and L. Robinet, "X-ray powder diffraction data for selected metal soaps," *Powder Diffraction*, vol. 17, no. 1, pp. 52-60, 2002.
- [42] J. J. Hermans, K. Keune, A. van Loon, R. W. Corkery and P. D. Iedema, "The molecular structure of three types of long-chain zinc(II) alkanoates for the study of oil paint degradation," *Polyhedron*, vol. 81, p. 335–340, 2014.
- [43] M. Cotte, P. Dumas, G. Richard, R. Breniaux and P. Walter, "New insight on ancient cosmetic preparation by synchrotron-based infrared microscopy," *Analytica Chimica Acta*, vol. 553, pp. 105-110, 2005.

- [44] M. Cotte, E. Checroun, J. Susini and P. Walter, "Micro-analytical study of interactions between oil and lead compounds in paintings," *Applied Physics A*, vol. 89, p. 841–848, 2007.
- [45] A. Lluveras-Tenorio, A. Andreotti, I. Bonaduce, S. Boularand, M. Cotte, J. Roqué, M. P. Colombini and M. Vendrell-Saz, "Mass Spectrometric and Synchrotron Radiation based techniques for the identification and distribution of painting materials in samples from paints of Josep Maria Sert," *Chemistry Central Journal*, vol. 6, no. 45, 2012.
- [46] G. Osmond, J. J. Boon, L. Puskar and J. Drennan, "Metal Stearate Distributions in Modern Artists' Oil Paints: Surface and Cross-Sectional Investigation of Reference Paint Films Using Conventional and Synchrotron Infrared Microspectroscopy," *Applied Spectroscopy*, vol. 66, no. 10, pp. 1136-1144, 2012.
- [47] S. Hageraats, K. Keune, M. Réfrégiers, A. van Loon, B. Berrie and M. Thoury, "Synchrotron Deep-UV Photoluminescence Imaging for the Submicrometer Analysis of Chemically Altered Zinc White Oil Paints," *Analytical Chemistry*, vol. 91, pp. 14887-14895, 2019.
- [48] C. Cennini, *Il libro dell'arte*, Vicenza: Neri Pozza Editore, 2017.
- [49] E. Catelli, G. Sciutto, S. Prati, M. V. Chavez Lozano, L. Gatti, F. Lugli, S. Silvestrini, S. Benazzi, E. Genorini and R. Mazzeo, "A new miniaturised short-wave infrared (SWIR) spectrometer for on-site cultural heritage investigations," *Talanta*, vol. 218, p. 121112, 2020.
- [50] S. Legrand, M. Alfeld, F. Vanmeert, W. De Nolf and K. Janssens, "Macroscopic Fourier transform infrared scanning in reflection mode (MA-rFTIR), a new tool for chemical imaging of cultural heritage artefacts in the mid-infrared range," *Analyst*, vol. 139, no. 10, pp. 2489-2498, 2014.
- [51] S. Prati, G. Sciutto, E. Catelli, A. Ashasina and R. Mazzeo, "Development of innovative embedding procedures for the analyses of

- paint cross section in ATR FTIR microscopy,” *Analytical and Bioanalytical Chemistry*, vol. 405, no. 2-3, pp. 895-905, 2013.
- [52] R. Dávalos Navarro, Interaction between pigments and binders: Study on the formation of metal carboxylates, Ravenna: Univeristy of Bologna, 2019.
- [53] F. Vanmeert, W. De Nolf, S. De Meyer, J. Dik and K. Janssens, “Macroscopic X-ray Powder Diffraction Scanning, a New Method for Highly Selective Chemical Imaging of Works of Art: Instrument Optimization,” *Analytical Chemistry*, vol. 90, pp. 6436-6444, 2018.
- [54] W. De Nolf, F. Vanmeert and K. Janssens, “XRDUA: crystalline phase distribution maps by two-dimensional scanning and tomographic (micro) X-ray powder diffraction,” *Journal of Applied Crystallography*, vol. 47, pp. 1107-1117, 2014.
- [55] M. Vagnini, C. Miliani, L. Cartechini, P. Rocchi, B. G. Brunetti and A. Sgamellotti, “FT-NIR spectroscopy for non-invasive identification of natural polymers and resins in easel paintings,” *Anal. Bioanal. Chem.*, vol. 395, p. 2107–2118, 2009.
- [56] M. M. Mikhailov, V. V. Neshchimenko and C. Li, “Optical properties of zinc oxide powders modified by nanoparticles ZrO₂, Al₂O₃, TiO₂, SiO₂, CeO₂ and Y₂O₃ with various concentrations,” *Dyes and Pigments*, vol. 131, pp. 256-263, 2016.
- [57] V. Neshchimenko, C. Li, M. Mikhailov and J. Lv, “Optical radiation stability of ZnO hollow particles,” *Nanoscale*, vol. 10, p. 22335, 2018.
- [58] J. J. Workman JR., “Interpretive Spectroscopy for Near Infrared,” *Applied Spectroscopy Reviews*, vol. 31, no. 3, pp. 251-320, 1996.
- [59] S. Carlesi, Optical Spectroscopies: Application to the Study of Paint Models, Florence : University of Florence, 2015.

- [60] F. Rosi, L. Cartechini, L. Monico, F. Gabrieli, M. Vagnini, D. Buti, B. Doherty, C. Anselmi, B. G. Brunetti and C. Miliani, "Tracking Metal Oxalates and Carboxylates on Painting Surfaces by Non-invasive Reflection Mid-FTIR Spectroscopy," in *Metal Soaps in Art. Cultural Heritage Science*, Springer, 2019, pp. 173-193.
- [61] S. Garrappa, E. Kočí, S. Švarcová, P. Bezdička and D. Hradil, "Initial stages of metal soaps` formation in model paints: The role of humidity," *Microchemical Journal*, vol. 156, p. 104842, 2020.
- [62] G. I. Osmond, Zinc oxide-centred deterioration of modern artists' oil paint and implications for the conservation of twentieth century paintings, Queensland: University of Queensland, 2014.
- [63] C. Invernizzi, T. Rovetta, M. Licchelli and M. Malagodi, "Mid and Near-Infrared Reflection Spectral Database of Natural Organic Materials in the Cultural Heritage Field," *International Journal of Analytical Chemistry*, 2018.
- [64] L. Svečnjak, G. Baranović, M. Vinceković, S. Prđun, D. Bubalo and I. Tlak Gajger, "An Approach for Routine Analytical Detection of Beeswax Adulteration Using FTIR-ATR Spectroscopy," *Journal of Apicultural Science*, vol. 59, no. 2, 2015.
- [65] E. G. Palacios, G. Juárez-López and A. J. Monhemius, "Infrared spectroscopy of metal carboxylates II. Analysis of Fe(III), Ni and Zn carboxylate solutions," *Hydrometallurgy*, vol. 72, pp. 139-148, 2004.

Acknowledgments

I would like to express my gratitude to Rebeca Dávalos Navarro for the invaluable help in the analytical experimentation and data processing.

I would also like to thank Dr. Ilaria Bonaduce and Dr. Francesca Modugno from the University of Pisa for the access to the GC-MS analysis and their support in the data processing.

Thanks to the students Hugues Malservet and Mathilde Romé from the Sorbonne University for their great effort and help in the experimental phase of this research, and to Dr. Yiming Jia for the help in the synthesis of metal soaps, the elaboration of calibration curves for FT-IR and the measurement of samples.

I would like to thank Stijn Legrand, Gert Nuyst, Ermanno Avranovich Clerici, Steven De Meyer, Dr. Frederik Vanmeert and Prof. Dr. Koen Janssens from AXES group from the University of Antwerp for the access to the MA-XRPD, XRPD, and MA-FT-IR instrumentation and the help in the data interpretation. The internship at the University of Antwerp was funded by the Marco Polo scholarship from the University of Bologna.

Conclusions

Colourants are very important in cultural heritage because they produce one of the most important features of artwork: the colour. Their preservation and study allow preserving the aesthetic values of an artefact, understanding possible modification suffered by degradation, and reconstructing, in a theoretical way, the possible original appearance of the object.

Because of the complexity of the polychrome systems, the study of colourants in cultural heritage requires a multi-analytical approach. Spectroscopy is of great utility and today is commonly used for analysing cultural heritage. In the three projects presented in the previous chapters, we illustrated the application of some advanced spectroscopic methodologies for studying different types of colourants.

Two FT-IR enhanced methodologies were proposed to reduce sample amount and pre-treatment. The results of the used of MU-ATR technique is a promising method that allows the characterization of artists' materials even in complex mixtures in a fast a simple way, and without sample preparation, using a small amount of sample (around $\sim 300 \mu\text{m}$). Besides, the application of TLC/MU-ATR using AgI@Au plates shows promising results for identifying degraded dyes in a fast and simple way and it was possible to evaluate the effect of light in dye fading.

Further studies on real samples from paintings and historical textiles will allow us to understand the potentiality of the two systems. In particular, more detailed experimentation to improve the synthesis of AgI and its deposition over the Au plate can help in improving the reproducibility and resolution of the TLC separation.

μ -FT-IR and μ -Raman combined with SR based X-ray techniques allow us to gain insights on the oxidation process of orpiment and its interaction with

metallic Ag, as well as the influence of factors such as light and humidity in the degradation process. The results indicate that Ag plays a key role in the degradation of orpiment when it is mixed with it, by increasing the oxidation of the pigment probably due to an ion interchange mechanism.

Further analysis of mock-ups containing realgar (AsS or As₄S₄) and mixtures with other pigments (i.e., minium) will offer more detailed information regarding the degradation of As pigments and the interaction of their degradation products with others materials present in their vicinity.

Finally, we obtained further evidence on the formation and crystallization of metal carboxylates in different binding media. The results show the limitation of SWIR and rFT-IR non-invasive methodologies and their advantages in particular for the monitoring of oil paintings ageing. We identified differences on the formation of carboxylates according to the type of binder, being the most stable beeswax. The pigments presented also a different reactivity; it was confirmed the high reactivity of zinc white and the faster reaction of minium in comparison with the lead white.

This project is still in process and further analysis using GC-MS will offer more information regarding the presence of FMCs and FFAs in advance degradation stages.

Appendix 1

Current trends in scientific literature

To understand the current trend of the scientific research, a bibliometric analysis about the spectroscopic methodologies used to the study of colourants in cultural heritage was performed. The analysis included publications from 1982 to June 2020. We used a bibliometric methodology because the bibliometric data offers information regarding the current status of a particular scientific field and identify areas of research that are developing or regressing, it also give insights on the volume of research and geographical distribution as well as the knowledge flow based on the relations between the different actors [1].

Bibliometric method

The bibliometric analysis was done considering articles indexed in Scopus and Web of Science between 1982 and 2020, the search was limited only to documents related to the application of spectroscopy to the study of colourants used in cultural heritage. The data was obtained on June 2020.

To maximise the number of relevant articles, different search strategies were tested. The search was done using the terms “spectroscopy” and “cultural heritage” as base terms, combined with “colorants”, “colourants”, “pigments”, “dyes”, and “lakes”.

General searches were performed to reach publications that do not contain the specific categories of colourants as indexed keywords. The

search was tailored using operators to eliminate possible documents not related to the field of interest, for example: “spectroscopy” AND “paintings” AND “cultural heritage” AND NOT “binder” AND NOT “cleaning” or “spectroscopy” AND “artworks” AND NOT “binder” AND NOT “cleaning” AND NOT “cellulose” AND NOT “polymer”. The final number of articles was revised, using Zotero software, to eliminate duplicates, include variations in names, and eliminate document not related with colourants.

Co-authorship maps were done using vosViewer software with a full counting method including authors with a minimum of 2 documents, retaining 817 from the 3479 authors identified. The clustering method is explained in Waltman and van Eck [2]. Analysis of indexed keywords was done by co-occurrence using a full counting and a minimum of 2 occurrences, a selection of keywords was done previous the mapping to eliminate general terms such as “cultural heritage”, “art history”, “spectroscopy” or “conservation”.

Results

The search in the databases selected yielded a total of 1032 registers. The data suggest that the number of publications increased since 2005 (Figure 1), however, after 2016 the number of publications slightly decreased.

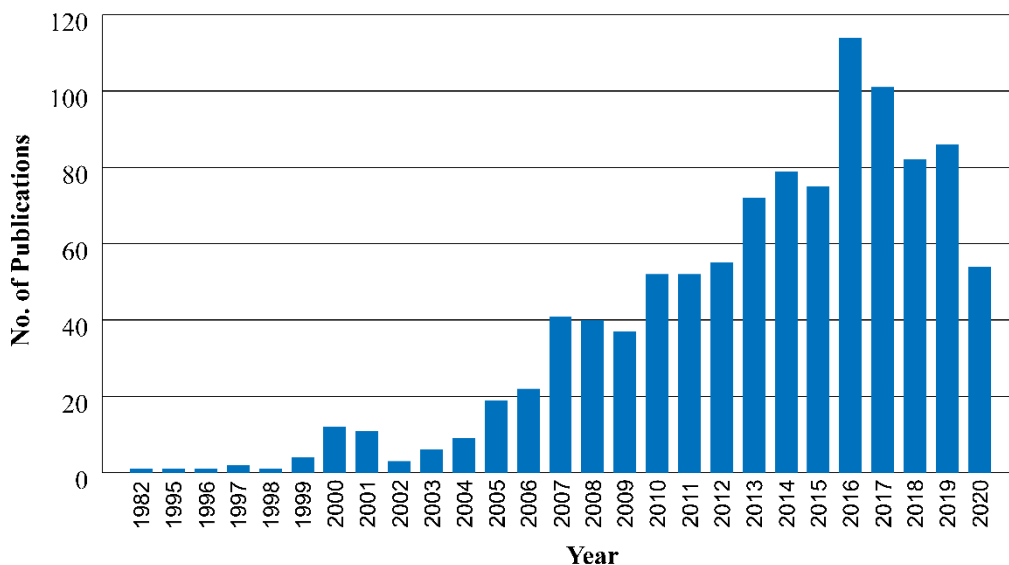


Figure 1. Number of publications indexed in Scopus and Web of Science between 1982 and June 2020.

Regarding the keywords indexed, “pigments/ pigment” are the terms with the higher occurrence in the literature, followed by “dyes/dye” and “red lakes” (Figure 2). It is interesting how the term lakes is always associated with the colour red, meaning the research so far has been focusing mainly in this typology of lakes and specialist have not associate directly that term to other lakes such as Maya blue that has been called “hybrid

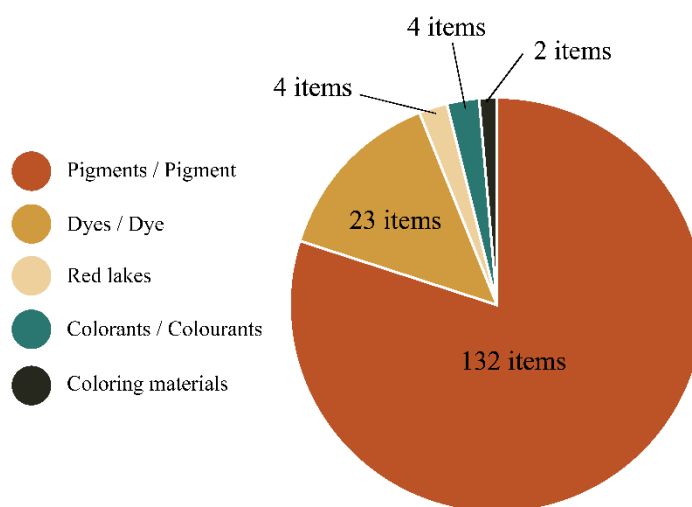


Figure 2. Graph of the occurrence of keywords based on the classification of colourants. The number of items per each term is indicated, no percentages are calculated since not all the keywords are included in the chart.

pigment". The term "coloring materials" is used in two publications as a general term.

The keyword occurrence suggest that the scientific research has been focused mainly on pigments and dyes. Less attention has been paid to lakes, probably due to the complexity a difficulty in their detection, and due to the fact that were less used than pigments. Is worth noting that some researcher classified lakes as organic pigments or hybrid pigments. This shows that today still there is some misunderstanding and confusion on the proper classification of colourants and their terminology among specialists.

With respect to the authorship, 3479 authors were identified and the 20 most productive authors in the period analysed and the institutions were they developed their main research activity are summarized in table 1 (next page). Europe is the main region were this researches are conducted followed by the United States of America (USA). Based on the affiliation institution of the first author, Italy is the country with the highest number of publications followed by USA, France and Belgium. Among the first 20 authors, most of them are affiliated to one of the institutes that are part of the Italian National Council of Research (CNR).

Table 1. List of the 20 most productive researchers based on the number of publications focused on the application of spectroscopic techniques for the study of colourants in cultural heritage. The data was revised to eliminate duplicates.

Name	h-index	Institution	Country	Registers
Picollo, M.	19	IFAC - CNR	Italy	33
Miliani, C.	37	ISPC - CNR	Italy	30
Cucci, C.	15	IFAC - CNR	Italy	28
Madariaga, J. M.	37	University of Basque Country	Spain	28
Castro, K.	36	University of Basque Country	Spain	27
Anglos, D.	39	FORTH	Greece	26
Romani, A.	41	University of Perugia, ISTM-CNR	Italy	22
Conti, C.	39	University of Rome, La Sapienza	Italy	21
Vandenabeele, P.	54	University of Ghent	Belgium	21
Janssens, K.	38	University of Antwerp	Belgium	19
Detalle, V.	19	C2RMF	France	18
Moens, L. J.	68	University of Antwerp	Belgium	15
Leona, M.	23	Metropolitan Museum of Art	USA	14
Casadio, F.	22	School of the Art Institute of Chicago	USA	14
Brunetti, B. G.	37	University of Perugia	Italy	13
Edwards, H. G. M.	59	University of Bradford	UK	13
Palleschi, V.	43	iCCOM-CNR	Italy	13
Rosi, F.	25	ISTM-CNR	Italy	13
Carvalho, M. L.	30	Universidade Nova de Lisboa	Portugal	13
Cotte, M.	36	ESRF	France	13

The co-authorship map (Figure 3) shows an intense collaboration between researchers. 23 clusters were identified, each one group according to the collaboration between the researchers and their co-authorship in the publications. It is not surprising that the clusters are in accordance to the institutions and the type of analytical techniques used by the researchers.

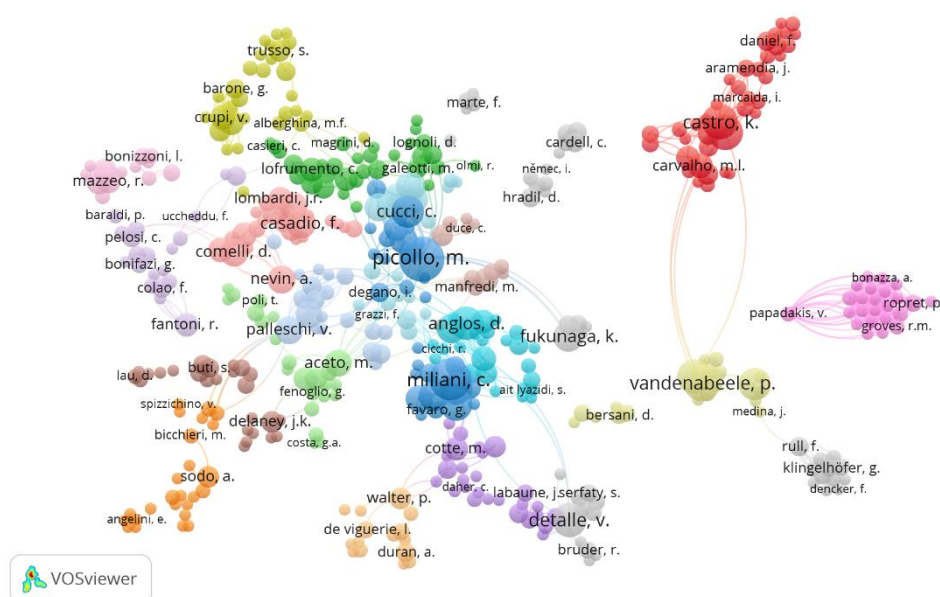


Figure 3. Co-authorship map showing the largest set of connected items from the 817 registers obtained from the databases. In total 468 authors were considered in the mapping. The colours indicate the different clusters.

The map of co-occurrence of the indexed keywords shows 24 clusters containing 263 terms. It clearly shows a predominance of Raman spectroscopy and pigments as most common keywords indexed in the publications (Figure 4, next page). Other commonly used techniques are by FT-IR and XRF (Figure 5, next page). Table 2 (page VII) summarized the characteristic of some of the techniques used for the study of colourants in cultural heritage.

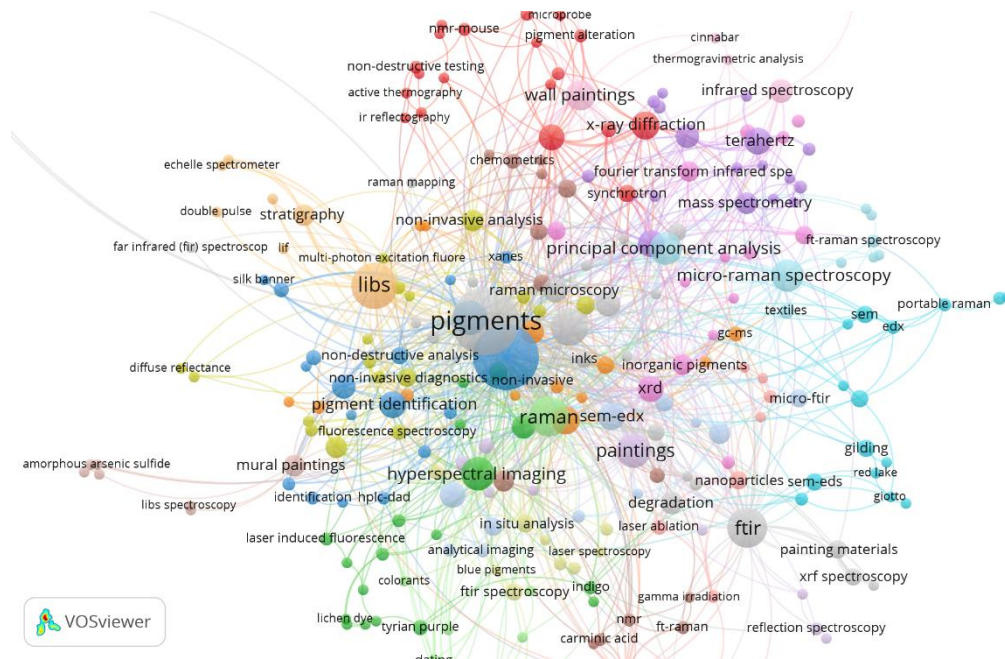


Figure 4. Map of co-occurrence of Keywords indexed in the literature review between 1982-June 2020, it is clear the predominance of “pigments” and “Raman” as the most recurrent keywords used in publications.

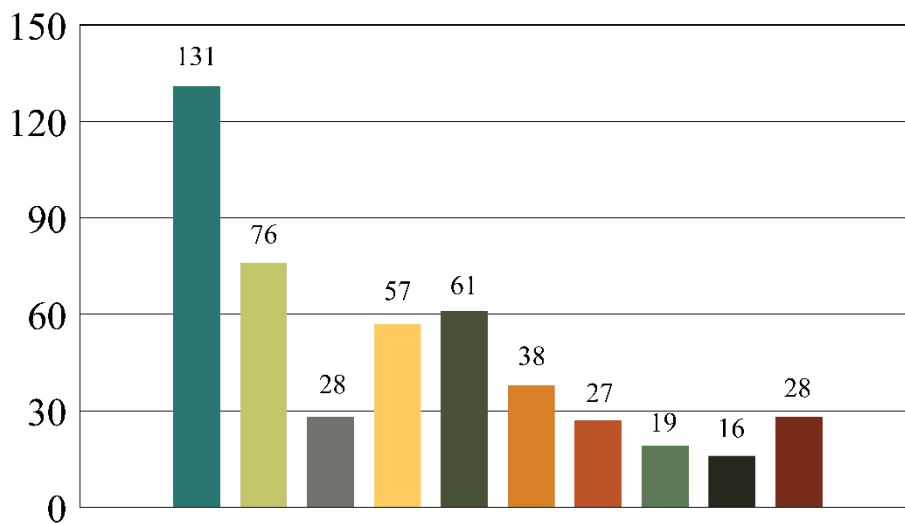
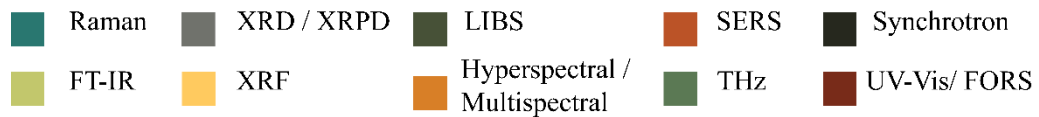


Figure 5. Number of documents per technique based on the keyword occurrence.

Table 2. Comparison of different techniques for colourants analysis. Adapted from [3].

Technique	Type of information	Sensitivity	Spatial resolution	Portable/ <i>In situ</i> analysis
Raman	Molecular	Good	<1 μm	✓
FT-IR	Molecular	Fair	~20 μm	✓
UV-Vis	Molecular	Good	~10 μm	✓
LIBS	Elemental	Excellent	~20 μm	✓
XRF	Elemental	Good	~1 μm	✓
XPS	Elemental	Good	~1 μm	✓
SEM-EDS	Elemental	Good	<1 μm	✗
XRPD	Molecular	Fair	~10 μm	✓

Type of study and information

Spectroscopic methods have been used to study different aspects of colourants used in cultural heritages; the main application is the identification of materials in different artefacts. These publications are focused on a) cases of study with particular conditions (uncommon materials, specific artists or objects, etc.), b) identification of modern materials as aid for authentication/dating, or c) set-up of analytical protocols (new applications or improvement of the existing conditions).

The study of the degradation phenomena is another aspect that has been constantly addressed in scientific investigations; a deep knowledge on the degradation causes constitutes a framework for the preventive conservation strategies, offers evidence of the object's original appearance and in some cases helps in dating the object or its modifications [4, 5]. The complexity of these systems makes impossible to achieve a complete understanding using a single technique, making necessary a multi-analytical approach [6].

The great application of spectroscopic techniques for studying colourants in cultural heritage have led to the publication reviews where scientist discuss the advances, advantages and limitations of each technique, or the challenges that particular materials represent.

References

- [1] É. Gauthier, «Bibliometric Analysis of Scientific and Technological research: A User's Guide to the Methodology,» Observatoire des Sciences et des Technologies (CIRST), Canada, 1998.
- [2] L. Waltman y N. J. van Eck, «A New Methodology for Constructing a Publication-Level Classification System of Science,» *Journal of the American Society for Information Science and Technology*, vol. 63, nº 12, pp. 2378-2392, 2012.
- [3] R. J. H. Clark, «Pigment identification by spectroscopic means: an arts/science interface,» *C. R. Chimie*, vol. 5, p. 7–20, 2002.
- [4] C. Miliani, L. Monico, M. J. Melo, S. Fantacci, E. M. Engelin, A. Romani y K. Janssens, «Photochemistry of Artists' Dyes and Pigments: Towards Better Understanding and Prevention of Colour Change in Works of Art,» *Angewandte Chemie International Edition*, vol. 57, pp. 7324-7334, 2018.
- [5] M. Cotte, J. Susini, V. A. Sole, Y. Taniguchi, J. Chillida, E. Checroun y P. Walter, «Applications of synchrotron-based micro-imaging techniques to the chemical analysis of ancient paintings,» *J. Anal. At. Spectrom.*, vol. 23, p. 820–828, 2008.
- [6] M. Cotte, E. Welcomme, V. A. Sole, M. Salome, M. Menu, P. Walter y J. Susini, «Synchrotron-Based X-ray Spectromicroscopy Used for the Study of an Atypical Micrometric Pigment in 16th Century Paintings,» *Analytical Chemistry*, vol. 79, nº 18, pp. 6988-6994, 2007.

Appendix 2

Table 1. Information about the paint manufacturers reported in the colour charts studied in Chapter 1 [1, 2, 3, 4, 5, 6].

Company	Date and place of foundation	Information
Pelikan	Hanover, Germany, 1838.	Initiated as an ink company, currently active offering different kind of products.
Redeker & Hennis A.-G.	Nürnberg, Germany	Registered a patent for watercolours and oil colours in USA in May 1903 that was renewed in May 1933 and assigned by mesne assignment to The Chemical Foundation Inc. Adolf Hitler possessed a watercolour metallic box of this brand produced in 1910.
G. Siegle & Co. GmbH	Munich/Stuttgart, Germany, 1845.	The company was founded by Heinrich Siegle in Munich in 1845, and in 1848 moved the company headquarters to Stuttgart. In 1917, the company Pabst & Lambrecht from Nuremberg took over Siegle.
Herrmann Neisch & Co	Dresden, Germany, 1871	The tempera tuber commercialized by this company after 1875 contained egg and oil. In the last part of the 19 th century also produce casein paint. It was taken over the Caparol Industrial Solutions GmbH in 1969.
Bössenroth	Dachau, Germany, 1905.	Small company founded by the painter Carl Bössenroth (1863-1935) that patented pastel-tempera colours.
Flamuco, Vereinigte Farben- und Lackfabriken GmbH	Munich, Germany	In 1910 the central was in Munich and factories in Augsburg, Strasbourg, Reinhafen, Stuttgart, Nurnberg, and Wels. In 1969 was acquired by Hoechst, by the time had six offices in Germany and 100 retail shops.

Referencias

- [1] D. Rothemel, «Company History,» 11 July 2014. [En línea]. Available: <https://www.pelikan-collectibles.com/en/Pelikan/Company-History/index.html>. [Último acceso: 30 03 2020].

- [2] Caparol Industrial Solutions GmbH, «History,» 2020. [En línea]. Available: <https://www.caparol-cis.de/en/company/history/more-history.html>. [Último acceso: 30 03 2020].
- [3] S. Beisiegel, «'I explored every means of painting back then, notably every tempera': Hermann Prell's research on tempera,» de *Tempera Painting 1800–1950. Experiment and Innovation from the Nazarene Movement to Abstract Art*, P. Dietemann, W. Neugebauer, E. Ortner, R. Poggendorf, E. Reinkowski-Häfner y H. Stege, Edits., Munich, Archetype Publications Ltd, 2019, pp. 107-116.
- [4] . A. Gieseler, «G. Siegle & Co., GmbH, Farbenfabriken,» 2009. [En línea]. Available: http://www.albert-gieseler.de/dampf_de/firmen0/firmadet3755.shtml. [Último acceso: 30 03 2020].
- [5] «The coloured world of surfaces,» *Pigment & Resin Technology*, vol. 3, nº 7, pp. 7-8, 1974.
- [6] E. A. Seemann, *Münchener kunsttechnische Blätter.*, p. no. 19, 1910/1911.

Appendix 3

μ -ATR-FTIR and μ -Raman Band assignment

Table 1. μ -ATR-FT-IR bands assignment of whole egg tempera [1, 2].

Wavenumber (cm^{-1})	Assignment	Wavenumber (cm^{-1})	Assignment
3279	N-H stretching	1536	Amide II bending
2923	CH_2 stretching	1195	Ester stretching
2853	CH_2 stretching	1158	Ester stretching
1743	C=O stretching	1090	Ester stretching
1640	Amide I stretching	1536	Amide II bending

Table 2. μ -Raman band assignment of orpiment [3].

Wavenumber (cm^{-1})	Assignment
382	As-S-As bridges
354	pyramids AsS_3 vibrations
311	pyramids AsS_3 vibrations
292	pyramids AsS_3 vibrations
202	As-S-As bridges
180	pyramids AsS_3 vibrations
136	pyramids AsS_3 vibrations

Table 3. μ -ATR-FT-IR bands assignment of linseed oil [1, 4].

Wavenumber (cm ⁻¹)	Assignment	Wavenumber (cm ⁻¹)	Assignment
3211	O-H stretching	1374	CH ₃ umbrella mode
2921	CH ₂ stretching	1236	C-O ester stretching
2852	CH ₂ stretching	1160	C-O ester bond
1707	C=O stretching	1094	C-O ester bond
1456	$\delta_{as}CH_3$	724	$\delta C=C-H$ (cis)

References

- [1] R. J. Meilunas, J. G. Bentsen and A. Steinberg, "Analysis of Aged Paint Binders by FTIR Spectroscopy," *Studies in Conservation*, vol. 35, pp. 33-51, 1990.
- [2] N. D. Singho, N. A. Che Lah, M. . R. Johan and R. Ahmad, "FTIR Studies on Silver-Poly(Methylmethacrylate) Nanocomposites via In-Situ Polymerization Technique," *Int. J. Electrochem. Sci.*, no. 7, pp. 5596 - 5603, 2012.
- [3] H. Cheng, Y. Zhou and R. L. Frost, "Structure comparison of Orpiment and Realgar by Raman Spectroscopy," *Spectroscopy Letters*, vol. 50, no. 1, pp. 23-29, 2017.
- [4] J. van der Weerd, A. van Loon and J. J. Boon, "FTIR Studies of the Effects of Pigments on the Aging of Oil," *Studies in Conservation*, vol. 50, p. 3–22, 2005.

Appendix 4

GC-MS analyses

FFA: Free fatty acids, FMC: Free metal carboxylates, P: palmitic acid, S: Stearic acid, A: Azelaic acid, O: oleic acid, Σ D: total amount of dicarboxylic acids.

Table 1. Data summary of GC-MS quantification of linseed oil samples aged naturally for 10 weeks.

Mock-ups	Natural ageing				
	FFA	σ	FFA+FMC	σ	FMC
ZWO _{natural}	0.3 %	0.1 %	0.6 %	0.1 %	0.3 %
LWO _{natural}	0.8 %	0.3 %	1.9 %	0.0 %	1.1 %
MO _{natural}	0.2 %	0.0 %	0.4 %	0.1 %	0.2 %

Table 2. Ratios obtained from the GC-MS quantification from linseed oil samples naturally aged for 10 weeks.

Mock-ups	Molecule	P/S		A/P		O/S		Σ D	
		Total	σ	Total	σ	Total	σ	Total	σ
ZWO _{natural}	FFA	1.4	0.2	0.1	0.0	1.1	0.5	4 %	2 %
	FMC	2.2	0.9	4.1	0.7	3.4	1.7	61 %	3 %
LWO _{natural}	FFA	1.3	0.0	0.7	0.4	0.6	0.0	28 %	12 %
	FMC	1.5	0.4	0.7	0.3	0.0	0.0	31 %	11 %
MO _{natural}	FFA	2.2	0.1	0.1	0.0	2.8	0.6	5 %	2 %
	FMC	0.4	0.5	1.2	1.7	0.3	0.5	24 %	33 %

Table 3. Data summary of GC-MS quantification of linseed oil samples artificially aged for 10 weeks.

Mock-ups	Artificial ageing				
	FFA	σ	FFA+FMC	σ	FMC
ZWO _{10weeks}	0.4 %	0.2 %	1.2 %	0.1 %	0.8 %
LWO _{10weeks}	0.9 %	0.1 %	2.3 %	0.3 %	1.4 %
MO _{10weeks}	0.6 %	0.1 %	1.2 %	0.1 %	0.6 %

Table 4. Ratios obtained from the GC-MS quantification from linseed oil samples artificially aged for 10 weeks.

Mock-ups	Molecule	P/S		A/P		O/S		Σ D	
		Total	σ	Total	σ	Total	σ	Total	σ
ZWO _{10weeks}	FFA	1.5	0.1	0.1	0.1	1.3	0.1	5 %	4 %
	FMC	3.0	0.9	2.6	1.2	2.8	1.2	56 %	10 %
LWO _{10weeks}	FFA	1.6	0.0	0.4	0.1	1.3	0.1	16 %	4 %
	FMC	1.7	0.4	8.9	1.3	1.5	0.8	82 %	1 %
MO _{10weeks}	FFA	2.3	0.7	0.2	0.0	2.9	1.1	8 %	1 %
	FMC	0.3	0.5	14.2	8.1	0.6	0.8	83 %	18 %

Table 5. Data summary of GC-MS quantification of whole egg samples aged naturally for 10 weeks.

Mock-ups	Natural ageing				
	FFA	σ	FFA+FMC	σ	FMC
ZWE _{natural}	0.3 %	0.1 %	0.7 %	0.4 %	0.4 %
LWE _{natural}	0.6 %	0.1 %	1.1 %	0.3 %	0.6 %
ME _{natural}	0.4 %	0.2 %	1.0 %	0.7 %	0.6 %

Table 6. Ratios obtained from the GC-MS quantification from whole egg samples naturally aged for 10 weeks.

Mock-ups	Molecule	P/S		A/P		O/S		Σ D	
		Total	σ	Total	σ	Total	σ	Total	σ
ZWE _{natural}	FFA	2.5	0.7	0.0	0.0	3.6	1.5	1 %	1 %
	FMC	1.1	0.1	0.2	0.1	0.4	0.1	10 %	8 %
LWE _{natural}	FFA	2.8	1.0	0.0	0.0	4.2	2.2	2 %	2 %
	FMC	1.5	0.4	0.1	0.0	0.7	0.4	8 %	3 %
ME _{natural}	FFA	2.2	0.7	0.0	0.0	2.3	0.8	2 %	0 %
	FMC	2.0	0.4	0.2	0.1	0.5	0.4	14 %	8 %

Table 7. Data summary of GC-MS quantification of whole egg samples artificially aged for 10 weeks.

Mock-ups	Artificial ageing				
	FFA	σ	FFA+FMC	σ	FMC
ZWE _{10weeks}	1.2 %	2.0 %	2.6 %	0.5 %	1.4 %
LWE _{10weeks}	0.8 %	0.3 %	1.1 %	0.3 %	0.5 %
ME _{10weeks}	1.7 %	0.4 %	3.8 %	2.0 %	2.2 %

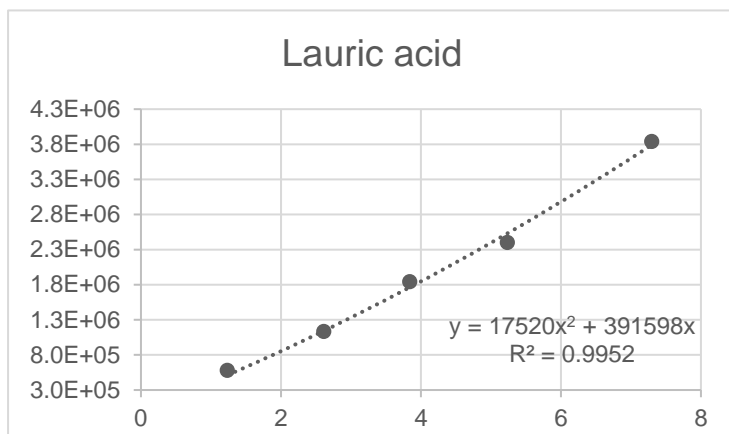
Table 8. Ratios obtained from the GC-MS quantification from whole egg samples artificially aged for 10 weeks.

Mock-ups	Molecule	P/S		A/P		O/S		Σ D	
		Total	σ	Total	σ	Total	σ	Total	σ
ZWE _{10weeks}	FFA	2.1	0.5	0.0	0.0	2.0	0.3	0 %	0 %
	FMC	3.7	1.9	0.1	0.1	2.1	1.3	8 %	3 %
LWE _{10weeks}	FFA	3.1	0.0	0.0	0.0	3.2	0.1	0 %	0 %
	FMC	0.8	0.8	0.7	0.8	0.9	1.0	15 %	13 %
ME _{10weeks}	FFA	2.5	0.7	0.0	0.0	2.9	0.8	1 %	0 %
	FMC	3.8	1.2	0.2	0.1	1.9	0.6	11 %	6 %

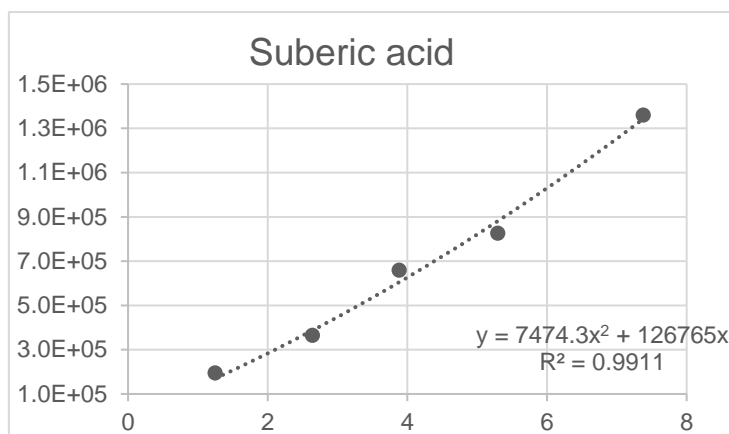
Calibration curves for the GC-MS procedure

Calibration curves with C13 (tridecanoic acid)

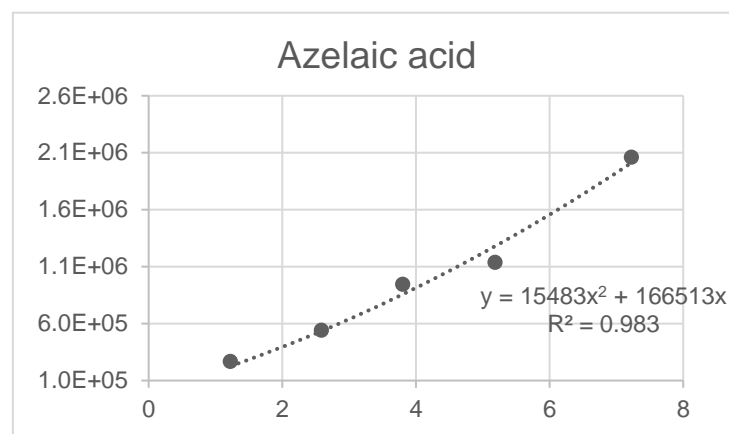
HMDS Derivatization



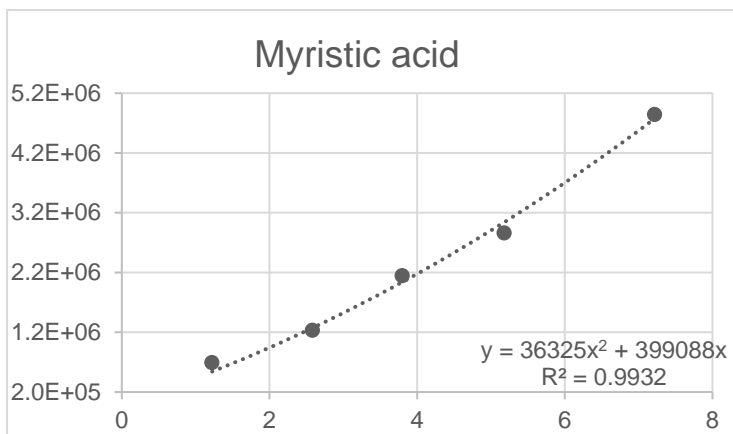
Conc/ ppm	Area/ x10 ⁶
1.24	0.578
2.61	1.132
3.84	1.841
5.24	2.400
7.30	3.837



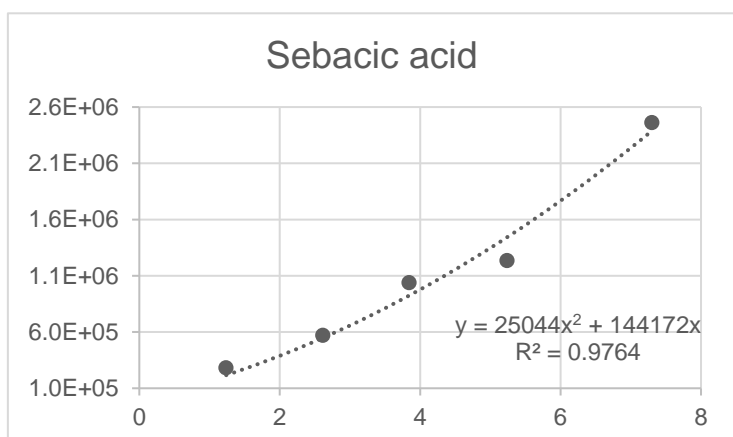
Conc/ ppm	Area/ x10 ⁶
1.25	0.193
2.64	0.364
3.89	0.658
5.30	0.825
7.38	1.359



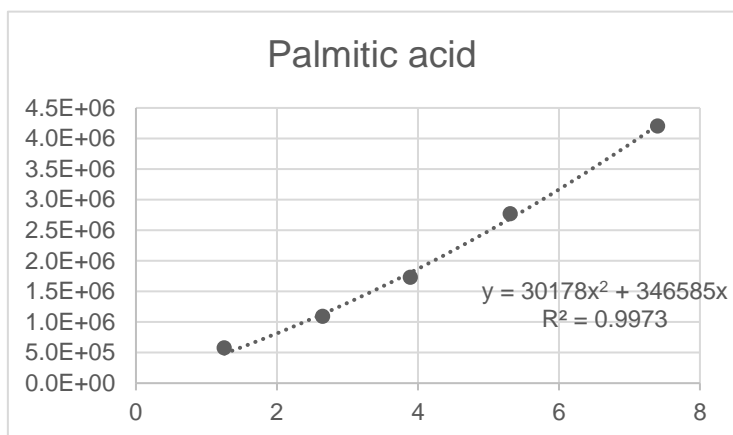
Conc/ ppm	Area/ x10 ⁶
1.22	0.268
2.59	0.541
3.80	0.944
5.19	1.136
7.23	2.059



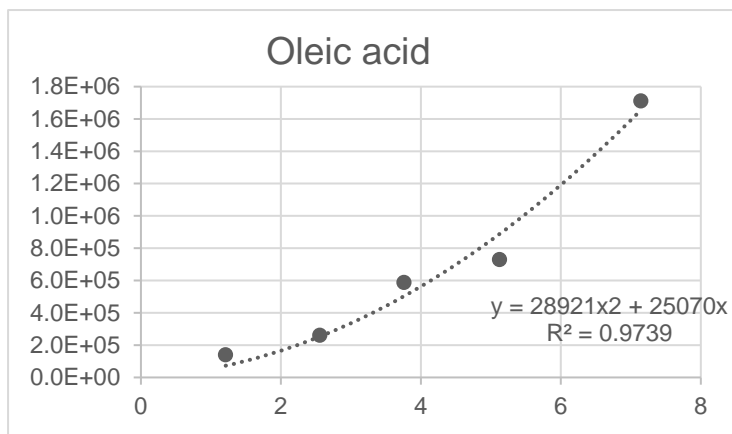
<i>Conc/ ppm</i>	<i>Area/ x10⁶</i>
1.22	0.690
2.58	1.231
3.80	2.144
5.18	2.860
7.22	4.840



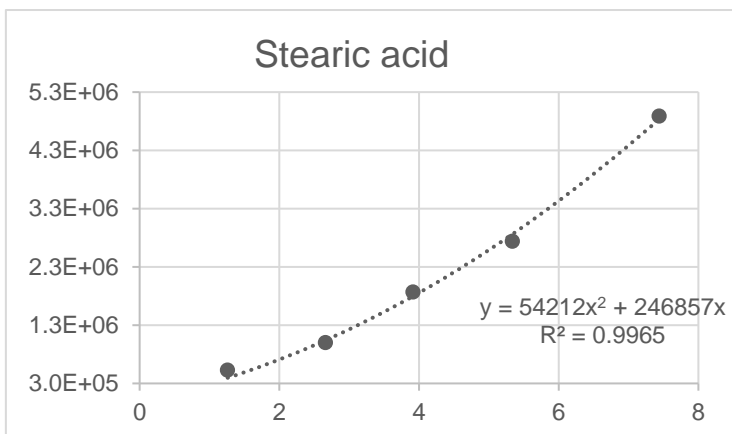
<i>Conc/ ppm</i>	<i>Area/ x10⁶</i>
1.24	0.281
2.62	0.569
3.84	1.038
5.24	1.233
7.30	2.460



<i>Conc/ ppm</i>	<i>Area/ x10⁶</i>
1.25	0.576
2.65	1.090
3.90	1.729
5.31	2.768
7.40	4.203

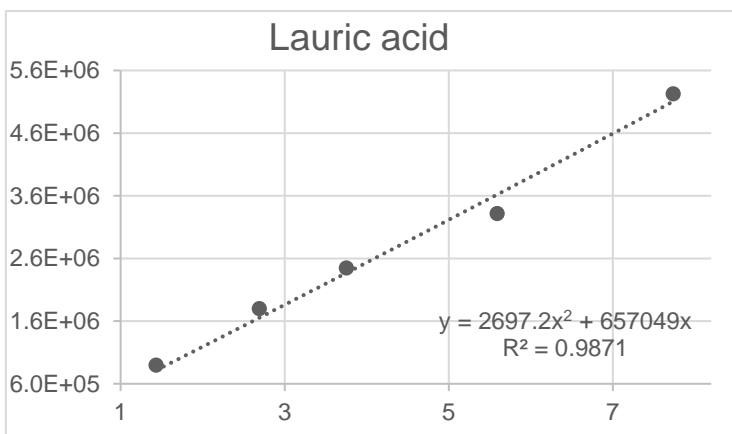


<i>Conc/ ppm</i>	<i>Area/ x10⁶</i>
1.21	0.140
2.56	0.260
3.76	0.587
5.13	0.729
7.15	1.711

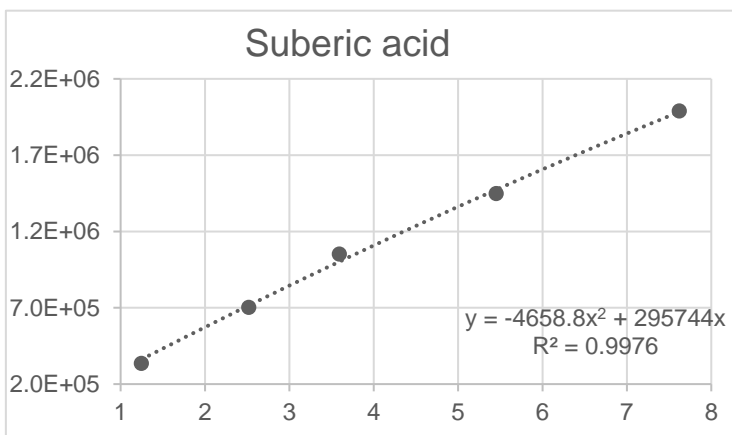


<i>Conc/ ppm</i>	<i>Area/ x10⁶</i>
1.26	0.527
2.66	0.998
3.92	1.867
5.34	2.739
7.44	4.886

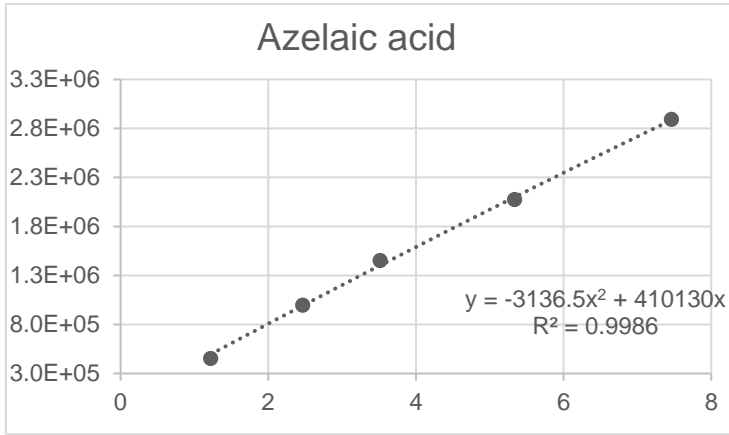
BSTFA Derivatization



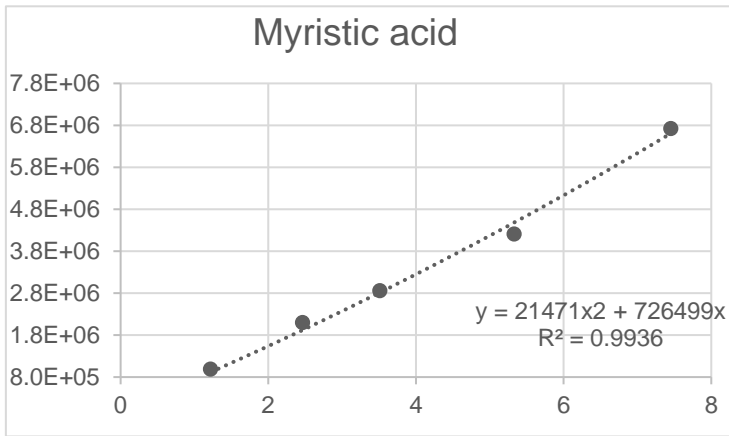
<i>Conc/ ppm</i>	<i>Area/ x10⁶</i>
1.23	0.895
2.49	1.797
3.55	2.448
5.39	3.316
7.53	5.226



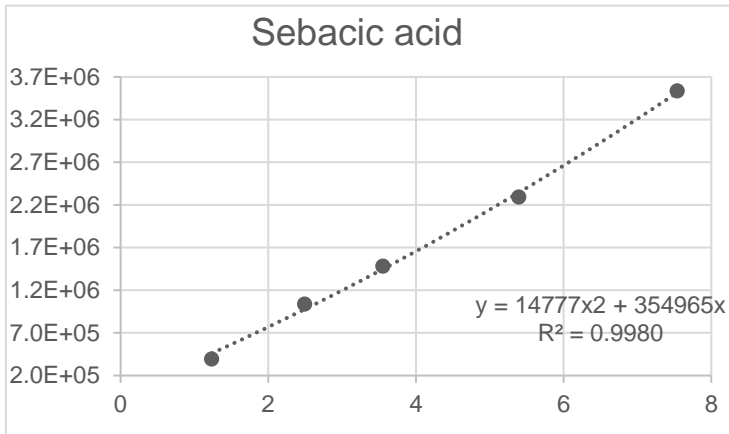
<i>Conc/ ppm</i>	<i>Area/ x10⁶</i>
1.24	0.334
2.52	0.702
3.59	1.051
5.45	1.447
7.62	1.988



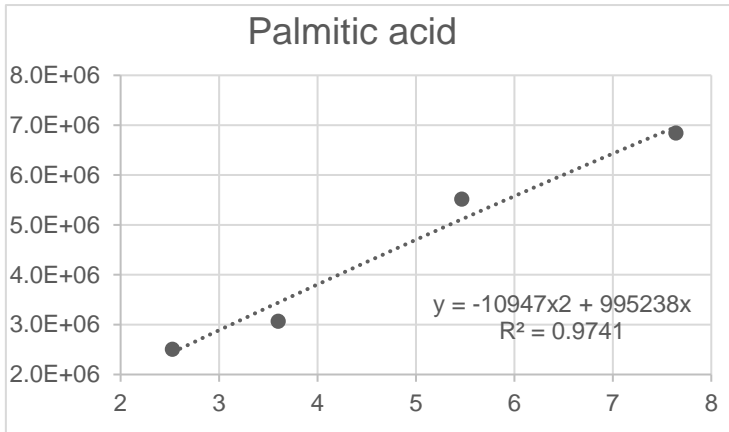
<i>Conc/ ppm</i>	<i>Area/ x10⁶</i>
1.22	0.451
2.46	0.994
3.51	1.450
5.33	2.073
7.46	2.890



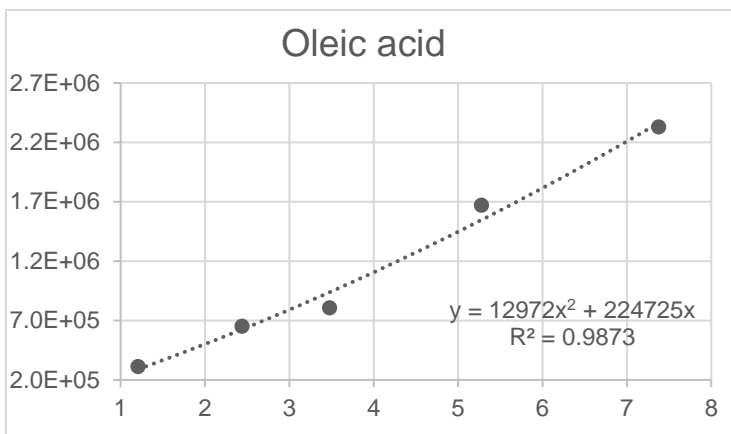
<i>Conc/ ppm</i>	<i>Area/ x10⁶</i>
1.22	0.985
2.46	2.095
3.51	2.854
5.33	4.207
7.45	6.721



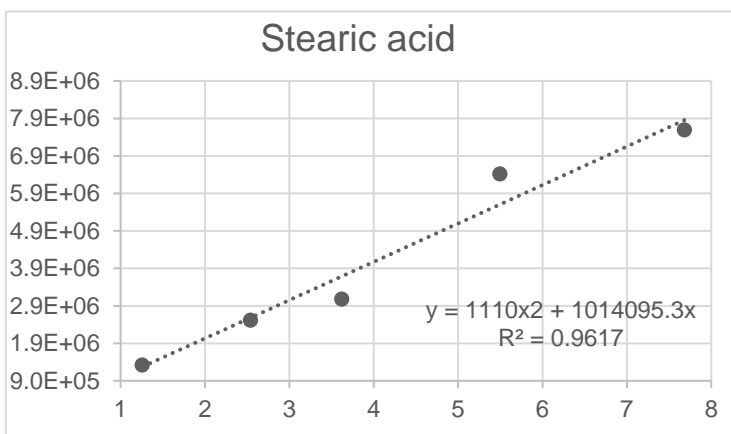
<i>Conc/ ppm</i>	<i>Area/ x10⁶</i>
1.23	0.392
2.49	1.035
3.55	1.479
5.39	2.291
7.54	3.533



<i>Conc/ ppm</i>	<i>Area/ x10⁶</i>
1.25	1.352
2.52	2.505
3.60	3.064
5.46	5.515
7.64	6.839



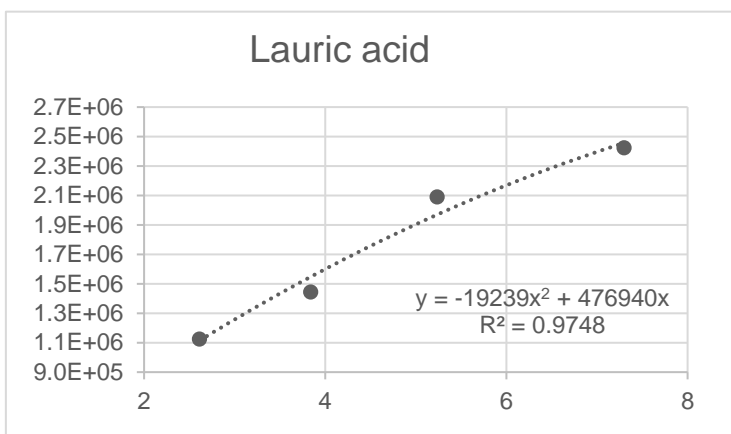
<i>Conc/ ppm</i>	<i>Area/ x10⁶</i>
1.20	0.311
2.44	0.650
3.47	0.806
5.27	1.669
7.37	2.328



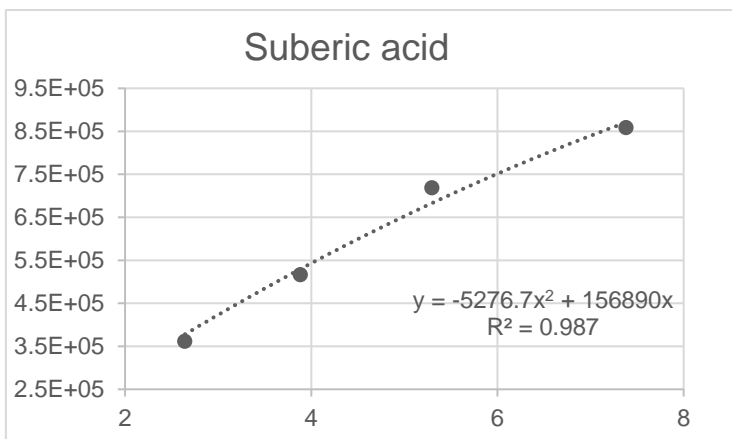
<i>Conc/ ppm</i>	<i>Area/ x10⁶</i>
1.25	1.315
2.54	2.513
3.62	3.074
5.49	6.413
7.68	7.589

Calibration curves with C17 (heptadecanoic acid)

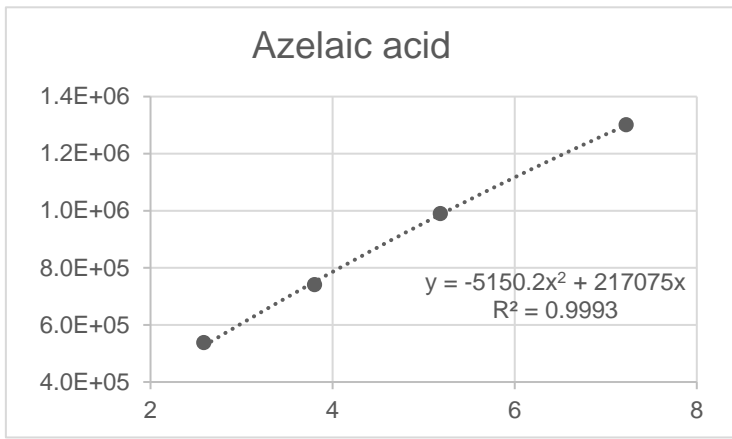
HMDS derivatization



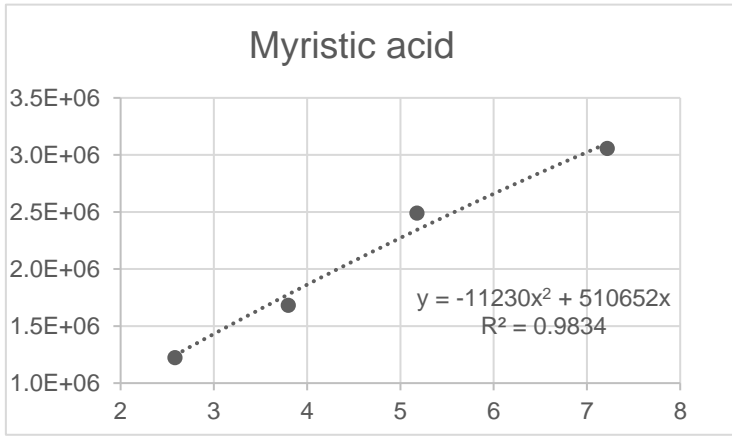
<i>Conc/ ppm</i>	<i>Area/ x10⁶</i>
1.24	0.578
2.61	1.124
3.84	1.443
5.24	2.089
7.30	2.423



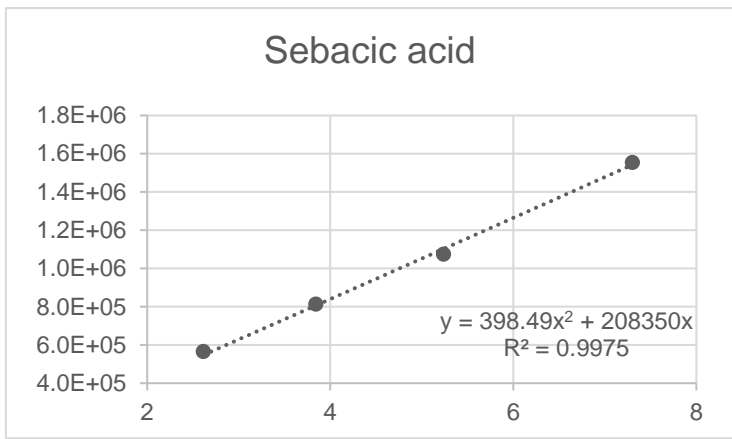
<i>Conc/ ppm</i>	<i>Area/ x10⁶</i>
1.25	0.193
2.64	0.361
3.89	0.516
5.30	0.718
7.38	0.858



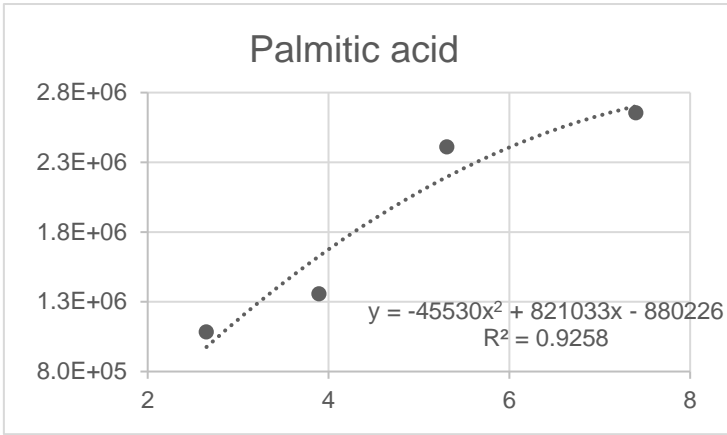
<i>Conc/ ppm</i>	<i>Area/ x10⁶</i>
1.22	0.268
2.59	0.537
3.80	0.740
5.19	0.989
7.23	1.300



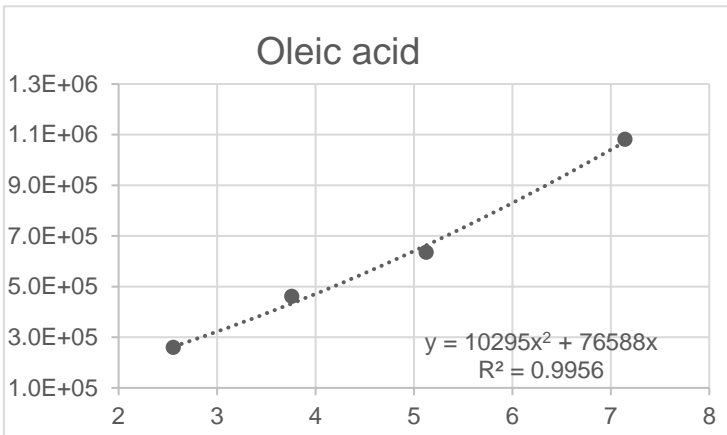
<i>Conc/ ppm</i>	<i>Area/ x10⁶</i>
1.22	0.690
2.58	1.221
3.80	1.680
5.18	2.489
7.22	3.056



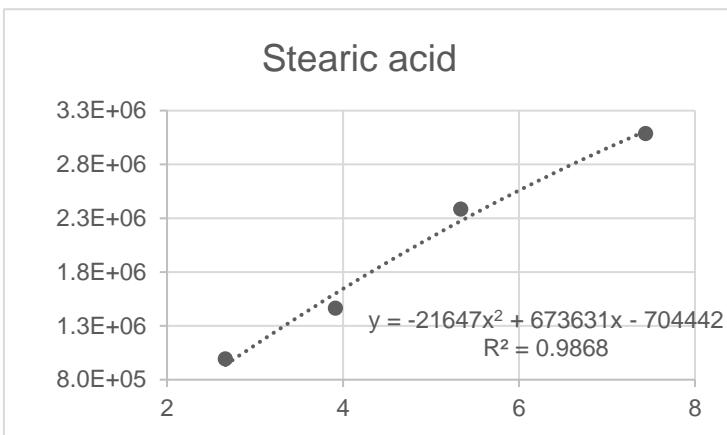
<i>Conc/ ppm</i>	<i>Area/ x10⁶</i>
1.24	0.281
2.62	0.565
3.84	0.813
5.24	1.073
7.30	1.553



<i>Conc/ ppm</i>	<i>Area/ x10⁶</i>
1.25	0.576
2.65	1.082
3.90	1.355
5.31	2.409
7.40	2.654

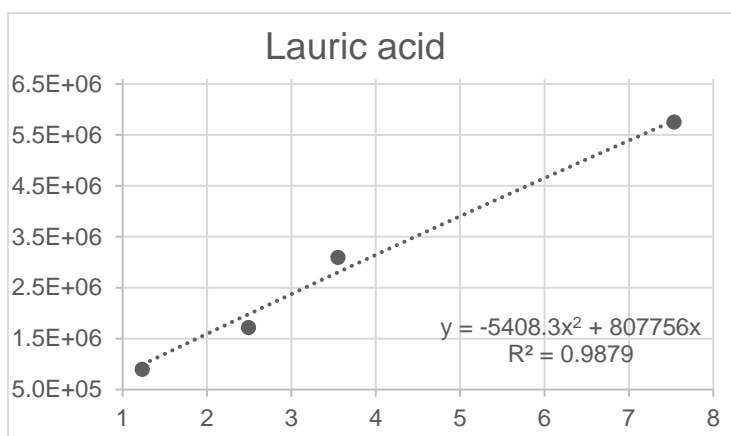


<i>Conc/ ppm</i>	<i>Area/ x10⁶</i>
1.21	0.140
2.56	0.259
3.76	0.460
5.13	0.634
7.15	1.080

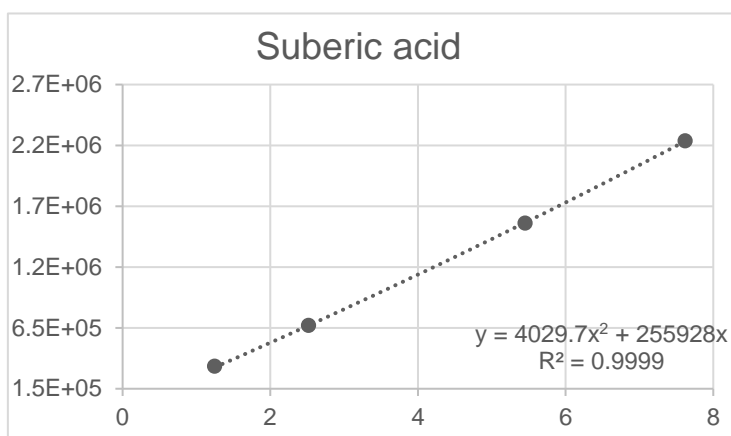


<i>Conc/ ppm</i>	<i>Area/ x10⁶</i>
1.26	0.527
2.66	0.991
3.92	1.463
5.34	2.384
7.44	3.085

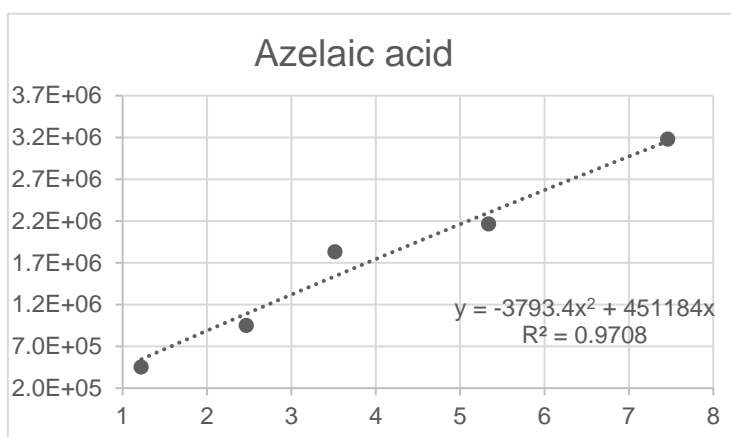
BSTFA derivatization



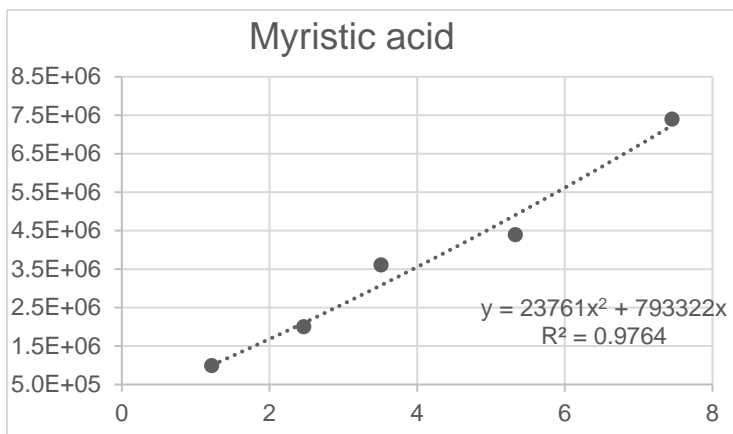
<i>Conc/ ppm</i>	<i>Area/ x10⁶</i>
1.23	0.895
2.49	1.714
3.55	3.090
5.39	3.461
7.53	5.749



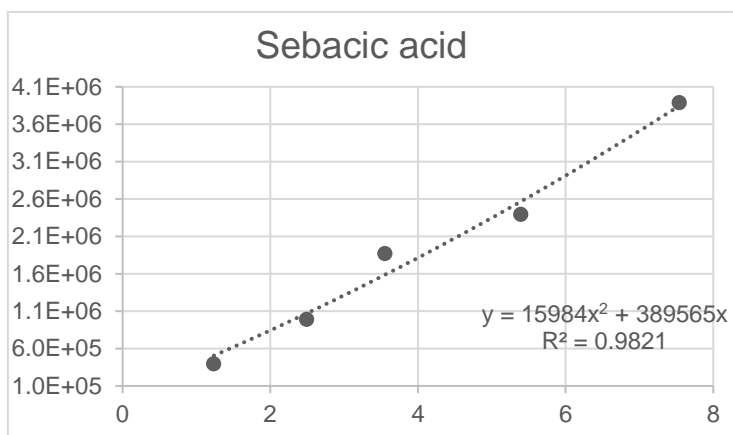
<i>Conc/ ppm</i>	<i>Area/ x10⁶</i>
1.24	0.334
2.52	0.669
3.59	1.327
5.45	1.511
7.62	2.187



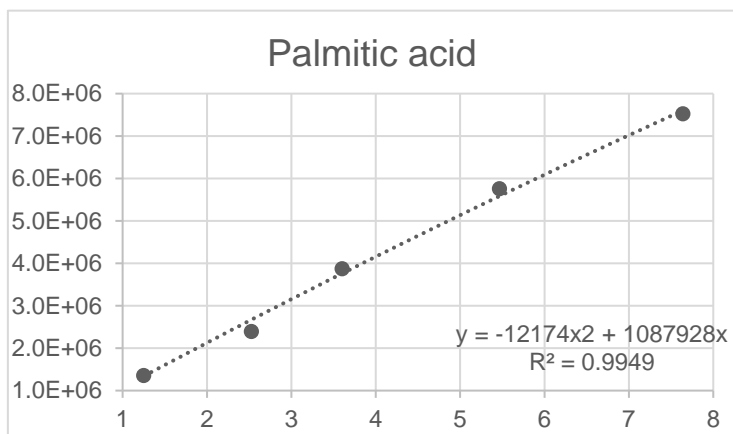
<i>Conc/ ppm</i>	<i>Area/ x10⁶</i>
1.22	0.451
2.46	0.948
3.51	1.831
5.33	2.163
7.46	3.179



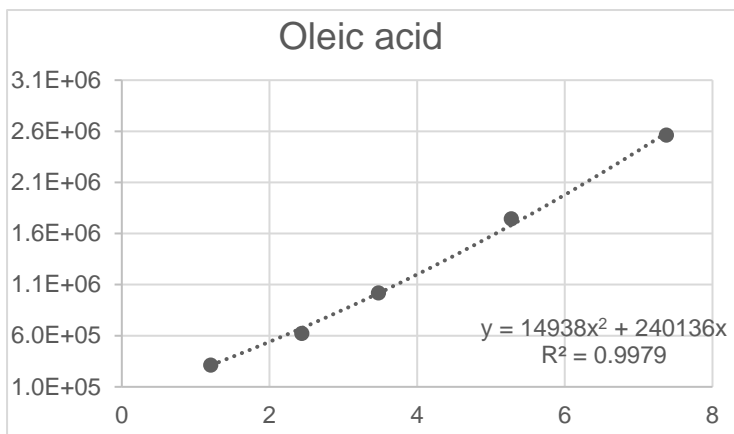
<i>Conc/ ppm</i>	<i>Area/ x10⁶</i>
1.22	0.985
2.46	1.998
3.51	3.603
5.33	4.391
7.45	7.393



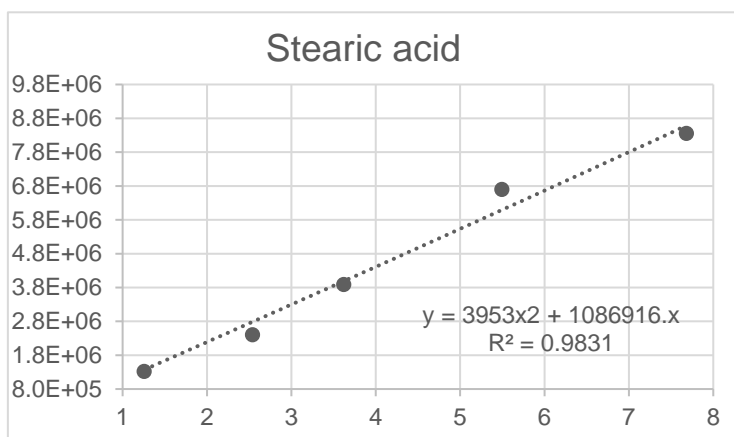
<i>Conc/ ppm</i>	<i>Area/ x10⁶</i>
1.23	0.392
2.49	0.987
3.55	1.867
5.39	2.391
7.54	3.887



<i>Conc/ ppm</i>	<i>Area/ x10⁶</i>
1.25	1.352
2.52	2.389
3.60	3.868
5.46	5.756
7.64	7.523



<i>Conc/ ppm</i>	<i>Area/ x10⁶</i>
1.20	0.311
2.44	0.620
3.47	1.017
5.27	1.741
7.37	2.560



<i>Conc/ ppm</i>	<i>Area/ x10⁶</i>
1.25	1.315
2.54	2.397
3.62	3.881
5.49	6.692
7.68	8.347

Acknowledgements

I want to thank my supervisor Prof. Rocco Mazzeo and co-supervisors, Prof. Silvia Prati, and Dr. Giorgia Sciutto for their useful comments on the present research.

Thanks to my colleagues from the M2ADL for their contributions: Dr. Emilio Catelli, Gianluca Chiapponi, Lucrezia Gatti, Dr. Yiming Jia, Marco Chávez and Francesca Ramacciotti.

I would also like to express my gratitude to all my colleagues and the students involved in the different projects included in this thesis.

Thanks to Prof. Dr. Koen Janssens, Dr. Frederik Vanmeert, Dr. Alba Álvarez Martin, Gert Nuyts, Stijn Legrand, Steven De Meyer, Ermanno Avranovich Clerici, Ehab Alemam, and Olivier Voet from the University of Antwerp for their support and kindness.

I would also like to thank Prof. Aldo Romani and Dr. Letizia Monico from the University of Perugia/CNR for providing the synchrotron data as well for their support and comments on the text of the second chapter.

Thanks to Dr. Heike Stege and Dr. Clarimma Sessa from the Doerner Institut for providing the paint samples and share the Raman and SERS data used in the first chapter.

I would also like to thank Dr. Illaria Bonaduce and Francesca Modugno from the University of Pisa for their support for the GC-MS analysis.

Thanks to Prof. Mariangela Vandini, Dr. Flavia Fiorillo, Dr. Sara Fiorentino, and Chiara Matteucci from the Cultural Heritage Laboratory from the University of Bologna for the access to the Raman instrumentation.

Finally, yet importantly, I would like to thank the students that collaborate in this research. Caterina Bordin, Gianluca Ghetti, Rebeca Dávalos Navarro, Hugues Malservet, Mathilde Romé, Zelan Li.